



HAL
open science

Morphological, electrophysiological and topographic characterization of layer V subcortical projection neurons in a mouse model of neurodevelopmental disease

Chiara Tocco

► **To cite this version:**

Chiara Tocco. Morphological, electrophysiological and topographic characterization of layer V subcortical projection neurons in a mouse model of neurodevelopmental disease. Molecular biology. Université Côte d'Azur, 2021. English. NNT : 2021COAZ6004 . tel-03964281

HAL Id: tel-03964281

<https://theses.hal.science/tel-03964281v1>

Submitted on 31 Jan 2023

HAL is a multi-disciplinary open access archive for the deposit and dissemination of scientific research documents, whether they are published or not. The documents may come from teaching and research institutions in France or abroad, or from public or private research centers.

L'archive ouverte pluridisciplinaire **HAL**, est destinée au dépôt et à la diffusion de documents scientifiques de niveau recherche, publiés ou non, émanant des établissements d'enseignement et de recherche français ou étrangers, des laboratoires publics ou privés.

THÈSE DE DOCTORAT

Caractérisation morphologique, électrophysiologique et topographique des neurones de la couche V dans un modèle murin de maladie neurodéveloppementale

Chiara TOCCO

Institut de Biologie Valrose

Présentée en vue de l'obtention du
grade de **Docteur en Sciences de la
Vie et de la Santé** d'Université Côte
d'Azur

Dirigée par : **Michèle Studer**

Soutenue le : **29 janvier 2021**

Devant le jury, composé de :

Barbara Bardoni, PhD, IPMC Institut de
Pharmacologie Moléculaire et Cellulaire
Valbonne, France

Isabelle Dusart, PhD, IBPS Institut de
Biologie Paris – Seine, Paris, France

Marta Nieto, PhD, CNB Centro Nacional
de Biotecnología, Madrid, Espagne

Caractérisation morphologique, électrophysiologique et topographique des neurones de la couche V dans un modèle murin de maladie neurodéveloppementale

Morphological, electrophysiological and topographic
characterization of layer V subcortical projection neurons
in a mouse model of neurodevelopmental disease

Jury :

President du jury :

Barbara Bardoni, PhD, IPMC Institut de Pharmacologie Moléculaire et Cellulaire
Valbonne, France

Rapporteurs :

Isabelle Dusart, PhD, IBPS Institut de Biologie Paris – Seine, Paris, France

Marta Nieto, PhD, CNB Centro Nacional de Biotecnología, Madrid, Espagne

Resumé

Chez les mammifères, la bonne exécution des mouvements volontaires fins repose sur des réseaux neuronaux complexes qui relient diverses régions du cerveau, tel que le cortex, les ganglions de la base, les noyaux pontins, le cervelet et le thalamus. La compréhension des mécanismes génétiques et moléculaires qui sous-tendent l'organisation neuronale de ces circuits améliorera notre connaissance de la façon dont les réseaux moteurs sont normalement établis au cours du développement et affectés dans les maladies neurodéveloppementales. Les neurones pyramidaux de la couche V à projection sous-corticale (LVPN) sont, entre autres, au cœur de ce circuit.

Nous avons précédemment montré que la perte génétique du facteur de transcription Nr2f1 dans le cortex en développement affecte l'organisation des aires fonctionnels du néocortex, la région évolutivement plus récente du cortex cérébral, et la spécification moléculaire des neurones LVPN, entraînant des fonctions motrices volontaires défectueuses tant chez les modèles murins que chez les patients humains présentant une haploinsuffisance du gène NR2F1. Pour mieux évaluer la contribution de Nr2f1 dans l'établissement des réseaux sous-corticaux, nous avons utilisé deux lignées de souris mutantes pour Nr2f1 et avons étudié les caractéristiques électrophysiologiques, morphologiques et de connectivité des neurones LVPN à différents stades de développement.

Nos données électrophysiologiques et morphologiques révèlent que les neurones mutants postnatals sont caractérisés par une excitabilité intrinsèque accrue et une complexité réduite des dendrites, ce qui indique que Nr2f1 joue un rôle clé dans la maturation fonctionnelle des LVPN pendant le développement cortical. En outre, le traçage génétique des projections dans les cerveaux mutants montre une cartographie topographique anormale entre le cortex et les noyaux pontins, ce qui implique que les neurones corticaux doivent normalement acquérir une propre identité positionnelle avant d'établir des projections sous-corticales appropriées. Dans l'ensemble, nos données indiquent que le gène Nr2f1 est impliqué dans l'établissement des propriétés fonctionnelles et structurelles des neurones LVPN, ainsi que dans l'organisation topographique des projections cortico-pontines, premiers acteurs du circuit cortico-ponto-cérébelleux impliqués dans la motricité fine.

Mot clés : Neurones pyramidaux de la couche V, faisceau corticospinal, topographie, maladie neurodéveloppementale

Abstract

In mammals, the proper execution of fine voluntary movements relies on complex, but highly organized neuronal networks connecting various regions of the brain, such as the cerebral cortex, basal ganglia, pontine nuclei, cerebellum and thalamus. Understanding the genetic and molecular mechanisms underlying the neuronal organization of these circuits may improve our knowledge of how motor networks are normally established during development and affected in neurodevelopmental diseases. Among others, subcortically projecting Layer V Pyramidal Neurons (LVPNs) are central to this circuit.

We have previously shown that the genetic loss of the transcription factor *Nr2f1* in the developing neocortex, the evolutionary most recent region of the cerebral cortex, affects areal organization and molecular specification of LVPNs, leading to defective voluntary motor functions in both mouse models and human NR2F1 haploinsufficient patients. To further assess the contribution of *Nr2f1* in the establishment of cortico-subcortical networks, we used two independent *Nr2f1* conditional mutant mouse lines and investigated electrophysiological, morphological and connectivity features of LVPNs at different developmental stages.

Our electrophysiological and morphological data reveal that postnatal mutant LVPNs are characterized by increased intrinsic excitability and reduced dendrite complexity, indicating that *Nr2f1* plays a key role in LVPN functional maturation during cortical development. Moreover, genetic tracing of LVPN projections in mutant brains shows abnormal topographic mapping between the cortex and pontine nuclei, implying that LVPNs need to acquire their proper areal identity to establish normal subcortical projections.

Overall, our data indicate that *Nr2f1* is involved in the establishment of functional and structural properties of LVPNs, as well as in the topographic organization of cortico-pontine projections, first players of the cortico-ponto-cerebellar circuit involved in fine motor skills.

Key words: Layer V Pyramidal neurons, corticospinal tract, topography, neurodevelopmental disease

If you could see me now
I hope that I'm making you proud.

Acknowledgements

To all the people who accompanied and guided me through these last 4 years I want to say: thank you, from the bottom of my heart. It has not been always easy, and I could not do it without you all. Thanks, from bringing knowledge, wisdom, happiness and affection to my PhD days.

First and foremost, I want to thank my supervisor and mentor, Dr. Michèle Studer, for supporting me all these years and for believing in me more than I did myself. I am been the most insecure person since forever, unable to see my potential, until you came along and decided this had to change. Although the path is still long ahead of me before I stop second-guessing every step I take, it is thanks to you if I even took this path at all.

Thanks to my colleagues, from the present and from the past, for always being available for me every time I needed advices and help. A special heartfelt thanks to Michele, who not only is a great person to work with but also one of the best friends I could imagine finding around and I cannot express with words how much your support in and outside of the lab has been important to me.

A big thank you to all the members of the iBV that I met along the way. *I don't know half of you half as well as I should like; and I like less than half of you half as well as you deserve.* To my friends Marika and Anna, I wish to say my biggest thank you, for being there for me every time I needed someone to talk with, being it a happy talk, or an angry talk. If I'm not insane by now is mostly because of you; I owe you big time.

I want to thank the members of my jury, Drs Barbara Bardoni, Isabelle Dussart and Marta Nieto for having accepted to correct my thesis and evaluate my doctorate work. Thanks for the kind word you wrote in your report. As previously said, I am the very last person to see the good in my work, so I could not believe my eyes when I read your extremely positive comments, I cannot stress enough how much reading them boosted my spirit.

And of course, although they are quite far away geographically speaking, they have always been very close to my heart and thoughts. A big virtual hug to my family and friends. Thanks for your support and unconditional love. Particularly this last year, it has been very important to have you all around. The world might have crumbled under our feet and we might have found ourselves isolated and alone, but we were never lonely (also thank you Zoom, I appreciate you). And today as four years ago, it reassures me to know that I can always count on your affection, wherever my path will lead. Also, I will keep coming back home, if you offer good food and wine!

List of abbreviations

A1	primary auditory cortex	Mc	magnocellular nucleus
ASD	autistic spectrum disorders	MdV	ventral part of the medullary
BBSOAS atrophy syndrome	Bosch-Boonstra-Schaaf optic	reticular nucleus	
BMP	bone morphogen protein	MG	thalamic medial geniculate nucleus
cKO	conditional KO	mS1	motorized primary somatosensory
CNS	central nervous system	cortex	
COUP-TFI	chicken ovalbumin upstream	NEc	neuroepithelial cell
promoter - transcription factor 1		NR2F1	nuclear receptor family 2 member 1
CP	corticopontine	P0	postnatal day 0
CSp	corticospinal	PCrt	parvocellular reticular nucleus
CST	corticospinal tract	PIL	thalamic posterior intralaminar
CSt	corticostriatal	nucleus	
CTh	corticothalamic	PN	pontine nuclei
DBD	DNA binding domain	PoM	thalamic posteromedial nucleus
dLG	thalamic dorsolateral geniculate	ps8	pseudo-rhombomere 8
nucleus		r6	rhombomere 6
E(10.5)	embryonic day 10.5	RGC	radial glial cell
EGF	epidermal growing factors	S1	primary somatosensory cortex
FGF	fibroblast growth factor	S2	secondary somatosensory cortex
Gi	gigantocellular nucleus	SHH	sonic hedgehog
GW11	gestational week 11	SpV	spinal trigeminal nucleus
KO	knock-out	SpVe	spinal ventricular nucleus
LBD	ligand binding domain	V1	primary visual cortex
LDVL	thalamic lateralodorsal ventrolateral	Ve	vestibular nucleus
nucleus		VL	thalamic ventrolateral nucleus
LII-III	layers II and III	VP	thalamic ventroposterior nucleus
LIV	layer IV	VPL	thalamic ventral posterolateral
LV	layer V	nucleus	
LVI	layer LVI	VPM	thalamic ventral posteromedial
LVPN	layer V pyramidal neuron	nucleus	
LP	thalamic lateral posterior nucleus	VZ	ventricular zone
M1	primary motor cortex	WNT	vertebrate orthologue of wingless

List of figures and tables

INTRODUCTION:

- Figure 1** – Principal cortical cell populations and their migratory streams
- Figure 2** – The lamination of the mouse neocortex
- Figure 3** – Projection neuron diversity in the mouse neocortex
- Figure 4** – Brodmann functional areas in the human brain
- Figure 5** – Arealization of the mouse neocortex
- Figure 6** – Differential layering of human primary motor and somatosensory areas
- Figure 7** – Thalamocortical topographic map in mice
- Figure 8** – Maturation of murine LVPNs
- Figure 9** – Critical steps of CST development
- Figure 10** – Voluntary movement network
- Figure 11** – Somatotopic representation of body parts in human and mouse neocortex
- Figure 12** – Cytoarchitecture of the cerebellar cortex
- Figure 13** – Migratory stream of pontine cells
- Figure 14** – Innervation patterns in the pontine nuclei
- Figure 15** – NR2Fs protein structures
- Figure 16** – Nr2f1 molecular mechanisms of regulation
- Figure 17** – Arealization defects in *Nr2f1 null* and *Emx1-cKO* animals
- Figure 18** – Laminar specific genes in *control* and *Nr2f1 cKO* neocortices
- Figure 19** – Loss of cortical *Nr2f1* influences the targeting of subcerebral projection neurons
- Figure 20** – Arealization defects in *Nex-cKO* animals
- Figure 21** – Laminar specific genes in control and *iz-hNr2f1* mouse neocortices
- Figure 22** – *NR2F1* pathologic mutations

MATERIAL AND METHODS:

- Figure 23** – Schematic of the analysed alleles, relative primers and representative PCR
- Figure 24** – In utero electroporation schematics
- Figure 25** – pCAG-mCherry plasmid map
- Figure 26** – Inducible pCAG-Bhlhb5-IRES-GFP plasmid map
- Figure 27** – pCAG_smFP TAG plasmid map
- Figure 28** – iDisco tissue clearing and immunostaining timeline
- Table 1** – Nr2f1 PCR reaction mix and primers
- Table 2** – Cre PCR reaction mix and primers
- Table 3** – *Thy1-eYFP-H* PCR reaction mix and primers

Table 4 – PCR program

Table 5 – List of used antibodies

Table 6 – List of qPCR primers

Table 7 – List of home-made solutions used in the KCl acute depolarization assay

Table 8 – List of home-made solutions used in 2D immunofluorescence protocol

Table 9 – List of home-made solutions used in iDisco protocol

RESULTS:

Figure 29 – Graphical summary

Figure 30 – *Nr2f1* cortical expression pattern

Figure 31 – Graphical summary

Figure 32 – Loss of *Nr2f1* leads to reduction of spines in *Nex-cKO* adult brains

Figure 33 – Loss of *Nr2f1* does not affect spine maturation in *Nex-cKO* mutants

Figure 34 – Assessing *Nr2f1/Bhlhb5* functional relationship via *in utero* electroporation

Figure 35 – Neuromorpho.org cells classification

Figure 36 – Example of Neuromorpho archive

Figure 37 – Example of cell sheet

Figure 38 – Panel of selected representative cells

Figure 39 – Sholl curves of four example cells

Figure 40 – Assessing optic nerve malformations via tissue clearing and 3D imaging techniques

Table of contents

Resumé	i
Abstract	iii
Acknowledgements	vii
List of abbreviations	ix
List of figures and tables	x
Prologue	xvi
INTRODUCTION.....	19
The development of the neocortex.....	20
Early stages of telencephalic development	20
The Neocortex	21
Lamination	22
Arealization	26
The topographic organization of cortical afferences and efferences	29
Generation and maturation of neocortical LV pyramidal neurons (LVPNs)	32
Fast growth phase	33
Intermediate growth phase	34
Slow growth phase	34
Morphological and electrophysiological features of mature LVPNs	35
Corticospinal tract development	37
Corticospinal neurons specification and differentiation - Fig. 9i	38
The pallial-subpallial boundary and internal capsule - Fig. 9ii	38
The telencephalic-diencephalic boundary and the cerebral peduncles - Fig. 9iii	38
The mesencephalic-rhombencephalic boundary - Fig. 9iv	38
The pyramidal decussation - Fig. 9v	39
Spinal cord - Fig. 9vi	40
Structural and functional characteristics of the voluntary movement circuitry.....	41
Intracortical connections and descending corticospinal tract	42
The side-loop to the basal ganglia	44
The Brainstem nuclei	45

Cerebral and Cerebellar cortices: differences in cytoarchitecture and topographic representation	46
The cortico-ponto-cerebellum network	47
Cell specification	48
Cell migration	48
Nucleogenesis	49
Corticopontine connectivity and function	50
Voluntary movement defects in human pathologies and animal models	52
Overview on behavioural tests to study dexterity in mice	54
Nr2f1 deficient mice as a genetic model to study corticospinal tract development.....	56
Nr2f1 structure and pattern of expression	56
Role of Nr2f1 during cortical development	59
Nr2f1 impaired arealization and layering influence axon growth and voluntary movement execution	62
Mitotic <i>versus</i> postmitotic Nr2f1 function in area specification	63
NR2F1 expression in humans and the Bosch-Boonstra-Schaff Optic Atrophy Syndrome	66
Common features and dissimilarities between BBSOAS patients and available mouse models	68
Thesis main objectives.....	72
MATERIAL AND METHODS.....	74
Animals	75
<i>Nr2f1^{flox/flox}; Emx1-Cre</i> mouse line	75
<i>Nr2f1^{flox/flox}; Nex-Cre</i> mouse line	75
<i>Thy1-eYFP-H</i> reporter mouse line	75
DNA extraction and genotyping	76
Nr2f1	76
CRE	77
Thy1-eYFP-H	77
Protein extraction and Western blot analysis of postnatal cortices.....	79
qPCR.....	80
Stereotaxic injections	81

In utero electroporation	81
Material preparation	81
Procedure	82
Plasmids	84
pCAG-mCherry	84
Inducible pCAG-Bhlhb5-IRES-GFP	85
pCAG_smFP FLAG	86
Intracardiac perfusion and tissue dissection	87
Tissue sectioning.....	87
KCl ex vivo depolarization assay	88
<i>Table 7 - List of the home-made solutions used in the KCl acute depolarization assay</i>	<i>88</i>
2D immunofluorescence.....	89
Imaging	90
Laser scanning confocal microscopy	90
Epifluorescence microscopy	90
Image Analysis	90
Statistical analysis	91
idisco clearing and 3D imaging	92
RESULTS	94
1. Paper One	95
2. Paper Two.....	143
3. Additional results	193
a. Assessing dendrites spine density of cortical layer V pyramidal neurons in <i>Nr2f1 cKO</i> models	193
i. Spine density dynamics variation relative to the developmental stage, cell type and cortical region of belonging	194
ii. The structure of mature dendritic spines	194
iii. Functions and pathological dysfunctions of dendritic spines	195
iv. Results	197
a. Assessing topographic map of thalamo-cortical and cortico-pontine projections in a genetic rescue model for <i>Nr2f1</i> loss of function.	200
Annex A.....	204

Publication of LVPNs P7 reconstructed cells on the neuromorpho.org database	204
LVPNs present morphological differences among classes and genotypes	207
Annexe B	209
Whole brain tissue clearing and imaging as a tool to study tract malformations in <i>Nr2f1</i> mutant animals.	209
DISCUSSION AND PERSPECTIVES	212
References	224

Prologue

Everything we do, any action we make during our life can be reduced and classified as an interaction of our body with the surrounding environment. All these interactions are the result of continuous elaboration and information processing that takes place in the brain. For this reason, the brain is considered the most important organ of our body. At least, according to the Brain!

Provocation aside, it is well acknowledged that the brain and more generally the Central Nervous System (CNS) plays key roles in our ability to survive and adapt to the changing world. One particular important feature of the CNS activity is the regulation of movement execution, a set of functions we use to navigate in the space we live, interact with objects and other individuals and perform basic and complex tasks, all with the ultimate goal of keeping ourselves alive and increasing the fitness of the species.

Historically, movements have been classified into three main categories: reflexive, rhythmic and voluntary movements (Kandel et al., 1991; Squire et al., 2013). We refer to reflexes when we talk about all those actions that are involuntarily coordinated in response to peripheral sensorial stimuli (the withdrawals reflex of a limb, coughing, sneezing and swallowing) and which outcome is mainly the avoidance of potentially dangerous situations. Rhythmic movements are also automatically regulated and, at least in principle, are the result of repetitive, alternated and stereotyped actions. Examples of rhythmic movements are all the different forms of locomotion, such as swimming and walking, but also chewing and breathing.

Differently from reflexes and rhythmic movements, voluntary movements are initiated to accomplish a specific goal and can improve with practice. Moreover, their coding, regulation and execution is, by a great extent, achieved by the CNS and specifically by the cerebral cortex.

In this work, I will focus on the first path of a complex neural circuit deputed to voluntary movements, and on the genetic, physiological and connectivity aspects of cortical layer V neurons, key players in the execution of skilled movements that result often altered in human neurodevelopmental disorders.

In the first chapter of the introduction, I will introduce cerebral cortex development and the major modifications this structure undergoes until reaching adulthood. I will describe its structure at both the macroscopic level, introducing the concept of functional areas and topographic representation, and the microscopic cellular level, describing some of the several neuronal populations populating the cerebral cortex including their functional significance and their connectivity patterns.

In the second chapter, I will further describe one of those cell populations, the pyramidal neurons of the cortical layer V, for their important role in the voluntary movement network. In this part, I will present their differentiation and maturation processes, as well as their morphology and electrophysiological profiles.

In chapter three, I will describe the circuits involved in the coordination and execution of voluntary movements, from the main cortico-spinal tract to their collaterals and additional connections and structures involved in the network. Furthermore, I will provide an overview on known human syndromes characterized by defects in the execution of voluntary movements and, in parallel, the available mouse models used to assess both motor defects and molecular mechanisms of pathogenesis.

In the fourth chapter, I will introduce Nr2f1 (also known as COUP-TFI) by describing what is known about its role in brain development, and by reporting a list of known human mutations in the NR2F1 gene and their pathological effects. In this part, I will also introduce the Nr2f1 deficient mouse models that I have used in my thesis work.

Finally, in the fifth and last chapter, I will summarize what it is known about Nr2f1 involvement in voluntary movement regulation and introduce the aims of my thesis work.

INTRODUCTION

The development of the neocortex

To better understand the functions elicited by the cerebral cortex during voluntary movement execution, it is imperative to discuss how this complex structure develops, prior to discuss how the circuits are formed.

Early stages of telencephalic development

The neocortex, together with the hippocampus, olfactory bulbs, basal ganglia and amygdala, represents one of the main components of the dorsal telencephalon, also known as pallium (Reviewed in Nat et al., 2013). The pallium and its ventral counterpart, the subpallium, constitute the telencephalon, the most complex and evolutionarily advanced brain structure. At early stages of development, the pallium is further subdivided into three major regions (**Fig. 1a**), dorsal, medial and lateral, which give rise to the neocortex, the hippocampal formation (archicortex) and the paleocortex (olfactory and limbic areas), respectively. Similarly, the subpallium is subdivided into three regions: medial, lateral and caudal (**Fig. 1a**) eminences and comprise the generation sites of migrating interneurons that will invade and populate the forming cerebral cortex and olfactory bulbs at later stages (Reviewed in Nat et al., 2013).

Neurons populating the mature telencephalon belong to two main classes, namely the glutamatergic projection (pyramidal) neurons and the GABAergic neurons (**Fig. 1b**). The glutamatergic class includes the vast majority of cortical neurons (70-80%), which are generally excitatory and are produced *in loco* at the germinative zone of the developing neocortex (Reviewed in Molyneaux et al., 2007). GABAergic neurons instead, include various subpopulations of cortical inhibitory interneurons, that represent the 20-30% of the whole cortical neuronal population, and are generated in the ventral telencephalon, prior to migrate and settle in the developing cortex (Reviewed in Nat et al., 2013).

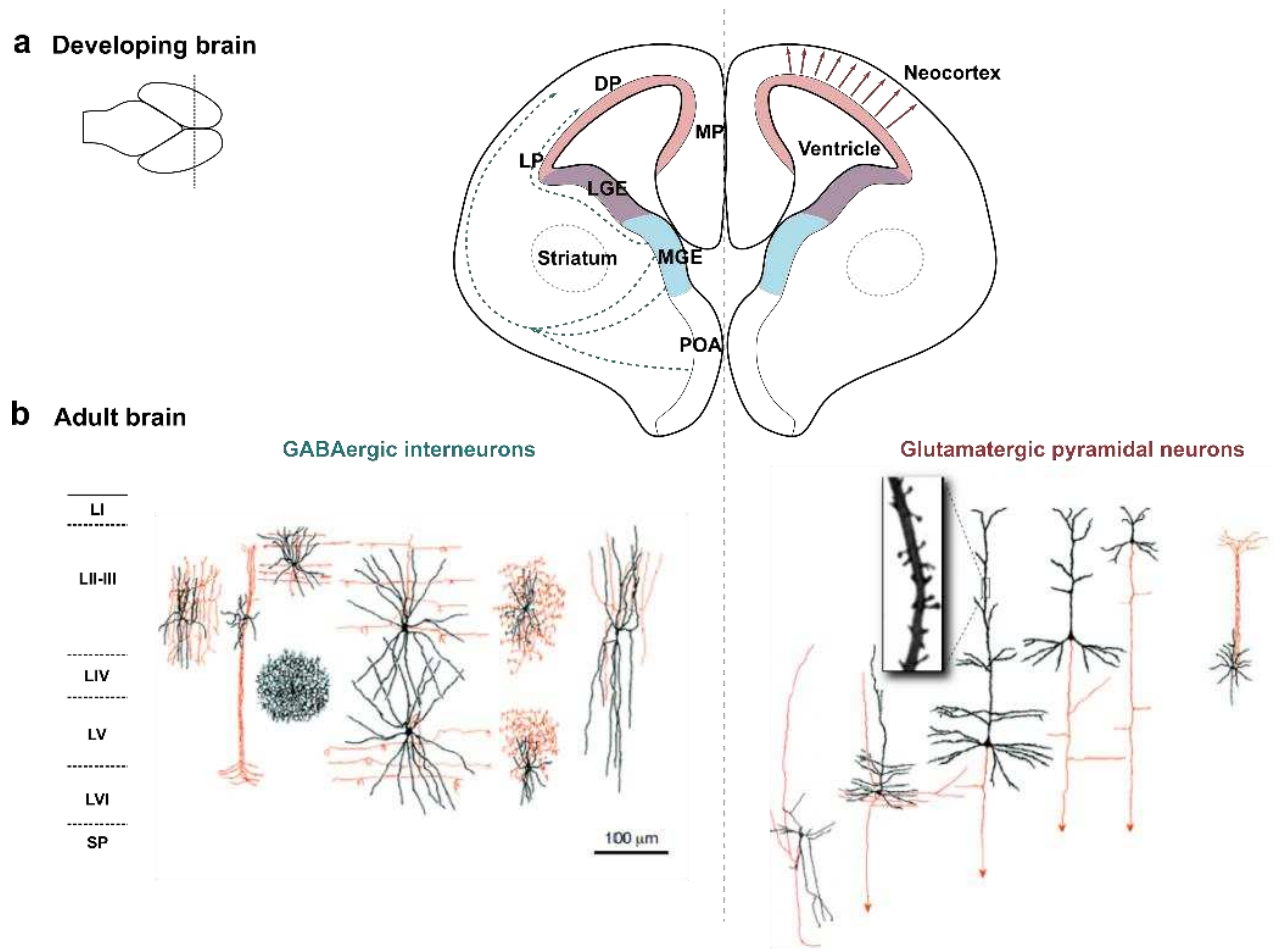


Figure 1 - Principal cortical cell populations and their migratory streams. **a)** Schematics of a coronal section of the mouse developing brain and principal migration paths of GABAergic interneurons (blue, dashed arrows) and glutamatergic pyramidal neurons (red arrows). **b)** Shape and distribution of cortical populations of interneurons (left) and excitatory neurons (right).

MP, DP, LP: medial, dorsal and lateral pallium; LGE, MGE: lateral and medial ganglionic eminence; POA: preoptic area; LI to LVI: layer I to layer VI; SP: subplate. (Adapted from Kwan et al., 2012; Tan et al., 2013).

In this manuscript I will mainly focus on the neocortical development and its glutamatergic component, leaving aside details and information concerning other telencephalic structural and cellular components, which are not strictly necessary for the understanding of my project.

The Neocortex

From an evolutionary point of view, the neocortex is considered the most recent region of the mammalian brain, seat of higher cognitive function, sensory perception and consciousness. This region, which underwent a dramatic expansion during mammalian evolution and especially in primates, retains a highly stereotyped development process, named corticogenesis. During a time

span of several days of mouse development, the various cellular components of the neocortex are produced within specific time windows and following very precise trajectories of differentiation and maturation (Reviewed in Greig et al., 2013; Molyneaux et al., 2007).

The first neural cells, the neuroepithelial (NE) cells, are generated from the blastocyst pluripotent stem cells during the transition from ectoderm to neuroectoderm, during a process called neural induction. Once formed, NE cells aggregate to form the neural plate and later the ventricular zone (VZ) of the neural tube at embryonic day (E)10.5. There, at the onset of corticogenesis (E11.5), NE cells will transform into radial glia cells (RGCs) and start giving birth to the different subpopulations of cortical pyramidal neurons, in a process called lamination (Reviewed in Greig et al., 2013). At the same time, the growing neocortex is subjected to the action of morphogens and transcription factors which guide the newly produced neuronal cells to organize themselves into distinct functional areas and networks, through a process called arealization (Alfano et al., 2013; Cadwell et al., 2019; O'Leary et al., 2008).

Although the duration of this process is varying massively among different mammalian species, it always culminates with the production of a highly structured, regionalized and six-layered cortex. Thus, for a matter of simplicity and unless necessary, I will refer only to the corticogenesis process as it occurs in rodents, and in general, to the mouse neocortex and other subcerebral structures.

Lamination

The process of lamination (**Fig.2**) starts approximatively at E11.5 when the first postmitotic cells form the preplate that then split in two layers by the emerging cortical plate, the precursor of cortical layers II-VI (Olson, 2014). The preplate splitting starts in the lateral neocortex and proceeds dorsally and caudally and produces two layers of pioneer cells, a deep layer called subplate and superficial one called marginal zone (Olson, 2014). Both structures are crucial for cortical development organization (Ayoub et al., 2009; Martínez-Cerdeño et al., 2014). The subplate is a transitional layer home of a heterogeneous population of glutamatergic and GABAergic neurons, involved in the patterning of early neuronal interaction and guidance of thalamocortical axons (Kostovic et al., 1990; Supèr et al., 1998). The marginal zone is also a transient prenatal structure; its equivalent adult structure is the cortical layer I. It is composed by several glia and neuron

populations and reelin-positive Cajal Retzius cells (Martínez-Cerdeño et al., 2014). Cajal Retzius cells are known to control both the scaffolding of the developing neocortex and neuron migration by secreting reeling into the extracellular matrix of the marginal zone. From there, the molecule diffuses into a gradient towards the ventricular zone and binds to lipoprotein receptors expressed on RGCs axons. Ultimately, the reelin signalling cascade mediate the reorganization of the cytoskeleton, promoting actin dynamics and cell motility (Frotscher et al., 2009).

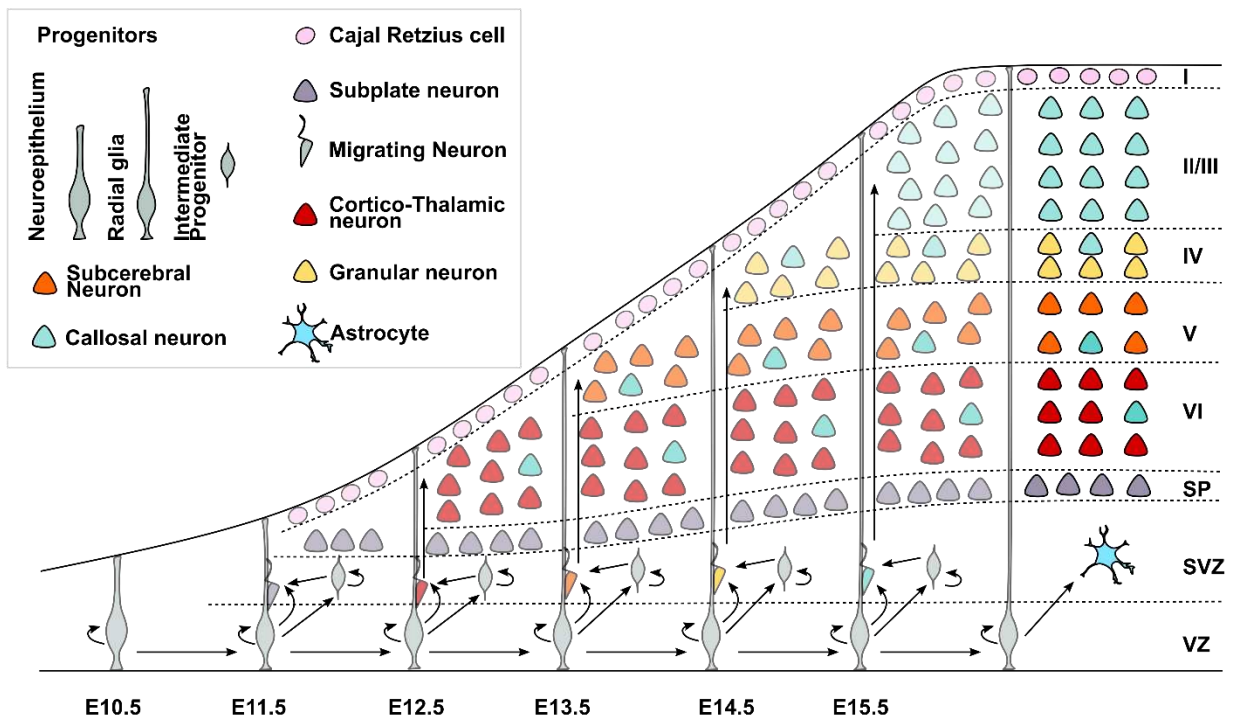


Figure 2 - The lamination of the mouse neocortex. Schematic representation of the sequential generation of neocortical projection neuron subtypes over the course of mouse embryonic development. Before the onset of neurogenesis, Cajal–Retzius (CR) cells primarily migrate into neocortical layer I from non-cortical locations. At E11.5, Radial glia cells (RGCs) in the ventricular zone (VZ) start producing projection neurons, which then migrate towards their final location using the RGCs basal process as scaffold, and intermediate progenitors which will populate the subventricular zone (SVZ) and contribute to neuronal production. Distinct projection neuron subtypes are born during sequential and partially overlapping time windows. Times indicated in the figure represent the peak of production of corresponding represented neurons: E11.5 subplate (SP) neurons, E12.5 Corticothalamic projecting neurons (CTHPNs), E13.5 Subcerebral projection neuron (SCPNs or layer V pyramidal neurons LVPNs), and E14.5 Granular neurons of the layer IV (GNs). Callosal projection neurons (CPNs) are mainly produced from E15.5 to E16.5 although some CPNs start to be produced at E12.5 and migrate to deep layers. After completion of neurogenesis, RGCs transit to a gliogenic mode, and start generating astrocytes and oligodendrocytes. (Adapted from Greig et al., 2013).

As previously mentioned, the split of the preplate is the result of the cortical plate formation. This process consists of sequential and partially overlapping waves, during which all the different

subpopulations of pyramidal neurons are produced at the VZ and radially migrate to populate the cortical plate. The first neurons to settle are the deep layer neurons of layer VI (which peak of production is at E12.5) and of layer V (E13.5). Those neurons are followed by the granular neurons of layer IV at E14.5 and finally the upper layer neurons of layers II and III from E15.5 to E16.5.

At the same time, other classes of cells are produced either *in loco* as the astrocytes (Bayraktar et al., 2015) or in other locations within the brain, such as Cajal-Retzius cells, which originate from the pallial-subpallial border, the cortical hem and the septum (Kilb et al., 2016), GABAergic interneurons, originating from the lateral and medial ganglionic eminences of the subpallium (Wonders et al., 2006) and oligodendrocytes, originating in (van Tilborg et al., 2018). Furthermore, microglial cells, the primary immune system cells of the CNS, originate from progenitors in the yolk sac and invade the cortex at early developmental stages in the embryo (Swinnen et al., 2013).

Each layer is composed mainly, but not exclusively, by specific cell populations of projection neurons (reviewed in Greig et al., 2013; Molyneaux et al., 2007). Generally, these neurons can be classified according to whether they project within the same hemisphere (associative), throughout the midline and towards the contralateral hemisphere (commissural), or even outside of the cortex (corticofugal) (**Fig. 3**). Associative projection neurons (**Fig. 3a**) are present in all layers and can be both short and long-distance projection neurons, which extend axons nearby or to other cortical areas, respectively. Commissural neurons (**Fig. 3a**) reside mainly in upper layers II and III, even though a smaller population is also found in lower layers V and VI. They cross the midline through two main commissures, named corpus callosum and anterior commissure, and extend their axons to reach mirror-image locations in the contralateral hemicortex (Fame et al., 2011). And finally, corticofugal projection neurons are the most various populations of pyramidal neurons in the neocortex. They can be further split into corticothalamic (**Fig. 3b**), corticotectal, corticopontine and corticospinal projection neurons, depending on their specific targets. These last three populations are collectively known as subcerebral projection neurons (**Fig. 3c**). Corticothalamic (CTh) neurons (**Fig. 3b**) are mainly found in layer VI, but also in layer V and project to various nuclei of the thalamus, according to their specific function. Corticotectal neurons (**Fig. 3c**) are located in the visual cortex and maintain primary projections to the superior colliculus as well as collateral projections to the rostral pontine nuclei. Corticopontine (CP) and corticospinal (CSp) neurons (**Fig. 3c**) are located in

the motor and somatosensory neocortex and constitute the main layer V neuron populations. They either project directly to the pontine nuclei or to the spinal cord with collateral projections to the striatum and pontine nuclei.

During the early '90 and beginning of 2000, tracing experiments helped in elucidating the existence and incidence of dual projection neurons, representing those neurons maintaining double projections towards distinct targets in adult stages and after pruning (Akintunde et al., 1992; Mitchell et al., 2005). In rodents, a percentage of cells of all classes of neurons (associative, callosal and subcerebral) retains double projections at adult stages (Reviewed in Molyneaux et al., 2007). Specifically, 13-66% of premotor associative neurons for example, retain collateral projections through the corpus callosum and to the contralateral hemisphere, and represents the class of neurons with the higher rate of dual projection neurons (Mitchell et al., 2005). Right after, callosal neurons of the sensorimotor cortex show collateral associative projections in 4-33% of cases (Mitchell et al., 2005). Within the subcerebral projection neurons, only a few cells retain dual projections (an average of 2% among the different subpopulations), with the vast majority of cells having individual projections to a specific target (Akintunde et al., 1992; Greig et al., 2013).

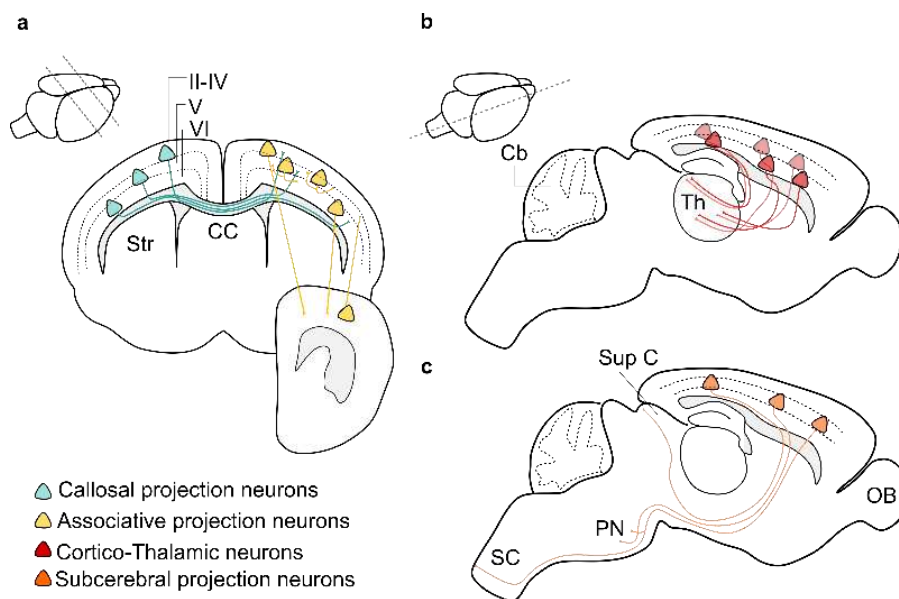


Figure 3 - Projection neuron diversity in the mouse neocortex. Schematic representation of **a)** callosal (cerulean) and associative (yellow) projection neurons, **b)** thalamo-cortical projection neurons (mainly in LVI -deep red-, but also in LV -faded red-) and **c)** subcerebral projection neurons.

Cb: cerebellum, CC: corpus callosum, OB: olfactory bulb, PN: pontine nuclei, SC: spinal cord, Str: striatum, Th: thalamus, II-IV: layers II, III and IV, V: layer V and VI: layer VI. (Adapted from Greig et al., 2013).

In the following chapters, I will focus on layer V pyramidal neurons, both as single neurons projecting towards the spinal cord or the pontine nuclei, as well as the small dual projecting population.

Despite corticogenesis being a process simultaneously happening throughout the whole neocortex, it is nevertheless characterized by slightly different spatially controlled time windows of neuronal subtype production. This ultimately produces cytoarchitectonic differences among different regions of the neocortex, and have been found to reflect area-specific functions (Creutzfeldt, 1977). This part will be further developed in the following paragraph.

Arealization

The term of “areas” in humans and primates was originally proposed by the German neuroanatomist Korbinian Brodmann, who first described this cytoarchitectural map in 1909 (Brodmann et al., 2006). Since then, Brodmann divisions have been further characterized *via* histological staining techniques, and functionally by Nuclear Magnetic Resonance Imaging. Four major areas can be distinguished in all placental mammals: three of them, the primary sensory areas, receive from the environment sensory inputs of different nature, such as visual, auditory and somatic information. The fourth, the primary motor area, receives motor information from subcerebral regions such as the striatum and the cerebellum, as well as sensory information from other cortical regions. Its role is to integrate all these data and in response to codify a motor execution output (**Fig.4**).

The process of area patterning, or arealization, is defined as the process by which a particular cell acquires in time and space its spatial identity along the different axes of the neocortex. During this complex process, cells start to express fate determinant genes which in turn regulate how those cells mature into specific subset of cortical neurons, by precisely integrating into local and subcortical networks, ultimately leading to distinct area cytoarchitecture and functions. Historically, two hypotheses have been proposed for the establishment of this process. The “protomap” hypothesis contemplate that cortical areas are intrinsically determined by the interplay between morphogens and locally expressed transcription factors in progenitor cells and before the arrival of the first wave of sensory inputs from the periphery *via* the thalamus (Rakic, 1988; Rakic et al., 2009). Conversely, the “protocortex” hypothesis proposed that cortical areas are not intrinsically pre-patterned but shaped by extrinsic cues deriving from thalamic afferences, which act on postmitotic neurons, during the first postnatal stages (López-Mascaraque et al., 2004; O’Leary, 1989; O’Leary et

al., 1992). To date, these two hypotheses are both considered valid and complementing each other. During early stages, area identity is imparted by cell intrinsic factors in progenitors and post mitotic neurons, whereas thalamic afferents are further influencing and refining area functions (O’Leary et al., 2008).

Lateral view

Medial view

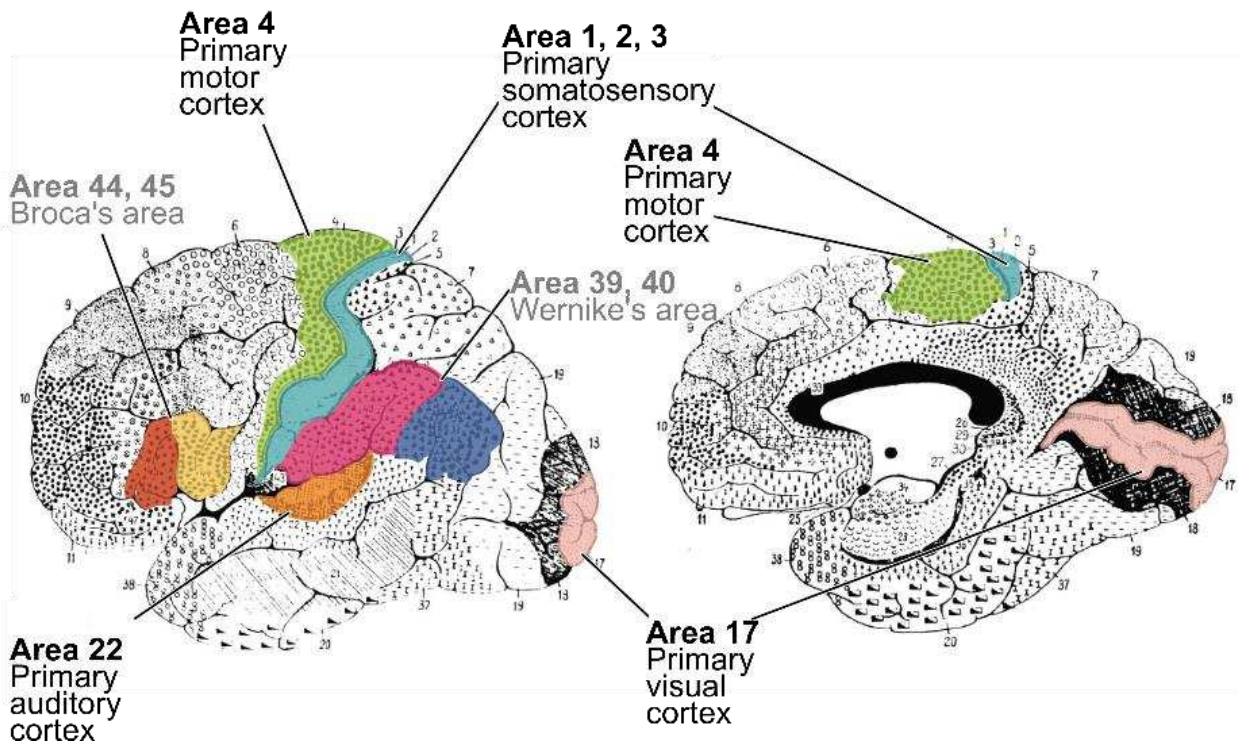


Figure 4 - Brodmann functional areas in the human brain. Lateral and medial views of the human brain including Brodmann’s area representations. The main areas are highlighted as follows: Areas 1-3, primary somatosensory, in cerulean. Area 4, primary motor, in green. Area 17, primary visual in pink and Area 22, primary auditory, in orange (adapted from Brodmann et al., 2006; Kandel et al., 1991).

During early stages of area patterning, the cortical primordium is controlled by the coordinate expression of morphogens, such as fibroblast growth factors (FGFs), sonic hedgehog (SHH), bone morphogenic proteins (BMPs), vertebrate orthologues of *Drosophila’s* wingless (WNTs) and epidermal growing factors (EGFs) (Fig. 5a). These molecules are expressed as early as E9.5 from localized patterning centres and form gradients within the forming protomap to regulate cell proliferation, specification and survival of neural progenitors (Alfano et al., 2013; O’Leary et al., 2007; Rubenstein et al., 1999). Furthermore, morphogens control by either inducing or repressing graded expression of transcription factors (Fig. 5b) in progenitor cells in the VZ (Fukuchi-Shimogori

et al., 2001; Grove et al., 2003). Finally, area specific expression of transcription factors in cortical plate postmitotic neurons controls the specification of precise neuronal subtype (Arlotta et al., 2005; Bedogni et al., 2010; Harb et al., 2016; Zhenyong Huang et al., 2009; Joshi et al., 2008; Weimann et al., 1999). The interplay between these factors is essential to start specifying individual functional areas. Among these factors, *Pax6* (Manuel et al., 2007), *Emx2* (Hamasaki et al., 2004), *Nr2f1* (Armentano et al., 2007; Borello et al., 2014) and *Sp8* (Borello et al., 2014) are the most studied and representative patterning genes, known to impart to the forming neocortex proper rostro-caudal and medio-lateral axes (Alfano et al., 2013; Grove et al., 2003; O’Leary et al., 2008). These factors are expressed as early as E9.5 in progenitor cells and, apart from *Nr2f1* which is also maintained in postmitotic neurons, the other three are restricted to progenitor cells and cease to be expressed soon after neuronal differentiation. While the combination of *Pax6* and *Sp8* in more rostral regions drives the specification towards motor identity, the expression of *Emx2* and *Nr2f1* is key for sensory specification (**Fig. 5c**) (reviewed in Bertacchi et al., 2019). Despite that, the topographic organization of the neocortical functional areas is not completed until early postnatal stages, when activity-dependent sensory stimuli reach the cortex through the thalamus and by refining area function, they reinforce the distinctions between areas (**Fig. 5d**).

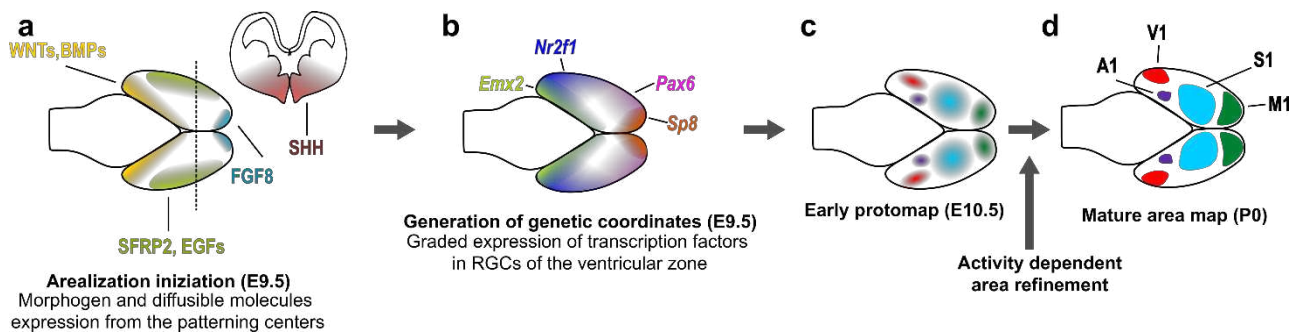


Figure 5 - Arealization of the mouse neocortex. **a)** Starting from E9.5, morphogens are secreted from distinctly located patterning centres and diffuse in the developing neocortex to form gradients and regulate **b)** graded expression of transcription factors in cortical progenitor cells (also called radial glia cells). **c)** Specifically, strong caudal expression of *Emx2* and *Nr2f1* promotes the specification of sensory areas, while rostral high expression of *Pax6* and *Sp8* drives the specification of motor identity. This “protomap” is then **d)** refined with the arrival of thalamic axons, which convey sensory information from the environment to the forming neocortex (adapted from Bertacchi et al., 2019).

As previously anticipated, the cytoarchitectonic structure of the different functional areas varies according to their specific function. As an example, the primary motor cortex (M1) shows an enlarged layer V (LV) and layer VI (LVI), seats of long-range projection neurons and corticothalamic neurons, whereas the granular layer IV (LIV), which is responsible of receiving and integrating sensory information coming from the environment through the thalamus, is greatly reduced (**Fig. 6 left**). On the contrary, the primary somatosensory cortex (S1) shows a prominent LIV (**Fig. 6 right**), which is in line with its main function of receiving and integrating inputs from the body (Creutzfeldt, 1977).

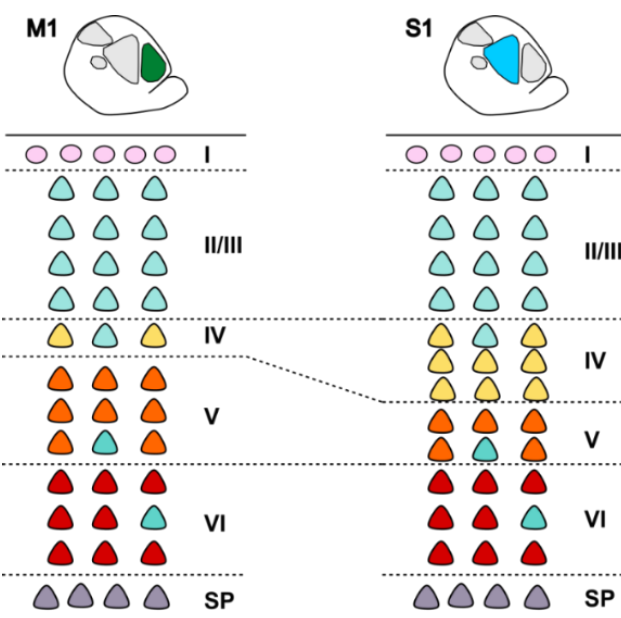


Figure 6 - Differential layering of murine primary motor and somatosensory areas. Schematic representation of area specific layering in primary motor and somatosensory mouse areas. A more expanded LV in the motor area is supportive of the fact that its main function is to relay movement information to subcerebral targets, whereas the expanded LIV typical of sensory areas reflects their main function as receivers of thalamic sensory inputs.

The topographic organization of cortical afferences and efferences

The arrival of thalamocortical projections to the neocortex is a fundamental event mediating activity-dependent refinement of functional areas. For this reason, the establishment of thalamocortical and corticothalamic paths has been thoroughly investigated, revealing that specific nuclei of the thalamus project to distinct regions of the cortex (Caviness et al., 1980) and vice versa, from the cortex efferences project back to the thalamus following the same route. On a large scale, this pattern of connections constitutes a topographic map between cortical functional areas and thalamic nuclei.

The thalamus is composed of several nuclei that can be classified in two main groups: aspecific nuclei, which projects to wide cortical regions, and specific nuclei, which instead target single cortical areas and their terminals mainly innervate layers IV and VI and, in a smaller proportion, the layer V. Reversely, corticothalamic projections arise mainly from layer VI but also V, and target the same thalamic region from which they received afferences. Specifically, S1 receives projections from the ventral posteromedial and posteromedial nuclei (VPM and PoM). Projections from the VPM reach layers IV, Vb and VI, whereas those from the PoM target the layer Va (Bureau et al., 2006). The auditory cortex receives afferences from the medial geniculate and the posterior intralaminar nuclei (MG and PIL) (Hofstetter et al., 1992; Hu, 2003) and the visual cortex is innervated by axons arising from the dorsal lateral geniculate and lateral posterior nuclei (DLG and LP) (Simmons et al., 1982). Finally, M1 receives afferences from the ventrolateral, ventral posterolateral and lateral dorsal ventrolateral nuclei (VL, VPL and LDVL) (Terashima et al., 1987; Tlamsa et al., 2010) (**Fig. 7**).

Although the establishment of the topographic map between cortex and thalamus is yet to be completely described, many factors influencing the process have been identified and they are expressed either at the level of pallium and subpallium, thalamus or specifically along the axons. As an example, the complex Netrin-1 (expressed in a rostral-high to caudal low gradient in the subpallium) and its receptors DCC and Unc5A-C (expressed along thalamocortical axons) are responsible of rostrally attracting the afferences (Powell et al., 2008). Several molecules of the Ephrin family are also important for the rostral targeting of thalamocortical axons. In fact, in mice deficient for either EphrinA4 or A7 or in double EphrinA5 and A4 knockouts, all the projections are caudally shifted, with motor axons projection into the S1 area (Dufour et al., 2003).

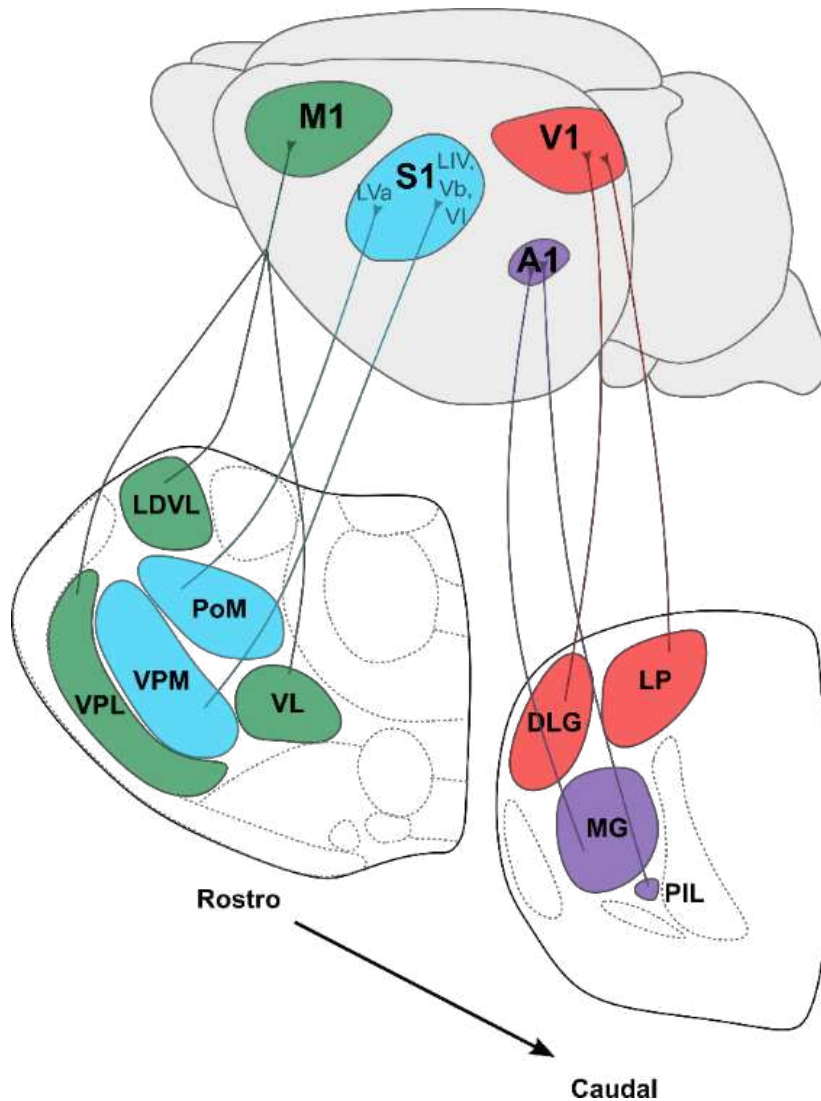


Figure 7 - The Thalamocortical topographic map in mice.

Schematic representation of main connections between thalamic nuclei and primary functional areas of the neocortex. Same colour represents a cortical region and its relative thalamic nuclei.

M1: primary motor; S1: primary somatosensory; V1: primary visual; A1: primary auditory; LDVL: lateral dorsal ventrolateral; PoM: posteromedial; VPM: ventral posteromedial; VPL: ventral posterolateral; VL: ventrolateral; LP: lateral posterior; DLG: dorsolateral geniculate; MG: medial geniculate; PIL: posterior intralaminar.

Furthermore, other guidance molecules (such as the semaphorins) as well as cell adhesion molecules (such as L1-CAMs and NrCAM) contribute to the thalamocortical afferences pathfinding

(Bagnard et al., 2001; Demyanenko, Riday, et al., 2011; Demyanenko, Siesser, et al., 2011; Gu et al., 2003; Maness et al., 2007; Wright et al., 2007). Finally, genes contributing to cortical arealization can also influence the topography of corticothalamic and thalamocortical innervations. For example, the cortical expression of the nuclear receptor Nr2f1 is fundamental for the correct establishment of both corticothalamic and thalamocortical connectivity, and loss of its function leads to the caudal shift of thalamocortical axons and the concomitant defective connectivity of corticothalamic projections (this topic will be further analysed in a following section) (Alfano et al., 2014; Armentano et al., 2007).

Generation and maturation of neocortical LV pyramidal neurons (LVPNs)

LVPN neurons are generated from RGCs at the VZ surface of the neocortex around E13.5, and their specification and differentiation is mediated by sequential and combinatorial expression of several transcription factors, such as *Fezf2* and *Ctip2* (B. Chen et al., 2008; McKenna et al., 2011). These two transcriptional regulators are highly expressed by LV neurons and are required for the early specification and axon outgrowth of subcerebral projection neurons, respectively, as demonstrated by the absence of the corticospinal tract (CST) in *Fezf2 knock-out (KO)* (B. Chen et al., 2005) and by its reduced outgrowth in *Ctip2 KO* (Arlotta et al., 2005) mice. Furthermore, the absence of *Ctip2* expression in *Fezf2 KO* animals, and the rescue of the projections defects by restoring *Ctip2* expression, suggest that this gene is a downstream factor of *Fezf2* in the regulation of CST development. This combinatorial expression is specifically found in LV but not in LVI corticofugal neurons, that express instead high levels of *Tbr1*, a transcription factor mediating corticothalamic differentiation, possibly through the inhibition of the *Fezf2-Ctip2* pathway (McKenna et al., 2011)

Despite *Fezf2* and *Ctip2* being the most popular factors influencing early subcerebral projection development, many other factors have been described to be involved in this process. Several studies have shown that loss of function of *Sox5* (Lai et al., 2008), *Satb2* (Alcamo et al., 2008; Britanova et al., 2008), *Nr2f1* (Tomassy et al., 2010) and/or *Bhlhb5* (Joshi et al., 2008) are not only involved in LVPN specification, but also in CST formation. In fact, the deregulation of such genes can lead to axonal misrouting and in some cases to axonal defasciculation, suggesting that these transcription

factors play different roles during CST formation. Finally, other factors which are acting at later stages, such as *Ldb1/Ldb2* and *Sip1* (Leone et al., 2017; Srivatsa et al., 2015), act more on LVPN differentiation, maturation and guidance.

After being generated, postmitotic subcerebral projection neurons settle in layer V, where they complete their differentiation and maturation. There, they integrate within the local network and start extending a primary axon through the internal capsule, the cerebral peduncle and pyramidal tract towards the spinal cord, pontine nuclei and the superior colliculus both directly and *via* collateral projections. At a later time point and through activity-dependent processes, unnecessary connections are eliminated in a process called pruning, which is ultimately leading to S1 and M1 LVPNs maintaining projections to caudal pontine nuclei and spinal cord, whereas visual cortex LVPNs project towards rostral pontine nuclei and superior colliculus (reviewed in Oswald et al., 2013).

LVPNs are characterized by a triangular shaped soma and two main dendritic domains: one, the basal domain, composed of primary neurons arising from the base of the soma, branch and expand within layer V, and an apical domain, mainly composed of a single apical dendrite, which then produce several secondary oblique dendrites close to the soma, and a greatly articulated terminal apical tuft innervating layer I (reviewed in Ramaswamy and Markram, 2015). During the first week after birth, from postnatal day (P)0 to P7, the dendritic structure of LVPNs increases in size and complexity, with progressive formation of secondary and tertiary basal branches, as well as oblique dendrites.

After this initial period, the maturation process (**Fig. 8**) is subdivided into three main stages: from P7 to P14 they undergo a generalized *fast growth phase* followed by, from P14 to P21, an *intermediate and localized growth phase* and finally, a third *slow growth phase*, starting from P21.

Fast growth phase

During this first maturation phase (**Fig. 8**), LV somata acquire a prevalently round or triangular shape while the dendrites generally undergo a substantial and rapid development. Basal dendrites grow in length and increase their radial reach, oblique ramifications increase both in terms of length and

thickness reaching almost maximal values, whereas the apical tuft dendrites start extending depicting already a wide variety of tuft shapes at this stage.

Intermediate growth phase

At this stage, the vast majority of somata have acquired their definitive triangular shape (**Fig. 8**). Meanwhile, basal dendrites continue growing in length at a comparable rate as the precedent phase, but no more branches appear, oblique dendrites reach their final state in term of numbers and length, whereas apical tufts expand in length, reaching 92% of their maximal value.

Slow growth phase

Finally, in the last step several new basal segments further increase in length, oblique dendrites terminal segments grow in thickness, whereas the intermediate and terminal segments of the apical tuft get shortened (**Fig. 8**).

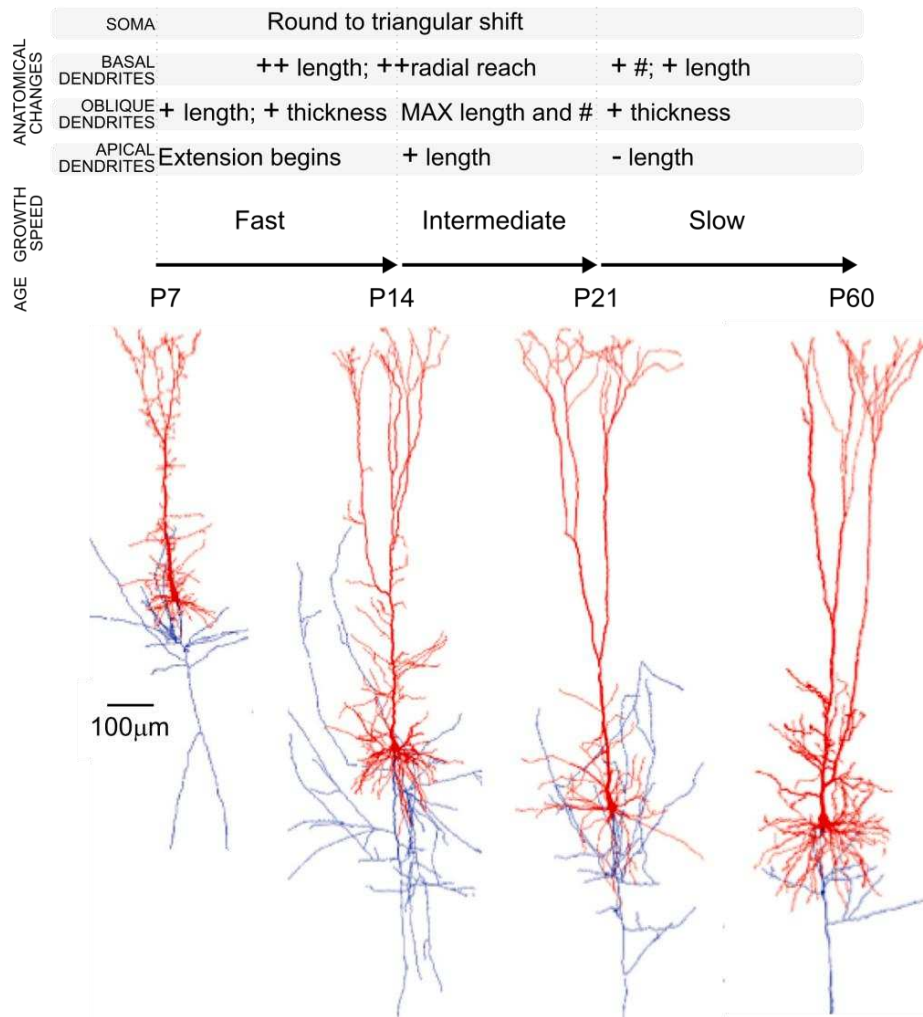


Figure 8 - Maturation of murine LVPNs. Illustration of the notable anatomical modifications occurring during LV neurons maturation and across different time points (P7, P14, P21 and adulthood, from P60 onwards). In the morphological reconstructions, axons are represented in blue, whereas dendrites are in red. (Adapted from Ramaswamy and Markram, 2015).

In summary, the rate of modification is higher in the first phase and diminishes over time; if changes are more generalized in the first phase when they affect the whole population of dendrites and segments in different domains, they become more and more restricted and localized through the process and finally, although dendrites can be both extended and thickened, these two phenomena never happen simultaneously at the same segment (reviewed in Ramaswamy and Markram, 2015).

Morphological and electrophysiological features of mature LVPNs

Once LVPNs reach maturity, they can be classified based on their targets. In fact, neurons residing in layer V can individually project to the spinal cord, the thalamus, the *zona incerta* of the subthalamus and the pontine nuclei, and sprout to the striatum and the pontine nuclei. Finally, a small population of callosal neurons is also present in layer V (Oswald et al., 2013). Although

subcerebral individual projection neurons are by far the more abundant, some of those populations have been partially neglected in the past, and to date they lack a comprehensive electrophysiological and morphological characterization. This is the case for the Corticopontine (CP) subpopulation of LVPNs, which is expected to present characteristics similar to the corticospinal (CSp) class (Suter et al., 2013) although the two subpopulations most probably have distinct features.

Based on their general morphology, three out of four of subcerebral neuron subtypes (corticospinal-corticopontine, corticothalamic and corticostriatal) are classified as thick-tufted neurons and are mainly residing in the lower part of LV (layer Vb), whereas callosal neurons are called slender-tufted neurons, for the absence of an articulated apical tuft, and are predominantly found in upper layer V (layer Va). Multiple studies have contributed in shedding light on the great variability that characterize the LVPN population (R. H. Cho et al., 2004; Gao et al., 2004; Oswald et al., 2013; Tseng et al., 1993). The result is a more precise classification of LVPNs in four different subtypes based not only on their targets, but also soma size and positioning within layer V, dendrite morphology and electrophysiological properties.

For instance, by analysing the cell shape, Oswald and colleagues (Oswald et al., 2013) observed how corticospinal-corticopontine (CSp-CP) and corticothalamic (CTh) neurons are generally the biggest ones, in terms of soma size, apical dendrite shaft thickness and overall arborization, whereas corticostriatal (CSt) and cortico-cortical callosal (CC) neurons both show very small profiles. Hence, to really discriminate between CSp and CTh and between CSt and CC neurons, they had to resolve to more subtle differences. For example, CSp-CP and CTh both show a highly developed apical tuft but differ in shape. Specifically, CSp-CPs tend to branch more and are more packed than CThs, which instead show a wider lateral extension. In contrast, in the basal domain, CTh neurons are the ones that branch most. Distinguishing CSt and CC neurons proved even harder since they share an almost identical Sholl profile; thus, the only real morphological difference turns to lie in their soma shape, with CC neurons having more rounded and less elongated somata than CSt.

Moreover, different studies have addressed the diversity of electrophysiological profiles that LVPNs exhibit (Hattox et al., 2007; Oswald et al., 2013; Ramaswamy et al., 2015). For instance, CSp-CP

neurons present the fastest and regular firing pattern among all classes, CTh neurons have a firing pattern that slightly accelerates in time, whereas CSt and CC neurons firing pattern slows down. This inversely correlates with CSt and CC neurons showing a larger hyperpolarization-activated current (called I_h), an inward current activated by hyperpolarization from the resting potential, than CSp-CP and CTh. In fact, the I_h current is considered to be a pacemaker current and mediates spike frequency adaptation, so that neurons with higher I_h values show less adaptation than neurons with lower I_h current. Furthermore, CSp-CP neurons are more depolarized than any other LV population, and the input resistance of CSp-CP and CTh neurons is found to be lower compared to CSt and CC neurons. Like intrinsic excitability properties, action potential (AP) features vary between LVPN subpopulations: CSp-CP and CTh neurons have lower AP thresholds than CSt and CC neurons as well as smaller AP half width, the latter pointing to faster APs in CSp-CP and CTh (Oswald et al., 2013).

Despite having described LVPNs as containing at least 4 different subgroups, the main subject of my thesis relies mainly on two sub-populations composing the corticospinal tract, the CSp and CP LVPNs.

Corticospinal tract development

To reach their final targets, CSp and CP neurons extend their axons that eventually cluster into a compact tract namely the corticospinal tract (CST). This structure, which arose quite recently during evolution, is only found in mammals and except for some inter-species differences, its organisation is highly conserved (reviewed in Welniarz et al., 2007). Previous studies in mice help describing the CST developmental process and point out to the existence of several critical steps, in which the axons change their direction, cross boundaries or leave the main path, to ultimately reach secondary targets. Many genes are involved in each of these steps: axon guidance factors, or molecules involved in signalling pathways, cell adhesion proteins, and also transcription factors (**Fig. 9**). In the following paragraphs, I will briefly describe these critical steps and the molecules involved in each of them.

Corticospinal neurons specification and differentiation - Fig. 9i

As previously mentioned, CSp and CP neurons are generated in the neocortex starting at E13.5, and their specification and differentiation is mediated by sequential and combinatorial expression of several transcription factors (reviewed in Greig et al., 2013; Molyneaux et al., 2007), such as the early specification factors Fezf2 (B. Chen et al., 2005; Molyneaux et al., 2005), Ctip2 (Arlotta et al., 2005; B. Chen et al., 2008), Sox5 (Lai et al., 2008), Satb2 (Alcamo et al., 2008; Britanova et al., 2008), Nr2f1 (Tomassy et al., 2010) and Bhlhb5 (Joshi et al., 2008), and the late differentiation factors Ldb1/Ldb2 and Sip1 (Leone et al., 2017; Srivatsa et al., 2015).

The pallial-subpallial boundary and internal capsule - Fig. 9ii

The process guiding CSp axons across the cortex and through the internal capsule is still under great investigation and many hypotheses have been proposed, as well as molecular players such as DRAXIN-DCC/Neurogenin1 (Shinmyo et al., 2015), Celsr3/Frizzle3 (WNT pathway) (Tissir et al., 2005; Y. Wang et al., 2002) and Pax6, by regulating Sema3A and 3C expression (Jones et al., 2002).

The telencephalic-diencephalic boundary and the cerebral peduncles - Fig. 9iii

Once CSp axons enter the internal capsule, they take a separate path from the one of thalamocortical neurons and start heading to the diencephalon, before turning laterally towards the cerebral peduncles. Among the involved molecules, one of the key players is Nkx2.1. Its loss of function produces CST misrouting as fibres fail to enter the diencephalon. Although the mechanism is far from being completely understood, the leading hypothesis is that Nkx2.1 positively regulates Slit2 in the telencephalon, which in turn act as a repulsive cue, forcing the fibres to project out of the telencephalon and towards the diencephalon (Bagri et al., 2002; Marín et al., 2002). Other factors involved in a similar process are the receptors Robo1 and 2 (Bagri et al., 2002; López-Bendito et al., 2007).

The mesencephalic-rhombencephalic boundary - Fig. 9iv

After passing through the cerebral peduncle to enter the rhombencephalon at approximately E17.5, the CST partially unbundle, and collaterals start innervating pontine nuclei. One potential

molecule that could act in this process is Sema6A (Rünker et al., 2008). Its absence leads to aberrant trajectories, with very few axons effectively reaching the rhombencephalon, but whether Sema6A is directly involved in allowing collaterals to innervate the pontine nuclei is not known. The mechanisms, through which Sema6A is acting, are not yet completely described and its known receptors, PlexinA2 and PlexinA4 seem to be only partially involved, as their loss of function is either not at all or only partially reproducing the *Sema6A KO* phenotype.

The pyramidal decussation - Fig. 9v

After crossing the pons, the CST is once again compact and run along the midline before crossing at the level of the caudal medulla, forming the pyramidal decussation. To do so, the CST drastically changes its direction, a phenomenon that is accompanied as well by a partial fibre defasciculation. Due to the high complexity of this process, it is not surprising that a high number of players are involved in it. L1 and NCAM, for example are crucial for the fibres to decussate and in their absence the CST still projects dorsally without crossing the midline (Cohen et al., 1991; Dahme et al., 1997). Sema6A and its receptors PlexinA3 and PlexinA4 are also playing a role at this stage and loss of function mouse models show altered CST projections and decussation, with different degrees of penetrance. Specifically, Sema6A KO animals presented severe CST mistargeting at the level of the pyramidal decussation, with high number of fibres failing to cross turn dorsally and instead diverging to the ventral aspect of the spinal cord. A slightly less severe phenotype was observed in PlexinA3/PlexinA4 double KO animals. In this model, roughly 50% of the fibres was still able to turn dorsally at the pyramidal decussation. And finally, in PlexinA3 and PlexinA4 simple KO animals, only a few portion of fibres failed to decussate, suggesting the two genes partially compensate for each other's loss of function (Faulkner et al., 2008; Rünker et al., 2008). Lastly, absence of Netrin1 receptors DCC and Unc5C, results in no crossing at all, or in an heterogeneous population of axon that either do not cross or aberrantly cross and project to the spinal cord (Finger et al., 2002).

Spinal cord - Fig. 9vi

And finally, once the CST has crossed the midline, it starts travelling along the spinal cord and yet other factors, such as ephrins (Coonan et al., 2001; Dottori et al., 1998; Leighton et al., 2001), molecules of the WNT signalling pathway (Y. Liu et al., 2005) and even an insulin growing factor (Özdinler et al., 2006) guide the fibres down their path and help them in finding their correct positioning.

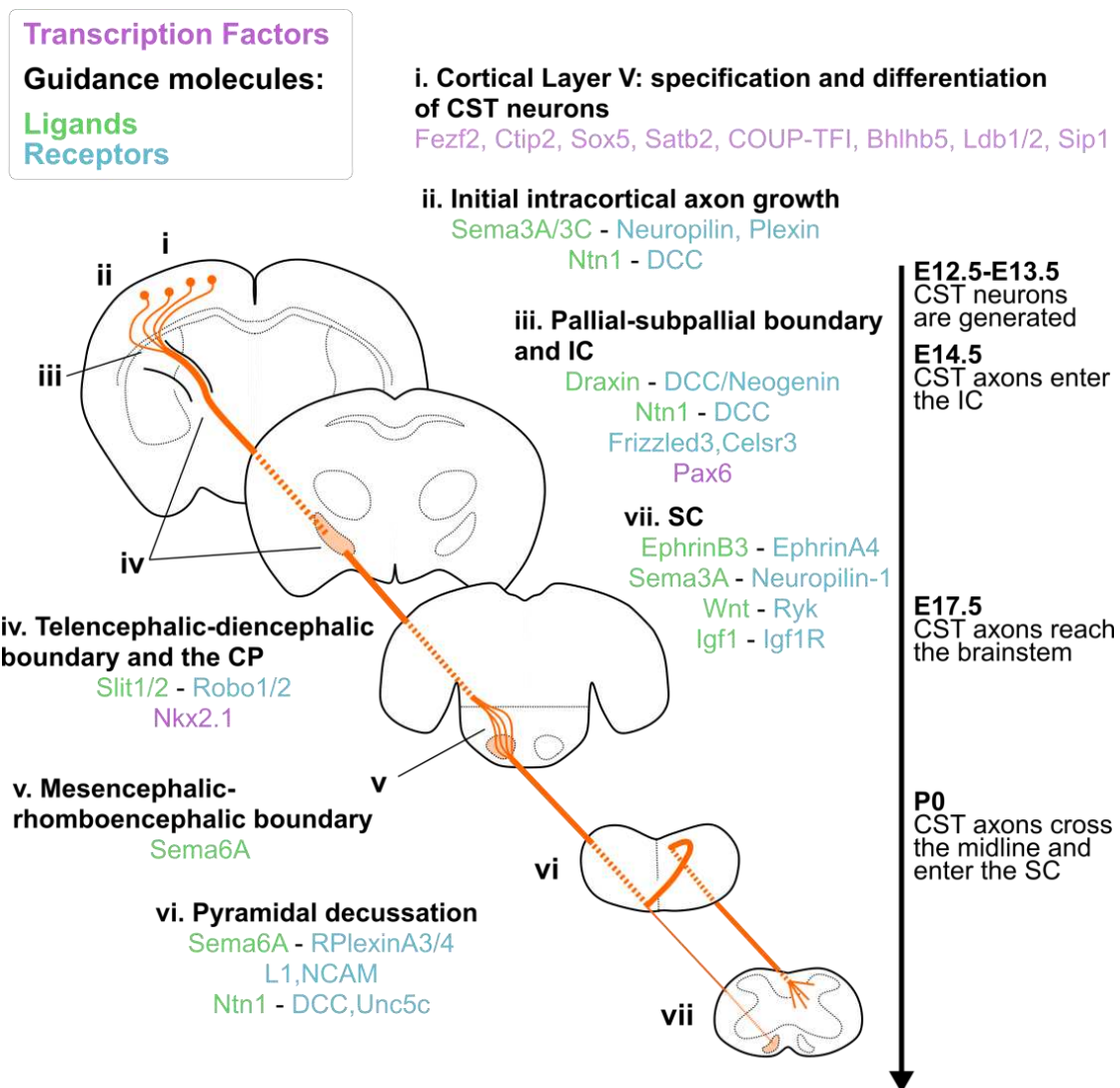


Figure 9 - Critical steps of CST development. Main events are also reported in the timescale on the right. For each step, known molecules are listed and classified based on whether they are transcription factors (purple), guidance cues (green) guidance factors' receptors (light blue).

CP: cerebral peduncle, CST: corticospinal tract, IC: internal capsule, SC: spinal cord. (Adapted from Welniarz et al., 2007).

Structural and functional characteristics of the voluntary movement circuitry

As previously anticipated, voluntary movements differ from reflexes and rhythmical movement since they are voluntarily planned before the initiation and can improve with practice. Such improvement can be achieved through both feedback and feed-forward mechanisms acting during motor planning and execution. All the needed information for these two mechanisms to work, is coded in the so called “motor plan”, an internal representation integrating various sensory information, such as spatial features as well as required forces for the coming movement (Arber et al., 2018; Brodal, 2010). Due to its high complexity, it is not surprising that the execution of voluntary movement relies on one of the most developed pathways in the CNS (**Fig. 10**). Historically, the main circuit was known as the cerebro-cerebellar pathway and uniquely cerebral and cerebellar cortices were considered as computational regions (Brodal, 2010). However, several studies in the last decades showed how other brain regions, specifically the pontine nuclei and the ventrolateral nuclei of the thalamus (VL), are not only relay stations as they were initially considered, but also retain an active role in the regulation of distinct voluntary movements (Schwarz et al., 1999). Finally, other information are coded and transmitted through parallel pathways, such as the side-loop connecting the CST to the basal ganglia (DeLong, 1972).

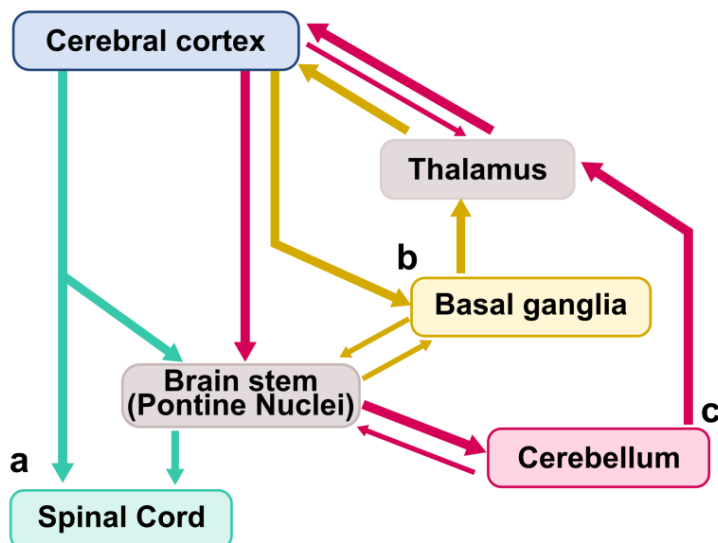


Figure 10 - Voluntary movement network. Schematic representation of principle regions and tracts involved in the regulation and execution of voluntary movements. From the cortex, fibres project *a*) directly or indirectly (through the brain stem) to the spinal cord; *b*) to the basal ganglia, which then send back information through the thalamus; *c*) to the cerebellum (via the pontine nuclei) and receives projections from the cerebellum via the ventrolateral nuclei of the thalamus.

In this third chapter I will focus on the main structures and tracts involved in the voluntary movement network. Furthermore, I will describe some of the major anomalies reported in human patients and when possible, the relative existing animal models.

Intracortical connections and descending corticospinal tract

In human, different functional areas of the neocortex are interconnected among each other to integrate various signals and ultimately control motor commands. M1 for example receives afferences from secondary motor areas as well as S1 and the secondary somatosensory areas and *vice versa*, sends back feedback information to all these regions (Kaneko et al., 1994). Interestingly, both M1 and S1 are characterized by a somatotopic representation of body parts, and the two maps show a high degree of resemblance (Schellekens et al., 2018). In both cases, limbs are represented in more medial positions, whereas regions relative to the head and the tongue are more laterally located. Furthermore, the number of neurons and hence area sizes strongly depend on the amount of precision tasks their relative body part can accomplish. For this reason, head and hands relative areas are bigger compared to regions dedicated to lower limbs and feet (**Fig. 11a**). To visually represent these proportions, the human body can be represented in a distorted way so that upper limbs and the face are proportionally bigger than lower limbs, eyes and genitals. Historically, this representation goes under the name of homunculus: a weird-looking little man with giant lips and hands and very small feet and eyes (**Fig. 11b**).

In rodents, a similar distribution can also be observed (Welker, 1971) and the relative position of body representation is maintained and fundamentally no overlap is observed, among projections from distinct body parts (**Fig. 11c**). Starting from the caudal midline, the first representations encountered are those relative to tail, trunk and hindlimb. Then, lateral to the hindlimb area, we find the forelimb representation, followed by several areas processing information relative to distinct part of the face. In rodents, the most prominent area is the barrel field, which process information from the whiskers, in line with the rodents highly relying on those structures for spatial navigation. Interestingly, forelimb representation is more extended than hindlimb, consistently with forelimb being involved in fine motor tasks, such as grasping and object manipulation. Similarly to

the homunculus, researchers came up with a stereotypical representation of body parts proportions in the cortex: the big-headed small-footed “*musunculus*”, as I propose to call it (Fig. 11d).

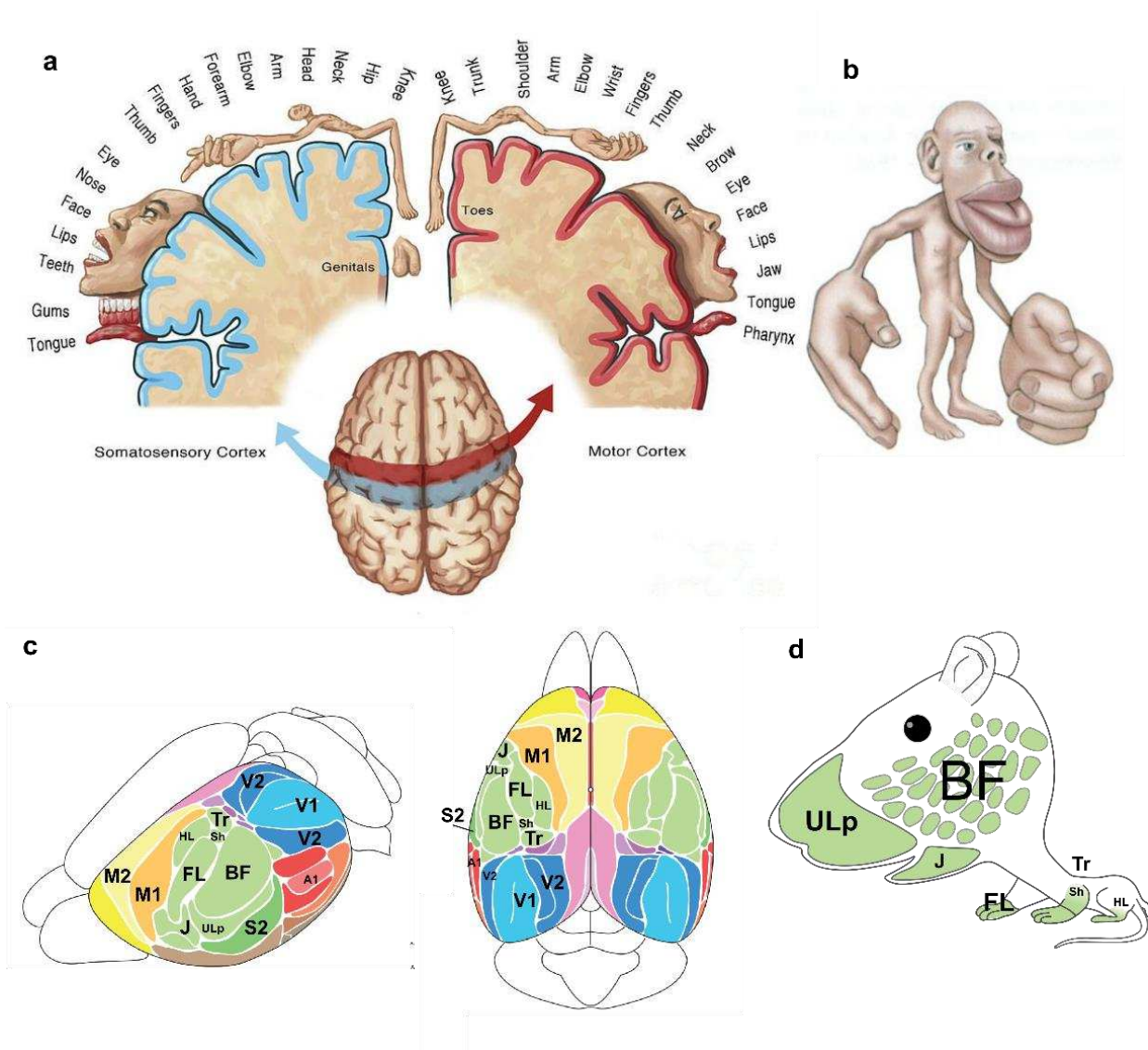


Figure 11 - Somatotopic representation of body parts in human and mouse neocortex. a) Medio-lateral distribution of body part representation in the somatosensory (left, in blue) and motor (right, red) cortex in humans. **b)** The homunculus, which represents the relative proportions of body parts as they are represented within the brain. **c)** Lateral and dorsal views of the mouse brain showing the spatial distribution of the main functional areas. Motor areas are depicted in yellow-orange, somatosensory in green, visual in blue and auditory in red. **d)** “Musunculus”, the mouse equivalent of the homunculus.

A1: primary auditory; BF: barrel field; FL: forelimb; HL: hindlimb; J: jaw; M1: primary motor; M2: secondary motor; S2: secondary somatosensory; Sh: shoulder; Tr: trunk; ULp: upper lip; V1: primary visual; V2: secondary visual. (adapted from Watson et al., 2012; Zembrzycki et al., 2013)

The main role of S1 is to process tactile information and provide a constant update of the body interaction with the surrounding environment and objects. Vice versa, the major role of M1 is to

convey motor command to the spinal cord motor neurons. Nevertheless, the boundary between M1 and S1 has been proven to be rather fluid, both anatomically and functionally. For instance, in humans as well as in other species, there is an intermediate region between M1 and S1 which is constituted by a mixed population of cells and that can simultaneously receive peripheral input as S1 and process to produce motor command output as M1 (Donoghue et al., 1982). Moreover, S1 itself can contribute directly to movements. For example, M1 and S1 are known to control opposite whisker motions. Specifically, whether activation of a specific region of M1 is regulating protraction of the whiskers, another location in S1 is regulating retraction and the two movements are independently regulated (Matyas et al., 2010). In another study, it has been demonstrated that S1 neurons modulate M1 excitability in order to achieve precision during the planning and execution of fine, skilled movements (Tamburin et al., 2002).

As already mentioned, the CST encompasses the main efferences of the neocortex and is composed by axons originating from M1 neurons and other secondary motor areas as well as S1 and S2 regions. Projections from these regions fasciculate while entering the internal capsule and through the cerebral peduncle, partially defasciculate in proximity of the pontine nuclei as well as at the level of the pyramidal decussation, in the spinal cord. Whereas M1 axons are massively involved in direct connections with spinal motor neurons, which key function is to transmit a motor command, axon arising from S1 and other regions have less direct access (**Fig. 10a**), and are thought to be more involved in the transmission of sensory information (Brodal, 2010).

Ultimately, CST fibres directly or indirectly control subcortical regions involved in fine motor movements, such as the basal ganglia and the cerebellum, via the pontine nuclei. Both connections and their role will be discussed further in the coming sections.

The side-loop to the basal ganglia

The nuclei of the basal ganglia are involved in a side loop of the descending CST, where fibres from the cortex target the different nuclei and subsequently from there axons send back feedback information through the thalamus *via* thalamo-cortical projections back to the cerebral cortex (**Fig. 10b**) (Brodal, 2010). Since different structures are connected to different regions of the cortex, the basal ganglia are composed of several anatomically and functionally distinct units. Studies show that

the information conveyed by the basal ganglia is subsequently sent to motor regions of the cortex in order to influence both direct and indirect motor control. In particular, the majority of fibres arising from the basal ganglia targets secondary motor areas, suggesting they might cover a role in motor planning, such as coordination of several individual movements to produce a more complex one, or integrate sensory information to produce an adequate motor response (Simonyan, 2019).

Nevertheless, the basal ganglia neurons are not only targeting motor regions, since they project also towards the prefrontal area (Simonyan, 2019), a region which is not directly involved in motor control, but instead covers a role in cognitive functions, such as memory and behaviour planning. Due to the existence of these connections, the basal ganglia are thought to contribute to linking motivation and emotions to motor control, as well as selection and adaptation in behaviour (change of attention from one target to another, in response to unexpected changes in the environment).

The Brainstem nuclei

Historically, the spinal cord has been described as the major centre for motor execution, but it has become evident that its sustained movement is not generated *in loco* (Arber, 2017). A proof of this concept comes from patients with complete spinal cord injury that fail to control movement of all the body parts innervated below the site of the injury, despite retaining functional local circuits.

The question on where exactly action commands originate in the brain led to the discovery of distinct regions in the brainstem that are responsible for conveying specific signals to the spinal cord motor neurons, and hence affect and control the different aspects of body part movements. The ventral part of the medullary reticular nuclei (MdV), the parvocellular reticular nuclei (PCRt) and the spinal trigeminal nuclei (SpV) in the caudal brainstem seem to specifically connect and regulate the activity of forelimb motor neurons (Esposito et al., 2014). Differently, the vestibular nuclei (Ve) and the spinal vestibular nuclei (SpVe) connect monosynaptically to hindlimb motor neurons (Esposito et al., 2014). Finally, other complexes, such as the magnocellular reticular (Mc), the pontine (PN) and the gigantocellular reticular nuclei (Gi) show indiscriminate connectivity with both populations (reviewed in Arber, 2017). Notably, these nuclei appear to be responsible for controlling only one specific aspect of the final movement. For example, the MdV is responsible for regulating fine motor forelimb execution (Esposito et al., 2014), while the Ve coordinates posture and balance (Basaldella

et al., 2015). To date, a specific function has yet to be discovered for many other brainstem formations, whereas the pontine nuclei, which receive projections from several cortical areas, have been recognized to process different kind of information and to cover several different functions. For their motor-related functions, the PN are an important integration and codification centre for motor and sensory information originating from the cortex and directed to the cerebellum. To better understand the role of the PN in motor command and execution, I will briefly introduce in the next chapter the cerebellum histological organization and functions, prior to focus on the PN and its functions.

Cerebral and Cerebellar cortices: differences in cytoarchitecture and topographic representation

To fully appreciate the central role of the PN in the cortico-cerebellar path, it is worth spending some time in comparing the organization of body parts information in the cerebral and the cerebellar cortex as well as their dissimilarities in terms of cellular organization. Differently from the cerebral cortex, the cerebellar cortex is organized in three layers; in the outer layer only sparse cells are present, whereas the majority of the volume is occupied by dendrites, the middle layer is composed by a monolayer of Purkinje cells and finally the most internal granular layer is composed by a huge population of granule cells. Granule cells project through the Purkinje layer, and to the more external layer, where they contact Purkinje cells dendrites (Brodal, 2010) (**Fig. 12**).

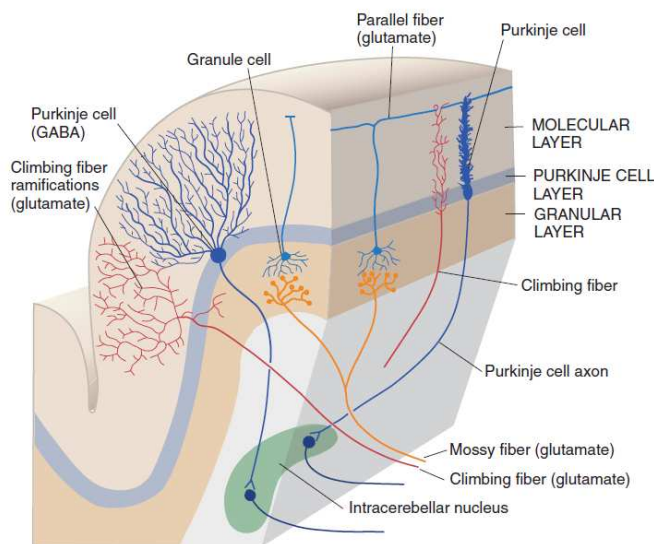


Figure 12 - Cytoarchitecture of the cerebellar cortex. The internal granular layer contains the majority of cerebellar cells. The intermediate layer consists of a monolayer of Purkinje cells. Both cell populations project into the external molecular layer. Granule and Purkinje cells also receive afferences from the pontine mossy fibres and climbing fibres of the inferior olivary nucleus respectively (Brodal, 2010).

This organization is homogeneous throughout all the cerebellar cortex, thus the only way to distinguish distinct areas can be done in

accordance with their function and connectivity. The most ventral as well as most primitive part of the cerebellum, for example, is named vestibulocerebellum, a part receiving afferences from vestibular nuclei. The middle most part of the cerebellum, the spinocerebellum, receives afferences from the spinal cord, whereas the rest of the hemispheres compose the cerebrocerebellum, and receive inputs from the cerebral cortex. Finally, all the three regions send back feedback outputs to the regions from which they have received afferences (Brodal, 2010).

Differently from the cerebral cortex, where both M1 and S1 areas are storing body part information following a somatotopic map, in the cerebellar the same information is scattered in discrete patches, each one being defined by sensory inputs from a specific body part and with multiple spread patches for every body part (F.Nitschke et al., 1996). This intrinsic difference in terms of spatial organization requires that cerebral and cerebellar topographic maps are aligned to allow communication between the two structures. As previously demonstrated in experiments conducted in monkeys, the stimulation of a specific body part representation in S1 or the tactile stimulation of the corresponding body part are activating very similar regions in the cerebellum (Dow, 1942). In the last decades, several studies have demonstrated that the PN are the prominent sites where this alignment takes place (Trygve B. Leergaard et al., 2006; Schwarz et al., 1999). In fact, on one side, the PN retain a somatotopic organization of body parts representation, although significantly different from the one we observe in the cerebral cortex (see below). On the other side, pontine mossy cells projects to scattered regions of the cerebellum to translate the topographic information received by the cortex (Trygve B. Leergaard et al., 2006).

The cortico-ponto-cerebellum network

Another tract involved in the voluntary movement network, is the loop connecting the cerebral neocortex to the cerebellum. The neocortex projects to the cerebellum through the PN and *vice versa* the cerebellum sends feedback signals to the neocortex through the ventrolateral (VL) nucleus of the thalamus (**Fig. 10c**). In humans, up to 90% of the neocortical layer V projections are estimated to target the PN, a percentage that is even higher in rodents, where almost the whole LVPNs population is projecting towards these structures. Similarly, up to 90% of pontine mossy cells are sending their axons to the cerebellum. Once the information reaches the cerebellum, it is further

elaborated and a feedback output is sent back to the neocortex, through the VL (Schwarz et al., 1999).

To better understand the connectivity involving the PN, it is important to introduce how they are generated during embryogenesis.

Cell specification

The PN are the largest of the precerebellar nuclei, a neuronal assembly within the hindbrain that provides input to the cerebellum. Cells that populate the PN originate in the rhombic lip and then tangentially migrate to reach their final position (**Fig. 13**). Overall, the process takes place between E12.5 and E18.5 (Hatanaka et al., 2016; Okada et al., 2007). Pontine cells derive from a population of progenitor cells located in a neuroepithelial domain spanning the rhombomere 6 (r6) and the pseudorhombomere 8 (ps8) of the rhombic lip (**Fig. 13a**). This domain is characterized by the expression of several different genes such as *Hoxa5*, *WNT1*, *Olig3*, *Pax6* and *Atoh1*, which have been shown to be actively involved in the process (revised in Kratochwil et al., 2017).

Cell migration

After pontine cells are generated, they migrate from the rhombic lip to their final destination, following a trajectory that can be split into three segments: during phase I, neurons leave r6-pr8 and migrate ventrally; they then switch to a rostrally oriented trajectory during phase II, while trespassing r5-r4 and finally, during phase III, they enter r3-r2, where they turn again ventrally, towards the midline (**Fig. 13a-b**) (Geisen et al., 2008). Several factors, including guidance molecules, transcriptional and post-transcriptional regulators have been found to influence all or distinct phases of pontine cell migration. Among others, the facial nucleus produced *Slit1* and *Slit2*, which act as repulsive cues for ventrally migrating neurons (**Fig. 13a**) expressing *Robo1* and *Robo2* receptors and which start migrating rostrally (phase I to phase II transition) (Di Meglio et al., 2008; Geisen et al., 2008). Once they overcome the *Slits* expression site, migrating pontine cells start again migrating ventrally and towards the midline, attracted by *Netrin1* (**Fig. 13a**). The balance between *Netrin1* receptor-mediated attraction (such as *DCC* and *Rig1/Robo3*) and those mediating repulsion

(i.e. *Unc5b*) ensure that the target is restricted to the correct area (Kim et al., 2011; Marillat et al., 2004; Zelina et al., 2014).

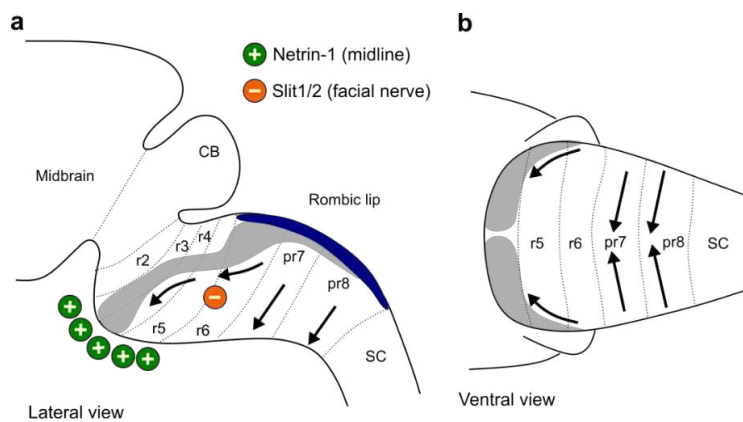


Figure 13 - Migratory stream of pontine cells.

Pontine cells originate from rhombomere (r)6–pr8 rhombic lip and take a rostroventral path and settle ventrally at the level of r3 and r4. Migratory streams are shown in grey from lateral (a) and ventral (b) views of the developmental rhombencephalon.

CB: cerebellum; pr7-8: pseudorhombomere 7 and 8, r2-6 rhombomere 2 to 6, SC spinal cord. (Adapted from Kratochwil et al., 2017).

A recent study has started to unravel the type of molecular control of migration of pontine cells. Postmitotic expression of *Hoxa5*, a Hox gene involved in spatial patterning, in a specific subset of migrating pontine neurons, is predisposing them to settle posteriorly in the pontine nuclei in a *Unc5b* dependent manner. To prove the key role of *Hoxa5* in this very specific migratory route, the authors induced the ectopic expression of the gene all along the rhombic lip and showed how cells, normally populating the PN all along the anterior-posterior axes, were accumulating posteriorly (Maheshwari et al., 2020). Moreover, the expression of *Hoxa5* in migrating pontine cells not only prompt them to follow a specific path and settle in a defined region of the pontine nuclei, but it also influences the subtype of cortical projections they will receive. This topic will be further discussed later on in the section.

Nucleogenesis

Migration is then followed by the aggregation of pontine cells and the formation of the nuclei. This process in mice occurs between E14.5, when the first neurons arrive, and E18.5. Early-born early-arriving neurons shift from tangential to radial migration, as soon as they reach the ventral PN and start migrating dorsally. Conversely, late-born late-arriving neurons do not have the capacity to migrate radially, and instead accumulate in more ventral positions. In addition to the dorso-ventral growth, PN also develop along the medio-lateral and rostro-caudal axes. For instance, a subset of

both early-born and late-born pontine cells acquire the ability to migrate laterally, finally settling in more distal positions. Migration along the rostro-caudal axes is rather infrequent and mostly involve early-born neurons (Shinohara et al., 2013).

Almost simultaneously, pontine neurons extend their axons toward the cerebellum. At present, few studies investigated the molecular players involved in the process and thus, very few of them are known. For instance, Neph2 is responsible to orchestrate cell migration within the nuclei and its loss of function cause the neurons to accumulate at the ventral midline, whereas other genes, like Barhl1 and Mbh2 for example, seem to be important for cell survival (S. Li et al., 2004)

Corticopontine connectivity and function

The PN are predominantly innervated by neocortical LVPNs, but also by several subcortical inputs such as the superior and inferior colliculus, the mammillary body, the trigeminal nuclei and the dorsal column nuclei. As for their targets, pontine mossy cells mainly project towards the cerebellum, reason for which the nuclei are considered as the integrative centre for cortical information, prior to their delivery to the cerebellum.

Similar to thalamocortical and corticothalamic projections, also corticopontine fibres are organized in a well-defined topographic map. In fact, corticopontine projections are characterized by a precise pattern of innervation, with distinct regions of the cortex being connected to relatively segregated regions in the nuclei, with very little overlap. Hence, projections from auditory and visual cortex innervate the dorso-lateral parts of the PN, from the motor cortex rostral and medial parts and finally, neurons from the somatosensory cortex project to the caudal regions of the PN. How exactly this is established, is not yet completely understood, and the vast majority of knowledge we have so far relies on studies performed on rats. For instance, classic experiments show that corticopontine afferences reach the pontine nuclei around E20 and the first projections within them are very wide and diffuse (P0-P7). Then, during the following two/three weeks, this pattern is refined and by P18 it becomes more focused and restricted to specific regions of the nuclei (Mihailoff et al., 1984). Generally, corticopontine fibres invade the nuclei from two entry zones, forming an anterior and a posterior bundle (Trygve B. Leergaard et al., 1995). It has been also reported that different subtypes of corticopontine afferences reach the PN at different times depending on their cortical

location. Specifically, afferences from more anterior cortical regions reach the pons around E20 and then start projecting within the PN at P0-P1, whereas more caudally originating afferences reach the pons and innervate the nuclei with a two-days delay (O'Leary et al., 1988) (**Fig. 14a**).

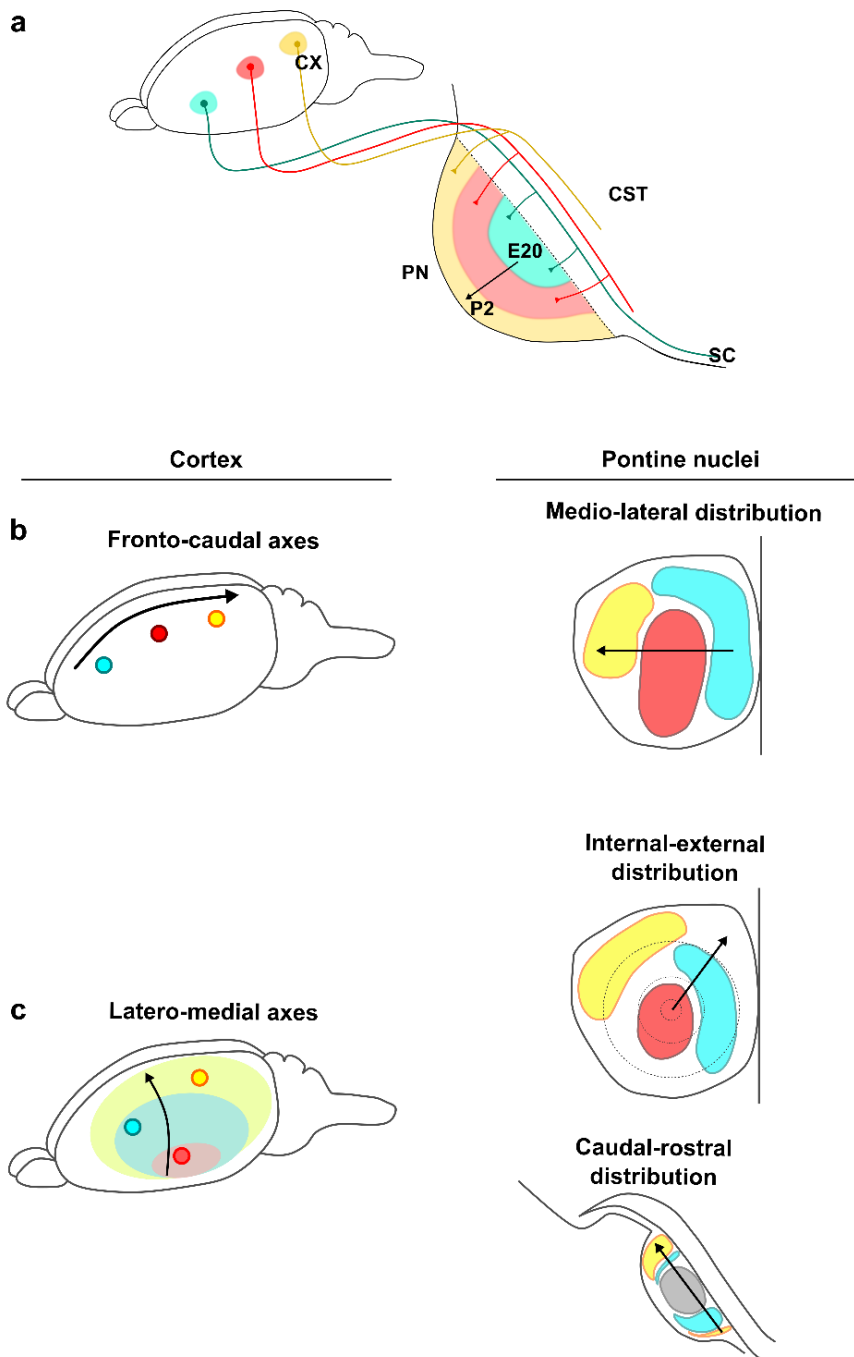


Figure 14 - Innervation patterns in the pontine nuclei. **a)** In function of their site of origin within the cortex, cortico-pontine axons reach and innervate the PN at specific timepoints. The inner core, composed by early-born pontine cells, is the site receiving projections from neurons in the antero-lateral cortex. The most occipital corticopontine neurons instead target late-born pontine neurons, which constitute the more external region of the PN. **b)** Neurons distributed along the fronto-caudal axes in the cortex project into the PN following a mediolateral pattern. **c)** Neurons distributed along the latero-medial cortical axes project into the PN in concentric regions, following an internal-external pattern. Moreover, a caudal-rostral shift is also observed

CST: corticospinal tract; CX: cortex; PN: pontine nuclei; SC: spinal cord (adapted from Leergaard et al., 1995).

Another important feature of corticopontine projections is the relationship between their cortical origin and pattern of innervation in the PN. In Leergard et al. 1995, the authors describe three main cortical axes and relative pattern distributions:

The fronto-caudal axes in the cortex are translated in a medio-lateral distribution within the PN (**Fig. 14b**).

Afferences originating from the anterolateral region of the cortex project to the central core of the PN. Fibres originating more medially tend to project in concentric layers in the PN. This pattern is called internal-external distribution (**Fig. 14c**).

Following the same anterolateral to medial axes, a shift from the caudal bundle to the rostral one can be observed in the pontine nuclei. This phenomenon is less evident than the previous two, since the two bundles are always present, but the proportion of fibres composing them is changing (**Fig. 14c**).

To date, how corticopontine projections are organized into the mature topographic map is still under debate. One hypothesis is that projections are attracted towards their specific target by the activity of locally expressed markers. An evidence in support of this scenario, is that *Hoxa5* cells from the posterior pontine nuclei attract S1 projections, specifically from the region representing the hindlimbs. When *Hoxa5* is ectopically expressed in other subsets of pontine cells which normally receive projections from other regions of the cortex, they start attracting fibres arising from S1 (Maheshwari et al., 2020).

A second hypothesis contemplates a possible involvement of the cortex, and more specifically of the somatotopic map of the cortex. It is possible to hypothesize that the spatial identity of cortical LVPNs and the mechanisms regulating this identity along the different axes of the neocortex are instrumental in forming the topographic map in the PN. To date and to our knowledge, no supporting evidences have been proposed so far.

Voluntary movement defects in human pathologies and animal models

Voluntary movement control relies on the perfect implementation of several distinct regions and tracts, each carrying a specific function. Hence, any damage or malformation at any step of the

network may cause different impairments in motor tasks execution. The origins of these defects can either be traumatic events that lead to network interruption, developmental defects or degenerative diseases. If the traumatic events are a key source of information to dissect the network in its basic components to understand the specific functions of each centre and tract, the study of developmental defects have greatly helped in deciphering the mechanisms underlying network ontogenesis.

Focusing on the CST, developmental defects can be broadly classified into two different categories: hypoplasia and aplasia on one end, and projection defects on the other end. In the first case, CST development can be impaired by defective neurulation, leading to complete agenesis of the tract in anencephalic patients and partial agenesis in holoprosencephalic patients (Chow et al., 1985; Marcorelles et al., 2010; Ten Donkelaar et al., 2004). Other common causes might be attributed to defects in neural progenitor proliferation resulting in microcephaly, or neuronal migration, resulting in lissencephaly (Roessmann et al., 1985; Ten Donkelaar et al., 2004; R. S. Williams et al., 1984). Finally, reduction in the CST volume can also be attributed to axon guidance defects. Moreover, aberrances in axon guidance can also cause a plethora of abnormalities affecting CST projection toward subcerebral targets and, ultimately, to the spinal cord. Generally, those defects affect specifically CST lateralization and are mainly caused by altered expression of axon guidance cues expressed at the midline, the level of the pyramidal decussation or the spinal cord, as well as defects in the expression of cue receptors within CST neurons. Some examples are the Kallmann and the Klippel-Feil syndromes. In the past decades, several patients have shown defective or absent pyramidal decussation (Farmer et al., 1990; Gunderson et al., 1968; Koenigkam-Santos et al., 2010; Krams et al., 1999; Mayston et al., 1997; Vale et al., 2017). Also, syndromes affecting the brainstem development, such as the HAPPS (acronym for Horizontal Gaze Palsy with Progressive Scoliosis), can affect the CST path. In these patients, mutations in the gene coding for one of the Slit receptors, ROBO3, lead to defects in the pyramidal decussation (Bosley et al., 2005; Haller et al., 2008; Jen et al., 2004).

Studies conducted in mice elucidated the role of several molecules in the process of CST development (see also Chapter 2) by highlighting critical sensitive steps, where CST projections might be impaired, and causing voluntary movement defects. Examples are transcription factors

which guide CST neurons maturation and specification in the cerebral cortex (i.e., *Fetzf2*, *Ctip2*, *Sox5*, *Satb2*, *Nr2f1* or *Bhlhb5*). Mutations in these genes lead to defects in CST projection and fasciculation. Loss-of-function of molecules and receptors involved in guiding the axons from the cortex into the internal capsule, such as *WNT* and *FRIZZLED3*, can cause CST agenesis (Tissir et al., 2005; Y. Wang et al., 2002). Mutations on any of the many axon guidance genes involved in the CST decussation in the brainstem (i.e. *DCC-ntn1*, *Slit1/2-Robo1/2*, *Sema6a-PlexinA4/A3* and *L1/NCAM*) can cause partial or complete absence of the pyramidal decussation (Bagri et al., 2002; Cohen et al., 1991; Dahme et al., 1997; Rünker et al., 2011; Welniarz, Morel, et al., 2017). And finally, mutations carried by genes involved in CST navigation along the spinal cord (i.e. *EphrinA4/A3*) can cause the fibres to aberrantly re-cross the midline (Coonan et al., 2001; Dottori et al., 1998; Paixão et al., 2013).

Overview on behavioural tests to study dexterity in mice

The CST is responsible to convey motor commands to the spinal cord and to motor neurons and specifically it acts on fine motor control of distal extremities. Most of the information on the CST functional role comes from classical studies conducted in monkeys after CST dissection (Lemon et al., 2012). In more recent years, many tests have been performed using mice as experimental models, and several different behavioural tasks have been used to highlight particular aspects of voluntary movements execution. The *single pellet skilled reaching test* for example, in which a food pellet can be reached only through a small fissure *via* the paws and not the snout (Farr et al., 2002), as well as the *tape removing test*, where a small piece of adhesive tape is applied to one of the mouse paws (Bouet et al., 2009; Starkey et al., 2005), are used to measure mouse dexterity and speed in performing fine unilateral movements and complete the task (grasp the food and remove the adhesive tape, respectively). Their ability is impaired if damage occurs at the level of the cortex, CST or brainstem. Another test evaluating handling skills called the *capellini handling task*, in which the mouse is supplied with a small piece of a capellini pasta that needs to be synchronously moved to be eaten (Tennant et al., 2010), is used to specifically assess bilateral movement execution. Furthermore, several tests have been developed to more precisely evaluate CST lateralization defects. For instance, the *obstacle avoidance test*, consisting in a small treadmill supplied with fixed obstacles with different shapes and height (Asante et al., 2010). How the animal is moving to avoid these obstacles is based on its ability to read and adapt to the environment. And finally, the

exploratory reaching task, where the mouse is placed inside a glass cylinder (Schallert et al., 2000; Starkey et al., 2005) and its movements against the wall (classified as asymmetric movements) are carefully analysed. If CST lateralization in the spinal cord is affected, then the mouse is more likely to perform symmetric movements.

To conclude, despite some structural differences between humans and mice, the CST retains a high degree of similarity in terms of organization, especially at the level of the pyramidal decussation, function (in both species it mediates voluntary movement regulation and execution) and finally, at the molecular level during important steps of development, with the majority of axon guidance genes being conserved. This, and the fact that mice can execute several fine motor tasks, make these animals, a good experimental model to test CST functionality.

Nr2f1 deficient mice as a genetic model to study corticospinal tract development

As described in previous chapters, transcription factors acting in the cortex during development can affect generation and correct growth of the CST, ultimately affecting voluntary movement execution.

In our lab, we largely study one of these factors, namely Nr2f1 (also known as COUP-TFI), and its multiple roles in cortical arealization (reviewed in Alfano and Studer, 2013; Bertacchi et al., 2019), cell proliferation (Bertacchi et al., 2020), cell migration (Alfano et al., 2011), post-mitotic cell specification of both pyramidal neurons (Alfano et al., 2014) and interneurons (Lodato et al., 2011; Touzot et al., 2016). Since absence of Nr2f1 affects the development of the hippocampus (Flore et al., 2016; Parisot et al., 2017) and as a consequence impairs cognitive tasks, such as learning and memory, the lab also uses several tasks that have allowed to unveil cortex-dependent behavioural impairments, such as abnormal activity, anxiety and/or fine motor tasks execution (Tomassy et al., 2010 ; Contesse et al., 2019). Moreover, Nr2f1 has also been reported to act during the generation of non-neural organs including testes, ovaries, prostate, skin, kidneys, lungs, stomach pancreas and salivary glands, although at present very little is known about its functions in these regions (reviewed in Bertacchi et al., 2019).

In the next chapter, I will focus on what we know about Nr2f1 function during cortical and CST development and differentiation. Finally, I will introduce a newly emerging pathology related to NR2F1 haploinsufficiency in human patients.

Nr2f1 structure and pattern of expression

Nr2f1 was originally known as COUP-TFI, which stands for “Chicken Ovalbumin Upstream Promoter Transcription Factor 1” but it is now more commonly named Nr2f1 in mouse and NR2F1 in humans for “Nuclear Receptor Family 2 Member 1”. The origin of the COUP-TF acronym is connected to the first reported activity of this gene. In fact, it was originally known to bind the chicken ovalbumin regulatory sequence and to directly modulate its expression. Nr2f1 with its homolog Nr2f2 are members of the superfamily of steroid/thyroid hormone receptors and are considered orphan

nuclear receptors, since their physiological ligands have not been identified (reviewed in Bertacchi et al., 2019). Nr2fs protein structure resembles the one of other members of the same family, with two highly conserved domains, specifically a DNA binding domain (DBD) formed by two zinc-finger domains, and a putative ligand binding domain (LBD). Moreover, both human and mouse NR2F1/Nr2f1 and NR2F2/Nr2f2 proteins show a high degree of homology in the two conserved domains, whereas differs more in the rest of the sequence (**Fig. 15**).

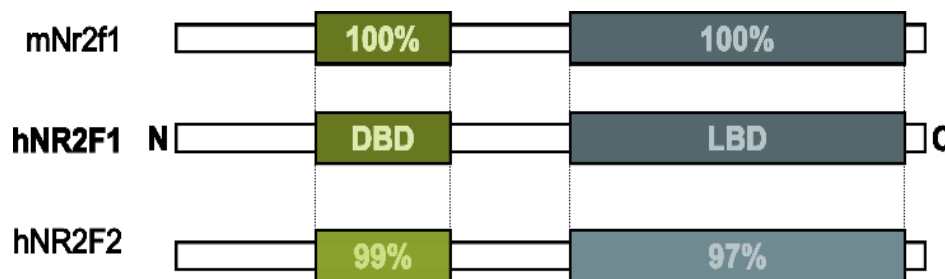


Figure 15 – NR2Fs protein structures. Simplified linear representation of human and mouse NR2F1/Nr2f1 and human NR2F2 proteins. Percentages represent the degree of homology with hNR2F1. C: carboxy-terminus DBD: DNA binding domain; LBD: ligand binding domain, N: amine-terminus. Adapted from (Bertacchi, Parisot, et al., 2019).

As a nuclear factor, Nr2f1 has been reported to act both as a positive and negative regulator of gene expression. Moreover, repression and activation can both be elicited by Nr2f1 direct binding to the regulatory sequences of target genes (**Fig. 16a-b**) (Cooney et al., 1992; Hwung et al., 1988; Montemayor et al., 2010), or by indirect mechanisms, where Nr2f1 can either act as a sponge and sequester proteins important for the transcription machinery (indirect repression **Fig. 165c**) (R. M. Evans et al., 2014) or as co-factor of other transcription factors (indirect activation, **Fig. 16d-e**) (Leng et al., 1996).

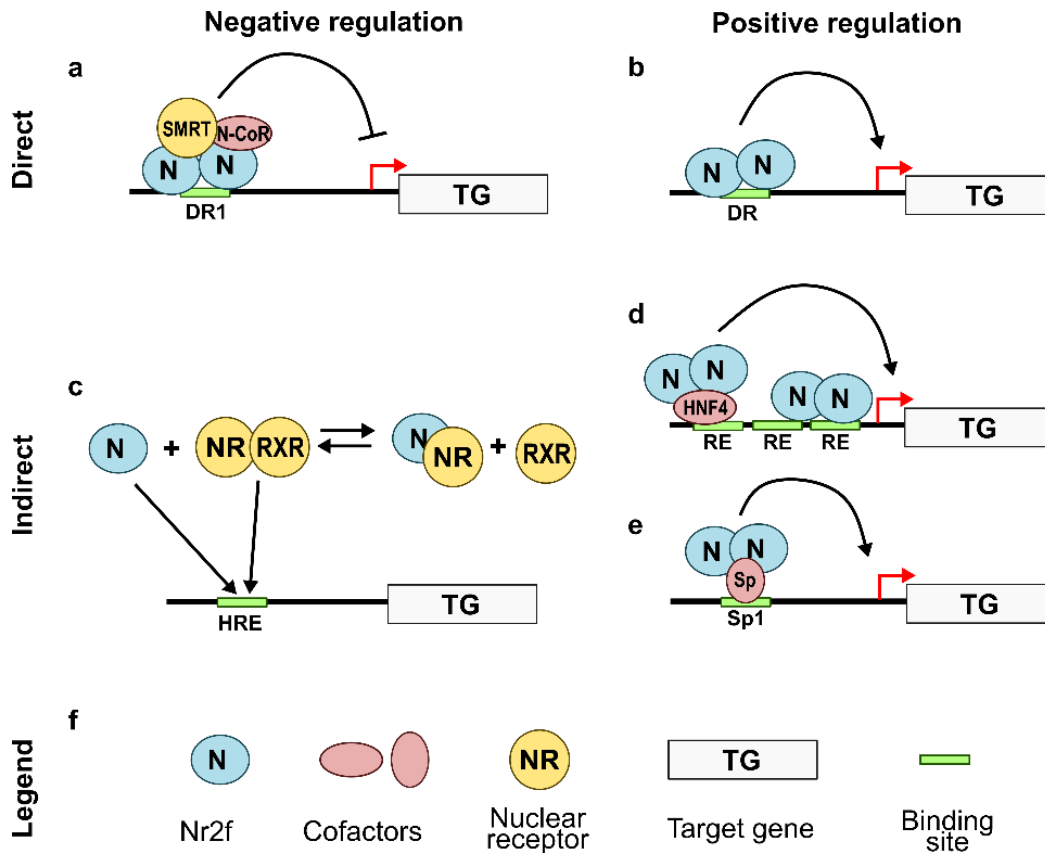


Figure *Nr2f1 molecular mechanisms of gene regulation.* *Nr2f1* can act as a direct inhibitor (a) or activator (b) by binding the regulatory sequence of their target genes. In other instances, *Nr2f1* acts indirectly, sequestering protein and blocking the transcription cascade (c) or binding to other factors to induce the target gene transcription (d-e). DR: direct repeats (GGTCA-spacer-GGTCA); HRE: hormone response element; N-CoR: nuclear receptor co-repressor; RE: response element; RXR: retinoid X receptor; SMRT: silencing mediator of retinoic acid and thyroid hormone receptor. (Adapted from Bertacchi et al., 2019).

Nr2f1 expression in the mouse neuroectoderm initiates as early as E8.5, when the anterior neural plate start closing (Armentano et al., 2006; Y. Qiu et al., 1994). Then, at later stages during development, it expands in several regions of the telencephalon, including the cerebral cortex (Armentano et al., 2006). Its expression is generally higher during gestation and decreases after birth, although it is still preserved in restricted regions (Q. Liu et al., 2000; Parisot et al., 2017; Cheng Zhou et al., 1999).

One of its major characteristics is to be expressed in gradients in various structures during development. For example, in the future neocortex, its expression is higher in caudo-lateral and lower in rostro-medial regions (Armentano et al., 2006; Liu et al., 2000; Tomassy et al., 2010; Zhou et al., 2001). This gradient is initially established in progenitors and then maintained by post-mitotic

neurons during differentiation and migration and it is particularly important to impart area identity in the neocortical map.

Role of Nr2f1 during cortical development

The particular expression gradient observed in the cortical primordium has suggested a role for Nr2f1 in area patterning. However, how exactly Nr2f1 was acting in cortical area specification has not always been clearly defined. In fact, due to its expression not only limited to the neocortex but also present in subcerebral regions, such as the thalamus, it was difficult to discriminate whether Nr2f1 was intrinsically acting in neocortical cells (following the protomap hypothesis) or in the thalamus controlling thalamic inputs (following the protocortex hypothesis) during the process of area mapping. The first experiments were conducted in a constitutive *Nr2f1 knock-out* (named *KO* or *null*) mouse line and showed no clear cortical area subdivision (C. Zhou et al., 2001) (**Fig. 17**). However, thalamocortical afferences, which are supposed to reach the cortical plate and innervate the cortical layer IV at approximately E16.5 (Moreno-Juan et al., 2017), failed to do so in *null* animals, causing the premature death of layer IV neurons (C. Zhou et al., 2001). This evidence leads to the hypothesis that the absence of defined areas could have been a consequence of the lack of thalamic inputs. To validate this hypothesis and prevent any influence from the thalamus, cortical-specific *Nr2f1 conditional KO (cKO)* mouse lines were generated (Alfano et al., 2014; Armentano et al., 2007). In these model, my host lab could demonstrate arealization impairments despite correct innervation of early thalamo-cortical axons, thus pointing to an intrinsic role of Nr2f1 in driving area identity of the developing neocortex, independent of thalamic inputs, and in accordance with the protomap model (Armentano et al., 2007).

In the first *cKO* mouse model generated in the lab, Nr2f1 was inactivated solely in the cortex by using a *Cre-recombinase* line placed under the promoter of the *Emx1* gene, a transcription factor expressed specifically in cortical radial glial cells from E9.5 (Armentano et al., 2007). In these mice, for simplicity named *Emx1-cKO*, loss of Nr2f1 function does not affect the overall cortical surface, but instead acts on the size and location of functional areas, as demonstrated by the use of several regionalized molecular markers and improper thalamo-cortical topography. For instance, area-specific markers, such as *Lmo4*, *Cad8*, and others, showed that primary somatosensory (S1), visual

(V1) and auditory (A1) areas were all caudally misplaced and their size drastically reduced (**Fig. 17**). Although shifted, this study showed that the relative area positions were maintained, even if the S1 barrel field was dramatically reduced (Armentano et al., 2007).

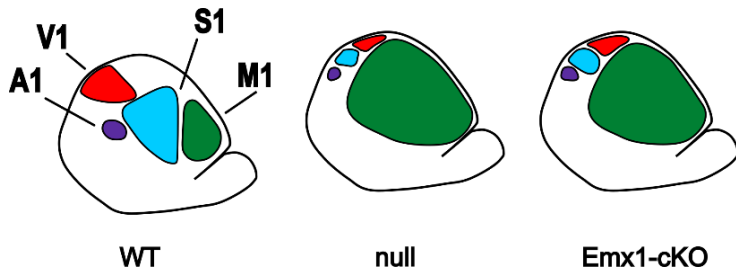


Figure 17 - Arealization defects in *Nr2f1* null and *Emx1-cKO* animals. Schematic of M1 (green), S1 and mS1 (light blue), V1 (red) and A1 (purple) areas in control (WT), full *Nr2f1* KO (null) and *Emx1-cKO* animals. M1 expands whereas S1, A1 and V1 areas are scaled down and caudally displaced. (adapted from Bertacchi et al., 2019).

Molecularly, *Nr2f1* loss-of-function influenced the expression of cortical S1 markers, such as *Rorβ* (an orphan nuclear receptor specifically expressed by LIV sensory neurons) and *MDGA1* (a cell adhesion molecule expressed by LII-III pyramidal neurons throughout the whole cortex and specifically by S1 LIV and LVI). These markers were absent in the presumptive S1 of mutant parietal cortices but retained in the miniaturized caudally-shifted areas located at the occipital pole (Armentano et al., 2007) (**Fig. 18**). On the contrary, molecular markers typical of the frontal motor cortex, such as the transcription factors *Id2*, *FOXP2* and *Igfbp4* as well as *Cadherin 8* (a cell adhesion protein) and *Crim1* (a cysteine rich protein) appeared to be expressed within the parietal presumptive S1 area (**Fig. 18**), some of them as early as E16.5 (Armentano et al., 2007; Tomassy et al., 2010). Furthermore, the transcription factor *CTIP2*, which normally is expressed at high levels in the LV and lower levels in the LVI, in line with the abundance of layer V neurons in M1, was abnormally highly expressed in LVI, in a similar fashion as normally depicted in M1 (Tomassy et al., 2010) (**Fig. 18**). Other genes, such as *Fezf2* and *Tbr1* (a transcription factor normally highly expressed in LVI and less prominently in LII and III of M1 and V1 areas), were also abnormally expressed in *Emx1-cKO* presumptive S1 (**Fig. 18**). Because of the similar expression patterns observed between normal M1 and mutant S1, the study concluded that *Nr2f1*-deficient S1 was mimicking molecular properties of M1, and this area was therefore denominated motorized S1 (mS1) (Armentano et al., 2007; Tomassy et al., 2010).

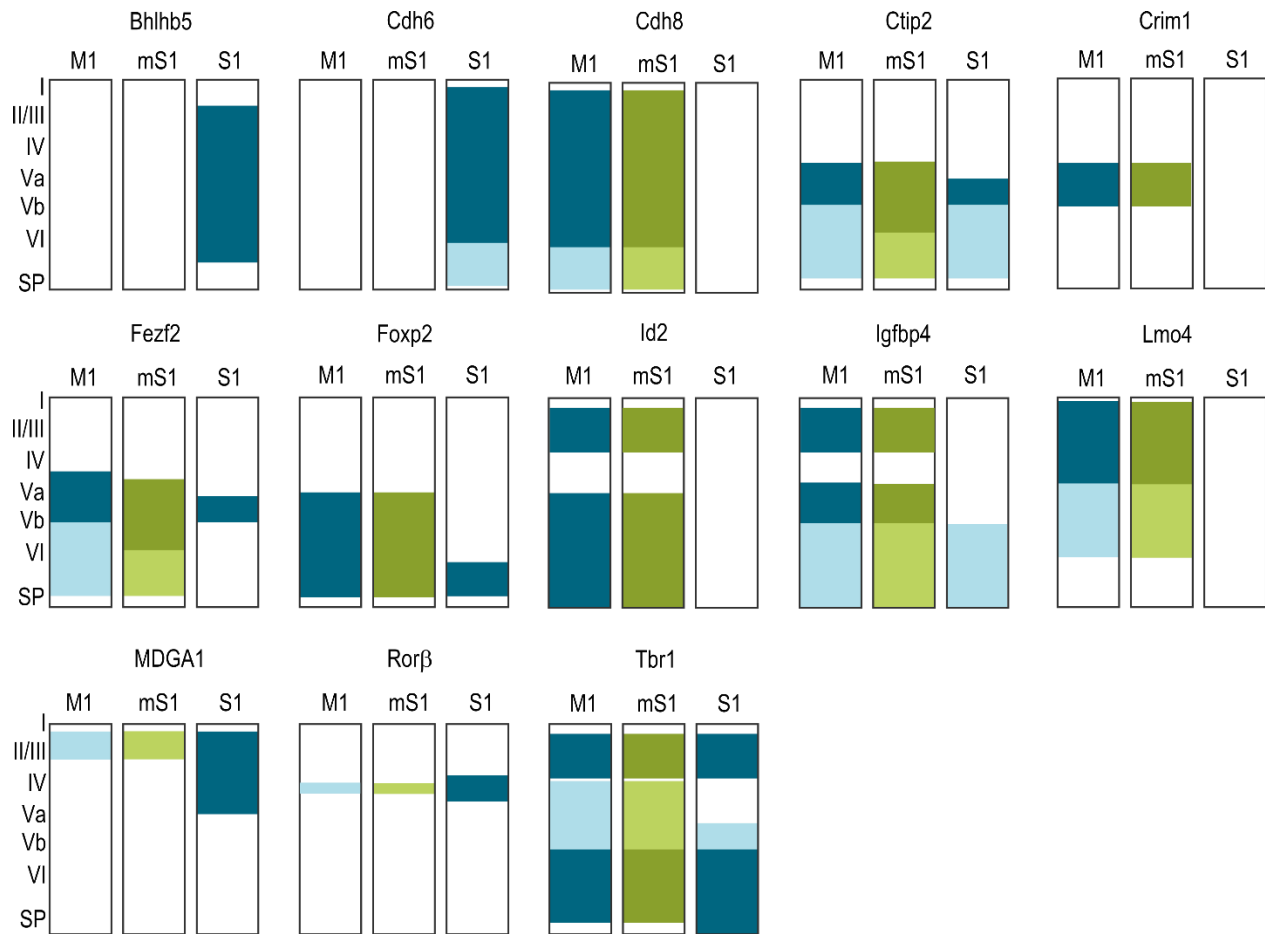


Figure 18 - Laminar specific genes in control and *Nr2f1* cKO neocortices. Schematic representation of laminar-specific expression patterns in control M1 and S1 areas compared (depicted in blue) to cKO (m)S1 (in green). Dark blue and green refer to high levels of expressions, whereas light blue and green refer to low levels of expression. SP: subplate.

Despite the several evidences supporting a sensory-to-motor conversion in *Nr2f1* deficient animals, some other observations were not fitting with a straightforward change of fate. As an example, the molecular markers FOXP2/TBR1 on one side and CIP2 on the other side, are normally expressed by two almost entirely segregated cell subpopulations in the LVI and LV, respectively. In the *Emx1-cKO* mutants instead, those two population are partially overlapping, with hybrid cells expressing either both FOXP2/CTIP2 or TBR1/CTIP2, suggesting that tangentially-organized areas and radially-developing layers are tightly linked during corticogenesis and that *Nr2f1* plays a key role in this process. In its absence, LVI corticothalamic and LV corticospinal neurons fail to properly differentiate and a large amount of neurons with mixed identity is generated (Tomassy et al., 2010).

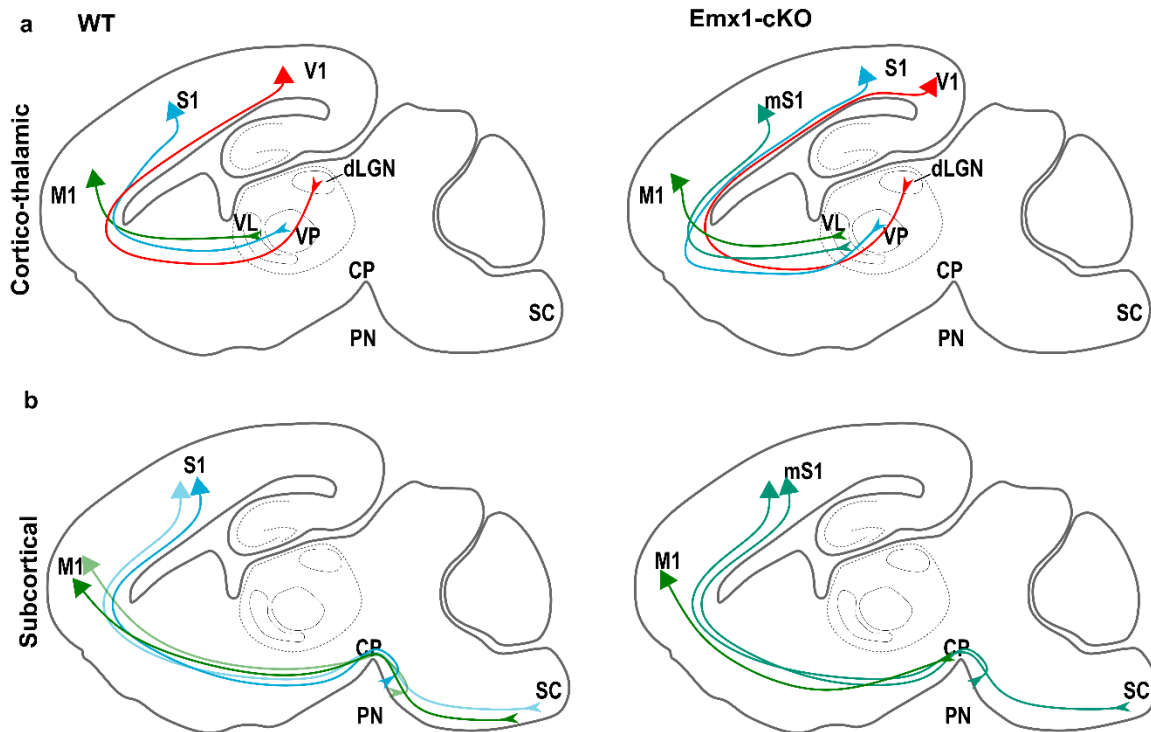
Nr2f1 impaired arealization and layering influence axon growth and voluntary movement execution

Since topography between the neocortex and the thalamus is a landmark of areal organization, studies of the host lab focused on the behaviour of afferent and efferent projections to and from the cortex in *Nr2f1* mutant animals. In *Emx1-cKO* cortices, thalamo-cortical axons reached the cortical plate at E16.5-E18.5, but were aberrantly attracted to more caudal regions where the misplaced and contracted S1 was localized (Armentano et al., 2007). Additionally, cortico-thalamic projections were affected too. In normal conditions, projections from M1 principally reach the ventrolateral (VL) nucleus, those from S1 the ventroposterior nucleus (VP) and those from V1 the dorsolateral geniculate nucleus (dLGN). On the contrary, *Emx1-cKO* projections from both M1 and mS1 projected to the VL nucleus, with caudally-displaced S1 projections targeting the dLGN and overall only very few projections reaching the VP (Armentano et al., 2007) (**Fig. 19**). Further, while subcerebral projection neurons from M1 and S1 normally follow slightly different paths, with M1 axons reaching the cerebral peduncle through the internal capsule, and S1 axons almost exclusively targeting the thalamus, in mutant brains, both populations equally projected to the cerebral peduncle and retrograde labelling from the cerebral peduncle highlighted the contribution of LV neurons and ectopic mS1 LVI neurons to the formation of subcerebral projection neurons (Armentano et al., 2007; Tomassy et al., 2010) (**Fig. 19**). More specifically, while retrograde labelling from the spinal cord showed a mislocalized and reduced contribution of cortico-spinal neurons in upper LVI, labelling from the CP, instead, depicted an increased population of corticofugal neurons (Tomassy et al., 2010). These observations led to the conclusion that loss of *Nr2f1* might have affected the cortical specification of different subtypes of subcerebral projection neurons of layer V (**Fig. 19**).

The Tomassy study also showed that this misrouting had a high impact on *Nr2f1 cKO* animal dexterity and voluntary movement execution. During the *tape removing test* for instance, mutant animals spent more time in coordinating their movements to get rid of the adhesive tape located on their paws, and during the *single pellet skilled reaching task*, mutant animals poorly coordinated their reaching and grasping fine movements and registered a lower rate of pellet recovery than their WT counterpart. Conversely, when tested for more general motor functions (such as speed,

travelled distance or latency to fall) they failed to show any defects, demonstrating that Nr2f1 loss of function specifically affects the voluntary movement network (Tomassy et al., 2010).

Figure 19 - Loss of cortical Nr2f1 influences the targeting of subcerebral projection neurons. Drawings of sagittal



sections of control (left) and *Emx1-cKO* (right) P7 brains. Pyramidal neurons are depicted in green (M1), teal (*mS1*), light blue (S1) and red (V1). **a)** In control conditions, corticothalamic projections from M1 reach the VL, from S1 the VP and from V1 the dLGN. In mutant conditions, neurons from *mS1* abnormally project towards the VL and the genuine S1 projecting to the VP is caudally shifted. **b)** In controls, subcerebral neurons from M1 mainly project to the spinal cord (SC) and a minor proportion to the pontine nuclei, whereas from S1 they mainly target the pontine nuclei with fewer projections towards the SC. In mutant animals, projections to the spinal cord are generally reduced, and mostly originate in the *mS1* whereas M1 axons stop at the CP.

CP: cerebral peduncle; dLGN: dorsal lateral geniculate nucleus; M1: primary motor area; *mS1*: motorized primary somatosensory area; PN: pontine nucleus; S1: primary somatosensory area; SC: spinal cord; V1: primary visual area; VL: ventrolateral nucleus; VP: ventroposterior nucleus.

Mitotic versus postmitotic Nr2f1 function in area specification

Among the patterning genes involved in area mapping, Nr2f1 graded expression is maintained in postmitotic neurons and loss of cortical Nr2f1 shows the strongest areal defect described so far (Grove et al., 2003; O’Leary et al., 2008). This raised the question of whether postmitotic cells could play a role in area specification during corticogenesis. Accordingly, some studies revealed that loss

of transcription factors expressed in early postmitotic cells, such as *Bhlhb5* or *Tbr1*, depicted an impairment in area formation (Bedogni et al., 2010; Joshi et al., 2008), although not as severe as in mice deficient for *Nr2f1* (Armentano et al., 2007).

Since *Nr2f1* is expressed both in progenitor cells and postmitotic neurons, the host lab tested whether postmitotic expression alone could play a role in areal specification. To this purpose, a second *conditional KO (cKO)* mouse line was generated and named *Nex-cKO* (Alfano et al., 2014). In this line, recombination of the lox sites flanking the *Nr2f1* third exon (see *Materials and Methods* for more details) was elicited by the activity of the *Cre-recombinase* placed under the promoter of the gene *Nex*, also known as *Neurod6*, a transcription factor which expression coincides with the generation of postmitotic neurons during corticogenesis (Goebbels et al., 2006).

Similarly to what observed in the *Emx1-cKO* mouse line, the analysis of layering and arealization markers showed a caudal expansion of the fronto-motor area at the expense of the somatosensory parietal area (Alfano et al., 2014; Armentano et al., 2007). Regionalized genes, such as *Bhlhb5*, *Rorb* and *Cadherin6 (Cad6)*, highly expressed in S1 but missing in motor cortex in WT cortices, were downregulated in the parietal presumptive S1 region in *Nex-cKO* animals (**Fig. 18**). On the contrary, *Lmo4* and *Cad8*, which are normally restricted to the M1 area, expanded caudally in *Nex-cKO* cortices. The layer V factor *Ctip2*, normally highly expressed in M1, but only restricted to layer Vb in S1, was radially enlarged in *Nex-cKO* cortices, suggesting that S1 has acquired motor-like properties, similar to the case of *Emx1-cKO* (**Fig. 20**). These results showed that, at least at the level of molecular markers, the lack of *Nr2f1* exclusively from postmitotic neurons was enough to impair area specification (Alfano et al., 2014).

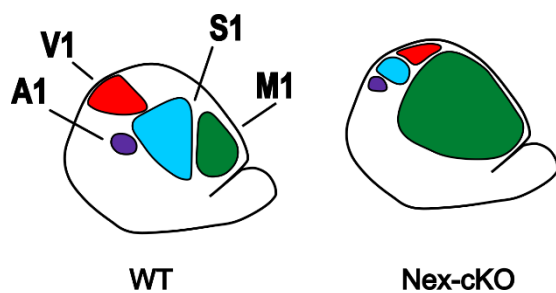


Figure 20 - Arealization defects in *Nex-cKO* animals. Schematic of M1 (green), S1 and mS1 (light blue), V1 (red) and A1 (purple) areas in control (WT) and *Nex-cKO* animals. M1 expands whereas S1, A1 and V1 areas are scaled down and caudally displaced. (adapted from Bertacchi et al., 2019).

Furthermore and similarly to what happened in *Emx1-cKO* mice, cortico-thalamic projections from occipital regions that normally reach the dLGN (visual-related nucleus), were ectopically found in the VPM nuclei (S1-related region), supporting the model of a caudal shift of S1 (Alfano et al., 2014), and maintained topography albeit the shifted areas.

To ultimately prove that *Nr2f1* expression was necessary and sufficient to impart sensory identity in postmitotic neurons, the lab deployed a *Nr2f1* overexpression mouse model. This mouse model carried a *Cre-inducible* construct expressing a human *Nr2f1* allele (*CAGGS-lox-stop-lox-hNr2f1*) (Wu et al., 2010) crossed to the *Nex-Cre* line and in a constitutive *Nr2f1 KO* background, thus allowing re-expression of *Nr2f1* only in postmitotic cells (called *iz-hNr2f1*). Due to the complete lack of *Nr2f1*, those animals were not vital after birth, and thus all the experiments were performed until P0. Interestingly, the sole postmitotic activity of *Nr2f1* was sufficient to re-establish normal patterns of expression of regionalized transcription factors like *Sp8*, *Cad8*, *Id2*, *Ctip2* and *Rorβ* in the parietal S1 cortex (**Fig. 21**). Conversely, in the fronto-motor region, the ectopic expression of postmitotic *Nr2f1* induced S1-like expression pattern of sensory proteins, such as *Cad8* and *Bhlhb5* and reduced the rostral motor marker *Lmo4* (**Fig. 21**) (Alfano et al., 2014).

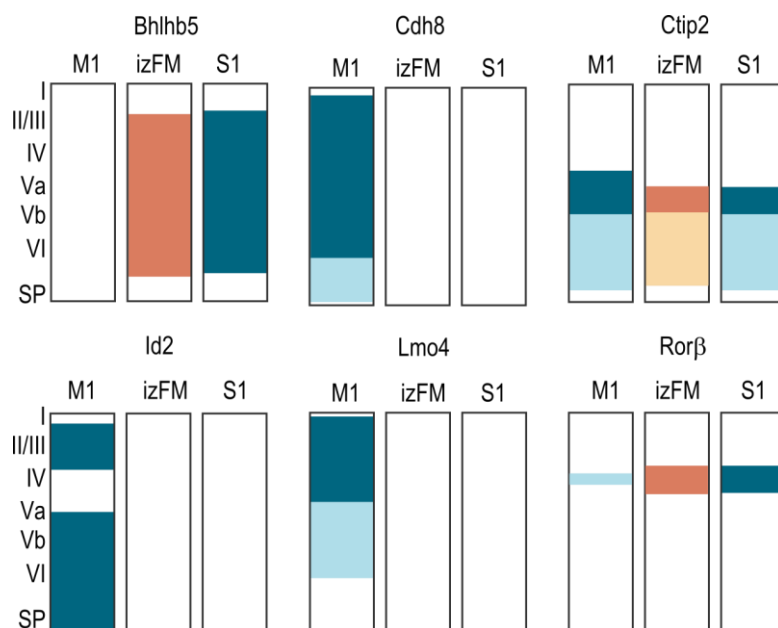


Figure 21 – Laminar specific genes in control and *iz-hNr2f1* mouse neocortex. Schematic representation of layering marker pattern of expression in control M1 and S1 areas (depicted in blue) compared to *iz-hNr2f1* neocortex (in orange). Dark blue and dark orange refer to high levels of expression, whereas light blue and light orange refer to low levels of expression.

izFM: frontomotor area in *hNr2f1* KI experiments; *SP*: subplate.

These experiments ultimately proved that *Nr2f1* impinges a sensory identity in postmitotic differentiating neurons in the developing neocortex and not in progenitors, as previously suggested (O’Leary et al., 2007, 2008), and uncovered multiple roles spanning several developmental stages.

For this reason, the two mouse lines represent interesting models to discriminate between early and late activity of Nr2f1 during corticogenesis by helping to further elucidate the complex processes of arealization, network wiring, and topography.

NR2F1 expression in humans and the Bosch-Boonstra-Schaaf Optic Atrophy Syndrome

In 2014, a new rare neurodevelopmental disease due to haploinsufficiency of *NR2F1*, was officially presented as *Bosch-Boonstra-Schaaf optic atrophy syndrome* (BBSOAS, OMIM 615722, ORPHA 401777), named after the clinicians who first described the syndrome (Bosch et al., 2014). These first patients experienced developmental delays, autistic-like disorders, epileptic seizures, hypotonia, feeding problems and visual impairments. The high penetrance of optic atrophy in patients with characteristic symptoms of neurodevelopmental diseases allowed the clinicians to propose a new syndrome and to identify the causative gene (Bosch et al., 2014; Chen et al., 2016). Today, more than 100 patients with point-mutations in the *NR2F1* gene have been identified worldwide, and most probably more will be found in the future.

The majority of point mutations or in-frame deletions are concentrated around the DBD, and patients with these mutations depict more severe clinical features than those with non-sense substitutions or frameshifts in the LBD, and even whole gene deletions (**Fig. 22**). A first interesting genotype-phenotype correlation has been described between classes of mutations and severity of the symptoms. This analysis showed that patients with missense and in-frame mutations on the DBD are overall those with the most severe diagnosis, whereas patients carrying mutations on other part of the gene, as well as patients completely lacking one allele, show overall milder symptoms (Rech et al., 2020). This phenomenon has been initially proposed after analysing transcriptional activity of different pathological variants of *NR2F1* (C. A. Chen et al., 2016). Specifically, DBD mutated variants produce a drastic reduction of the activity (measured as luciferase activity) to almost zero, whereas any other mutation led to a more modest activity reduction.

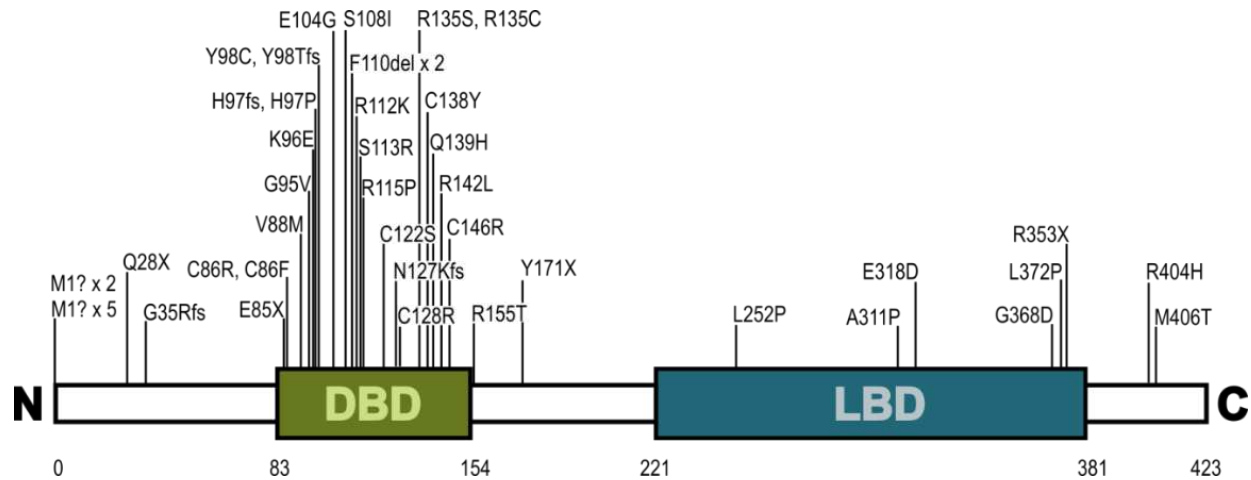


Figure 22 – NR2F1 pathologic mutations. Protein structure of NR2F1 showing some of the mutations identified in patients. Note the highest number in the DBD domain. C: carboxy-terminus; DBD: DNA binding domain; LBD: ligand binding domain; N: amine-terminus.

BBSOAS is a very complex pathology, with a huge asset of different clinical features, which are represented in the cohort with variable penetrance. The most common symptoms are developmental and speech delay, vision impairment and hypotonia (present in at least the 89% of individuals). Other common features are autistic spectrum disorders (ASD) which are present in almost 80% of individuals, cognitive/behavioural anomalies (70%) and feeding difficulties (70-84%) (Rech et al., 2020). Furthermore, some patients also present defects associated with voluntary movement regulation. In most of the cases (40%), patients with movement disorders perform repetitive behaviours (Rech et al., 2020), whereas other patients show reduced accuracy when performing visual assisted saccade and anti-saccade tests, as well as reduced accuracy and reaction time in the oculomotor and manual motor stop signal test (Bojanek et al., 2020). In the visual assisted saccade and anti-saccade tests, when requested to focus a central clue, BBSOAS patients are less accurate than controls in shifting their attention to peripheral targets -saccade- or to a mirror position -anti-saccade- when performing this task. Similarly, during stop signal test trials, where individuals were asked to either respond or not to peripheral targets appearing if a cross or STOP signal respectively were shown in the centre, BBSOAS patients were generally less accurate and slower than their control counterparts (Bojanek et al., 2020). So far, these tests have been adapted to only one patient, thus we do not know yet the prevalence of this specific set of symptoms in the cohort of patients.

Common features and dissimilarities between BBSOAS patients and available mouse models

The use of constitutive (*null*) or conditional (*cKO*) *Nr2f1* knock out mouse models have been extremely helpful in investigating molecular and physiological mechanisms that could explain the different BBSOAS symptoms in humans. For instance, feeding defects observed in some patients can depend on malformation of cranial nerves, a feature also observed in *null* animals (Yuhong Qiu et al., 1997). The corpus callosum hypoplasia observed in 24% of the BBSOAS individuals, has also been detected in both *null* and *cKO* animals (Alfano et al., 2011; Armentano et al., 2006). The complex visual phenotype characteristic of the vast majority of patients, has been thoroughly studied in a recent publication published by the host lab (Bertacchi, Gruart, et al., 2019), specifically optic nerve atrophy, optic disc malformations as well as visual impairment. Although many features of the human pathology are recapitulated by mouse models, some others are not reproduced, as for example epileptic seizures (observed in more than 20% of the patients cohort, but never in mouse models), supporting the idea that despite the available models have been very useful so far for a first broad characterization of BBSOAS symptoms, more specific models carrying human point mutations are anyhow needed for more detailed and precise analysis (Bertacchi et al., 2019).

At present, only one animal model carrying a specific homologues patient NR2F1 mutation has been generated (K. Zhang et al., 2020). In this recent publication, Zhang and colleagues selected a human point mutation (R112K) of NR2F1, found in a BBSOAS patient with autistic features, and managed to introduce the corresponding mutation into fertilized mouse eggs via CRISPR/Cas9. Resulting mutant animals were viable when the mutated allele was found in heterozygosity (*Nr2f1^{+/m}*), whereas homozygosity (*Nr2f1^{m/m}*) led to lethality. In mutant embryos, the authors reported reduced expression of dorsal telencephalic markers and simultaneously increased expression of ventral markers. This translated, in later stages of development, into a reduction of cortical excitatory pyramidal neurons and an augmentation of inhibitory interneurons in the S1 region. Curiously, only the interneuron population, and not pyramidal one, resulted affected in the M1. This imbalance between excitatory and inhibitory neurons could be recorded by altered electrophysiological activity: mEPSCs frequency was lower and mIPSCs higher than in control conditions. It has been proposed how excitatory/inhibitory imbalance might underlie behavioural deficits in several

neurodevelopmental disorders (Buxbaum et al., 2002; Cossette et al., 2002; Fatemi et al., 2009; Robertson et al., 2015), which prompted the authors to test those animals for social and anxiety behaviours. In a three-chamber test, *Nr2f1^{+/-m}* animals preferred inanimate objects to age-matched animals and familiar animals to novel ones, suggesting a reduced sociability compared to control animals. Moreover, *Nr2f1^{+/-m}* showed excessive self-grooming and when placed into a Y maze, they rarely chose alternating direction, and most frequently repeated the same path over and over. Both behaviours can be interpreted as readouts of repetitive movements. Finally, several anxiety tests (dark-light emergency, elevated plus maze and open field) pointed up to increased anxious behaviours in *Nr2f1^{+/-m}* when compared to control animals. All these evidences recapitulated most of the symptoms observed in the NR2F1-R112K patient, specifically ASD, intellectual disability and obsessive-compulsive behaviours.

Thanks to the availability of foetal human tissue, it is now possible to study NR2F1 expression in human tissues and compare its protein distribution with *Nr2f1* in the mouse. Characteristic *Nr2f1* mouse patterns of expressions have been lately confirmed also in human foetal brains. For instance, in the developing neocortex (gestational week GW11 and GW14), NR2F1 has been found to follow a latero-posterior to medio-anterior gradient of expression, as previously described in mice. Furthermore, both apical and basal progenitors highly express NR2F1, whereas differentiated neurons show a much lower content (Bertacchi et al., 2020).

A key structural difference between mouse and human cerebral cortex is the presence of gyra and sulci, i.e. cerebral convolutions, in the human brain. During development, the human brain hemispheres fold as they grow in size, ultimately leading to a huge increase in cortical surface, relatively to the whole brain volume. The first primary convolutions arise as early as GW9 and become more evident between GW13 and GW15.

This process greatly relies on basic developmental mechanisms, such as cell proliferation and migration, and any disruption might lead to cortical malformations, a broad and heterogeneous group of neurodevelopmental diseases (Juric-Sekhar et al., 2019). Whenever cell proliferation or survival are affected, the result is a smaller, usually smooth underdeveloped brain, a phenomenon that is called microcephaly or micro-lissencephaly (Barbelanne et al., 2014). On the other hand,

when migration is altered, it can lead to ectopic aggregation of cells and cellular heterotopia. Moreover, it has been proposed that defective migration might also lead to aberrant formation of convolutions, such as polymicrogyria, a brain malformation characterized by an increased number of defectively shaped gyra (Barkovich et al., 2012; Parrini et al., 2016; Sun et al., 2014). Generally, those defects are associated with intellectual disability, seizures and impaired oromotor skills (Jansen et al., 2005; Parrini et al., 2016). A recent study from the lab showed that six BBSOAS patients with developmental delay, speech difficulties and ASD like features, carry brain malformations and polymicrogyria-like features (Bertacchi et al., 2020). Interestingly, NR2F1 has been found to be expressed at low levels in prospective sulci and highly expressed in folded regions, where a high number of progenitors are formed, proliferate and produce an excess of neurons leading to tangential expansion. Moreover, the analysis of *Nr2f1* involvement into neuronal progenitor physiology in constitutive *Nr2f1 heterozygotes* and *null* embryos, unveiled an important role in the regulation of the transition between proliferation and differentiation, leading to longer and more abundant proliferation upon reduced *Nr2f1* expression levels. Importantly, *Nr2f1* has been proven to be a cell cycle regulator. In fact, *Nr2f1 null* animals showed an accelerated cell cycle progression (Bertacchi et al., 2020). These data suggest that *Nr2f1* role in controlling neural progenitor proliferation rate could be one of the causes of the polymicrogyria-like features observed in BBSOAS patients. Due to the limitation of using a lissencephaly model, such as the mouse, in the study of cerebral convolutions, alternative models start to be implied in the field. 3D human brain organoids, for example, can be utilized to study the involvement of specific human genes in cell proliferation and differentiation, and eventually in the formation of the first convolutions, representing a more suitable model to study human corticogenesis (Y. Li et al., 2017).

Among the various symptoms affecting BBSOAS patients, clinicians observe delayed motor development with poor motor planning and coordination, as well as stereotyped repetitive movements characteristic of autistic children. Most of the reported motor impairments can be traced back to defects of the voluntary movement network. The fronto-striatal system, for example, is responsible for the inhibition of stereotyped repetitive movements, and its impairment has been associated with repetitive movements in ASD patients (Mosconi et al., 2009). Reaction time and

movement accuracy instead, rely greatly on the activity of the cerebro-ponto-cerebellar pathway (Bojanek et al., 2020).

Regarding motor impairments and as anticipated in the previous paragraph, *Nr2f1 cKO* animals are characterized by reduced dexterity and voluntary movement execution in the context of general normal motor capabilities (apart from hyperactivity) (Tomassy, 2010; Contesse, 2019), making them a reliable mouse model for further understanding the impaired development and/or affected wiring of circuits at the origin of a voluntary movement execution. Indeed, unravelling the origin of this defect from the point of the motor and somatosensory cortex will be the focus of my thesis work (see more below).

Although *conditional cortical KO* animals are not high-fidelity models of the human pathology, they are nevertheless very useful in the moment we want to dissect the different pathological components and pinpoint the targeted cellular subtypes of the *Nr2f1* loss-of-function phenotype. In fact, human patients are characterized by congenital mutations on one allele of the gene; hence, the whole individual carries one functional copy of the gene and a mutated one (or none, depending on the specific case). In the *cKO* lines instead, the gene is removed only from the cortex and both alleles are missing. The result is a tissue-specific gene ablation that provides a strong, localized and specific phenotype, while ensuring the survival of the animal until adulthood. This is the reason why I will use in my thesis work the two cortical conditional mutants, the *Emx1-cKO* and *Nex-cKO* lines that will allow me to specifically analyse the intrinsic role of *Nr2f1* in the specification of layer V neurons involved in voluntary movements and also distinguish between its early and late functions. This will help us not only to unveil the function of cortical area patterning genes, such as *Nr2f1*, in the differentiation and maturation process of layer V neurons, but also to better elucidate the contribution of central defects in the pathogenesis of cognitive and motor impairments in human patients affected by neurodevelopmental diseases, such as BBSOAS.

Thesis main objectives

Cortical layer V pyramidal neurons are of great interest in neurobiology since they integrate inputs from many sources and distribute outputs to cortical and subcortical structures. They represent the first step of a complex circuit deputed to voluntary skilled movements. In order to contribute to our understanding of the intrinsic properties of layer V pyramidal neurons (LVPNs) in physiological and pathological conditions, my thesis work takes advantage of previous work in the host lab showing abnormal specification and laminar distribution of LVPNs in mouse mutant lines, in which *Nr2f1* is inactivated solely in the developing cortex and depict impaired execution of fine voluntary movements.

Nr2f1 is a well-studied transcriptional regulator involved in early corticogenesis, and one of the few to play a dual role in both progenitor cells and postmitotic neurons. In recent years, the characterization of a human syndrome caused by mutations in this gene enhanced the interest of the scientific and clinical community in *Nr2f1*/*NR2F1* functions within the complex picture of rare neurodevelopmental disease mechanisms. In the lab, we take advantage of region- and time-specific conditional *KO* mouse lines to help dissecting the complex pathophysiological phenotype arising from the loss of *Nr2f1* function in independent tissues and/or cell types. This will also contribute to further understanding its physiological role in the different cell types.

Our hypothesis is that *Nr2f1* plays a key role in the correct differentiation, maturation and projections of LVPNs involved in fine motor task codification and execution in rodents and humans. To this purpose, I have used several approaches to investigate the different aspects of LVPN specification and maturation, such as their morphological, molecular and structural differentiation, as well as their topographical innervation to the pontine nuclei, the first targets within the cortico-ponto-cerebellum network.

Specifically, the principal aims of my thesis work are the following:

To decipher the role of cortical *Nr2f1* in the morphological and functional shaping of LVPNs during early stages of maturation.

To study axonal projection patterns of LVPNs towards the pons and spinal cord and discriminate between mitotic and post-mitotic Nr2f1 expression in the corticospinal tract formation.

To evaluate the impact of improper cortical area mapping in the topographic projection map of the pontine nuclei known to impact on fine voluntary movement execution.

To identify and validate downstream Nr2f1 molecular targets involved in regulating the morphological, functional and connectivity traits of LVPNs.

MATERIAL AND METHODS

Animals

***Nr2f1^{flox/flox}; Emx1-Cre* mouse line**

This *conditional knock-out (cKO)* mouse line was already available in the lab and used to study several aspects of cortical patterning during development (Armentano et al., 2007) as well as behavioural consequences (Contesse et al., 2019b; Flore et al., 2016; Tomassy et al., 2010). To obtain this cortex-specific *Nr2f1 cKO* mouse line, *Nr2f1 floxed* mice were mated to the *Emx1-Cre* mouse line, known to drive site- and time-specific recombination in the dorsal pallium from embryonic developmental day (E)10.5 (Gorski et al., 2002). Mice homozygous for the *Nr2f1 flox* allele (*Nr2f1^{flox/flox}*) and heterozygous for *Emx1-Cre* are named ***Nr2f1^{flox/flox};Emx1-Cre*** or more simply ***Emx1-cKO*** throughout the whole manuscript (with the exception of the result - paper one section, in which they were named ***Nr2f1cKO***). *Nr2f1^{flox/flox}* littermates without the *Emx1-Cre* were used as controls.

***Nr2f1^{flox/flox}; Nex-Cre* mouse line**

This *cKO mouse* line was already available in the lab and used to specifically study the role of *Nr2f1* in the specification of postmitotic cortical neurons (Alfano et al., 2014). To obtain this conditional cortex-specific *Nr2f1 knock-out (cKO for conditional KO)* mouse line, *Nr2f1 floxed* mice were mated to the *NEX-Cre* mouse line, known to drive site- and time-specific recombination in early postmitotic neurons of the dorsal telencephalon, starting from approximately E11.5 (Goebbels et al., 2006). Mice homozygous for *Nr2f1 flox* (*Nr2f1^{flox/flox}*) and heterozygous for *NEX-Cre* are named ***Nr2f1^{flox/flox};NEX-Cre*** or more simply ***NEX-cKO*** throughout the whole manuscript. *Nr2f1^{flox/flox}* littermates without the *NEX-Cre* were used as controls.

***Thy1-eYFP-H* reporter mouse line**

This reporter mouse line (Porrero et al., 2010) was obtained from Jackson Labs and used as a reliable reporter line of layer V pyramidal cells from P14 onwards. *Emx1-cKO* and *NEX-cKO* animals, as well as their *Nr2f1^{flox/flox}* littermates were mated to animals carrying the *Thy1-eYFP* locus.

DNA extraction and genotyping

All the animals were subjected to ear clipping for the identification around postnatal day (P)14, one week before the weaning time. When animals were sacrificed before P14, toe clipping was performed around P5-P7 for the identification and tail biopsies were taken for the genotyping.

Resulting tissue biopsies were subsequently processed for the DNA extraction. Samples were incubated for 2-4 hours at 65°C in 500 µl of lysis buffer (50 mM Tris pH7.5, 100mM EDTA pH8, 100mM NaCl, 1% SDS implemented prior use with 0.2 µg/µl of proteinase K). For the DNA extraction, lysates were mixed with 500 µl of 2-propanol and then centrifuged for 5' at 16000 rcf. DNA pellets were then washed with 70% ethanol in H₂O, centrifuged for 2' at 16000 rcf and then air-dried. Finally, dried pellets were resuspended in 100-200 µl of deionized water.

Mice were genotyped by Polymerase Chain Reaction (PCR) and all the animals were tested for the presence of floxed, wild-type and null *Nr2f1* alleles, the Cre-recombinase and the Thy1-eYFP reporter gene. All the reactions were prepared using the GoTaq® Green Master Mix (Promega #M7423), a commercial mix containing the Taq polymerase enzyme, dNTPs and the reaction buffer in a 2x concentration. Reactions were done in a total volume of 10 µl (1:10 DNA in master mix).

Nr2f1

The resulting amplicons were 240bp for the WT allele (amplified by ARM531-Ex351 primers), 350bp for the floxed allele (amplified by ARM531-Ex351 primers) and 425bp for the null allele (amplified by ARM531-ARM402 primers) (**Table 1 and Fig 23 a-d**).

	Sequence	Annealing region	Volume
ARM 531 (10µM)	5' CTGCCTGTAGGAATCCTGTCTC 3'	Upstream the third exon	2µl
ARM 402 (10µM)	5' AAGCAATTTGGCTTCCCCTGG 3'	Third exon	1µl
Ex351 (10µM)	5' AATCCTCCTCGGTGAGA 3'	Downstream the second Lox site	1µl
H ₂ O			1µl
GoTaq® Green Master Mix 2x			5µl

Table 1 - Nr2f1 PCR reaction and primers

CRE

The resulting *Cre-recombinase* amplicon was a ~400bp-long fragment. Since the *Cre-recombinase* is an exogenous gene, we used primers against actin as an internal control. The resulting amplicon was 250bp long (**Table 2 and Fig. 23 b-d**).

	Sequence	Annealing region	Volume
Forward (10 μ M)	5'CCCGCAGAACCTGAAGATGT 3'	Cre coding sequence	1 μ l
Reverse (10 μ M)	5' TGATCCTGGCAATTTTCGGCT 3'	Cre coding sequence	1 μ l
CCRmR (10 μ M)	5' ATGTGGATGGAGAGGAGTCG 3'	Actin coding sequence	1 μ l
CCRmL (10 μ M)	5' AAACCGAGACCTTCCTGTTC 3'	Actin coding sequence	1 μ l
H ₂ O			1 μ l
GoTaq [®] Green Master Mix 2x			5 μ l

Table 2 - Cre PCR reaction and primers

Thy1-eYFP-H

The resulting *Thy1-eYFP-H* amplicon was approximately 350bp-long fragment. Since the *Thy1-eYFP-H* is an exogenous sequence, we used primers against actin as an internal control. The resulting amplicon was 250bp long (**Table 3 and Fig23c-d**).

Primer	Sequence	Annealing region	Volume
Thy1-Forward	5' TCTGAGTGGCAAAGGACCTTAGG 3'	Thy1 promoter sequence	1 μ l
eYFP-Reverse	5' CGCTGAACTTGTGGCCGTTTACG 3'	eYFP coding sequence	1 μ l
CCRmR	5' ATGTGGATGGAGAGGAGTCG 3'	Actin coding sequence	1 μ l
CCRmL	5' AAACCGAGACCTTCCTGTTC 3'	Actin coding sequence	1 μ l
H ₂ O			1 μ l
GoTaq [®] Green Master Mix 2x			5 μ l

Table 3 - Thy1-eYFP-H PCR reaction and primers

For the three reactions, we used a common PCR program (**Tab.4**).

Temperature	Duration	Number of repetitions
95°C	4'	1x
96°C (denaturation)	40''	35x
55°C (annealing)	40''	
72°C (elongation)	1'	
72°C	10'	1x

Table 4 - PCR program

All the amplifications were analysed either by gel electrophoresis, by using a 1.5% agarose gel or by Capillary electrophoresis, taking advantage of the QIAxcel Advanced Instrument (Qiagen, ID: 9001941) system (**Fig. 23**).

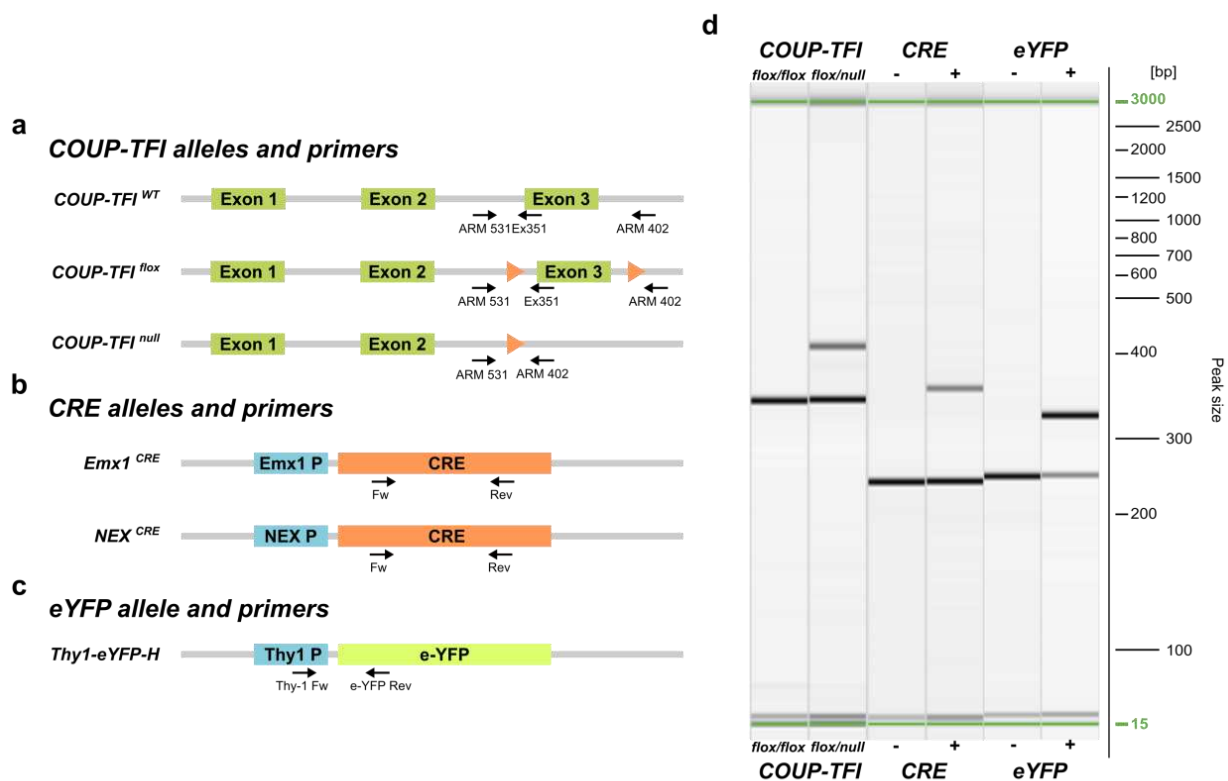


Fig.23 -Schematic of the analysed alleles and relative primers, and representative PCR. a) *Nr2f1* alleles and primers: wild-type (WT) which is amplified by the primers ARM531 and Ex351; Flox, amplified by the primers ARM531 and 351 and finally null, which is amplified by the primers ARM531 and ARM 402. **b)** CRE alleles and primers: *Emx1*-CRE which is active since the progenitor stage and the *NEX*-Cre, which is active starting from the postmitotic stage in the cortex. Both are amplified by a couple of primers, Forward (Fw) and Reverse (Rev) designed to target the coding sequence of the Cre recombinase. **c)** The presence of the *eYFP-H* allele is revealed by using A Forward primer laying on the promoter sequence

(Thy-1 Fw) and a reverse primer lying on the reporter gene sequence (eYFP Rev). **d)** Example of QIAxcel runs for the genotyping of the three gene of interest (Nr2f1 on the left, Cre in the middle and eYFP on the right).

Protein extraction and Western blot analysis of postnatal cortices.

Postnatal pups (P7-8) were sacrificed by decapitation and fresh tissues were dissected immediately after. Whole cortex samples were collected and lysed in RIPA buffer (10 mM Tris-Cl (pH 8.0), 1 mM EDTA, 1% Triton X-100, 0.1% sodium Deoxycholate, 0.1% SDS, 140 mM NaCl, 1 mM PMSF) implemented with cOmplete protease inhibitors (Roche). Protein quantity was then measured with the Pierce BCA protein assay KIT (ThermoScientific #23225). Equal amounts of proteins from tissue lysates were resolved by reducing SDS-PAGE, transferred to PolyVinylidene DiFluoride (PVDF; GE Healthcare #10600029) membrane and incubated with the indicated antibodies (**Table 6**). Immunoblots were developed using ECL Prime western blotting detection reagent (GE Healthcare # RPN2232). Signals were normalized on actin signal intensity.

Antigen	Company and Reference		Species	Working dilution	Experiment
AnkG	Antibodies Inc.	75-146	Ms	1:200	IF
CTIP2	Abcam	ab18465	Rat	1:500	IF
NeuN	Cell Signalling	24307S	Rb	1:100	IF
HCN1	Abcam	ab229340	Rb	1:100 1:1000	IF WB
b-actin	Abcam	ab8277	Rb	1:3000	WB
GFP	Abcam	ab13970	Ck	1:500	IF
GFP	Thermo Fisher	A11122	Rb	1:500	iDISCO
RFP	Abcam	Ab124754	Rb	1:500	IF
FLAG	Novusbio	NBP106712SS	Rat	1:200	IF; iDISCO
Ms IgG - AF 555	Thermo Fisher	A21422	Gt	1:500	IF
Rat IgG - AF 488	Thermo Fisher	A11006	Gt	1:500	IF
Rb IgG - AF 647	Thermo Fisher	A32733	Gt	1:500	IF
Rb IgG - AF 555	Thermo Fisher	A21428	Gt	1:100	IF
Ck IgY - AF 488	Thermo Fisher	A11039	Gt	1:500	IF
Rb IgG - HRP	Bio-Rad	1706515	Gt	1:3000	WB
Ms IgG - HRP	Bio-Rad	1721011	Gt	1:3000	WB

Table 5 - List of used antibodies.

qPCR

qPCRs on cDNA were performed using the Gotaq® qPCR Master Mix (Promega® #A6001) according to manufacturer's instructions. Samples were run on a LigthCycler II 480 (Roche) and the following primers were used:

Gene	Primers	
<i>GAPDH</i>	Fw: GTATGACTGCACTCACGGCAAA	Rev: TTCCCATTCTCGGCCTTG
<i>Cacna1A</i>	Fw: GGGCCCAAGAGATGTTCCAG	Rev: TCCACAGACTGGGAGTTGGG
<i>Cacna1B</i>	Fw: CACGCAGAGGACCCACGATG	Rev: CATCACAGCCAGTGTTCCTG
<i>Cacna1G</i>	Fw: TCAGCTGCCTGTCAACTCCC	Rev: CCCATCACCATCCACACTGG
<i>Cacna1H</i>	Fw: ACCTACACAGGCCCGGTAC	Rev: ATGGGACCTGGAAGGAGGTG
<i>Cacna2D1</i>	Fw: CAGGGAGGGCACTGATCTTC	Rev: TTGATAGTGACGGGCGAAGG
<i>Cacna2D3</i>	Fw: TTAGGTGTGGCGCTCTCCAG	Rev: GCCAAGGACACGTCAGGATG
<i>Hcn1</i>	Fw: TGCCACAGCTTTGATCCAGT	Rev: GCGCATGTCTAGCTGGTAACT
<i>Kcnab1</i>	Fw: TCCCATGGAAGAAATCGTTCCG	Rev: CTTCCATGATCTCCATCGCG
<i>Kcng3</i>	Fw: GGGAAGCCATAGAGGCAGTG	Rev: GTGGAGTTCTCTCCACACATCTG
<i>Kcnd2</i>	Fw: CAACCGCAGTCTGGATGACC	Rev: CGGTGAACCACCCTATGCAG
<i>Kcni1</i>	Fw: TTAGTGCCTTTATGGGTGATCC	Rev: GATGCCCTGACTCTCTCTCC
<i>Kcni5</i>	Fw: CTTTCCAGACCCAGGATGCC	Rev: TTGATTCAGTGGAGCGCCTG
<i>Kcnj6</i>	Fw: AACTGACGGAGAGGAATGGG	Rev: TGGGTTGGGTGAATTCTGGG
<i>Kcnk2</i>	Fw: ACGTGGCAGGTGGATCAGAC	Rev: AGTAGGCCAGCCCAACGAG
<i>Kcnmb4</i>	Fw: TTGAAAGATGAGATCGGTTCC	Rev: AAGCAGTGCAGGAGAGCAATC
<i>Kv2.1</i>	Fw: CGTCATCGCCATCTCTCATG	Rev: CAGCCCACTCTCTCACTAGCAA
<i>Gria1</i>	Fw: CTGGTGGTGGTGGACTGTG	Rev: TGTCCATGAAGCCCAGGTTG
<i>Gria2</i>	Fw: ATTTGGAATGGTATGGTTGGAG	Rev: AGGCTCATGAATGGCTTCGAG
<i>Gria3</i>	Fw: TCATTCTCACGGAGGATTCCC	Rev: CACAGCAAAGCGGAAAGCAC
<i>Gria4</i>	Fw: CCAGAGCCTCCCTGAAGACC	Rev: TGC GCGCTCTCTCTCTTTT
<i>Grik1</i>	Fw: AGTTGGTTCGCATGCTCTTCG	Rev: CGAACCTTGATGCCCAATAC
<i>Grik2</i>	Fw: CTGGTGGAGAGTGCTTTGGG	Rev: CCACACCCTTGCAACCCTG
<i>Grik3</i>	Fw: TCGCCAGATTACGCCCTTAC	Rev: GCCCATTCCAAACCAGAAGC
<i>Grik5</i>	Fw: GCCTGCGTTGGTAGAGGAC	Rev: TCTGCCTTCCGGTTGATGAG
<i>Grin1</i>	Fw: TCAGAGCACACTGTGGCTGC	Rev: ATCGGCCAAAGGGACTGAAG
<i>Grin2B</i>	Fw: GGAAGTGGGAGAGGGTGGG	Rev: CAGGACACATTGAGGCCAC
<i>Scn1a</i>	Fw: AACAAGCTTGATTCACATAACAATAAG	Rev: AGGAGGGCGGACAAGCTG
<i>NaV 1.2</i>	Fw: GGGAACGCCCATCAAAGAAG	Rev: ACGCTATCGTAGGAAGGTGG
<i>NaV 1.6</i>	Fw: AGTAACCCTCCAGAATGGTCCAA	Rev: GTCTAACCAGTTCCACGGGTCT

Table 6 – List of qPCR primers

For each reaction primers were used at 0.2 μ M using 10nl of total cDNA. Each sample was corrected to the housekeeping gene GAPDH.

Stereotaxic injections

P4-P5 pups were anesthetized for 5 minutes in ice, then immobilized using a home-made polystyrene holder. Then, the skull was opened with the use of a 25G needle, prior injection with a Hamilton syringe, equipped with a 22s needle (Hamilton, #7784-05). The viral vector (AAV9-CAG-tdTomato (MIRCen) a kind gift of the Dusart Lab) was diluted 1:50 in TE-Buffer (Qiagen, #1018499) to a final concentration of 1.75e12 vg/ml and approximately 0.5/1ml was injected unilaterally either in M1 or S1 area. Fast Green (Sigma-Aldrich, #F7252) was added to the mix to visualize the injection site. After the surgery, the pups were left recovering under an infrared lamp or a heating mat until fully awake, then put back into the cage with the mom until sacrifice.

In utero electroporation

The experimental procedure for the *in utero* electroporation (IUE) was performed according to (Saito et al., 2001) with several modifications as stated below.

Material preparation

Endofree-toxin plasmids were diluted in TE-Buffer (Qiagen, #1018499) until it reached the proper working concentration of 1 μ g/ μ l in a final volume of 20 μ l, including 1x Fast Green (Sigma-Aldrich, #F7252). For the co-electroporation of multiple plasmids, the concentration of each single plasmid has been lowered until they together reached a final concentration of maximum 2 μ g/ μ l.

Glass capillaries were generated by pulling glass tubes (Harvard-Apparatus, #30-0016), with a micropipette puller (Sutter Instrument, Model P-1000; Parameters: Heat 459, Pull 60, speed 75, Time/del 100, Pressure 200) and cut at approximately 60 μ m away from the tip. After being loaded

with 15 μ l of plasmid mix, capillaries were inserted into a metallic holder and connected to the microinjector (Eppendorf FemtoJet 5274 V2.02).

Injection parameters: injection pressure (P_i) 100-300hPA, injection duration (t_i) 0.7'', constant pressure (P_c) 7hPA.

Electroporation parameters: Without poring pulse; Transfer pulse voltage: 37, pulse length: 50 ms, pulse interval: 999 ms, number of pulses: 4, decay rate: 5%.

Procedure

After pregnancy duration of exact 13.5 days (E13.5), mothers were deeply anesthetized via Intraperitoneal (IP) injection of 10 μ l per gram body weight of a mix of Tiletamine-Zolazepam-Buprenorphine-Xylazine (or TZBX 80mg/kg). Then, the mice were shaved on the upper abdomen and cleaned with disinfectant (Pierre Fabre, #716431). Afterwards, a lateral laparotomy has been performed (**Fig. 24a**) and the uterus exposed by carefully pulling it out with ring forceps (**Fig. 24b**).

Then, plasmids were introduced into one of the two lateral ventricles via microinjection of approximately 1 μ l DNA mix (**Fig. 24c**). To allow the plasmids to enter the cells, an electroporation step was performed by placing tweezer electrodes (3 mm, Nepagene, #CUY650P3) onto the uterine wall with the plus node above the premature M1 or S1 area underneath, and applying square electric pulses via an electroporator device (Nepagene Superelectroporator, Nepa21 Typell) (**Fig. 24d**).

To finish, the uterus containing the embryos was repositioned into the original location and the incision was sewed up with sutures (Peters Surgical; 6/0 #87002F for peritoneum and 5/0 #87001F for skin) (**Fig. 24e**).

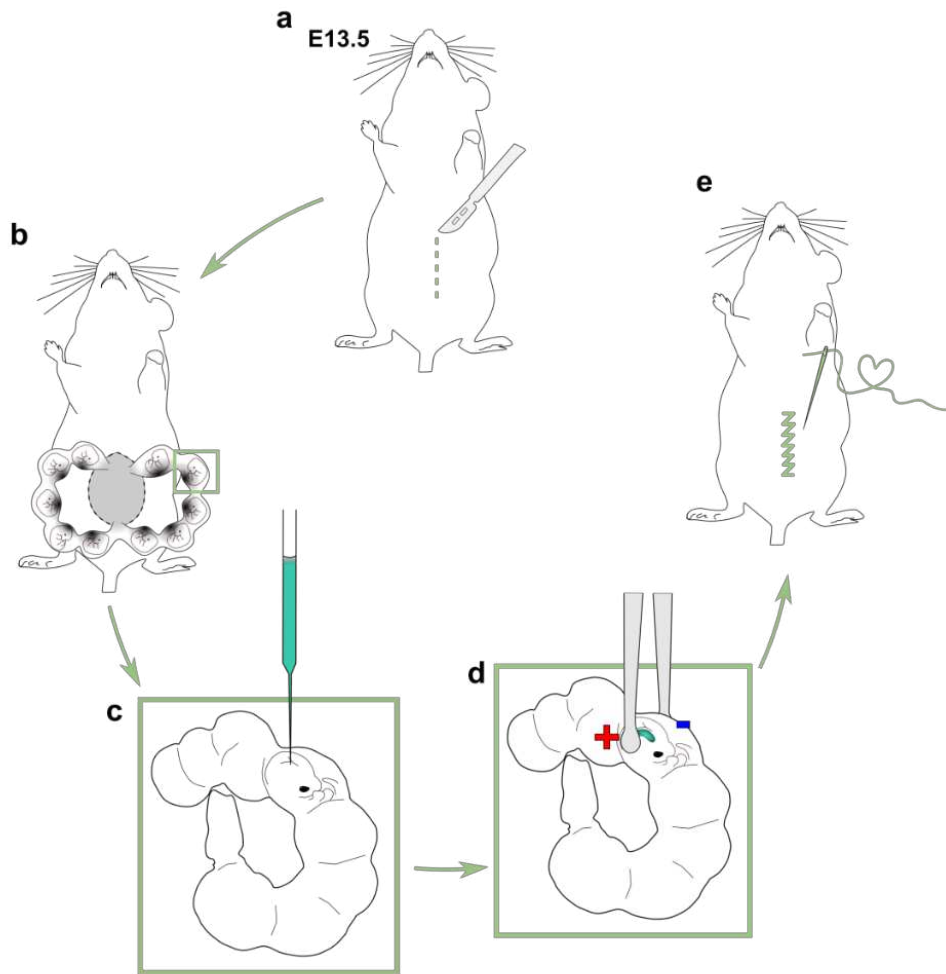


Fig.24 - In utero electroporation schematics. *a) After 13.5 days from the fertilization (E13.5) the pregnant female is anesthetized and then an abdominal laparotomy is performed. b) then, the uterus is exposed, c) the DNA mix is injected with a glass capillary in the lateral ventricle of the embryos, d) an electric current is applied with paddle electrodes and finally e) the uterus is put back in the abdomen and the surgical cut sutured.*

120µl Meloxicam (Metacam) and 200µl Gentamicin (1mg/ml, Sigma #G1272) were subcutaneously injected to prevent inflammation and reduce the post-surgery pain. Electroporated mice were then housed in solitary and in a ventilated black box for up to 24h before being finally re-introduced in the housing room where they were kept until the dissection day. Mouse lines with a B6D2 background (i.e. Nr2f1flox/flox, Emx1-cKO and NEX-cKO) were housed in a separate room to avoid stress and, one day before the expected delivery they were subcutaneously injected with a mix of 50µl Meloxicam and 50µl Buprenorphine to ease partum pain and avoid new-born elimination.

Plasmids

Several combinations of plasmids have been used for the electroporation experiments.

pCAG-mCherry

The plasmid, which is commercially available from addgene (#108685), has been used as a technical control for the electroporation, in all those experiments lacking an internal reporter gene (**Fig. 25**). The expression of the reporter gene mCherry (for monomer Cherry) is under the constitutive promoter of the chicken β -actin and the cytomegalovirus (CMV) enhancer sequence.

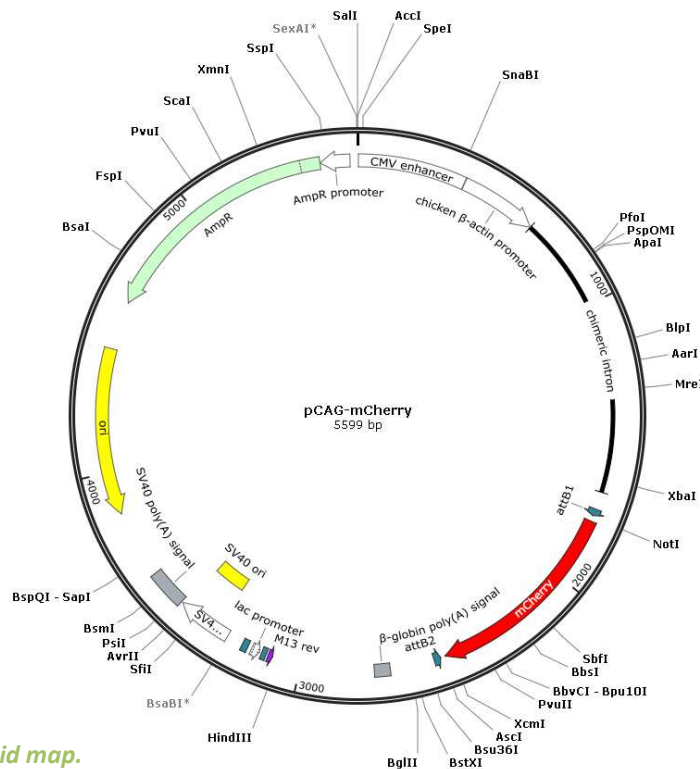


Fig.25 - pCAG-mCherry plasmid map.

Inducible pCAG-Bhlhb5-IRES-GFP

The plasmid, a kind gift from Ingo Bormuth in the Tarabykin Lab and successfully tested, was already available in the lab and is composed by a chicken β -actin promoter, a reporter mCherry protein flanked by loxP sites, the open reading frame (ORF) of the transcription factor Bhlhb5, an IRES sequence and finally the reporter gene EGFP (**Fig.26**). The expression of both Bhlhb5 and EGFP is activated only upon Cre-dependent homologous recombination of the loxP sites, which simultaneously leads to the removal of the mCherry sequence and allows establishing the correct frame for the Bhlhb5 and EGFP transcription. By injecting this plasmid into E13.5 neuronal progenitor cells of *NEX-cko* animals, we aim to restore *Bhlhb5* expression which lost upon *Nr2f1* removal (see **Additional experiments - b**).

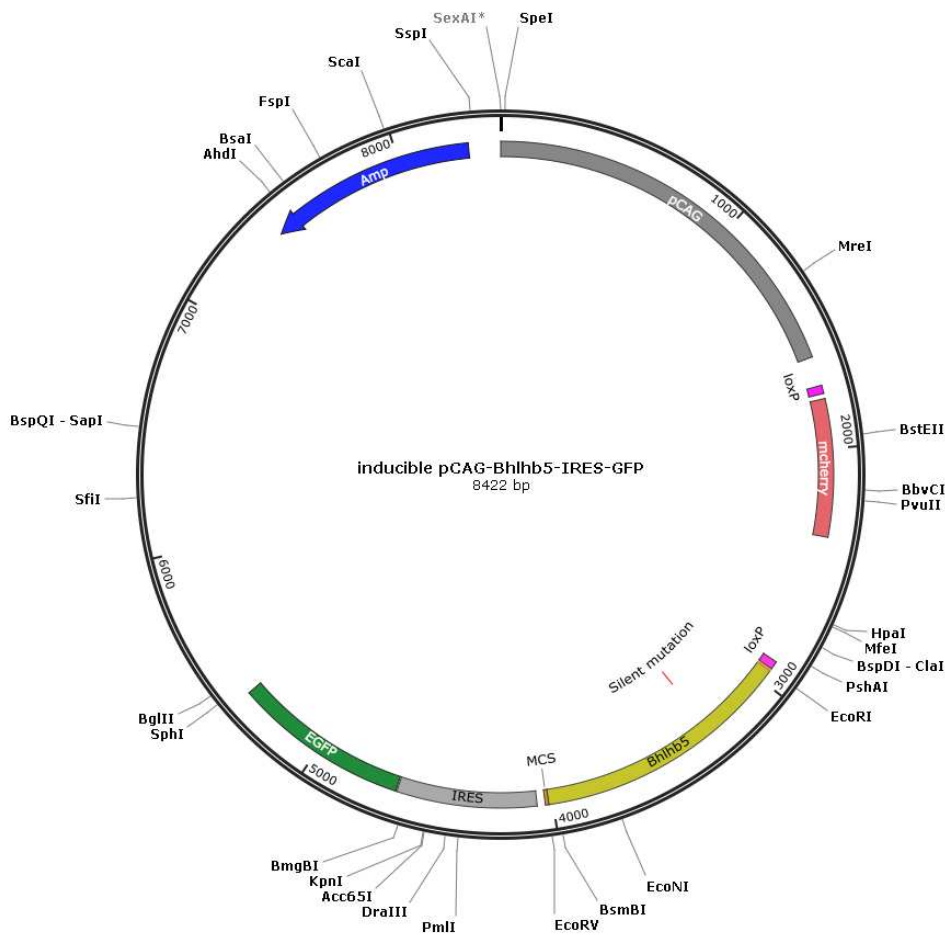


Fig.26 - Inducible pCAG-Bhlhb5-IRES-GFP plasmid map.

pCAG_smFP FLAG

This plasmid, which is commercially available from addgene (#59756), has been used to allow the visualization of long projections of layer V pyramidal neurons (**Fig.27**).

The plasmid contains the coding sequence of the so-called “spaghetti monster Fluorescent Protein (smFP)”, a GFP protein carrying a darkened chromophore, and several copies of the FLAG epitope. This engineered protein retains solubility and cell tolerance characteristic of fluorescent proteins and the presence of FLAG tags allows an efficient detection, thanks to the availability of highly reliable primary antibodies. Moreover, the elevated number of copies of these epitopes significantly reduces the amount of smFP needed (and consequently decreasing fluorescent proteins cluster formation high-doses toxicity) for an optimal labelling of thin processes, such as dendrites and axons (Viswanathan et al., 2015).

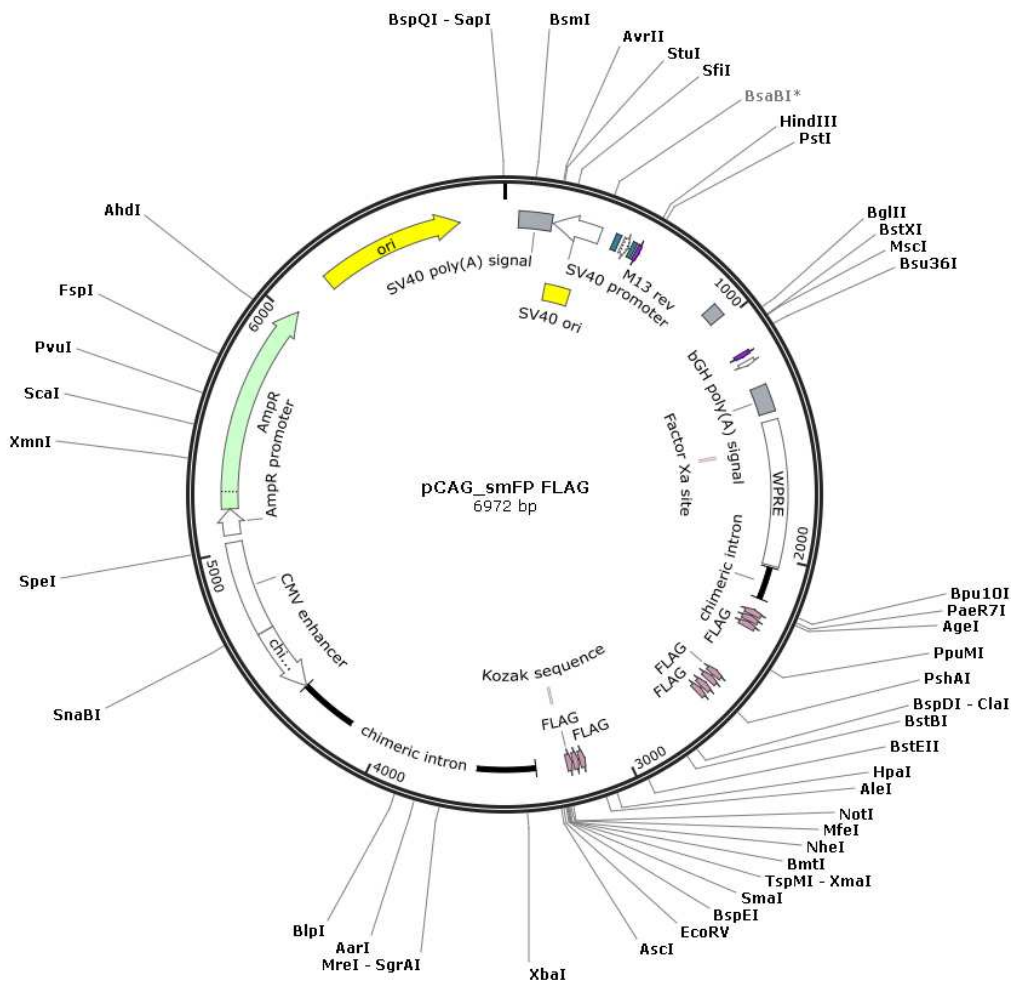


Fig.27 - pCAG_smFP TAG plasmid map.

Intracardiac perfusion and tissue dissection

At the planned developmental stage, mice underwent intracardiac perfusion of PBS for blood and hematic cells elimination, followed by 4% PFA (Sigma-Aldrich, #P6148) in PBS for tissue fixation.

Prior the perfusion, animals were anesthetized with an overdose of TZBX injected intraperitoneally. In order to expose the myocardium, the skin was first incised from the sternum to the neck, and then the diaphragm, as well as the ribs were cut and removed.

To initiate the perfusion, a butterfly needle (24G for P5-P8 animals and 21G for the adults; B.Braun # 4056370 and # 4056337 respectively) was inserted into the left valve of the heart and the opposite ventricle was cut in order to let the liquids flow out of the bloodstream.

Then, with a peristaltic pump, animals were perfused with PBS (10-15ml for P5-P8 animals, 30ml for the adults), followed by 4% PFA (10-15ml for P5-P8 animals, 30ml for the adults). For brain dissection, perfused animals were decapitated, skin and skull cut open and the brain detached and collected in PBS.

Finally, in the vast majority of experiments, brains were post-fixed in 4% PFA at 4°C for 2-4h depending on the developmental stage, then washed in PBS and stored in PBS-Azide (0.05%; Sigma-Aldrich, #S8032) at 4°C before being processed. The only exception was made for the brains used in the HCN1 immunostaining. Specifically, post-fixation step was just 30' long and after that tissues were immediately processed for the immunofluorescence as described below, to avoid degradation.

Tissue sectioning

Brains that had to be analysed by 2D imaging were then embedded in 4% Select Agar (Sigma-Aldrich, #A5054) in PBS. Therefore, 4g of Select Agar were dissolved in 100ml PBS and heated up with a microwave and then poured into a mould. As soon as the agar cooled down to 55°C, the brain has been placed in the fluid and correctly positioned. After complete solidification, the agarose block was glued to a metallic support and vibratome sectioned (Leica VT 1000S; Speed: 7, Frequency 7).

Depending on the experiment, brains were sectioned either sagittally or coronally and with a thickness of 100µm (exception made for those brains processed for the HCN1 staining, which thickness was 50µm). Sections were then preserved in PBS – Azide (0.05%) until further processing.

KCl ex vivo depolarization assay

Ctrl and Emx1-cKO P7 mice were sacrificed by decapitation and brains dissected into ice-cold aCSF saturated with 95% O₂ and 5% CO₂. 300µm-thick slices were produced by vibratome sectioning and then immersed into aCSF, kept at room temperature and constantly saturated with 95% O₂ and 5% CO₂. After 15 minutes of acclimatization, slices from both genotypes were split into two groups: an untreated group (called - **KCl**) and an experimental group (called + **KCl**). KCl was added to the aCSF of the experimental group by diluting a convenient amount of a 1M master solution of KCl diluted in aCSF in order to obtain a final concentration of 7mM, whereas control slices were kept in normal aCSF. After an incubation time of 6 hours (M. D. Evans et al., 2015), slices were washed for 15 minutes in aCSF and then processed for immunofluorescence (IF), as described below (**Table 7**).

Solution	Component	Concentration	Volume for 1L
aCSF	NaCl	124 mM	7.25 g
	KCl	3 mM	223.65 mg
	NaH ₂ PO ₄	1.25 mM	177.45 mg
	NaHCO ₃	26 mM	2.18 g
	Glucose	10 Mm	1.80 g
	CaCl ₂	2 mM	294.04 mg
	MgCl ₂	1 mM	203 mg
	PBS		Q.S.
aCSF high KCl	NaCl	124 mM	7.25 g
	KCl	7 mM	521.85 mg
	NaH ₂ PO ₄	1.25 mM	177.45 mg
	NaHCO ₃	26 mM	2.18 g
	Glucose	10 Mm	1.80 g
	CaCl ₂	2 mM	294.04 mg
	MgCl ₂	1 mM	203 mg
	PBS		Q.S.

Table 7 - List of the home-made solutions used in the KCl acute depolarization assay

2D immunofluorescence

For adult samples, floating slices were incubated in blocking buffer (**Table 8**) Over Night (ON) at 4°C, gently rocking, followed by a 3-day long incubation with the primary antibodies, diluted in blocking buffer to reach their working concentration. After a series of washes in PBS to remove the excess of antibodies, the sections were then incubated with the secondary antibodies (in concentration 1:500) and HOECHST (1:10k), ON at 4°C. Finally, sections were washed 3-5 times at room temperature and then mounted on SUPERFROST microscope slides (Thermo scientific #J1800AMNZ), let dry for approximately 30' before closing using Mowiol mounting media (**Table 8 8**) and glass coverslips (DiaPath #061061).

For pups, antibodies incubation times were reduced to one ON at 4°C for the primary antibodies and 1h at room temperature (RT) for the secondary antibodies. The only exception was made for the brains used in the HCN1 immunostaining. Specifically, blocking stem was 2-hour long, primary antibodies incubation 3-hour long and finally secondary antibodies incubation 1-hour long. All the steps were performed at 4°C and the blocking buffer was prepared without the triton-X100.

Solution	Component	Concentration	Volume for 50ml
Blocking buffer	Goat Serum	10%	5ml
	BSA	3%	1.5g
	Triton-X100	0.5% (pups), 1% (adults)	500µl
	PBS 1x		44.5ml
Mowiol	Glycerol		12g
	Mowiol		5g
	mqH ₂ O		12ml
	0.2M Tris pH 8.5		24ml

Table 8 – List of the home-made solutions used in the 2D immunofluorescence protocol

Imaging

Laser scanning confocal microscopy

Confocal imaging was performed using a Zeiss 710 or a Leica SP5 confocal microscopes equipped with a 405nm diode, an argon ion, a 561nm DPSS and a 647 HeNe lasers. Z-stacks of fixed cortical sections were imaged using a LD-LCI Plan-Apo 25x/0.8 NA or a LD Plan-Apo 63x/1.4 NA oil immersion lenses (710 Zeiss) or with a 20X multi-immersion (oil, glycerol, water) NA 0.7 or a HCX APO L 63X oil 1.4 NA (SP5 Leica). Confocal imaging was performed every time high resolution images were required in order to study subcellular structures, such as dendritic spines, dendrites and axons, as well as cell counting.

Epifluorescence microscopy

Epifluorescence imaging was performed using a Zeiss Apotome microscope, equipped with an automatic stage. Tiles mosaics were imaged in the software ZEN Blue, by using 2.5x or 10x depending on the needs. The high speed of the system was crucial to obtain a very big number of pictures in a reasonable amount of time, without drastically affecting image quality. For that reason, I took advantage of this system when acquiring series of sections for the projection mapping experiments which I performed at different developmental stages and with different aims (i.e. the functional rescue, the dissection of somato and motor cortico spinal and cortico pontine projections).

Image Analysis

Images from 2D IF experiments were analysed by using Fiji-ImageJ Software (Schindelin et al., 2015): cell counter plug-in was used to assess the number of cells expressing specific proteins, while measurement tools were used to determine signal intensity or Axonal Initial Segment (AIS) features such as length and distance from the soma. AIS average diameter measurement was performed via IMARIS software's tool filament tracer. AISs were semi-automatically reconstructed and an average diameter automatically measured for every AIS individually (see Results – Paper one section). CST

morphometric analysis was performed in Fiji-ImageJ, by using the measurement tools built in the software.

Morphological characterization of biocytin filled layer V pyramidal neurons (LVPNs) was analysed by using IMARIS software. Cell arborization was reconstructed in a semi-automatic manner, via the filament tracer module. Automatic length measuring tool was used to calculate the total dendritic length and the basal dendritic length. Branching points, branching point orders and tips were manually quantified for both basal and apical dendrites, as well as primary and lateral dendrites. The branch tip order is an integer value equivalent to the number of branching points a dendrite undergoes from its somatic origin to the terminal tip (see also Figure 2D for a graphic representation). Primary dendrites were identified as directly originating from the soma, lateral dendrites were categorized as originating from and perpendicular to the apical dendrite whereas total and basal branch tips were identified as the terminal ends of primary dendrites including or excluding the apical dendrite arborization respectively.

The basal Dendritic Complexity Index (bDCI) was calculated as follows:

$$bDCI = \frac{\sum \text{basal branch tip orders} + \text{basal branch tips}}{\text{Primary dendrites}} \text{Basal Arbor Length}$$

An automatic detection of Sholl intersections was used to compute Sholl profiles for every individual cell. Sholl intersections were identified as the number of dendrite intersections for concentric spheres of increasing radius and having as a centre the centroid of the cell body. Distance between radii was set at 10 μ m.

Statistical analysis

Statistical analyses were performed using GraphPad Prism7 and data are presented as mean \pm s.e.m. N values represent biological replicates from > 3 different brains. Whenever possible, both genotypes were processed in parallel. Data sets were tested for normality (Kolmogorov-Smirnov) or homoscedasticity (Leven test) before performing parametric (Student t-test, one-way or 2-way

ANOVA followed by Bonferroni's post-hoc test) or non-parametric tests (Welch's unequal variances t-test or Mann-Whitney test) used to determine p-values.

idisco clearing and 3D imaging

Embryos were collected at E13.5, and heads briefly rinsed in PBS prior incubation in PFA 4% for 3-4h at 4°C, with gentle shaking. Fixed tissues were then processed according to previously published protocols (Belle et al., 2017; Henning et al., 2019) with some modifications. To quench tissue auto-fluorescence and decolour the retina pigmented layer, heads were treated with 10% H₂O₂ in PBS, for 1h 30' at 55°C. Then, embryo heads were incubated in PBSGT blocking buffer (0.5% Triton-X 100, 0.2% Gelatin in PBS-Azide) overnight (O/N) at 37°C with gentle shaking or slow rotation. Heads were then incubated with the Tuj1 primary antibody (Sigma T8660; 1:500 in PBSGT) for 5 days at 37°C in slow rotation. After incubation, samples were repeatedly washed in PBST (0.5% Triton-X 100 in PBS) over the day at room temperature (RT) in slow rotation, then O/N at 4°C. Secondary antibody (Thermo Fisher scientific; anti-rabbit Alexa-fluor 555; 1:500 in PBSGT) was added and heads were incubated O/N at 37°C in slow rotation. After several washes in PBST, heads were dehydrated in increasing concentration of methanol in PBS pH 9.0 (20%; 40%; 60%; 80% and finally twice in 100%; 1h each step, 4°C in slow rotation). Lipid removal was obtained with 66% dichloromethane (DCM) in methanol by O/N incubation, followed by 1h-long incubation in 100% DCM at RT in slow rotation. Finally, refractive index matching and tissue clearing were obtained by submerging the samples in dibenzil-ether (DBE). Tissues were stored at RT and in the dark until imaging. (**Fig. 28 and Table 9**). 3D images from the clearing experiments were acquired via the Zeiss light-sheet Z.1 microscope equipped with 5x objective and Zen software. Image analysis, 3D rendering and signal segmentation, as well as video editing were performed using the IMARIS (Bitplane) software.

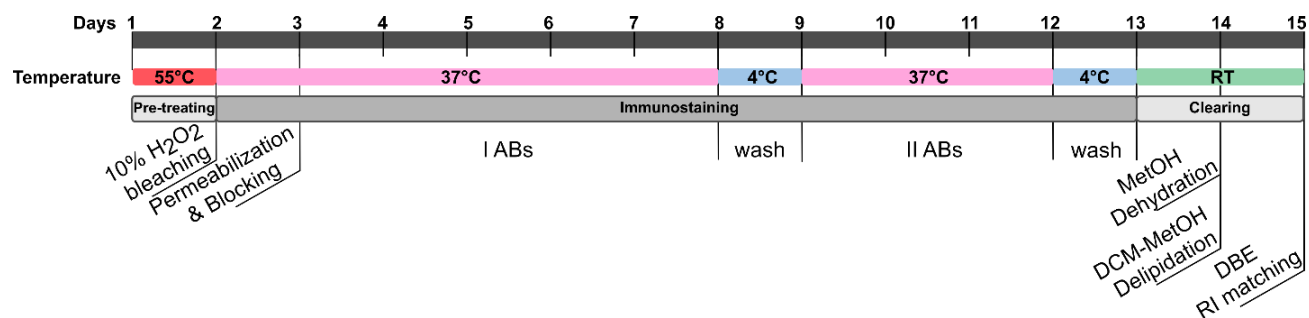


Fig.28- iDisco tissue clearing and immunostaining timeline. The pre-treating consists in a bleaching step (10% H₂O₂ in PBS for 1h30' at 55°C) that precedes the immunofluorescence. The immunostaining step can be adapted based on the characteristic of the samples. Small samples coming from young animals or embryos were treated with a milder buffer (0.5% Triton-X100) for all the steps. Blocking and permeabilization was usually ON at 37 °C in gentle rotation, primary antibodies incubation 5/6 days, same environmental conditions as previous step. Then, samples were washed for 24h in the cold room and under gentle rotation before the incubation with secondary antibodies (2/3 days, same conditions as primary antibodies incubation). Before proceeding with the clearing, tissues were once again washed for 24h as previously stated. Finally, the clearing step (performed at room temperature) consisted in tissue dehydration in incremental MetOH concentration, delipidation in DCM-MetOH and DCM and finally refractive index matching with DBE.

Solution	Component	Concentration	Volume for 50ml
MetOH-PBS	MetOH	20%, 40%, 60%, 80%, 100%	10ml, 20ml, 30ml, 40ml, 50ml
	PBS	80%, 60%, 40%, 20%, -	Q.S.
H ₂ O ₂ -MetOH	H ₂ O ₂	5%	8.3 (from stock solution at 30%)
	MetOH		Q.S.
PBST	Triton-X100	1% (adults), 0.5% (pups)	500µl
	PBS 1X		Q.S.
PBSGT	Triton-X100	1% (adults), 0.5% (pups)	500µl
	Gelatine	0.2%	(5ml from stock solution 2% in PBS)
	Sodium-Azide	0.05%	2.5ml
	PBS 1X		Q.S.

Table 9 – List of the home-made solutions used in the iDISCO protocol.

RESULTS

1. Paper One

Title: *COUP-TFI/Nr2f1 Orchestrates Intrinsic Neuronal Activity during Development of the Somatosensory Cortex*

At the onset of corticogenesis, expression of morphogens in the patterning centres directs the gradient expression of area patterning genes along the dorso-ventral and antero-lateral axes of the cortical primordium (Alfano et al., 2013; Greig et al., 2013; O’Leary et al., 2008). The dose-, time- and space-specific combinatorial expression of such transcription factors in progenitor and early postmitotic cells initiates the process of neuron fate determination and subtype specification and starts shaping the protomap of the future cortical functional areas (Greig et al., 2013; O’Leary et al., 2008). Simultaneously, patterns of local spontaneous activity within the developing neocortex set the basis of the future network organization (Andreae et al., 2018; Kirkby et al., 2013). Finally, both the area map and the activity network will require sensory-evoked activity for their refinement (Cadwell et al., 2019; Simi et al., 2018).

So far, although the regulation of local spontaneous activity by cortical genetic programs has been hypothesised, no evidences have been presented.

To test this hypothesis, we investigated the electrophysiological and morphological state of cortical Layer V pyramidal neurons in a cortical-specific conditional *KO* for the transcriptional regulator *Nr2f1*, to evaluate whether the gene, known to promote S1 specification during corticogenesis, would also affect the functional maturation of the network.

In this article, the activity and electrophysiological data have been produced by A. Marcantoni, E. Magrinelli and I. Del Pino and support the idea that peri- and postnatal *Nr2f1* mutant cortices show altered spontaneous activity patterns and synchronization defects, and that postnatal LVPNs have affected intrinsic bioelectric properties. Specifically, both spontaneous and network activity of cultured *Nr2f1*-deficient cortical neurons were affected, their activity profiles showed longer recording bursts (a period in time when a neuron, or a network of neurons repetitively fire several action potentials) with a lower firing frequency, and the network appeared to be less synchronized than in normal conditions. Further electrophysiological analyses showed that *Nr2f1* mutant neurons

retain aberrant intrinsic electric properties, such as increased resting membrane potential and reduced rheobase and sag current.

Neurons that normally fail to generate their expected electrophysiological profiles are also affected at the structural and morphological levels. As an example, neurons that are in a less excitable state tend to produce more dendrites and synaptic spines so to compensate and retain a normal activity pattern. *Vice-versa*, when a cell is intrinsically more prone to fire, its structure is generally simplified to avoid over-stimulation of the network (Tien et al., 2018).

To assess if this was the case, I performed a set of morphological and structural analyses on a pool of biocytin-filled LVPNs from postnatal control and mutant mouse brains. The results, which are included in this paper (**Fig. 4 and Supplementary Fig. 3 in Del Pino et al., 2020**), indicate that the basal dendritic structure is indeed affected by the absence of *Nr2f1*. These neurons are characterized by both a smaller number of primary dendrites, and a reduced complexity, measured as number of branching, than their control counterpart.

Another compartment that resulted compromised in the absence of *Nr2f1* is the axon initial segment (AIS), a specialized region localized between the somatic and the axonal compartments. This structure is characterized by high-density clusters of voltage-gated sodium (Nav) channels and represents the site of action potential (AP) initiation. In the AIS, Nav channels are recruited and stabilized through interactions with Ankyrin-G, an AIS-specific scaffold protein, and accumulate at this site, reaching concentrations that are up to 50 times higher than in the soma. This results in strong regionalized Na⁺ currents and confer to the AIS a lower AP threshold compared to the somatic compartment, making the generation of APs in this site easier than anywhere else in the cell. For this reason, structural modifications that affect the number and composition of the AIS Nav clusters will inevitably influence the firing properties of the cell (Petersen et al., 2017). The AIS compartment is very dynamic during development, and it adapts in response to changes in signal input and intrinsic excitability by extending or retracting along the axon, or even by shifting from and towards the soma, in an attempt to maintain a homeostatic physiological level of output signal (Kuba et al 2010). This phenomenon, called AIS plasticity, has been observed in both physiological and in pathological conditions during brain development (reviewed in Leterrier, 2018).

My analysis showed that both the AIS structure itself and its positioning relative to the soma are affected by the loss of Nr2f1 function and that inducing chronic depolarization *via* KCl treatment on *ex vivo* brain sections would only trigger AIS shortening in control but not mutant cells (**Fig. 5 and Supplementary Fig. 5 in Del Pino et al., 2020**).

Finally, we found that NR2F1 regulates, directly and indirectly, the expression of several ion channels, which can explain its influence on neuronal activity and morphology. One of the most interested channels that we found altered is the hyperpolarization-activated cation channel HCN1. Typically, HCN1 conducts the hyperpolarization-activated current (I_h) and is involved in the stabilization of resting membrane potential, the modulation of rhythmic oscillatory activity in individual neurons and neuronal networks, ultimately controlling neuronal excitability (Bonzanni et al., 2018; Z. Huang et al., 2009; Marini et al., 2018). In the absence of Nr2f1, HCN1 is downregulated at both transcriptional and protein level. Moreover, HCN1 is directly bound by Nr2f1, suggesting a possible direct regulation of HCN1 (**Fig. 6 in Del Pino et al., 2020**).

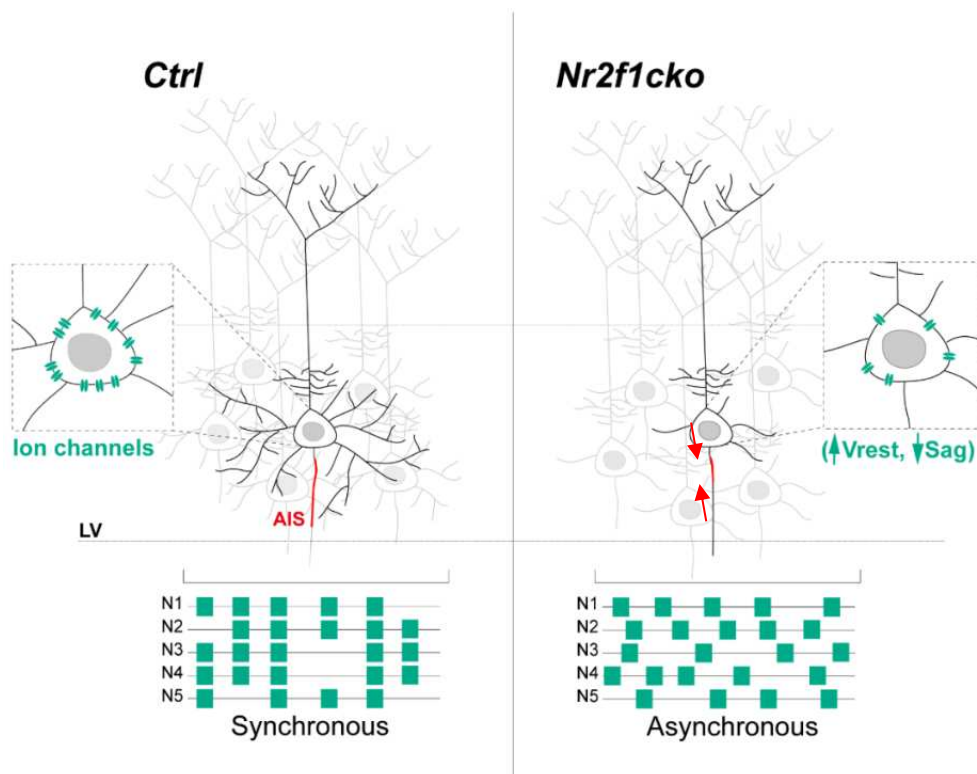


Figure 29 – Graphical summary. In the absence of NR2F1, cortical pyramidal neurons of the layer V are characterized by a smaller ion channel pool (in the dashed box), reduced basal dendrites ramification (main panel) and a shorter axon initial segment (AIS, in red in the main scheme). These molecular and structural changes lead to a generalized dysfunction of the electrophysiological state of these cells, characterized by higher resting membrane potential (V_{rest}) and reduced Sag current, and ultimately desynchronization of the network.



ORIGINAL ARTICLE

COUP-TFI/Nr2f1 Orchestrates Intrinsic Neuronal Activity during Development of the Somatosensory Cortex

Isabel Del Pino ^{1,4}, Chiara Tocco ², Elia Magrinelli ^{2,5},
Andrea Marcantoni ³, Celeste Ferraguto², Giulia Tomagra ³,
Michele Bertacchi ², Christian Alfano², Xavier Leinekugel ¹,
Andreas Frick ¹ and Michèle Studer ²,

¹Université de Bordeaux, Inserm U1215, Neurocentre Magendie, 33077 Bordeaux, France, ²Université Côte d'Azur, CNRS, Inserm, iBV, 06108 Nice, France, ³Dipartimento di Scienza e Tecnologia del Farmaco, Università di Torino, 10125 Torino, Italy, ⁴Present address: Centro de Investigación Príncipe Felipe, 46012 Valencia, Spain and ⁵Present address: Département des Neurosciences Fondamentales, Université de Lausanne, CH-1005 Lausanne, Switzerland

Address correspondence to Michèle Studer, Institut de Biologie Valrose (iBV), Univ. Nice Sophia Antipolis, Centre de Biochimie; UFR Sciences, Parc Valrose, 28 avenue Valrose, 06108 Nice Cedex 2, France. Email: Michele.studer@unice.fr

† Isabel del Pino, Chiara Tocco, Elia Magrinelli, and Andrea Marcantoni are co-first authors

‡ Xavier Leinekugel, Andreas Frick, and Michèle Studer are co-last senior authors

Abstract

The formation of functional cortical maps in the cerebral cortex results from a timely regulated interaction between intrinsic genetic mechanisms and electrical activity. To understand how transcriptional regulation influences network activity and neuronal excitability within the neocortex, we used mice deficient for *Nr2f1* (also known as *COUP-TFI*), a key determinant of primary somatosensory (S1) area specification during development. We found that the cortical loss of *Nr2f1* impacts on spontaneous network activity and synchronization of S1 cortex at perinatal stages. In addition, we observed alterations in the intrinsic excitability and morphological features of layer V pyramidal neurons. Accordingly, we identified distinct voltage-gated ion channels regulated by *Nr2f1* that might directly influence intrinsic bioelectrical properties during critical time windows of S1 cortex specification. Altogether, our data suggest a tight link between *Nr2f1* and neuronal excitability in the developmental sequence that ultimately sculpts the emergence of cortical network activity within the immature neocortex.

Key words: Nr2f1/COUP-TFI, intrinsic excitability, spontaneous activity, layer V pyramidal neurons, somatosensory cortex

Introduction

The area- and cell-type specific organization of the mammalian neocortex is a process involving coordinated interactions between cell intrinsic genetic programs and neural activity, an essential feature in specifying the composition and organization of neural circuits during all stages of development (Jabaudon 2017; Simi and Studer 2018). Before experience shapes neuronal

circuits *via* sensory-driven activity, the developing cortex is genetically primed to establish patterns of local spontaneous activity, which autonomously synchronizes large groups of neurons independently of sensory stimulation and contributes to the development of neuronal circuits (Kirischuk et al. 2017; Andrae and Burrone 2018; Luhmann and Khazipov 2018; Anton-Bolanos et al. 2019). These early patterns of spontaneous

activity are thought to set the initial blueprint of cortical network organization, and their alteration during cortical development leads to the formation of dysfunctional cortical circuits (Kirkby et al. 2013; Li et al. 2013). The embryonic thalamus also conveys spontaneous neuronal activity to the immature cortex, influencing the formation of a functional somatotopic map (Anton-Bolanos et al. 2019). Hence, local spontaneous activity in cortical and precortical relay stations during embryonic and early postnatal stages might prepare cortical areas and circuits for upcoming sensory input.

Spontaneous activity emerging during early development in different cortical areas in form of calcium (Ca^{2+}) waves has been reported already at embryonic day E16 in mice, most probably generated in proliferating radial glia cells (Kirschuk et al. 2017). Immature neurons express voltage-dependent ion channels, responsible for a highly synchronized spontaneous activity within small neuronal networks (Luhmann et al. 2016). Finally, certain features of immature cells, including high membrane resistance and prominent low-threshold calcium currents, seem to enhance excitability in neurons receiving little afferent sensory input (Moody and Bosma 2005).

Besides spontaneous activity, the neocortical primordium is under the control of distinct morphogens that establish proper coordinates along the developing anteroposterior and dorsoventral cortical axes (O'Leary and Sahara 2008; Alfano and Studer 2012; Greig et al. 2013). Functioning in a dose-, context-, and time-dependent manner, these signaling pathways modulate the gradient expression of area patterning genes, such as *Pax6*, *Sp8*, *Emx2*, and *Nr2f1* (also known as *COUP-TFI*), among others. These transcriptional regulators cooperatively instruct cell identity acquisition in cortical progenitors and early postmitotic neurons, building a rough primordial areal map, known as a protomap, which will be refined by sensory-evoked activity during postnatal stages (Simi and Studer 2018; Cadwell et al. 2019). Changes in dosage of these factors alter the size and position of primordial area maps with severe consequences in cell-type specification and circuit formation (Greig et al. 2013; Jabaudon 2017). Although the interaction between cortical patterning genes and onset of spontaneous activity during primary area mapping has been hypothesized, there is still no clear evidence on how this interaction is perpetrated.

To tackle this question, we used mice deficient for the nuclear receptor *Nr2f1*, a gene coding for a member of the superfamily of steroid hormone receptors and a key transcriptional regulator during cortical development, as a genetic model of altered primary somatosensory (S1) area mapping (Armentano et al. 2007). In humans, haploinsufficiency of the *NR2F1* gene leads to an emerging genetic neurodevelopmental disorder, named Bosch-Boonstra-Schaaf Optic Atrophy Syndrome. Patients affected by this autosomal-dominant disorder exhibit several clinical features, such as intellectual disability, epileptic seizures, autistic-like traits, abnormal fine motor coordination, and optic atrophy (Boschet et al. 2014; Chen et al. 2016; Bertacchi et al. 2019). In mice, *Nr2f1* represents a well-studied area patterning gene, which determines sensory identity, controls neuronal migration, and laminar specification; its loss of function leads to motor and cognitive impairments (Armentano et al. 2007; Tomassy et al. 2010; Alfano et al. 2014; Contesse et al. 2019). In the absence of cortical *Nr2f1* in progenitors or early postmitotic neurons, proper barrel fields do not form in the normal S1 region, which seems instead to be respecified into a motor-like cortex (thus named as motorized S1—mS1), as shown by molecular markers and early thalamocortical projections (Armentano et al. 2007;

Alfano et al. 2014). Nevertheless, sensory thalamocortical axons are still able to reach the pallial subplate of the affected S1 region in *Nr2f1* cortex-specific mutants, despite its very early acquisition of motor-like molecular identity (Armentano et al. 2007). Interestingly, at postnatal stages, thalamocortical axons fail to functionally innervate the cortical plate, implying that *Nr2f1* function within the developing S1 region is necessary for the correct establishment of thalamocortical projections but has little effect on their early arrival. Moreover, the abnormal crosstalk between mS1 and thalamocortical neurons, an important event for the correct development of cortical circuits, suggested that mS1 cells might display multiple functional defects besides the abnormal expression of area-specific molecular markers. To this end, and to understand whether the loss of cortical *Nr2f1* leads to a fully functional respecification of sensory to motor identity in mS1, we decided to compare spontaneous activity, as well as intrinsic electrophysiological and morphological properties of mutant mS1 neurons to control (Ctrl) S1 and motor (M1) cortical neurons. More generally, this allowed us to decipher the interactions between identity patterning genes and early activity function during the process of area mapping.

We found that mutant mS1 neurons fail to reproduce intrinsic spontaneous and network activity, as well as morphological and electrophysiological hallmarks, typical of either normal M1 or S1, suggesting a novel role for *Nr2f1* in controlling functional specification of S1 properties. Together, our data show that despite imparting a molecular identity of M1-like in S1 cortex, *Nr2f1* loss in the cortical primordium results in abnormal spontaneous activity and intrinsic excitability unique to mS1 and different from M1 and S1. This newly described function is accomplished by the transcriptional modulation of several ion channels involved in modulating excitability as well as morphological and structural features of layer V pyramidal neurons (LVPNs).

Materials and Methods

Mice

Nr2f1/COUP-TF1^{fl/fl} mice were crossed with *Emx1-Cre* mice to delete *Nr2f1/COUP-TFI* exclusively in cortical progenitors and their progeny (Armentano et al. 2007). These mice are named *Nr2f1cKO* throughout the text. Mice were genotyped as previously described (Armentano et al. 2007). Control and mutant littermates were *Nr2f1^{fl/fl}* and *Nr2f1^{fl/fl};Emx1-Cre*, respectively. For P21 studies, control (*Nr2f1^{fl/fl}*) and mutant *Nr2f1cKO* mice were crossed with *Thy1-eYFP-H* mice to specifically label layer V projection neurons (LVPNs), as previously reported (Harb et al. 2016). Midday of the day of the vaginal plug was considered as embryonic day 0.5 (E0.5). Control (*Nr2f1^{fl/fl}*) and mutant *Nr2f1cKO* mice were predominantly bred in a C57BL6 background. Both male and female embryos and pups were used in this study. All mouse experiments were conducted according to national and international guidelines, with authorization #15 349 and #15 350 by the French Ministry of Education, Research and Innovation and upon request of the local ethics committee—CIEPAL NCE/2019-548 (Nice) and CEEA50 (Bordeaux), and in accordance with the guidelines established by the Italian National Council on Animal Care and approved by the local Animal Care Committee of University of Turin (Authorization DGSAF0011710-P-26/07/2017).

MEA Recordings on Primary Cultures and Analysis of MEA Activity

Cortical neuronal cultures were obtained from E18 *Ctrl* and *Nr2f1cKO* mouse fetuses. Somatosensory cortices were rapidly

dissected under sterile conditions, kept in cold HBSS (4 °C) with high glucose, and then digested with papain (0.5 mg/ml) dissolved in HBSS plus DNase (0.1 mg/ml), as previously described (Gavello et al. 2018). Isolated cells were then plated at the final density of 1200 cells/mm² onto the MEA (Microelectrode Array, previously coated with poly-DL-lysine and laminin). Cells were incubated with 1% penicillin/streptomycin, 1% glutamax, 2.5% foetal bovine serum, and 2% B-27 supplemented Neurobasal medium in humidified 5% CO₂ atmosphere at 37 °C. Each MEA dish was covered with a fluorinated ethylene-propylene membrane (ALA scientific, Westbury, NY, USA) to reduce medium evaporation and maintain sterility, thus allowing repeated recordings from the same chip.

Multisite extracellular recordings from 59 electrodes were performed using the MEA-system, purchased from Multi-Channel Systems (Reutlingen, Germany). Data acquisition was controlled through MC_Rack software (Multi-Channel Systems Reutlingen, Germany), setting the threshold for spike detection at $-30\ \mu\text{V}$ and sampling at 10 kHz. Experiments were performed in a nonhumidified incubator at 37 °C and with 5% CO₂, without replacing the culture medium. Before starting the experiments, cells were allowed to stabilize in the nonhumidified incubator for 90 s; then, the spontaneous activity was recorded for 2 min.

Burst analysis was performed using Neuroexplorer software (Nex Technologies, Littleton, MA, USA) after spike sorting operations. A burst consists of high frequency firing of a neuron separated by periods of quiescence (Cotterill et al. 2016); thus, a threshold of at least 3 spikes and a minimum burst duration of 10 ms was set. Algorithm specifications such as maximum interval to start burst (0.17 s) and maximum interval to end burst (0.3 s) were set as in (Gavello et al. 2012; Gavello et al. 2018). Burst analysis was performed by monitoring the following parameters: mean frequency, number of bursts, and mean burst duration. Cross correlation probability values were obtained by means of Neuroexplorer software using $\pm 2\text{-s}$ and 5-ms bin size. All the data collected from active recording sites (i.e., firing activity with spike amplitude $>30\ \mu\text{V}$, i.e., $3\times$ noise value) were pooled by genotype for statistics (N = number of active recording sites, cf., Allio et al. 2015). Detailed number of MEAs recorded per genotype (Ctrl or *Nr2f1cKO*) is provided in Supplementary Table 5.

Ca²⁺ Imaging from *Ex vivo* Brain Slices Preparation and Analysis

Mouse pups at postnatal age (P)1 and P4 were anesthetized on ice, and brains were dissected in ice-cold high-Mg artificial cerebral-spinal fluid (aCSF, containing in mM 125 NaCl, 25 NaHCO₃, 2.5 KCl, 7 MgCl₂, 2 CaCl₂, 1.25 NaH₂PO₄, 10 glucose, and adjusted to pH 7.4) after decapitation. Horizontal 300- μm -thick slices were prepared using a Leica Vibratome 100 M in ice-cold high-Mg aCSF under 95% O₂, 5% CO₂ bubbling. Selected slices were incubated for 1 h at 37 °C in aCSF containing 0.63% Oregon Green BAPTA™ (ThermoFisher O6807 dissolved in DMSO) before proceeding to image acquisition. Slices were loaded on a 35-mm diameter petri dish with 1.3-mm glass bottom and immobilized with a custom nylon net while kept under a constant aCSF perfusion at 37 °C throughout the imaging process. After 30 min of equilibration in the microscope objective holder, time-lapse images were acquired for 15 min at 150-ms intervals using a spinning disk microscope (Olympus/Andor technology) equipped with a 40 \times air objective. Activity was recorded up to 200 μm below the pia margin.

Images were automatically corrected for drifting using the built-in Fiji function “Linear stack alignment with SIFT” (Schindelin et al. 2012). Single cell borders were manually generated as separate regions of interest (ROIs) using a customized MATLAB script. Each ROI was used to acquire BAPTA fluorescence intensity as the mean of intensity within each ROI area by frame, resulting in a matrix of single cell time series of BAPTA fluorescence signals as a readout of Ca²⁺ cytoplasmic concentration. Matrices were corrected by a moving average (Anderson 1975) normalizing each timepoint with the average of 60 s in each cell and generating a constant baseline over the progressive signal loss due to the bleaching of the BAPTA dye. As a cutoff for detecting cells actively displaying Ca²⁺ transients, we discarded from the analysis those cells whose first quartile of intensity did not contain at least 40% of its timepoints, since cells below this threshold showed values comparable to noise signals. For each experiment, we measured the ratio of active and inactive cells (see also Supplementary Fig. 2; Supplementary Table 1). For the remaining selected timeseries, Ca²⁺ transients were detected filtering BAPTA intensity on a threshold of 3 SD. The burst frequency of every selected cell was measured by dividing the number of transients above threshold by the sum of intervals between each burst. To evaluate activity coordination, we counted the ratio of transients occurring across cells in a sliding window interval of 3 s normalized by the total number of transients. All time-lapse analyses were performed using a custom MATLAB script.

Ex vivo Whole-Cell Electrophysiology and Analysis

P5 to P8 pups were decapitated, and brains were placed on ice-cold modified artificial cerebrospinal fluid (aCSF) containing (in mM): 87 NaCl, 25 NaHCO₃, 5 Glucose, 65 Sucrose, 2.5 KCl, 1.25 NaH₂PO₄, 0.5 CaCl₂, and 7 MgCl₂ saturated with 95% CO₂ and 5% O₂. Coronal slices of 300- μm thickness were cut using a vibratome (Vibratome 300 Plus, Sectioning Systems) and gently transferred to room temperature aCSF containing (in mM): 125 NaCl, 25 NaHCO₃, 25 Glucose, 2.5 KCl, 1.25 NaH₂PO₄, 2 CaCl₂, and 1 MgCl₂ saturated with 95% CO₂ and 5% O₂ (pH 7.4). Current-clamp recordings were performed at 32–34 °C using a potassium gluconate-based intracellular solution containing (in mM): 120 K-Gluconate, 20 HEPES, 0.5 EGTA, 15 KCl, 4 MgATP, and 0.3 NaGTP (pH 7.4) and osmolarity set to 299 mosmol/l. Biocytin (1.5–2 mg/ml) was added to the intracellular solution for *post hoc* immunohistochemistry. Neurons were visualized with an upright microscope (Zeiss Axio Examiner D1) equipped with an Evolve 512 EMCCD Camera (Photometrics) using a 63X/1.0 NA water-immersion objective (Zeiss) and infrared DodT contrast imaging. Recording pipettes (6–10 M Ω) were pulled from borosilicate glass using a Narishige P-10 puller. Data were acquired using a Dagan BVC-700A Amplifier, low-pass filtered at 3 kHz, and sampled at 20 kHz with ITC16 (Instrutech) and AxoGraph X software. Membrane voltage was recorded in the bridge mode. To determine the excitability of pyramidal neurons, 800-ms square current steps of 10 pA from -100 to $+150$ pA were set. The rheobase was defined as the minimum somatic current required to elicit an action potential (AP) from the resting membrane potential (V_{rest}) of the neuron. Input resistance (R_{in}) was calculated from voltage responses to -20 pA. Threshold potential was defined as $dV/dt = 10$ mV/ms. Interspike interval (ISI) was calculated as the difference between first and second AP at the minimal current to elicit >2 AP. The amplitude of APs was measured from spike threshold (see Supplementary Table 2). AP

width was measured at half of the maximum amplitude (APhalf-width or AP_{h-w}). Voltage sag was calculated as the difference between negative voltage peak and steady-state hyperpolarization from traces in which the difference between steady-state response and baseline fell within 20–30 mV. Firing frequency was calculated by dividing the number of APs by the duration of the current step (800 ms). Membrane time constant (τ_m) was calculated as the slow component of a double exponential fit of the decay (recovery) from the average of 10 hyperpolarizing current pulses (1 ms 400 pA). Capacitance was obtained as the ratio of membrane time constant over R_{in} .

Post Hoc Immunofluorescence

Brain slices were fixed overnight (ON) at 4 °C with 4% paraformaldehyde in 0.1 M phosphate buffer (PB) pH 7.4. The following day slices were washed 3 × 10 min with 0.1 M PB and incubated overnight (ON) at 4 °C with Alexa-Fluor®-conjugated streptavidin diluted 1:500 in 0.1 M PB. The day after, slices were washed 3 × 10 min with 0.1 M PB, stained with DAPI, and finally mounted with Mowiol.

KCl Ex Vivo Depolarization Assay

Ctrl and *Nr2f1cKO* P7 pups were sacrificed by decapitation and brains dissected into ice-cold aCSF saturated with 95% O₂ and 5% CO₂. 300- μ m-thick slices were produced by vibratome sectioning and then transferred into room temperature aCSF, and constantly saturated with 95% O₂ and 5% CO₂. After 15 min of acclimatization, slices from both genotypes were split into two groups: an untreated group (–KCl) and an experimental group (+KCl). KCl was added at the final concentration of 7 mM to the aCSF of the experimental group, whereas control slices were kept in normal aCSF. After an incubation time of 6 h (Dumitrescu et al. 2016), slices were washed for 15 min in newly prepared aCSF and then processed for immunofluorescence (IF), as described below.

Histology and Immunohistochemistry of Mouse Perinatal Cortices

P7 to P8 pups were anesthetized by using a mixture of Tiletamine-Zolazepam-Xylazine-Buprenorphine (TZXB) and intracardially perfused with PB Saline (PBS) followed by 4% paraformaldehyde (PFA) in PBS. Then, brains were dissected and postfixed for 4 h at 4 °C in 4% PFA and then vibratome-sectioned to obtain 100- μ m-thick, coronal, or sagittal floating sections. ON incubation at 4 °C in a solution of 0.5% Triton X-100, 3% BSA, 10% goat serum in PBS was performed to permeabilize the sections and reduce nonspecific binding of the antibodies. For IF, sections were incubated for 2 days at 4 °C with indicated primary antibodies in a solution of 0.5% Triton X-100, 10% goat serum in PBS, and then ON at 4 °C with relative secondary antibodies and HOECHST diluted in PBS. For the complete list of primary and secondary antibodies, see [Supplementary Table 4C](#). For HCN1 IF, brains were briefly postfixed for 30 min at 4 °C in 4% PFA and then immediately sectioned with the vibratome to obtain 50- μ m-thick, coronal floating sections. Permeabilization-blocking step was reduced to 2 h, primary antibody incubation to one ON and secondary antibody and HOECHST incubation to 2 h. Sections were then transferred on superfrost plus slides (ThermoScientific), let dry for 30 min to 1 h, and finally mounted with Mowiol mounting medium.

Microscopy and Image Analysis

Imaging was performed using a Zeiss 710 confocal microscope equipped with a 405-nm diode, an argon ion, a 561-nm DPSS, and a 647 HeNe lasers. Z-stacks of fixed cortical sections were imaged using a LD-LCI Plan-Apo 25x/0.8 NA or a LD Plan-Apo 63x/1.4 NA oil immersion lenses. Images from IF experiments were analyzed by using Fiji-ImageJ Software (Schindelin et al. 2012): cell counter plug-in was used to assess the number of cells expressing specific proteins, while measurement tools were used to determine signal intensity or axonal initial segment (AIS) features such as length and distance from the soma. For the AIS average diameter measurement, we took advantage of the IMARIS software tool filament tracer (Oxford Instruments). AISs were semi-automatically reconstructed, and an average diameter automatically measured for every AIS individually.

Morphological characterization of biocytin filled LVPNs was analyzed using IMARIS. Cell arborization was reconstructed in a semi-automatic manner, via the filament tracer module. Automatic length measuring tool was used to calculate the total and basal dendritic length. Branching points, branching point orders, and tips were manually quantified for both basal and apical dendrites, as well as primary and lateral dendrites. The branch tip order is an integer value equivalent to the number of branching points; a dendrite undergoes from its somatic origin to the terminal tip (see also [Fig. 4E](#) for a graphic representation). Primary dendrites were identified as directly originating from the soma; lateral dendrites were categorized as originating from and perpendicular to the apical dendrite, whereas total and basal branch tips were identified as the terminal ends of primary dendrites including or excluding the apical dendrite arborization, respectively.

The basal Dendritic Complexity Index (bDCI) was calculated as $[(\text{Basal branch tip orders} + \text{Basal branch tips}) / \text{Primary dendrites}] \times \text{Basal Arbor Length}$.

An automatic detection of Sholl intersections was used to compute Sholl profiles for every individual cell. Sholl intersections were identified as the number of dendrite intersections for concentric spheres of increasing radius (10- μ m difference) and having as a center the centroid of the cell body (see also [Supplementary Table 3](#)).

RNA Extraction and cDNA Synthesis

RNA for reverse transcriptase-PCRs (RT-PCRs) was extracted from P7 dissected neocortices separated from meninges of *Ctrl* and *Nr2f1cKO* mice ($n = 3$) using the RNeasy Mini kit (Qiagen) following manufacturer's instructions. RNA quantity and RNA quality were assessed with Nanodrop and gel electrophoresis. cDNA was synthesized from 1 μ g of total RNA using Super- script III First-Strand Synthesis System for RT-PCR (Invitrogen) following manufacturer's instructions.

qPCR RNA/cDNA Quantification

Quantitative polymerase chain reaction (qPCR) on cDNA was performed using KAPA Sybr Fast (Kapa Biosystems) according to manufacturer's instructions. Samples were run on a LigthCycler II 480 (Roche) with the primers listed in [Supplementary Table 4A](#). Each reaction consisted of 10ng total cDNA, with 200 nM forward-reverse primer mix. Amplification take-off values were evaluated using the built-in LightCycler relative quantification analysis function, and relative expression was calculated with

the 2^{- $\Delta\Delta$ Ct} method. Gene expression was normalized to the housekeeping gene GAPDH.

Dissection and Western Blot of Mouse Perinatal Cortices

P7-P8 pups were sacrificed by decapitation, and fresh tissues were dissected immediately after. Whole cortex samples were collected and lysed in RIPA buffer [10 mM Tris-Cl (pH 8.0), 1 mM EDTA, 1% Triton X-100, 0.1% sodium Deoxycholate, 0.1% SDS, 140 mM NaCl, 1 mM PMSF] implemented with Complete protease inhibitors (Roche). Protein quantity was then measured with the Pierce BCA protein assay KIT (ThermoScientific). Equal amounts of proteins from tissue lysates were resolved by reducing SDS-PAGE, transferred to PolyVinylidene DiFluoride membrane, and incubated with the indicated antibodies (see [Supplementary Table 4C](#)). Immunoblots were developed using ECL prime western blotting detection reagent (GE Healthcare). Signals were normalized to actin signal intensity.

Chromatin Immuno-Precipitation (ChIP)

The ChIP protocol was modified from [Alfano et al. \(2011\)](#) using protein Sepharose-A resin (SIGMA), prepared by washing in PBS and equilibration buffer (HEPES pH 7.4 20 mM, EDTA 1 mM, NaCl 150 mM, Triton 0.8%, SDS 0.1% PMSF 10 mg/ml). For each experiment ($n = 3$), cortices from 8 mice at P0 were collected in ice-cold HBSS and washed in DMEM. Samples were crosslinked in 0.9 formaldehyde for 10 min and blocked adding 1.1 mL of glycine 1.25 M for 5 min. Samples were rinsed in washing buffer (HEPES pH 7.4 20 mM, NaCl 150 mM, Glycine 0.125 M, PMSF 10 mg/ml). Nuclei were extracted in lysis buffer (HEPES pH 7.4 20 mM, NaCl 150 mM, Glycine 0.125 M, SDS 1% PMSF 10 mg/ml) and collected by centrifugation (2200rcf for 5 min) before sonication in 1.2-mL sonication buffer (HEPES pH 7.4 20 mM, NaCl 150 mM, Glycine 0.125 M, SDS 0.4% PMSF 10 mg/ml) six times for 5 s. DNA fragments were separated from cellular debris by spinning at 14000rcf for 10 min. After collecting the supernatant, fragmentation quality was evaluated by gel electrophoresis. DNA fragments were split in $3 \times 300 \mu\text{l}$ samples and precleared with resin Slurry solution (resin/equilibration buffer, 50/50 volume) by adding 50 μl of this solution to each sample and incubating for 1 h at 4 °C. Supernatant was collected after spinning at 800rcf for 2 min at 4 °C and incubated ON at 4 °C with 3 μg of dedicated antibodies: Nr2f1 antibody (Thermo Fisher PA5-21611) and GFP antibody (Abcam ab13970, as an internal negative control for aspecific binding). A sample called Mock was obtained using a blank volume of Sonication buffer with no antibody. About 50 μl of Slurry solution was added to each sample, and all samples were incubated 3 h at 4 °C and washed four times in ice-cold washing buffer A (HEPES pH 7.4 20 mM, NaCl 150 mM, Triton 100 1%, SDS 0.1% PMSF 10 mg/ml), four times in ice-cold washing buffer B (Tris pH 8.0 20 mM, EDTA 1 mM, LiCl 250 mM, NP-40 0.5%, Na-Deoxycholate 0.5%, PMSF 10 mg/ml), and two times in TE buffer (Tris HCl pH 8.0 20 mM, EDTA 1 mM, PMSF 10 mg/ml). Finally, DNA fragments were eluted by adding 300 μl of Elution buffer (NaHCO₃ 50 mM, 1% SDS) and incubating in rotation 1 h at RT. Input samples were generated by mixing 300 μl of elution buffer to 10 μl of the supernatant from the first washing of a sample without antibody. Fragments were separated from the resin and antibodies by spinning twice at 8000rcf for 2 min and recovering the supernatant. Next, we reversed crosslink by adding 12 μl of NaCl 5 M to the samples and by incubating ON at 65 °C. Any RNA contamination was

removed by adding 1 μl of RNase-A 10 mg/ml and incubating for 30 min at 37 °C; the reaction was blocked adding 6 μl of EDTA 0.5 M. Remaining proteins were digested by adding 12 μl of Tris HCl pH 8.0 and 1 μl of proteinase K 10 mg/ml for 1-2 h at 45 °C. Finally, samples were purified by phenol-chloroform extraction and precipitated into 20 μl of H₂Omq.

qPCR of ChIP Samples

qPCRs on ChIP were performed using KAPA Sybr Fast (Kapa Biosystems) according to manufacturer's instructions. Samples were run on a LigthCycler II 480 (Roche) with the primers listed in [Supplementary Table 4B](#). For each reaction of 0.5 μl of sample, 0.2 μM of primers were added. For proper quantification, a calibration curve was calculated, by running six sequential 1:10 dilutions of a sample with known starting concentration for each set of primers. Each reaction was carried out in three technical replicates: negative controls including the use of aspecific antibody, no antibody, and mock and input samples. Samples were normalized on the input and set to 1, and the fold change was then calculated as the ratio between specific antibodies samples to aspecific antibody controls.

Statistical Tests

Hierarchical clustering was performed with Euclidean distance, using both average burst frequency and correlation per condition. In [Figure 2](#), three-way ANOVA to determine relevant parameters driving differences for Ca²⁺ transient frequency, coordination, and frequency variability was used; *post hoc* testing was performed using Welch two-samples test. In [Figure 6A](#), Welch's unequal variances *t*-test analysis correcting the *P*-value for multiple testing using the Benjamini-Hochberg procedure, false discovery rate = 0.25 was utilized. Data analysis scripts were custom-prepared in R ([Computing RfFs 2018](#)) and MATLAB. Additional statistical analyses were also performed using Graphpad Prism7, and data are presented as mean \pm SEM. *n* values represent biological replicates from ≥ 3 different brains and ≥ 3 different litters as stated in each figure legends or supplementary tables. No statistical tests were used to predetermine sample size, but samples sizes were similar as reported in previous publications ([Del Pino et al. 2013](#); [Del Pino et al. 2017](#)) or as generally employed in the field. No randomization was used. Whenever possible, both genotypes were processed in parallel on the same day. *Ex vivo* electrophysiology experiments and analysis of all data were performed before genotyping. Differences were considered significant when $P < 0.05$. Data sets were tested for normality (Kolmogorov-Smirnov) or homoscedasticity (Levene test) before performing parametric (Student *t*-test, one-way, two-way, or three-way ANOVA followed by Bonferroni's *post hoc* test) or nonparametric tests (Welch's unequal variances *t*-test or Mann-Whitney test) used to determine *P*-values (See also [Supplementary Tables 1-5](#)).

Results

Altered Intrinsic Network and Bursting Activity in Cultured Nr2f1-Deficient Cortical Neurons

To understand whether early molecular misspecification of mS1 was accompanied by changes in intrinsic neocortical activity, we first assessed network activity in neocortices lacking *Nr2f1* independently of thalamic afferents by employing a conditional mutant mouse in which *Nr2f1* is exclusively deleted from the cortex (referred as *Nr2f1cKO*). We compared

network activity of dissociated mutant mS1 cortical neurons to that of *Ctrl* M1 and S1 neurons at E18.5 by culturing them onto microelectrode arrays (MEAs). This allowed us to follow activity in an *in vitro* embryo-derived model at different times of cortical network maturation in the absence of subcortical inputs and assess the possible effect of cell-autonomous developmental programs on functional network organization (Fig. 1 and Supplementary Fig. 1).

Our recordings of primary-cultured neuronal networks started at 9DIV, since 6DIV neuronal cultures failed to show any activity in either *Ctrl* or *Nr2f1cKO* conditions. A comparison of the average firing frequency of the earliest events taking place at 9DIV showed a significantly lower firing frequency in mS1 *Nr2f1cKO* than in *Ctrl* S1 and M1 networks (Fig. 1A–D). In addition, whereas there was no significant difference in the average number of bursts recorded from *Ctrl* S1 and *Nr2f1cKO* mS1 networks, both of them displayed significantly lower burst numbers when compared to *Ctrl* M1 networks (Fig. 1E). We also found that the burst duration of *Ctrl* M1 and mutant mS1 was higher than that of *Ctrl* S1 neurons (Fig. 1F). However, firing activity was more organized into bursts in *Nr2f1cKO* mS1 neurons than in *Ctrl* S1 and M1, resulting in a higher firing synchronization index (Fig. 1G–H). These findings show that at 9DIV, loss of *Nr2f1* leads to an overall reduced firing frequency but prolonged burst duration and increased network synchronization in mS1 neurons when compared to control M1 and S1.

To explore the maturation of this cortical network activity, we performed similar experiments in neuronal cultures at 15DIV and 20DIV (Supplementary Fig. 1). At 15DIV, we observed that the firing frequency of *Ctrl* cortical networks reached a higher value than at 9DIV and 20DIV (data not shown). We therefore compared firing parameters measured at 15DIV with those measured at 9DIV to assess whether network maturation was affected *in vitro*. Interestingly, the extent of developmental increase in firing activity, number of bursts, and burst duration was lower in *Nr2f1cKO* mS1 and *Ctrl* M1 neuronal networks than in *Ctrl* S1 (Supplementary Fig. 1A–C). Since network maturation correlates with the expression of synchronized events organized in bursts, the evaluation of the percentage of spikes organized in bursts and the cross correlation index represent two parameters of network maturation *in vitro* (Gavello et al. 2012; Gavello et al. 2018). We found that the percentage of spikes within bursts (Supplementary Fig. 1D), as well as the cross-correlation index (Supplementary Fig. 1E), were significantly smaller in both *Nr2f1cKO* mS1 and *Ctrl* M1 neurons compared to *Ctrl* S1 neurons. These data unveil that network properties, involved during maturation of *Ctrl* M1 neurons, are similar in *Nr2f1cKO* mS1 but not in *Ctrl* S1 neurons.

Finally, the differences in firing patterns here reported are determined by a combination of neuronal intrinsic and synaptic factors, such as network connectivity, potentially related to glial function. Despite glial cells being fundamental for neuronal function and network maturation, we have not specifically investigated potential changes in glial cell number or function in *Nr2f1cKO* mS1-derived cultures, and rather focused our investigation on neuronal factors.

Alterations in Ca²⁺ Transients and Synchronous Activity in Early Postnatal *Nr2f1*-Deficient Cortices

As a further step toward understanding how spontaneous cortical network activity develops in the immature *Nr2f1cKO*

mouse pups, we set up a Ca²⁺ imaging protocol in *ex vivo* acute brain slices of P1 and P4 mouse pups using the calcium indicator Oregon Green BAPTAM (TM superscript please). These two stages represent critical timepoints of early cortical somatosensory circuit establishment bridging the activity from spontaneous thalamic waves (Anton-Bolanos et al. 2019) to experience-driven thalamic inputs (Corlew et al. 2004). Cells that displayed Ca²⁺ transients as a result of prolonged neuronal activation typical of excitatory neurons were recorded over 15 min (Fig. 2, see Materials and Methods). To evaluate the level of cortical network maturation, we measured the correlation index of Ca²⁺ transients for each experiment. This index is a measure of simultaneously active cells during a specific transient and is calculated as the ratio of active neurons displaying a Ca²⁺ transient within a 3-s window, normalized on the total number of active neurons and the total amount of transients within the same experiment (Fig. 2A and Supplementary Fig. 2, see Materials and Methods).

At P1, we observed differences in Ca²⁺ transient frequency (Hz) between *Ctrl* M1 and S1 and between *Ctrl*s and *Nr2f1cKO* mS1, indicating that the mS1 network retains properties distinct from both S1 and M1 (Fig. 2B and Supplementary Table 1). At P1, the Ca²⁺ correlation index did not display differences across either areas or genotypes (Fig. 2C and Supplementary Table 1), implying that no evident circuit maturation differences were found at this stage. At P4, an overall increase of Ca²⁺ transient frequency (Hz) was observed in all conditions (Fig. 2B and Supplementary Table 1), in line with previous observations (Corlew et al. 2004). At this stage however, comparison of the correlation index among areas and genotypes showed a statistical difference between *Ctrl* M1 and S1 as well as between *Ctrl* S1 and *Nr2f1cKO* mS1 (Fig. 2C and Supplementary Table 1). This was accompanied by an overall decrease of the variability of Ca²⁺ transient frequency in *Ctrl* S1 and M1, indicating higher coherence of spontaneous activity across measured cells (Fig. 2D and Supplementary Table 1). On the other hand, *Nr2f1cKO* mS1 cells failed to show any significant decrease of the variability of Ca²⁺ transient frequency (Fig. 2D and Supplementary Table 1).

Taken together, our data show that loss of *Nr2f1* function alters Ca²⁺ frequency and Ca²⁺ correlation index of mutant mS1 cells at perinatal stages.

Abnormal Intrinsic Electrophysiological Properties in Early Postnatal *Nr2f1*-Deficient Cortical LVPNs

Since intrinsic electrophysiological properties are related to the expression of neural activity, we next examined the state of the intrinsic excitability of pyramidal neurons in *Nr2f1cKO* mouse cortices, previously shown to express an altered molecular signature (Tomassy et al. 2010; Harb et al. 2016). We measured their intrinsic excitability profile in *Ctrl* M1 and S1 as well as *Nr2f1cKO* mS1 in acute brain slices from 5- to 8-day old (P5–8) mouse pups. At this developmental stage, corticogenesis and neural migration already took place, and neocortical neurons have differentiated from an immature spiking phenotype, acquiring instead a regular type of spiking (Massengill et al. 1997). We employed whole-cell recordings in current-clamp mode and performed the measurements in the absence of synaptic blockers since, at this developmental stage, the number of synaptic inputs is very low (Favuzzi et al. 2019) and spontaneous activity rarely occurred in our recording conditions. In order to compare electrophysiological properties of *Ctrl* M1 and S1 with those of

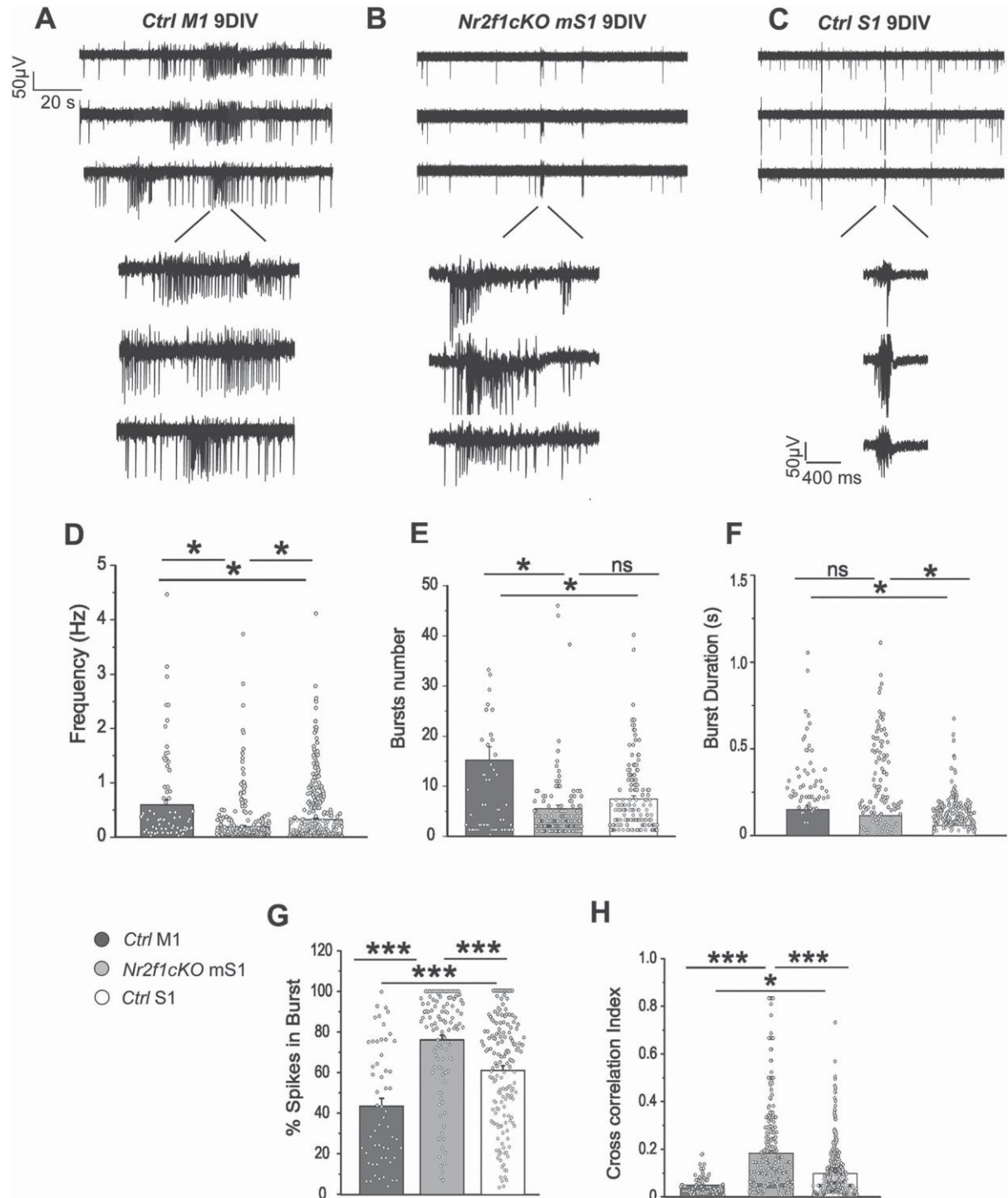


Figure 1. Impaired intrinsic network and bursting activity recorded in DIV 9 cultured *Nr2f1*-deficient cortical neurons. (A–C) Spontaneous firing of *Ctrl S1*, *Nr2f1cKO mS1*, and *Ctrl M1* cortical network recorded by three representative MEA at 9 DIV. In insets, representative bursts shown at expanded scale. Firing parameters from *Ctrl S1* ($N = 10$), *Nr2f1cKO mS1* ($N = 12$), and *Ctrl M1* ($N = 7$) MEAs are compared. (D) Average firing frequency from *Ctrl M1* MEA was 0.63 ± 0.16 Hz ($N_{\text{channels}} = 76$), from *Nr2f1cKO mS1* MEA was 0.30 ± 0.04 Hz ($N_{\text{channels}} = 208$), and from *Ctrl S1* MEA was 0.41 ± 0.04 Hz ($N_{\text{channels}} = 271$). (E) Average bursts number from *Ctrl M1* MEA was 14.91 ± 2.73 ($N_{\text{channels}} = 56$), from *Nr2f1cKO mS1* MEA was 5.51 ± 2.73 ($N_{\text{channels}} = 203$), and from *Ctrl S1* MEA was 7.21 ± 0.67 ($N_{\text{channels}} = 170$). (F) Average burst duration from *Ctrl M1* MEA was 0.38 ± 0.07 s ($N_{\text{channels}} = 56$), from *Nr2f1cKO mS1* MEA was 0.31 ± 0.02 s ($N_{\text{channels}} = 112$), and from *Ctrl S1* MEA was 0.15 ± 0.02 s ($N_{\text{channels}} = 169$). (G) Percentage of spikes in burst from *Ctrl M1* MEA was $43.08 \pm 3.88\%$ ($N_{\text{channels}} = 56$), from *Nr2f1cKO mS1* was $76.03 \pm 2.39\%$ ($N_{\text{channels}} = 114$), and from *Ctrl S1* MEA was $60.96 \pm 2.06\%$ ($N_{\text{channels}} = 167$). (H) Cross correlation index from *Ctrl M1* MEA was 0.05 ± 0.01 ($N_{\text{channels}} = 56$), from *Nr2f1cKO mS1* MEA was 0.18 ± 0.01 ($N_{\text{channels}} = 258$), and from *Ctrl S1* MEA was 0.09 ± 0.01 ($N_{\text{channels}} = 256$). Data are represented as mean \pm SEM. Significance is shown above: * $P < 0.05$; ** $P < 0.01$, *** $P < 0.001$. ns, not significant. Sampling and statistical test listed in Supplementary Table 5.

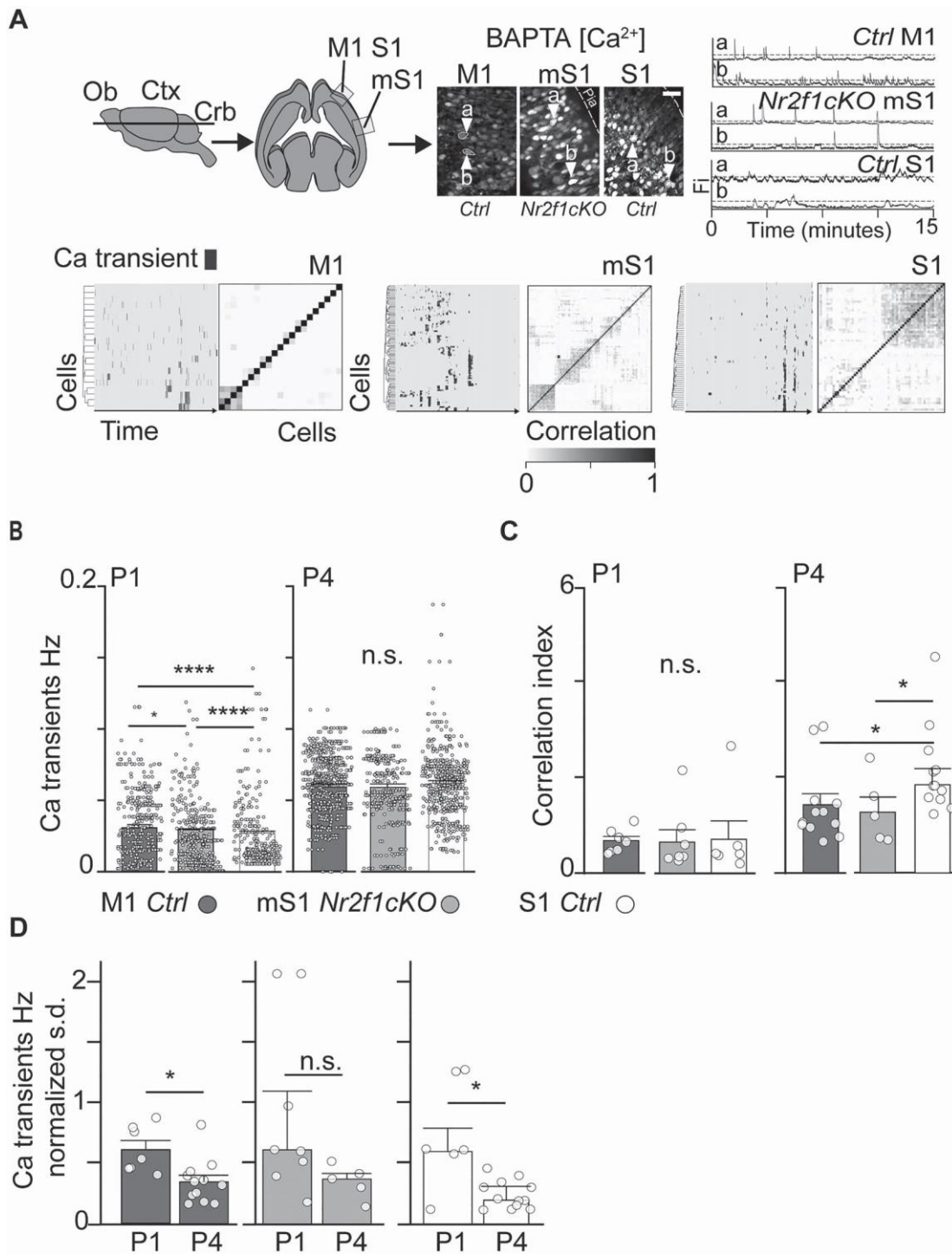


Figure 2. Altered Ca²⁺-dependent intrinsic activity upon *Nr2f1* loss. (A) Top left: schematics of the acute horizontal slice preparation, from which we recorded the primary motor (M1) and somatosensory (S1) areas (S1 and M1 in *Ctrl* and mS1 in *Nr2f1cKO* brains) based on their respective rostral and medial position. Top center: representative image of the Ca²⁺ BAPTA fluorescent signals for each area. Top right: time series of intracellular signals in manually defined cells (indicated in the previous panels with white arrowheads) corrected by moving average (F). Ca²⁺ transients are defined by distinct thresholds. Bottom: time series matrices of above threshold Ca²⁺. Single traces have been sorted by Euclidean distance (left). Pearson correlation matrices of single neuron signal traces within single experiment (right). Distribution of single cell Ca²⁺ transient frequency (Hz) (B) and transient intraneuron correlation (C) in P1 and P4 brains. For Ca²⁺ transients, single points indicate cells; for Ca²⁺ correlation, single points are single time-lapse images; some slices have been recorded multiple times; each animal was recorded over more slices. (D) Standard deviation (s.d.) of Ca²⁺ transients frequency normalized to the mean indicates a progressive decrease of frequency variability with age in both *Ctrl* M1 and S1, while no decrease is measured in *Nr2f1cKO* mS1. Statistical scripts were custom-prepared in R (Computing RFFS 2018). Sampling and statistical tests are listed in [Supplementary Table 5](#). Abbreviations: Ob, Olfactory bulb; Ctx, Cortex; Crb, Cerebellum; M1, motor cortex; mS1, motorized somatosensory cortex; P, postnatal day; and S1, somatosensory cortex. **P* < 0.05, ***P* < 0.01, *****P* < 0.001. Scale bar: 10 μm. See also [Supplementary Figure 2](#) and [Supplementary Tables 1](#) and [5](#).

Nr2f1cKO mS1 neurons, we focused on similar neuronal populations by selecting neurons that were identified as layer V pyramidal neurons (LVPNs), as defined by *post hoc* morphological reconstructions. Although LVPNs differentiate into two major types in terms of morphology and intrinsic physiology in adult brains, these two LVPN types are not well differentiated at the electrophysiological level during early postnatal stages (Kasper et al. 1994; Christophe et al. 2005). Among all recorded cells, we analyzed 28 *Nr2f1cKO* neurons in mS1 (from 7 different brains) as well as 10 *Ctrl* M1 and 19 *Ctrl* S1 neurons (from 8 different brains) located within the layer V and displaying a slowly adapting regular spiking firing pattern (Fig. 3A). Notably, specific changes in passive and active electrophysiological properties were observed in *Nr2f1cKO* mS1 neurons when compared to both *Ctrl* M1 and S1 neurons (Supplementary Table 2). Mutant mS1 LVPNs displayed a more depolarized resting membrane potential (V_{rest}) than *Ctrl* S1 LVPNs, but no significant differences when compared to *Ctrl* M1 LVPNs (Fig. 3B). In addition, mS1 LVPNs displayed a significantly decreased rheobase compared to *Ctrl* M1 and S1 LVPNs (Fig. 3C). Interestingly, *Nr2f1cKO* mS1 LVPNs also exhibited a reduced voltage sag in response to hyperpolarizing current steps, suggesting a more reduced I_h than *Ctrl* LVPNs (Fig. 3D). Finally, *Nr2f1cKO* mS1 LVPNs also exhibited a significantly higher maximum firing frequency than *Ctrl* M1 LVPNs, but no significant differences when compared to *Ctrl* S1 LVPNs (Supplementary Table 2). No significant changes in input resistance, AP threshold, AP amplitude, AP half-width, ISI, latency for AP generation, membrane time constant (τ_m), or capacitance were observed in mutant LVPNs (Supplementary Fig. 3 and Supplementary Table 2). Taken together, this functional characterization suggests that within the immature and *Nr2f1*-deficient mS1 cortex, LVPNs display alterations in their intrinsic excitability. Particularly, these neurons show a unique electrophysiological signature differing from *Ctrl* S1 and M1 LVPNs in some but not all intrinsic properties.

Reduced Dendritic Complexity of LVPNs in *Nr2f1* Mutant Cortices

To assess whether abnormal intrinsic excitability of P5-P8 mutant mS1 LVPNs was accompanied by changes in dendritic morphology, we reconstructed and analyzed the LVPNs that were filled with biocytin after patch clamp recording (Fig. 4A-C). We first evaluated dendritic arbor geometry and complexity by performing Sholl analysis. Comparison of Sholl profiles revealed that mS1 *Nr2f1cKO* LVPNs had a significantly reduced proximal dendritic branching pattern (20–100 μm from the soma) than both *Ctrl* M1 and S1 LVPNs (Fig. 4D and Supplementary Table 3), whereas minor or no differences were observed in distal regions (Supplementary Fig. 4A and Supplementary Table 3). Next, to evaluate more specific features of the dendrite geometry, we assessed the basal dendrite complexity index (bDCI), arbor length, number of primary dendrites, branching points and tips, and oblique formations of basal and apical dendrites of mutant mS1 and *Ctrl* M1 and S1 neurons (Fig. 4E-I and Supplementary Fig. 4B-D). Our morphological data point to a generally less elaborate basal dendrite formation in mutant mS1 LVPNs, whereas no significant differences were observed in apical and oblique dendrite geometry between *Nr2f1cKO* mS1 neurons and *Ctrl* M1 and S1 neurons. In particular, the bDCI was significantly reduced in *Nr2f1cKO* mS1 LVPNs compared to *Ctrl* cells from M1 and S1 cortices (Fig. 4E-F), as a result of a reduced number of primary dendrites, branching points,

and terminal tips (Fig. 4G-I). Overall, our data indicate that the loss of *Nr2f1* function affects the complexity of LVPN basal dendrite geometry in mS1 at early postnatal stages. Moreover, the structural differences observed between *Ctrl* M1 and mutant mS1 LVPNs show that despite expressing CTIP2, a *bona fide* marker for LVPNs (Armentano et al. 2007; Tomassy et al. 2010), these neurons differ in their morphological complexity and electrophysiological properties.

Reduced Conformation and Plasticity Properties of the Axon Initial Segment in Mutant *Nr2f1* LVPNs

Intrinsic excitability and dendritic changes are often associated with variations in the structural properties of the axon initial segment (AIS), a specialized structure playing a pivotal role in the integration of synaptic inputs and AP initiation (Kole and Stuart 2012; Yamada and Kuba 2016). It has been reported that distinct AIS features, such as length and/or location relative to the soma, are crucial for the homeostatic control of neuronal excitability in LVPNs (Hamada et al. 2016). The observed reduction of basal dendrite complexity, sag response, and the presence of a more depolarized resting membrane potential in mS1 (Fig. 3 and Supplementary Fig. 3) led us to hypothesize that structural changes of the AIS could occur in *Nr2f1cKO* LVPNs. This could act as a potential mechanism stabilizing AP generation, as observed in previous studies (Gulledge and Bravo 2016; Hamada et al. 2016). To test this hypothesis, we analyzed the AIS structure of P7 LVPNs *Ctrl* S1 and *Nr2f1cKO* mS1 cortices employing the cytoskeletal scaffolding protein Ankyrin G—a widely used marker of the AIS—(Kordeli et al. 1995; Zhou et al. 1998), together with CTIP2 (Arlotta et al. 2005), and NeuN, a neuronal marker labeling the soma (Fig. 5). Notably, we found a significantly reduced length and diameter of the Ankyrin-positive AIS as well as decreased distance from the soma in *Nr2f1cKO* mS1 compared with *Ctrl* S1 LVPNs (Fig. 5A-D). This suggests that altered intrinsic excitability and dendritic structure of mutant LVPNs might be correlated with changes in AIS conformation and localization (Grubb and Burrone 2010; Kuba 2010; Kuba et al. 2010; Wefelmeyer et al. 2016). Decreased length and diameter were also observed in P21 LVPNs (Fig. 5E-G), suggesting that altered AIS structure observed at P7 is most probably not the result of delayed neuronal maturation.

Finally, to assess whether the AIS of *Nr2f1*-deficient LVPNs would still respond to a plasticity-inducing stimulus despite its already reduced length and diameter, we applied a chronic depolarization protocol to *Ctrl* and *Nr2f1cKO* P7 acute brain slices (see Materials and Methods). In agreement with previous studies (Dumitrescu et al. 2016), the depolarization treatment reduced the relative AIS length of *Ctrl* LVPNs. In contrast, no significant changes were observed in the AIS size between depolarization and control treatment of *Nr2f1*-deficient LVPNs (Supplementary Fig. 5A,B). The failure of AIS response to increased neuronal activity in *Nr2f1*-deficient LVPNs suggests a common mechanism between increased excitability and loss of *Nr2f1* function.

Altered Expression of Ion Channels and Glutamate Receptors in Postnatal Cortices of *Nr2f1cKO* Mutants

Since neuronal intrinsic excitability is primarily determined by the expression, subcellular distribution, and biophysical properties of ion channels, we next tested the hypothesis that loss of *Nr2f1* function might alter neuron properties and

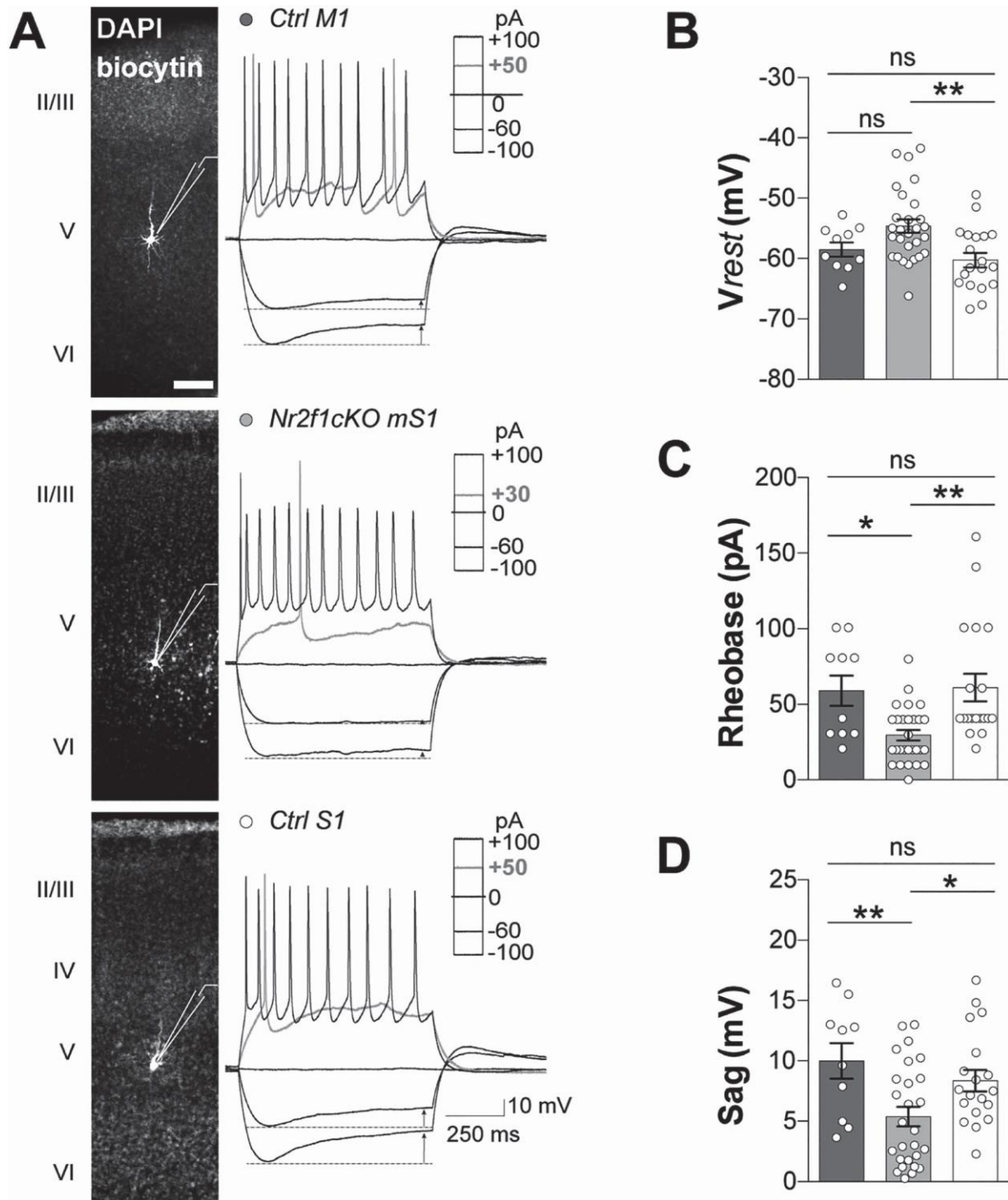


Figure 3. Abnormal intrinsic excitability of *Nr2f1*-deficient LVPNs. (A) LVPNs identified *post hoc* through fluorescent labeling for biocytin (in white) and DAPI (gray) in *Ctrl M1*, *Nr2f1cKO mS1* and *Ctrl S1* display slow-adapting regular spiking firing pattern. (B) Mean resting membrane potential (V_{rest}) is significantly different between the conditions (** $P = 0.0028$). Multiple comparisons show a significantly more depolarized V_{rest} in *Nr2f1cKO mS1* than in *Ctrl S1* neurons (** $P = 0.0025$) but not significantly different from M1 neurons ($P = 0.135$). (C) Rheobase is significantly different between the three conditions analyzed (** $P = 0.0017$). *Nr2f1cKO mS1* pyramidal neurons display a significantly reduced rheobase compared to *Ctrl M1* and *S1* neurons (* $P = 0.004$ in M1 vs. mS1 and ** $P = 0.003$ in S1 vs. mS1). (D) Sag is significantly different between the three conditions (** $P = 0.0063$). *Nr2f1cKO mS1* neurons display a significantly lower sag response to hyperpolarization compared to *Ctrl M1* (** $P = 0.0042$) and *S1* neurons (* $P = 0.020$). Abbreviations: II, III, IV, V, VI, cortical layers II–VI. Sampling and statistical test listed in [Supplementary Table 5](#). Data are represented as mean \pm SEM. Scale bar: 100 μ m. See also [Supplementary Figure 3](#) and [Supplementary Tables 2](#) and [5](#).

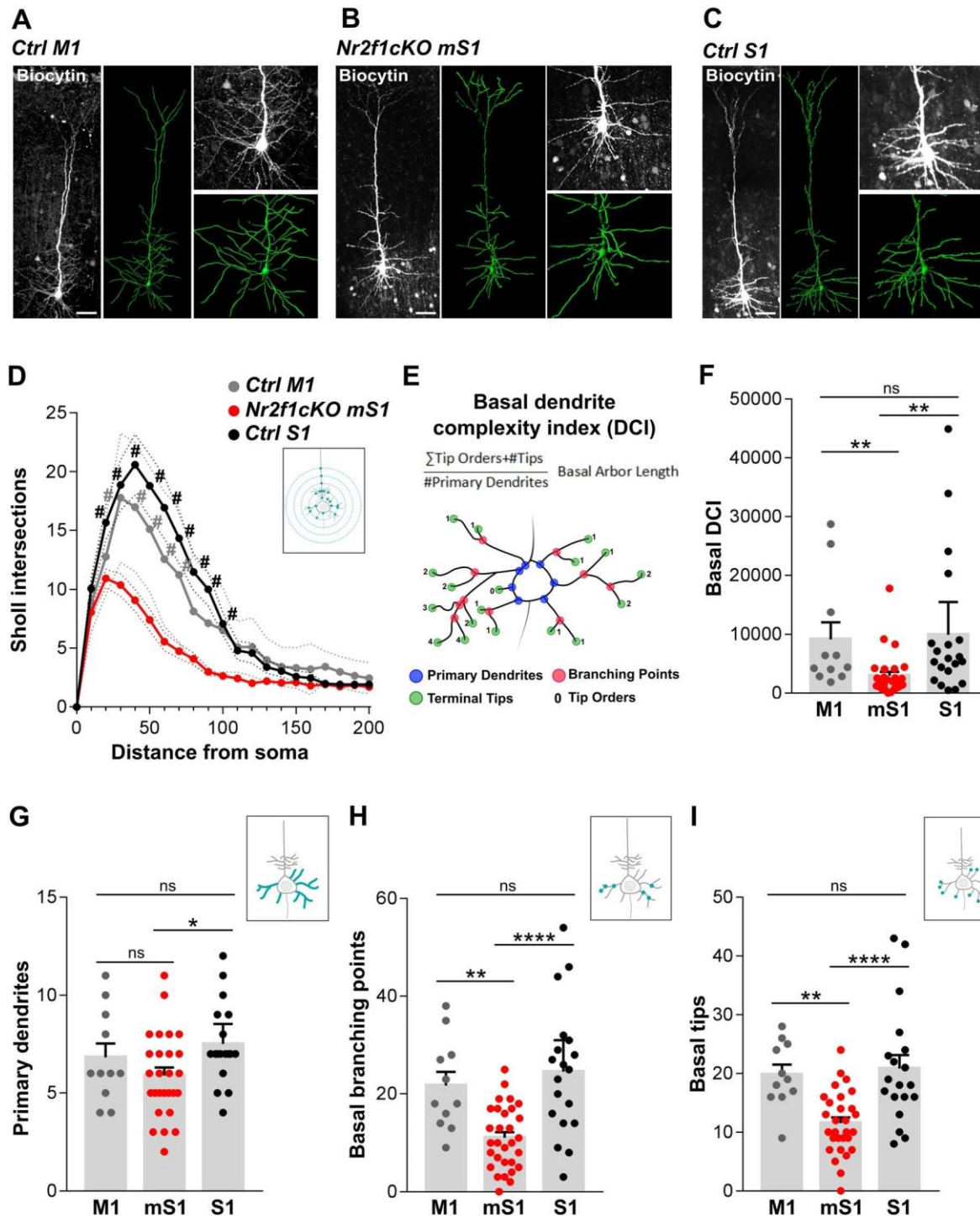


Figure 4. Reduced basal dendritic complexity of LVPNs in *Nr2f1* mutant cortices. Representative images of P7 *Ctrl M1* (A), *Nr2f1cKO mS1* (B), and *Ctrl S1* (C) LVPNs. In grayscale, maximum intensity projection of a multistack confocal image; in green, correspondent 3D reconstructions. On the right, magnifications of the basal structures. Scale bar: 50 μm. (D) Sholl analysis points to a reduction of the arborization complexity in *Nr2f1cKO mS1* LVPNs compared to both M1 and S1 control cells (# $P < 0.05$). For detailed statistics, see [Supplementary Table 3](#). (E) Basal DCI formula and schematic representation of primary dendrites, branching points, terminal tips, and tip orders. (F-I) Average basal DCI (*Ctrl M1*, 9148 ± 2838 ; *Nr2f1cKO mS1*, 2956 ± 658 ; *Ctrl S1*, 9902 ± 2650 ; *Ctrl S1* vs. *Nr2f1cKO mS1*, $P = 0.0025$; *Ctrl M1* vs. *Nr2f1cKO mS1*, $P = 0.0063$), number of primary dendrites (*Ctrl M1*, 6.82 ± 0.71 ; *Nr2f1cKO mS1*, 5.89 ± 0.41 ; *Ctrl S1*, 7.5 ± 0.49 ; *Ctrl S1* vs. *Nr2f1cKO mS1*, $P = 0.035$; *Ctrl M1* vs. *Nr2f1cKO mS1*, $P = 0.41$), basal dendrites branching point (*Ctrl M1*, 21.73 ± 2.81 ; *Nr2f1cKO mS1*, 11.03 ± 1.17 ; *Ctrl S1*, 24.58 ± 3.05 ; *Ctrl S1* vs. *Nr2f1cKO mS1*, $P < 0.0001$; *Ctrl M1* vs. *Nr2f1cKO mS1*, $P = 0.005$), and terminal tips (*Ctrl M1*, 19.82 ± 0.70 ; *Nr2f1cKO mS1*, 11.52 ± 0.99 ; *Ctrl S1*, 20.84 ± 2.265 ; *Ctrl S1* vs. *Nr2f1cKO mS1*, $P \leq 0.0001$; *Ctrl M1* vs. *Nr2f1cKO mS1*, $P = 0.0036$) are statistically reduced in mutant cells compared to controls. Data are represented as mean \pm SEM. Sampling and statistical test listed in [Supplementary Table 5](#). See also [Supplementary Figure 3](#) and [Supplementary Tables 3-5](#).

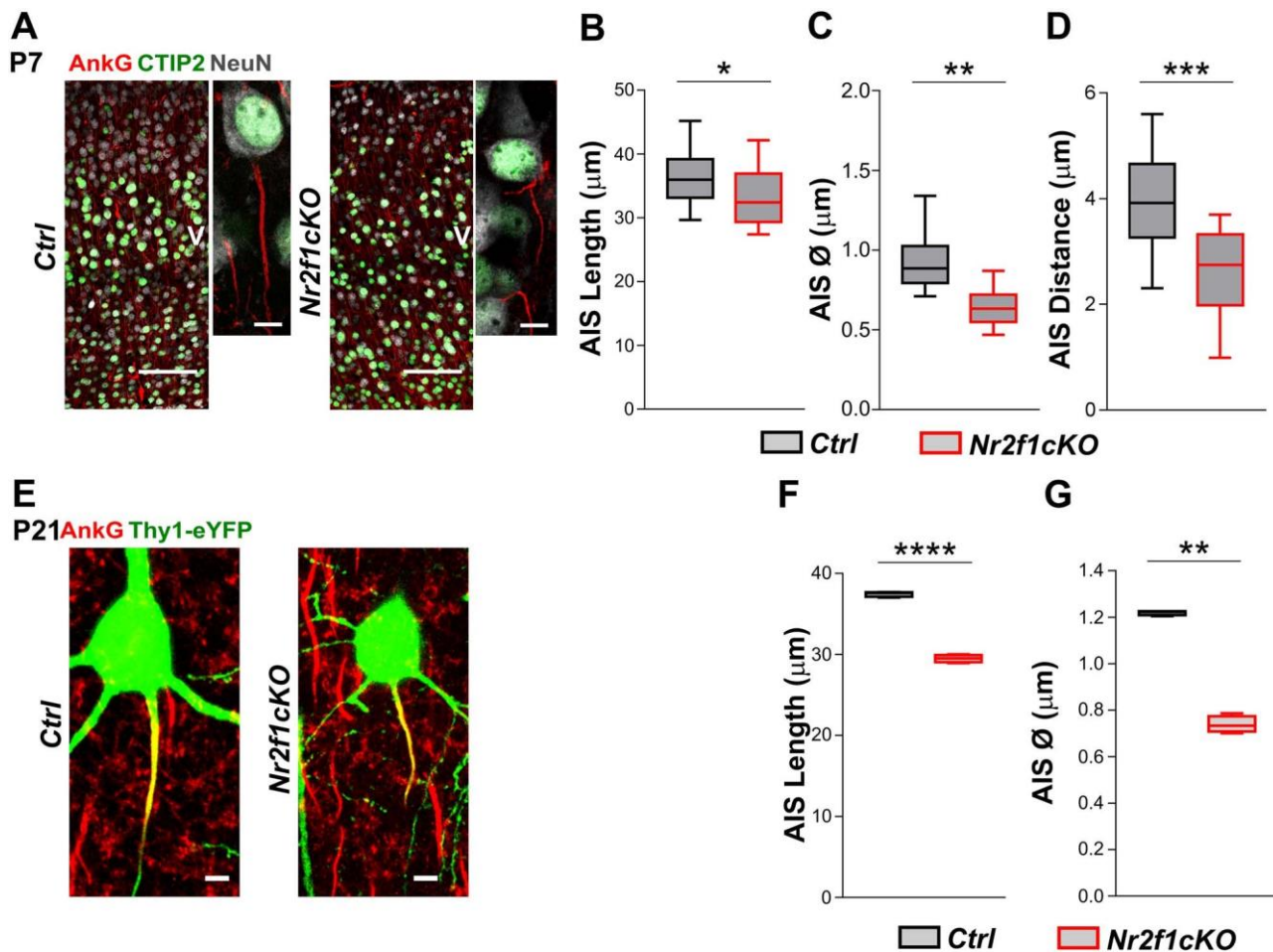


Figure 5. Abnormal structural features of the AIS in mutant *Nr2f1* LVPNs. (A) Left panel, coronal sections of P7 *Ctrl* S1 and *Nr2f1cKO* mS1 cortices labeled with CTIP2, for layer V identification, Ankyrin G for the AIS and NeuN as a somatic marker. Scale bar: 100 μ m. Right panel confocal images of triple stained *Ctrl* and *Nr2f1cKO* LVPNs. Scale bar: 10 μ m. (B–D) Average AIS length (*Ctrl*, 35.23 ± 0.67 ; *Nr2f1cKO*, 31.14 ± 0.32 ; $P = 0.0129$), diameter (*Ctrl*, 0.94 ± 0.006 ; *Nr2f1cKO*, 0.65 ± 0.004 ; $P = 0.0043$), and distance from the soma (*Ctrl*, 3.91 ± 0.21 ; *Nr2f1cKO*, 2.63 ± 0.2 ; $P = 0.0001$) are statistically reduced in *Nr2f1cKO* neurons compared with *Ctrl* at P7. (E) Confocal images of *Ctrl* (left) and *Nr2f1cKO* (right) LVPNs from P21 somatosensory cortices. In green, *Thy1-eYFP* reporter gene; in red, Ankyrin G. (F–G) Average AIS length (*Ctrl*, 37.46 ± 0.15 ; *Nr2f1cKO*, 29.51 ± 0.23 ; $P < 0.0001$) and diameter (*Ctrl*, 1.2 ± 0.005 ; *Nr2f1cKO*, 0.74 ± 0.02 ; $P < 0.0001$) are statistically reduced in *Nr2f1cKO* cells compared with controls at P21. Data are represented as mean \pm SEM. Sampling and statistical test listed in Supplementary Table 5. (See also Supplementary Fig. 5 and Supplementary Tables 4 and 5).

excitability through a modification of the expression of ion channels.

To this purpose, we performed RT-qPCR for an extensive list of K^+ , Na^+ , and Ca^{2+} channels specifically expressed in deep layers from *Ctrl* and *Nr2f1cKO* cortical lysates (Fig. 6A). Out of 33 ion channels that we could successfully test, we found a significant reduction in the mRNA levels of only *Hcn1*, *KCNAB1*, *Kcnk2*, *CACNA2D1*, *GRIA3*, and *Grin1* in *Nr2f1cKO* when compared to *Ctrl* brains (Fig. 6A and Supplementary Fig. 6). Notably, we found significantly decreased protein levels of the hyperpolarization-activated cation channel HCN1 (Shah 2014) in *Nr2f1cKO* (Fig. 6B and Supplementary Fig. 7). Moreover, double staining of HCN1 and CTIP2 on cortical sections at P7, when HCN1 expression becomes detectable in cell bodies (Fig. 6C), confirmed decreased HCN1 protein signal intensity in CTIP2-expressing LVPNs, as well as a reduced number of double CTIP2/HCN1 positive neurons in mutant neurons compared to *Ctrl*s (Fig. 6D,E), supporting overall reduction of HCN1 protein in layer V neurons of *Nr2f1cKO* mutant brains.

Finally, we investigated whether voltage-gated ion channels, whose transcript levels were found altered in mutant brains, were directly regulated by *Nr2f1*. To address this, we searched for evolutionary conserved binding sites for *Nr2f1* on the group of differentially expressed genes using the ECR browser tool (Ovcharenko et al. 2004; Loots and Ovcharenko 2007). By using MatInspector (Quandt et al. 1995) and ChromAnalyzer (Montemayor et al. 2010), we identified putative binding sites for *Nr2f1* at 25 kb of the 5'UTR of *Hcn1*, 3 kb of the 5'UTR of *KCNAB1*, and proximal to the 5'UTR of *Kcnd2* loci (Fig. 6F). These sites mainly match the *Nr2f1* canonical binding sequence consisting of direct repeats with variable spacer configurations, as previously described (Montemayor et al. 2010). Notably, we observed that the binding sequence on the *Hcn1* locus matched the expected consensus site (Fig. 6F, red nucleotides). To experimentally test the direct regulation of the expression of these ion channels by *Nr2f1*, we performed chromatin immunoprecipitation (ChIP) assay on whole newborn *Ctrl* cortices using a

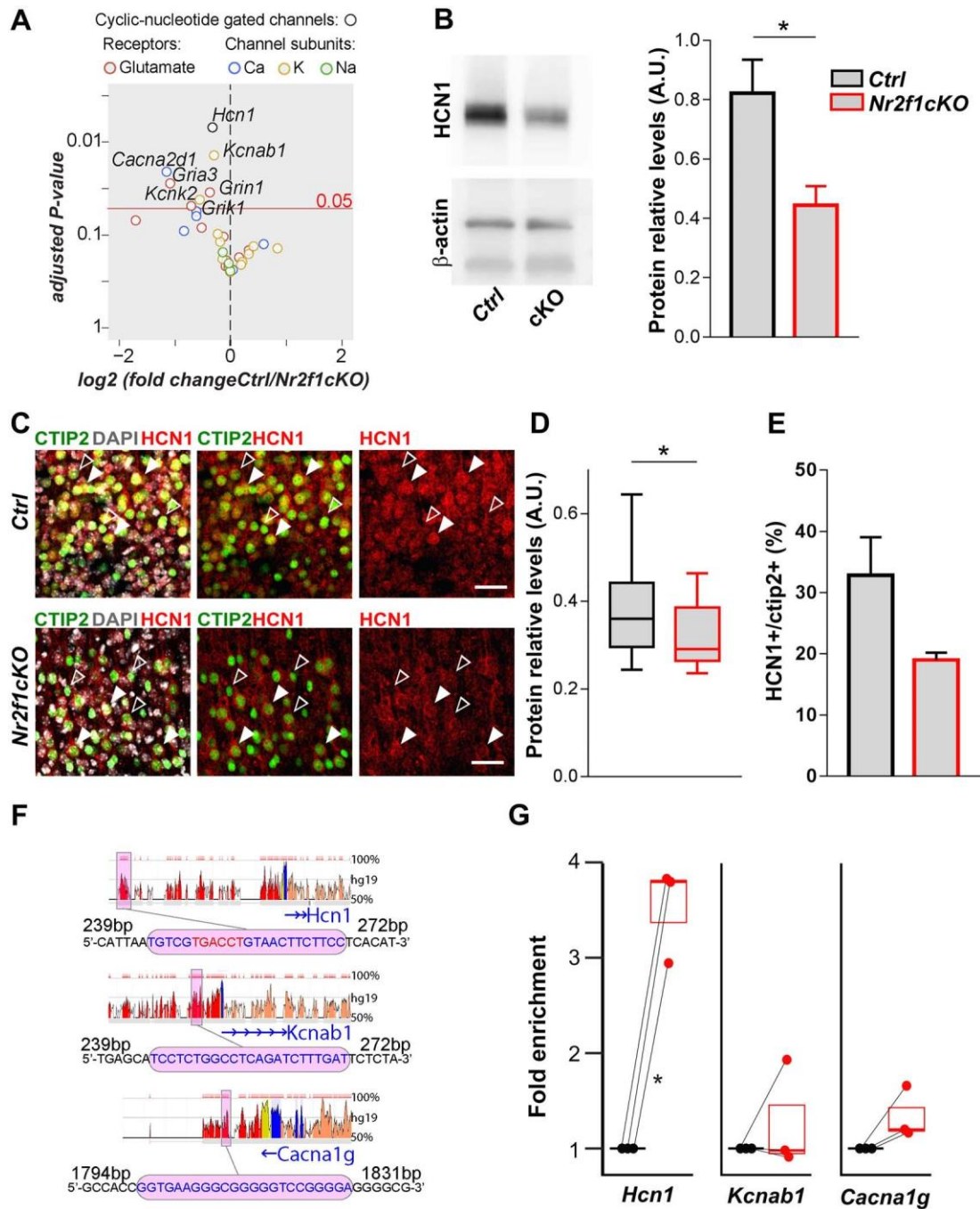


Figure 6. Regulation of ion channel-expression levels by *Nr2f1*. (A) Data plot of qPCR analysis on P7 *Ctrl* and *Nr2f1cKO* cortices. The red line represents the threshold for significance. Significantly downregulated genes are depicted in the upper left panel. (B) Western blot analysis of HCN1 protein shows a significant reduction in *Nr2f1cKO* P7 cortices (*Ctrl*, 0.822 ± 0.11 ; *Nr2f1cKO*, 0.44 ± 0.064 ; $P = 0.05$). (C) CTIP2-HCN1 double IF staining of P7 somatosensory cortices. (D) Box and whiskers plot distribution of HCN1 cell signal intensity points to a reduction of HCN1 in *Nr2f1cKO* LVPNs (*Ctrl*, 0.89 ± 0.03 ; *Nr2f1cKO*, 0.71 ± 0.01 ; $P = 0.015$). (E) The number of HCN1⁺ cells within the LVPN CTIP2⁺ population tends to be reduced in *Nr2f1cKO* cells (*Ctrl*, 32.81 ± 6.24 ; *Nr2f1cKO*, 18.99 ± 1.19 ; $P = 0.15$). (F) Snapshots from Evolutionary Conserved Regions browser showing *Nr2f1* binding location and sites (in pink; red nucleotides highlighting the canonical direct repeat of *Nr2f1* binding site: TGACCT); intergenic regions (red); UTR (yellow); exons (blue); and introns (orange). (G) Immunoprecipitation of chromatin (ChIP) indicates that *Nr2f1* binds these sites with different affinities. All data are expressed as “relative” fold enrichment and normalized against ChIP performed on the same samples with an anti-GFP as an aspecific antibody. Data are represented as mean \pm SEM. Sampling and statistical test listed in Supplementary Table 5. See also Supplementary Figure 6 and Supplementary Tables 4 and 5.

well-established Nr2f1 antibody (Alfano et al. 2011; Parisot et al. 2017). Quantitative PCR (qPCR) analysis of immunoprecipitated material showed a reproducible 3- to 4-fold significant enrichment of Nr2f1 versus GFP unspecific binding only on the *Hcni* locus and not on the *KCNAB1* or *CACNA1G* loci (Fig. 6G), despite their altered transcript levels quantified in mutant brains (Supplementary Fig. 6). These data on the molecular landscape of the somatosensory cortex indicate that while expression levels of several ion channels might be modulated by Nr2f1 during cortical development, only few of them seem to be directly controlled by this factor. We thus hypothesize that the changes in neuronal activity induced by Nr2f1 can have secondary consequences for a number of activity-dependent neuronal and network maturation processes. Overall, we identified *Hcni* gene, whose protein product is known to determine voltage sag and intrinsic excitability, as one of several putative direct targets (Brager et al. 2012; Zhang et al. 2014; Fan et al. 2016).

Discussion

Our work reveals early developmental alterations in spontaneous activity and intrinsic excitability of the neocortex in a mouse model of cortical patterning abnormalities. We propose that *Nr2f1* expression within the immature S1 cortex is required for the emergence of S1 area-specific features that go beyond molecular and topographic connectivity, as previously reported (Armentano et al. 2007; Alfano et al. 2014). Here, we show that Nr2f1 does not only play a key role in imparting somatosensory identity to young neurons (Alfano et al. 2014), but that it also regulates the development of proper neocortical activity patterns and bioelectrical properties. Therefore, our data provide an additional link between intrinsic genetic determination of proto-areas and spontaneous cortical activity in the immature cortex through the regulation of membrane ion channels in glutamatergic pyramidal neurons (summarized in Fig. 7).

Cortical and Thalamic Early Developmental Activity Governing Proper Formation of Somatosensory Maps

In this study, we show that loss of cortical Nr2f1, known to determine sensory identity of early differentiating neurons (Alfano et al. 2014), also impacts on intrinsic network activity within the immature neocortex. These findings indicate that, in addition to acquiring motor-like properties in terms of early molecular fate specification, mS1 neurons undergo unique changes in intrinsic electrophysiological properties in a manner that is different from S1 but also distinct from M1 electrophysiological identities.

A recent study reports that prenatal activity of thalamic neurons can influence somatosensory map formation in the cortex before the emergence of sensory inputs (Anton-Bolanos et al. 2019). Upon blockade of thalamic calcium waves, the neocortex becomes hyperexcitable, the columnar and barrel organizations are perturbed, and the somatosensory map lacks anatomical and functional structure. Perturbation of laminar and columnar development of the barrel cortex has also been observed in transgenic mice in which glutamatergic release was disrupted in thalamocortical axons (Li et al. 2013). This could imply that impaired organization of the somatosensory map observed in *Nr2f1* KO mutants is caused by the absence of prenatal thalamic inputs reaching the mutant cortex. This hypothesis, however,

is not entirely supported by our data, since thalamic axons do reach the subplate in *Nr2f1* mutant prenatal cortices (Armentano et al. 2007). Nevertheless, thalamocortical interactions in *Nr2f1* mutants may be dysfunctional due to pre- or postsynaptic mechanisms. For example, presynaptic alterations of incoming thalamocortical axons may be due to the altered expression of cortical molecular cues. A nonexclusive, interesting hypothesis that arises from our results, is that of altered properties of postsynaptic mis-differentiated S1 neurons in *Nr2f1* mutant cortices. We have demonstrated that neuronal intrinsic properties, morphology, and spontaneous activity are altered in the S1 region of mutant brains at a critical period for thalamocortical interactions that are crucial for proper laminar and columnar development of the barrel cortex. Hence, the early expression of arealization genes, such as *Nr2f1*, might be necessary to set up proper postsynaptic properties and synchronized activity patterns within the immature somatosensory cortex.

Nr2f1 Controls Determinants of Spontaneous Network Activity

Developmental spontaneous activity has already been described to follow a regionalized pattern in the cortex (Corlew et al. 2004; Uhlen et al. 2015) and to ultimately influence the assembly of long-range circuit connections (Tritsch et al. 2007; Blankenship et al. 2011; Yamamoto and Lopez-Bendito 2012; Schneggenburger and Rosenmund 2015; Anton-Bolanos et al. 2019). However, how spontaneous activity is first triggered and then finely modulated during the formation of the neocortical protomap is still unclear. In the mouse neocortex, large plateaus of synchronized network activity at birth are followed by early network oscillations and giant depolarizing potentials during the first postnatal week (Allene et al. 2008; Allene and Cossart 2010). Multiple aspects that relate to intrinsically regulated maturation of pyramidal neurons might influence the developmental sequence of cortical network activity. Our data provide a novel characterization at electrophysiological and molecular levels of intrinsic excitability features in S1 that are influenced by abnormal patterning of the somatosensory cortex in the absence of *Nr2f1* during the first postnatal week. Our hypothesis that *Nr2f1* expression could influence molecular determinants relevant for early neuronal network activity is corroborated by previous transcriptome analyses. Indeed, *Nr2f1* loss in postmitotic cortical cells regulates the expression of several activity-related genes, such as *CHRNA7*, *Kcnq3*, *Kcnlp4*, *Robo1*, and *Sv2b* (Alfano et al. 2014). However, the direct impact of these candidates on immature cortical neuron activity still remains to be investigated.

Several studies have also highlighted the role of cell intrinsic and presynaptic factors in determining cortical network development with potential long-term effects (Boillot et al. 2016; Murase et al. 2016). For example, the transcription factor Tbr1, known to regulate cortical layer identity, also alters the intrinsic excitability of neocortical neurons, by regulating HCN1 transcription in neonates and increasing sag response in layer VI (Fazel Darbandi et al. 2018). Thus, among several possible pathways involving ion channels, regulation of HCN1 levels is potentially an example of common mechanisms used by early transcriptional regulators to modulate spontaneous network activity within the developing cortex.

Within immature cortical networks, the earliest patterns of correlated spontaneous activity (synchronous plateau assemblies) are thought to arise from voltage-gated conductance and

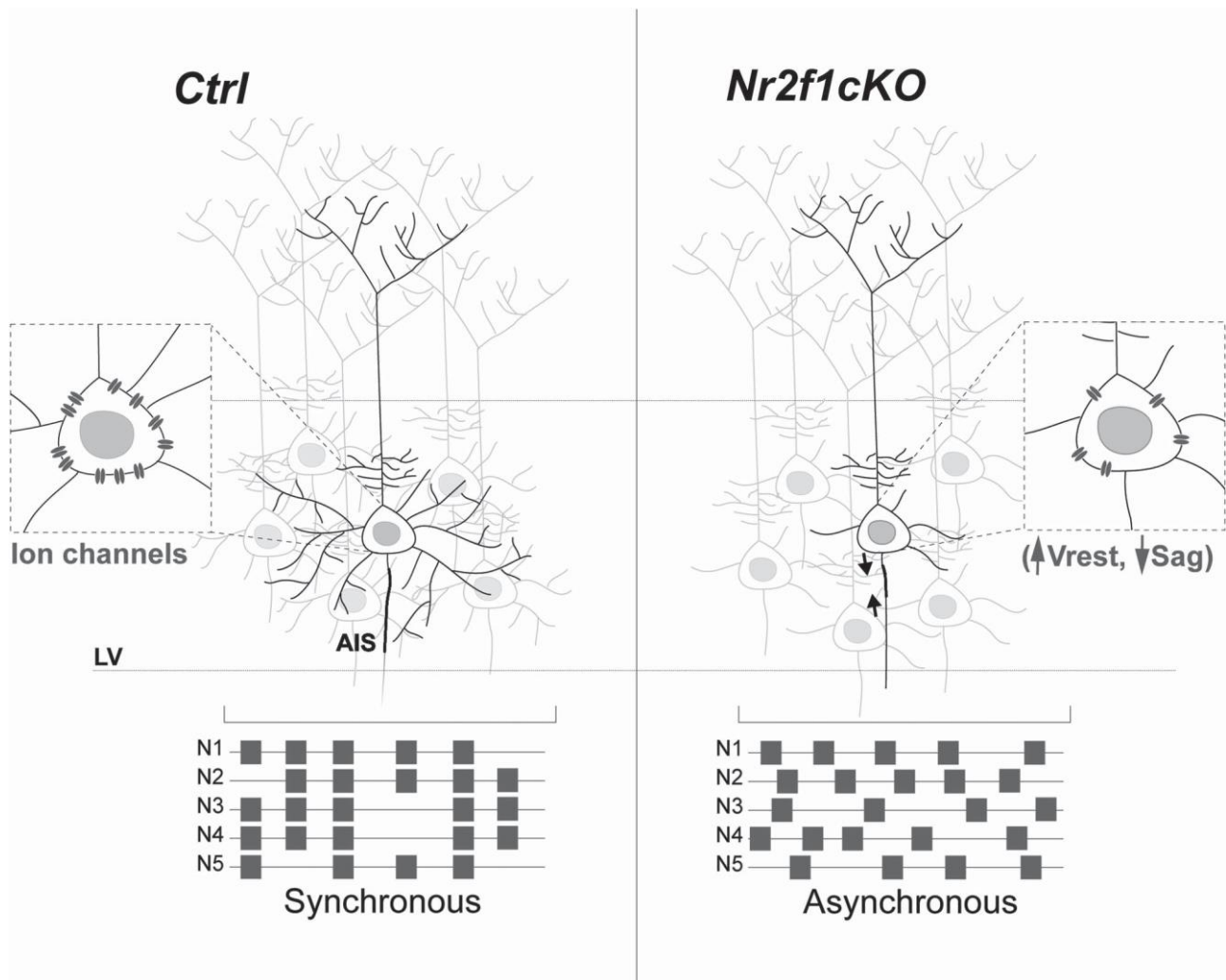


Figure 7. Schematics summarizing the changes in pyramidal neuron anatomy, bioelectric properties, and network synchronization upon Nr2f1 loss. The summary schema highlights a pyramidal neuron with less complex basal dendritic arbor, shorter AIS (in black), and reduced expression of ion channels (in the inset, in dark gray), leading to altered resting membrane potential (V_{rest}) and sag ratio (Sag) as well as asynchronous firing of neurons (below) within the cortical network of the immature somatosensory area, in the absence of *Nr2f1* (*Nr2f1cKO*) compared with a *Ctrl* neuron. Arrows point to the length of the AIS, which is reduced in mutant neurons.

gap junction coupling (Roerig and Feller 2000; Pearson et al. 2004; Allene et al. 2008; Blankenship et al. 2011; Cho and Choi 2012). These early events are followed by cortical early network oscillations (cENOs) generated by a glutamatergic synaptic and extrasynaptic drive (Garaschuk et al. 1998; Allene et al. 2008). In this context, it is important to note that *Nr2f1* loss also affects the expression of GRIN1 and many cell-adhesion-related genes (i.e., *Cdh4*, *Cdh11*, *Cdh12*, *FAT3*, and *NCAM2*) (Alfano et al. 2014). These could in turn impair gap-junction functionality, glutamatergic signaling, and therefore the expression of synchronous plateau assemblies and cENOs. Interestingly, intrinsic bioelectrical membrane properties prominently determine the occurrence of membrane potential spikes before gap-junction coupling takes place (Allene and Cossart 2010). Hence, it is tempting to speculate that *Nr2f1* function might involve early forms of activity within the embryonic brain together with regulating fate-specific determinants.

Concomitant Changes in Intrinsic Neural Excitability during Nr2f1-Dependent Neocortical Development

Our study reports several alterations of pyramidal glutamatergic neuron intrinsic properties, presumably due to the altered expression of HCN1 and other ion channels, such as the ones identified in our study (*Kcnab1*, *Grin1*, *Gria3*, *Cacna2d1*, and *Kcnk2*). Functionally, we have observed a reduced I_h and associated voltage sag, and other changes pointing to increased neuronal excitability, such as a more depolarized resting membrane potential (V_{rest}) and an increased maximum firing frequency. In mature glutamatergic neurons of the adult rodent neocortex, HCN1 is prominently localized to apical dendrites and regulates dendritic calcium electrogenesis, intrinsic high frequency, burst, and sustained firing (Kole et al. 2007; Thuault et al. 2013; Zhang et al., 2014). Its blockade results in a more hyperpolarized resting membrane potential but increased membrane resistance,

synaptic integration, and AP back-propagation efficacy, as previously described (Magee 1998; Williams and Stuart 2000; Berger et al. 2001; Chen et al. 2001; Lupica et al. 2001; Poolos et al. 2002; Wang et al. 2003; Williams and Stuart 2003; Nolan et al. 2004; Fan et al. 2005; Poolos et al. 2006; van Welie et al. 2006; Brager and Johnston 2007; Bender and Baram 2008; Zhang et al., 2014). In addition, intrinsic pacemaker properties through HCN1 expression have been hypothesized to generate and drive distinct synchronized activity patterns in immature networks (Luhmann et al. 2016).

Another factor that could lead to abnormal excitability is delayed maturation of pyramidal cells as a result of *Nr2f1* loss. Indeed, in our *ex vivo* electrophysiological analysis, some properties of *Nr2f1cKO* LVPNs, such as membrane resting potential, resemble those of less mature neurons. In contrast, other electrophysiological parameters, such as input resistance and capacitance, do not reflect any delay in maturation. Moreover, our analysis of AIS plasticity at P21 also does not indicate a maturation defect in individual neurons but rather favors the hypothesis of a homeostatic/compensatory effect leading to decreased dendritic complexity and AIS plasticity.

Finally, genetic or pharmacological dysfunction in HCN channels in mice results in behavioral phenotypes associated with somatosensory-motor coordination, for example, reduced forelimb reaching accuracy and atypical movements during a single-pellet skill reaching task (Boychuk et al. 2017). Similar behavioral phenotypes are displayed by *Nr2f1cKO* mice (Tomassy et al. 2010) and resemble symptoms of *NR2F1* haploinsufficient patients (Bosch et al. 2014; Chen et al. 2016; Rech et al. 2020). Together with the cellular and molecular role of *Nr2f1* during intrinsic area patterning, this study has unraveled neuronal intrinsic excitability and spontaneous activity as novel aspects of the phenotype related to reduced *Nr2f1* expression. These might prove useful to better understand axonal connectivity and circuit formation leading to abnormal behavior and cortical dysfunction in mice (Tomassy et al. 2010; Flore et al. 2017; Contesse et al. 2019) and in humans (Bosch et al. 2016; Chen et al. 2016; Rech et al., 2020).

Supplementary Material

Supplementary material is available at *Cerebral Cortex* online.

Author Contributions

Conceptualization, methodology, validation, and formal analysis, I.D.P., C.T., E.M., A.M., C.A., M.S., X.L., and A.F.; investigation, I.D.P., C.T., E.M., A.M., C.F., M.B., and G.T.; resources, M.S. and A.F.; writing—original draft and editing, I.D.P., C.T., E.M., A.M., and M.S.; writing—review, X.L. and A.F.; visualization, I.D.P., C.T., E.M., and A.M.; funding acquisition, M.S., X.L., A.F., and I.D.P.

Funding

Agence Nationale de la Recherche (grant # ANR-13-BSV4-0011-01 to M.S. and X.L.); Fondation Recherche Médicale; Equipe FRM 2015 (grant #DEQ20150331750 to M.S.) and 4th year FRM PhD fellowship #FDT201904008137 to C.T.; “Investments for the Future” LabEx SIGNALIFE (grant ANR-11-LABX-0028-01 to M.S.); Région PACA PhD fellowship (project R16097AA-CR PACA/Inserm 2016) to C.T. “Initiative d’Excellence (IdEx) del’ Université de Bordeaux” fellowship and Spanish Ministry of Science, Innovation and

Universities RTI2018-100872-J-I00 to I.D.P.; Inserm endowment to A.F.

Notes

We thank Dr M. Kole and Dr. N Dehorter for critical reading of the manuscript and members of the Studer and Frick laboratories for stimulating discussions. We also thank G. Lopez-Bendito for insightful suggestions. We are grateful to the iBV PRISM Microscopy facility and the Bordeaux Imaging Center, supported by Labex-BRAIN (ANR-10-LABEX-43), for the acquisition of some imaging data. The authors also thank the animal and genotyping facilities of the Neurocentre Magendie (supported by INSERM and LabEX-BRAIN ANR-10-LABX-43) and of the iBV.

Conflict of Interest: The corresponding author declares nonfinancial competing interest on behalf of all authors.

References

- Alfano C, Magrinelli E, Harb K, Hevner RF, Studer M. 2014. Postmitotic control of sensory area specification during neocortical development. *NAT Commun.* 5:5632.
- Alfano C, Studer M. 2012. Neocortical arealization: evolution, mechanisms and open questions. *Dev Neurobiol.* 73:411-447.
- Alfano C, Viola L, Heng JI, Pirozzi M, Clarkson M, Flore G, De Maio A, Schedl A, Guillemot F, Studer M. 2011. COUP-TFI promotes radial migration and proper morphology of callosal projection neurons by repressing *Rnd2* expression. *Development.* 138:4685-4697.
- Allene C, Cattani A, Ackman JB, Bonifazi P, Aniksztejn L, Ben-Ari Y, Cossart R. 2008. Sequential generation of two distinct synapse-driven network patterns in developing neocortex. *J Neurosci.* 28:12851-12863.
- Allene C, Cossart R. 2010. Early NMDA receptor-driven waves of activity in the developing neocortex: physiological or pathological network oscillations? *J Physiol.* 588:83-91.
- Allio A, Calorio C, Franchino C, Gavello D, Carbone E, Marcantoni A. 2015. Bud extracts from *Tilia tomentosa* Moench inhibit hippocampal neuronal firing through GABAA and benzodiazepine receptors activation. *J ETHNOPHARMACOL.* 172:288-296.
- Anderson OD. 1975. Moving average processes. *STATISTICIAN.* 24:283-297.
- Andreae LC, Burrone J. 2018. The role of spontaneous neurotransmission in synapse and circuit development. *J Neurosci Res.* 96:354-359.
- Anton-Bolanos N, Sempere-Ferrandez A, Guillamon-Vivancos T, Martini FJ, Perez-Saiz L, Gezelius H, Filipchuk A, Valdeolmillos M, Lopez-Bendito G. 2019. Prenatal activity from thalamic neurons governs the emergence of functional cortical maps in mice. *Science.* 364:987-990.
- Arlotta P, Molyneaux BJ, Chen J, Inoue J, Kominami R, Macklis JD. 2005. Neuronal subtype-specific genes that control corticospinal motor neuron development in vivo. *Neuron.* 45:207-221.
- Armentano M, Chou SJ, Tomassy GS, Leingartner A, O’Leary DD, Studer M. 2007. COUP-TFI regulates the balance of cortical patterning between frontal/motor and sensory areas. *NAT Neurosci.* 10:1277-1286.
- Bender RA, Baram TZ. 2008. Hyperpolarization activated cyclic-nucleotide gated (HCN) channels in developing neuronal networks. *Prog Neurobiol.* 86:129-140.
- Berger T, Larkum ME, Luscher HR. 2001. High I(h) channel density in the distal apical dendrite of layer V pyramidal cells

- increases bidirectional attenuation of EPSPs. *J Neurophysiol.* 85:855-868.
- Bertacchi M, Parisot J, Studer M. 2019. The pleiotropic transcriptional regulator COUP-TFI plays multiple roles in neural development and disease. *BRAIN Res.* 1705:75-94.
- Blankenship AG, Hamby AM, Firl A, Vyas S, Maxeiner S, Willecke K, Feller MB. 2011. The role of neuronal connexins 36 and 45 in shaping spontaneous firing patterns in the developing retina. *J Neurosci.* 31:9998-10008.
- Boillot M, Lee CY, Allene C, Leguern E, Baulac S, Rouach N. 2016. LGI1 acts presynaptically to regulate excitatory synaptic transmission during early postnatal development. *Sci Rep.* 6:21769.
- Bosch DG, Boonstra FN, de Leeuw N, Pfundt R, Nillesen WM, de Ligt J, Gilissen C, Jhangiani S, Lupski JR, Cremers FP et AL. 2016. Novel genetic causes for cerebral visual impairment. *Eur J Hum Genet.* 24:660-665.
- Bosch DG, Boonstra FN, Gonzaga-Jauregui C, Xu M, de Ligt J, Jhangiani S, Wiszniewski W, Muzny DM, Yntema HG, Pfundt R et AL. 2014. NR2F1 mutations cause optic atrophy with intellectual disability. *Am J Hum Genet.* 94:303-309.
- Boychuk JA, Farrell JS, Palmer LA, Singleton AC, Pittman QJ, Teskey GC. 2017. HCN channels segregate stimulation-evoked movement responses in neocortex and allow for coordinated forelimb movements in rodents. *J Physiol.* 595:247-263.
- Brager DH, Akhavan AR, Johnston D. 2012. Impaired dendritic expression and plasticity of h-channels in the *fmr1(-/y)* mouse model of fragile X syndrome. *Cell Rep.* 1:225-233.
- Brager DH, Johnston D. 2007. Plasticity of intrinsic excitability during long-term depression is mediated through mGluR-dependent changes in I(h) in hippocampal CA1 pyramidal neurons. *J Neurosci.* 27:13926-13937.
- Cadwell CR, Bhaduri A, Mostajo-Radji MA, Keefe MG, Nowakowski TJ. 2019. Development and arealization of the cerebral cortex. *Neuron.* 103:980-1004.
- Chen CA, Bosch DG, Cho MT, Rosenfeld JA, Shinawi M, Lewis RA, Mann J, Jayakar P, Payne K, Walsh L et AL. 2016. The expanding clinical phenotype of Bosch-Boonstra-Schaaf optic atrophy syndrome: 20 new cases and possible genotype-phenotype correlations. *Genet Med.* 18:1143-1150.
- Chen K, Aradi I, Thon N, Eghbal-Ahmadi M, Baram TZ, Soltesz I. 2001. Persistently modified h-channels after complex febrile seizures convert the seizure-induced enhancement of inhibition to hyperexcitability. *NAT Med.* 7:331-337.
- Cho MW, Choi MY. 2012. Spontaneous organization of the cortical structure through endogenous neural firing and gap junction transmission. *Neural Netw.* 31:46-52.
- Christophe E, Doerflinger N, Lavery DJ, Molnar Z, Chrapak S, Audinat E. 2005. Two populations of layer v pyramidal cells of the mouse neocortex: development and sensitivity to anesthetics. *J Neurophysiol.* 94:3357-3367.
- Computing RFFS. 2018. *R: A LANGUAGE AND Environment for STATISTICAL Computing.* R Foundation for Statistical Computing, In.
- Contesse T, Ayrault M, Mantegazza M, Studer M, Deschaux O. 2019. Hyperactive and anxiolytic-like behaviors result from loss of COUP-TFI/Nr2f1 in the mouse cortex. *Genes Brain BEHAV.* 18:e12556.
- Corlew R, Bosma MM, Moody WJ. 2004. Spontaneous, synchronous electrical activity in neonatal mouse cortical neurons. *J Physiol.* 560:377-390.
- Cotterill E, Charlesworth P, Thomas CW, Paulsen O, Eglén SJ. 2016. A comparison of computational methods for detecting bursts in neuronal spike trains and their application to human stem cell-derived neuronal networks. *J Neurophysiol.* 116:306-321.
- Del Pino I, Brotons-Mas JR, Marques-Smith A, Marighetto A, Frick A, Marin O, Rico B. 2017. Abnormal wiring of CCK(+) basket cells disrupts spatial information coding. *NAT Neurosci.* 20:784-792.
- Del Pino I, Garcia-Frigola C, Dehorter N, Brotons-Mas JR, Alvarez-Salvado E, Martinez de Lagran M, Ciceri G, Gabaldon MV, Moratal D, Dierssen M et AL. 2013. Erbb4 deletion from fast-spiking interneurons causes schizophrenia-like phenotypes. *Neuron.* 79:1152-1168.
- Dumitrescu AS, Evans MD, Grubb MS. 2016. Evaluating tools for live imaging of structural plasticity at the axon initial segment. *Front Cell Neurosci.* 10:268.
- Fan J, Stembkowski PL, Gandini MA, Black SA, Zhang Z, Souza IA, Chen L, Zamponi GW. 2016. Reduced hyperpolarization-activated current contributes to enhanced intrinsic excitability in cultured hippocampal neurons from PrP(-/-) mice. *Front Cell Neurosci.* 10:74.
- Fan Y, Fricker D, Brager DH, Chen X, Lu HC, Chitwood RA, Johnston D. 2005. Activity-dependent decrease of excitability in rat hippocampal neurons through increases in I(h). *NAT Neurosci.* 8:1542-1551.
- Favuzzi E, Deogracias R, Marques-Smith A, Maeso P, Jezequel J, Exposito-Alonso D, Balia M, Kroon T, Hinojosa AJ, E FM et AL. 2019. Distinct molecular programs regulate synapse specificity in cortical inhibitory circuits. *Science.* 363:413-417.
- Fazel Darbandi S, Robinson Schwartz SE, Qi Q, Catta-Preta R, Pai EL, Mandell JD, Everitt A, Rubin A, Krasnoff RA, Katzman S et AL. 2018. Neonatal Tbr1 dosage controls cortical layer 6 connectivity. *Neuron.* 100:831-845.e837.
- Flore G, Di Ruberto G, Parisot J, Sannino S, Russo F, Illingworth EA, Studer M, De Leonibus E. 2017. Gradient COUP-TFI expression is required for functional Organization of the Hippocampal Septo-Temporal Longitudinal Axis. *Cereb Cortex.* 27:1629-1643.
- Garaschuk O, Hanse E, Konnerth A. 1998. Developmental profile and synaptic origin of early network oscillations in the CA1 region of rat neonatal hippocampus. *J Physiol.* 507(Pt 1):219-236.
- Gavello D, Calorio C, Franchino C, Cesano F, Carabelli V, Carbone E, Marcantoni A. 2018. Early alterations of hippocampal neuronal firing induced by Abeta42. *Cereb Cortex.* 28:433-446.
- Gavello D, Rojo-Ruiz J, Marcantoni A, Franchino C, Carbone E, Carabelli V. 2012. Leptin counteracts the hypoxia-induced inhibition of spontaneously firing hippocampal neurons: a microelectrode array study. *PLoS One.* 7:e41530.
- Greig LC, Woodworth MB, Galazo MJ, Padmanabhan H, Macklis JD. 2013. Molecular logic of neocortical projection neuron specification, development and diversity. *NAT Rev Neurosci.* 14:755-769.
- Grubb MS, Burrone J. 2010. Activity-dependent relocation of the axon initial segment fine-tunes neuronal excitability. *NATURE.* 465:1070-1074.
- Gulledge AT, Bravo JJ. 2016. Neuron morphology influences axon initial segment plasticity. *eNeuro.* 3:ENEURO.0085-15.2016. doi: 10.1523/ENEURO.0085-15.2016.
- Hamada MS, Goethals S, de Vries SI, Brette R, Kole MH. 2016. Covariation of axon initial segment location and dendritic tree normalizes the somatic action potential. *Proc NATL ACAD Sci U S A.* 113:14841-14846.

- Harb K, Magrinelli E, Nicolas CS, Lukianets N, Frangeul L, Pietri M, Sun T, Sandoz G, Grammont F, Jabaudon D *et AL.* 2016. Area-specific development of distinct projection neuron subclasses is regulated by postnatal epigenetic modifications. *Elife*. 5:e09531.
- Jabaudon D. 2017. Fate and freedom in developing neocortical circuits. *NAT Commun*. 8:16042.
- Kasper EM, Larkman AU, Lubke J, Blakemore C. 1994. Pyramidal neurons in layer 5 of the rat visual cortex. II. Development of electrophysiological properties. *J Comp Neurol*. 339: 475-494.
- Kirischuk S, Sinning A, Blanquie O, Yang JW, Luhmann HJ, Kilb W. 2017. Modulation of neocortical development by early neuronal activity: physiology and pathophysiology. *Front Cell Neurosci*. 11:379.
- Kirkby LA, Sack GS, Firl A, Feller MB. 2013. A role for correlated spontaneous activity in the assembly of neural circuits. *Neuron*. 80:1129-1144.
- Kole MH, Brauer AU, Stuart GJ. 2007. Inherited cortical HCN1 channel loss amplifies dendritic calcium electrogenesis and burst firing in a rat absence epilepsy model. *J Physiol*. 578:507-525.
- Kole MH, Stuart GJ. 2012. Signal processing in the axon initial segment. *Neuron*. 73:235-247.
- Kordeli E, Lambert S, Bennett V. 1995. AnkyrinG, A new ankyrin gene with neural-specific isoforms localized at the axonal initial segment and node of Ranvier. *J Biol Chem*. 270:2352-2359.
- Kuba H. 2010. Plasticity at the axon initial segment. *Commun Integr Biol*. 3:597-598.
- Kuba H, Oichi Y, Ohmori H. 2010. Presynaptic activity regulates Na(+) channel distribution at the axon initial segment. *NATURE*. 465:1075-1078.
- Li H, Fertuzinhos S, Mohns E, Hnasko TS, Verhage M, Edwards R, Sestan N, Crair MC. 2013. Laminar and columnar development of barrel cortex relies on thalamocortical neurotransmission. *Neuron*. 79:970-986.
- Loots G, Ovcharenko I. 2007. ECRbase: database of evolutionary conserved regions, promoters, and transcription factor binding sites in vertebrate genomes. *BIOINFORMATICS*. 23: 122-124.
- Luhmann HJ, Khazipov R. 2018. Neuronal activity patterns in the developing barrel cortex. *Neuroscience*. 368: 256-267.
- Luhmann HJ, Sinning A, Yang JW, Reyes-Puerta V, Stüttgen MC, Kirischuk S, Kilb W. 2016. Spontaneous neuronal activity in developing neocortical networks: from single cells to large-scale interactions. *Front Neural Circuits*. 10:40.
- Lupica CR, Bell JA, Hoffman AF, Watson PL. 2001. Contribution of the hyperpolarization-activated current (I(h)) to membrane potential and GABA release in hippocampal interneurons. *J Neurophysiol*. 86:261-268.
- Magee JC. 1998. Dendritic hyperpolarization-activated currents modify the integrative properties of hippocampal CA1 pyramidal neurons. *J Neurosci*. 18:7613-7624.
- Massengill JL, Smith MA, Son DI, O'Dowd DK. 1997. Differential expression of K4-AP currents and Kv3.1 potassium channel transcripts in cortical neurons that develop distinct firing phenotypes. *J Neurosci*. 17:3136-3147.
- Montemayor C, Montemayor OA, Ridgeway A, Lin F, Wheeler DA, Pletcher SD, Pereira FA. 2010. Genome-wide analysis of binding sites and direct target genes of the orphan nuclear receptor NR2F1/COUP-TFI. *PLoS One*. 5:e8910.
- Moody WJ, Bosma MM. 2005. Ion channel development, spontaneous activity, and activity-dependent development in nerve and muscle cells. *Physiol Rev*. 85:883-941.
- Murase S, Lantz CL, Kim E, Gupta N, Higgins R, Stopfer M, Hoffman DA, Quinlan EM. 2016. Matrix Metalloproteinase-9 regulates neuronal circuit development and excitability. *Mol Neurobiol*. 53:3477-3493.
- Nolan MF, Malleret G, Dudman JT, Buhl DL, Santoro B, Gibbs E, Vronskaya S, Buzsaki G, Siegelbaum SA, Kandel ER *et AL.* 2004. A behavioral role for dendritic integration: HCN1 channels constrain spatial memory and plasticity at inputs to distal dendrites of CA1 pyramidal neurons. *Cell*. 119: 719-732.
- O'Leary DD, Sahara S. 2008. Genetic regulation of arealization of the neocortex. *Curr Opin Neurobiol*. 18:90-100.
- Ovcharenko I, Nobrega MA, Loots GG, Stubbs L. 2004. ECR browser: a tool for visualizing and accessing data from comparisons of multiple vertebrate genomes. *Nucleic Acids Res*. 32:W280-W286.
- Pariset J, Flore G, Bertacchi M, Studer M. 2017. COUP-TFI mitotically regulates production and migration of dentate granule cells and modulates hippocampal Cxcr4 expression. *Development*. 144:2045-2058.
- Pearson RA, Catsicas M, Becker DL, Bayley P, Luneborg NL, Mobbs P. 2004. Ca(2+) signalling and gap junction coupling within and between pigment epithelium and neural retina in the developing chick. *Eur J Neurosci*. 19:2435-2445.
- Poolos NP, Bullis JB, Roth MK. 2006. Modulation of h-channels in hippocampal pyramidal neurons by p38 mitogen-activated protein kinase. *J Neurosci*. 26:7995-8003.
- Poolos NP, Migliore M, Johnston D. 2002. Pharmacological upregulation of h-channels reduces the excitability of pyramidal neuron dendrites. *NAT Neurosci*. 5:767-774.
- Quandt K, Frech K, Karas H, Wingender E, Werner T. 1995. MatInd and MatInspector: new fast and versatile tools for detection of consensus matches in nucleotide sequence data. *Nucleic Acids Res*. 23:4878-4884.
- Rech ME, McCarthy JM, Chen C-A, Edmond JC, Shah VS, Bosch DGM, Berry GT, Williams L, Madan-Khetarpal S, Niyazov D *et AL.* Phenotypic expansion of Bosch-Boonstra-Schaaf optic atrophy syndrome and further evidence for genotype-phenotype correlations. *Am. J. Med. Genet. A*. <https://doi.org/10.1002/ajmg.a.61580>.
- Roerig B, Feller MB. 2000. Neurotransmitters and gap junctions in developing neural circuits. *BRAIN Res BRAIN Res Rev*. 32: 86-114.
- Schindelin J, Arganda-Carreras I, Frise E, Kaynig V, Longair M, Pietzsch T, Preibisch S, Rueden C, Saalfeld S, Schmid B *et AL.* 2012. Fiji: an open-source platform for biological-image analysis. *NAT Methods*. 9:676-682.
- Schneggenburger R, Rosenmund C. 2015. Molecular mechanisms governing ca(2+) regulation of evoked and spontaneous release. *NAT Neurosci*. 18:935-941.
- Shah MM. 2014. Cortical HCN channels: function, trafficking and plasticity. *J Physiol*. 592:2711-2719.
- Simi A, Studer M. 2018. Developmental genetic programs and activity-dependent mechanisms instruct neocortical area mapping. *Curr Opin Neurobiol*. 53:96-102.
- Thuault SJ, Malleret G, Constantinople CM, Nicholls R, Chen I, Zhu J, Panteleyev A, Vronskaya S, Nolan MF, Bruno R *et AL.* 2013. Prefrontal cortex HCN1 channels enable intrinsic persistent neural firing and executive memory function. *J Neurosci*. 33:13583-13599.

- Tomassy GS, De Leonibus E, Jabaudon D, Lodato S, Alfano C, Mele A, Macklis JD, Studer M. 2010. Area-specific temporal control of corticospinal motor neuron differentiation by COUP-TFI. *Proc Natl Acad Sci U S A*. 107:3576-3581.
- Tritsch NX, Yi E, Gale JE, Glowatzki E, Bergles DE. 2007. The origin of spontaneous activity in the developing auditory system. *Nature*. 450:50-55.
- Uhlen P, Fritz N, Smedler E, Malmersjo S, Kanatani S. 2015. Calcium signaling in neocortical development. *Dev Neurobiol*. 75:360-368.
- van Welie I, Remme MW, van Hooft JA, Wadman WJ. 2006. Different levels of Ih determine distinct temporal integration in bursting and regular-spiking neurons in rat subiculum. *J Physiol*. 576:203-214.
- Wang Z, Xu NL, Wu CP, Duan S, Poo MM. 2003. Bidirectional changes in spatial dendritic integration accompanying long-term synaptic modifications. *Neuron*. 37:463-472.
- Wefelmeyer W, Puhl CJ, Burrone J. 2016. Homeostatic plasticity of subcellular neuronal structures: from inputs to outputs. *Trends Neurosci*. 39:656-667.
- Williams SR, Stuart GJ. 2000. Site independence of EPSP time course is mediated by dendritic Ih in neocortical pyramidal neurons. *J Neurophysiol*. 83:3177-3182.
- Williams SR, Stuart GJ. 2003. Voltage- and site-dependent control of the somatic impact of dendritic IPSPs. *J Neurosci*. 23:7358-7367.
- Yamada R, Kuba H. 2016. Structural and functional plasticity at the axon initial segment. *Front Cell Neurosci*. 10:250.
- Yamamoto N, Lopez-Bendito G. 2012. Shaping brain connections through spontaneous neural activity. *Eur J Neurosci*. 35:1595-1604.
- Zhang Y, Bonnan A, Bony G, Ferezou I, Pietropaolo S, Ginger M, Sans N, Rossier J, Oostra B, LeMasson G et al. 2014. Dendritic channelopathies contribute to neocortical and sensory hyperexcitability in Fmr1(-/y) mice. *Nat Neurosci*. 17:1701-1709.
- Zhou D, Lambert S, Malen PL, Carpenter S, Boland LM, Bennett V. 1998. AnkyrinG is required for clustering of voltage-gated Na channels at axon initial segments and for normal action potential firing. *J Cell Biol*. 143:1295-1304.

SUPPLEMENTARY FIGURES

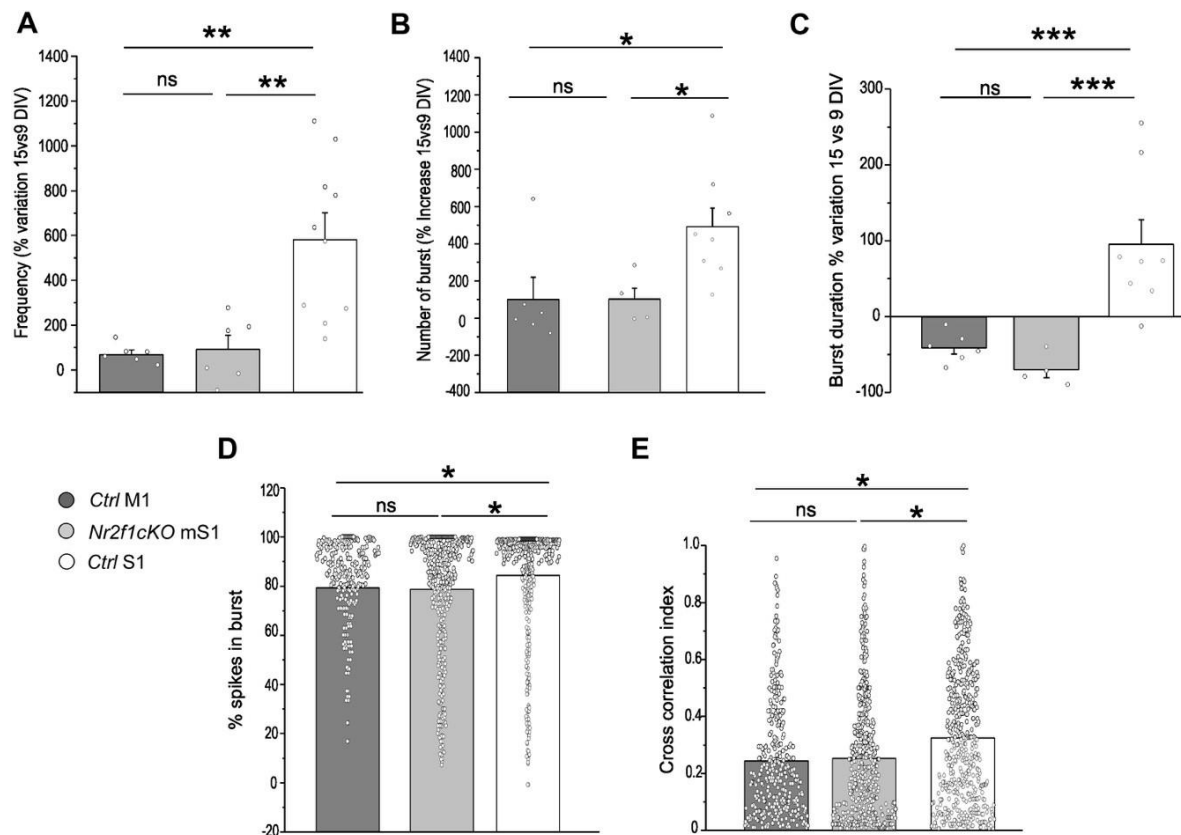


Figure S1. Firing parameters at 15 DIV. Changes of firing parameters recorded at 9 DIV were compared with those recorded at 15 DIV. **A)** From 9 to 15 DIV firing frequency in MEAs increased by $67.053 \pm 18.687\%$ in *Ctrl* M1 (N=6), $91.455 \pm 64.271\%$ (N=6) in *Nr2f1cKO* mS1 and $580.155 \pm 116.167\%$ (N=10) in *Ctrl* S1. **B)** From 9 to 15 DIV number of bursts increased by $98.15 \pm 120.22\%$ in *Ctrl* M1 (N= 6), $100.68 \pm 60.65\%$ in *Nr2f1cKO* mS1 (N=4) and $489.05 \pm 100.53\%$ in *Ctrl* S1 (N=8). **C)** From 9 to 15 DIV burst duration decreased by $40.52 \pm 8.06\%$ in *Ctrl* M1 (N= 6) and by $69.77 \pm 10.81\%$ in *Nr2f1cKO* mS1 (N= 4) but increased by $95.24 \pm 32.59\%$ in *Ctrl* S1 (N=8). **D)** At 15 DIV, the percentage of spikes in burst was 79.21 ± 1.16 in *Ctrl* M1 (N_{channels}=330), 78.71 ± 1.19 in *Nr2f1cKO* mS1 (N_{channels}= 377), and 94.29 ± 1.14 in *Ctrl* S1 (N_{channels}= 456). **E)** At 15 DIV, cross correlation index was 0.24 ± 0.01 in *Ctrl* M1 (N_{channels}= 329), 0.25 ± 0.01 in *Nr2f1cKO* mS1 (N_{channels}= 447) and 0.32 ± 0.01 in *Ctrl* S1 (N_{channels}=458). (* P<0.05; **P<0.01; ***P<0.001). Sampling and statistical tests in Table S5).

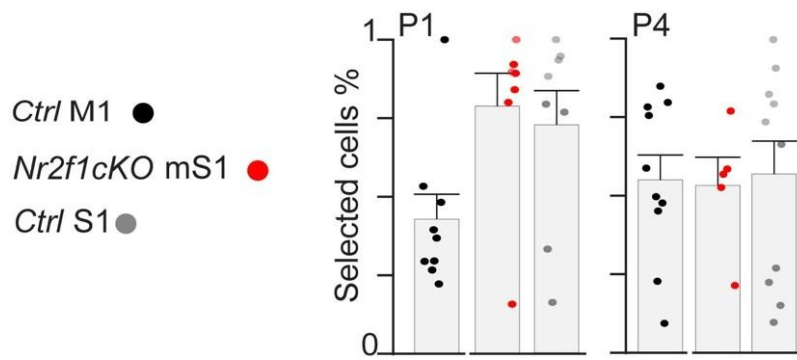


Figure S2. Ca^{2+} active cell parameters. Percentage of active cells in the total of manually selected ROI in each experiment of acute slice Ca^{2+} spontaneous recording. Sampling and statistical tests are listed in Table S5. Abbreviations: M1 - motor cortex, mS1 – motorized somatosensory cortex, P – postnatal day, S1 - somatosensory cortex. *See also Tables S1 and S5.*

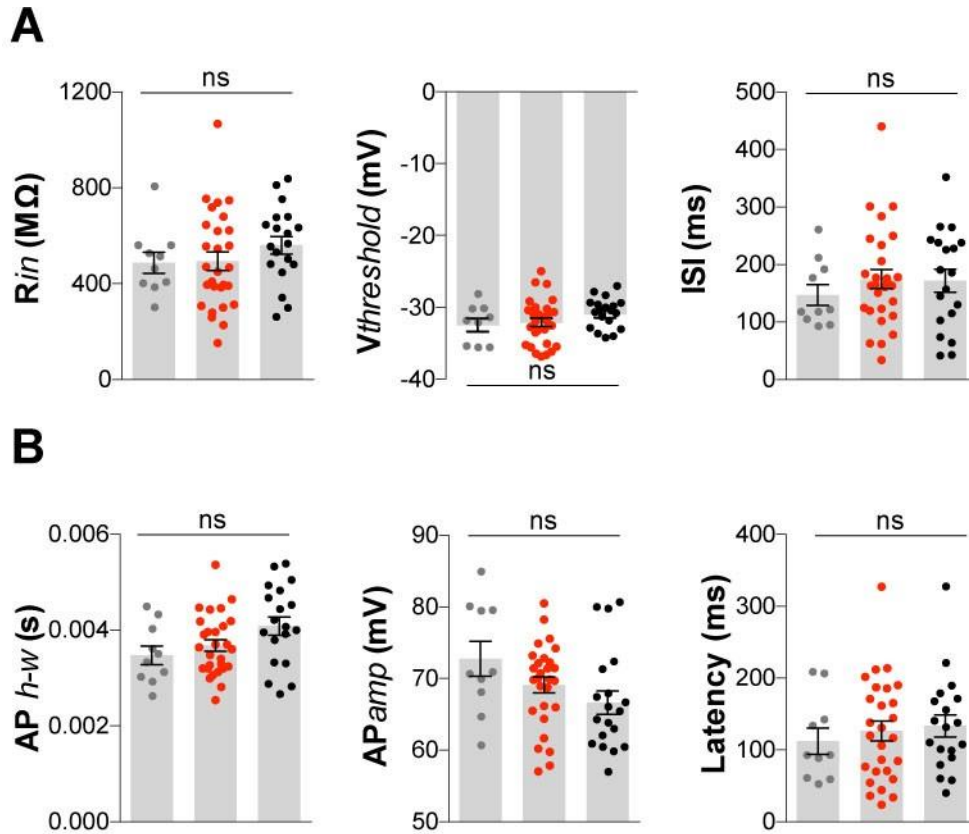


Figure S3. Specific intrinsic excitability features and input-output relationship remain unaltered in *Nr2f1* deficient layer V pyramidal neurons (LVPNs). **A)** LVPNs in *Ctrl* M1 (in gray), *Nr2f1cKO* mS1 (in red) and *Ctrl* S1 (in black) display similar input resistance, threshold for action potential and inter-spike interval. **B)** We also observed a similar action potential half-width, action potential amplitude and latency to display the first action potential at rheobase. Data are represented as mean \pm SEM. Sampling and statistical tests are listed in Table S5. *R_{in}*, input resistance; *V_{threshold}*, threshold for action potential; *AP_{h-w}*, half-width of action potential; *ISI*, inter-spike interval. *See also Figure 3 and Tables S2 and S5.*

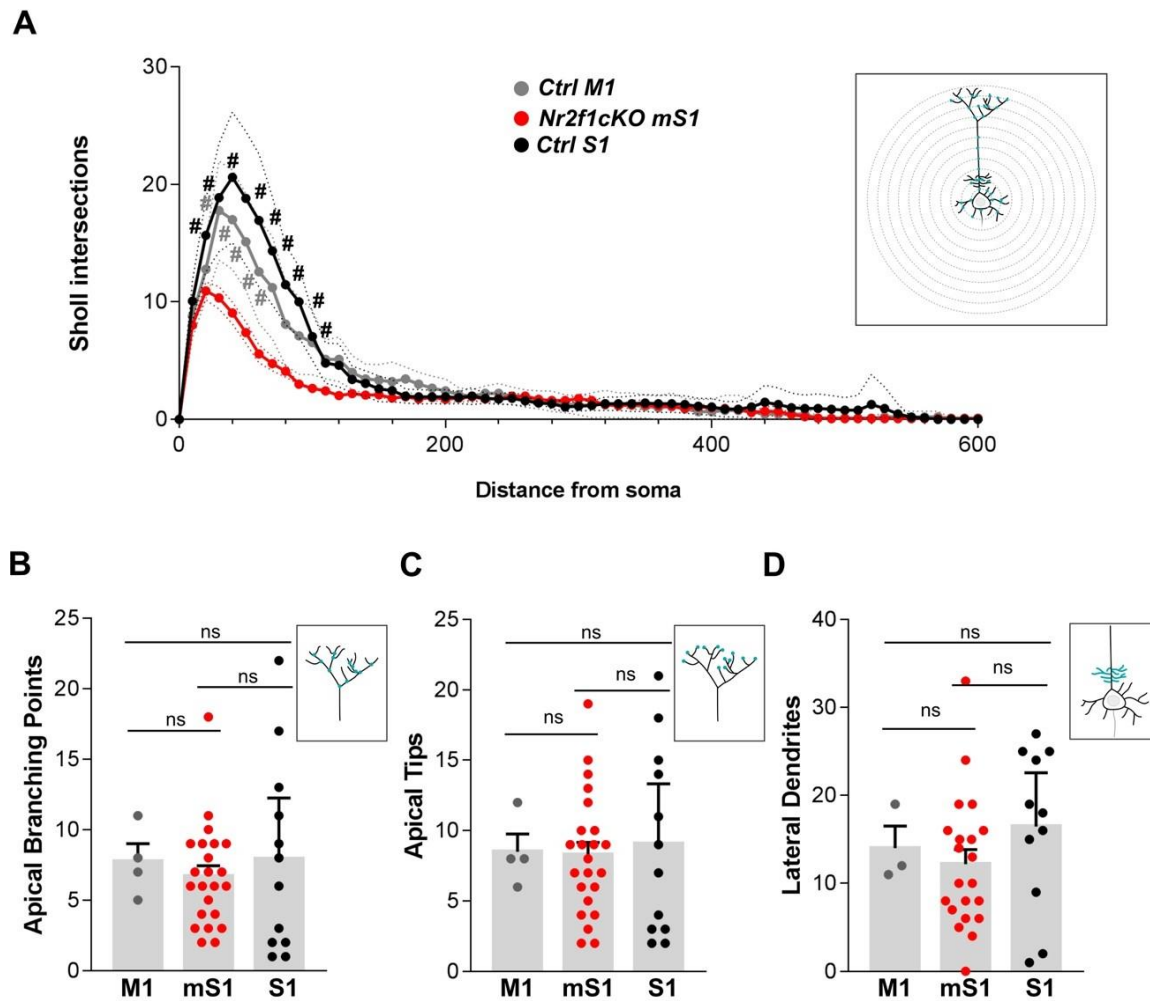


Figure S4. Apical dendritic complexity of layer V pyramidal neurons (LVPNs) is not affected in *Nr2f1* mutant brains. **A)** Sholl analysis shows no differences in complexity among *Ctrl* M1, *Nr2f1cKO* mS1 and *Ctrl* S1 P7 LVPNs, relative to distal dendrites ($\#P < 0.05$). (see also Table S3). **B-D)** Number of Apical Branching Points (*Ctrl* M1, 7.75 ± 1.25 ; *Nr2f1cKO* mS1, 5.14 ± 0.75 ; *Ctrl* S1, 7.92 ± 1.97 ; *Ctrl* S1 vs *Nr2f1cKO* mS1 $P = 0.73$; *Ctrl* M1 vs *Nr2f1cKO* mS1 $P = 0.90$), Apical Terminal Tips (*Ctrl* M1, 8.5 ± 1.26 ; *Nr2f1cKO* mS1, 8.26 ± 0.90 ; *Ctrl* S1, 9.08 ± 1.93 ; *Ctrl* S1 vs *Nr2f1cKO* mS1 $P = 0.88$; *Ctrl* M1 vs *Nr2f1cKO* mS1 $P = 1$) and Lateral dendrites (*Ctrl* M1, 14 ± 2.52 ; *Nr2f1cKO* mS1, 12.19 ± 1.65 ; *Ctrl* S1, 16.45 ± 2.75 ; *Ctrl* S1 vs *Nr2f1cKO* mS1 $P = 0.29$; *Ctrl* M1 vs *Nr2f1cKO* mS1 $P = 0.92$) are unaffected by the loss of *Nr2f1*. Data are represented as mean \pm SEM. Sampling and statistical tests are listed in Table S5. See also Figure 4 and Tables S3 and S5.

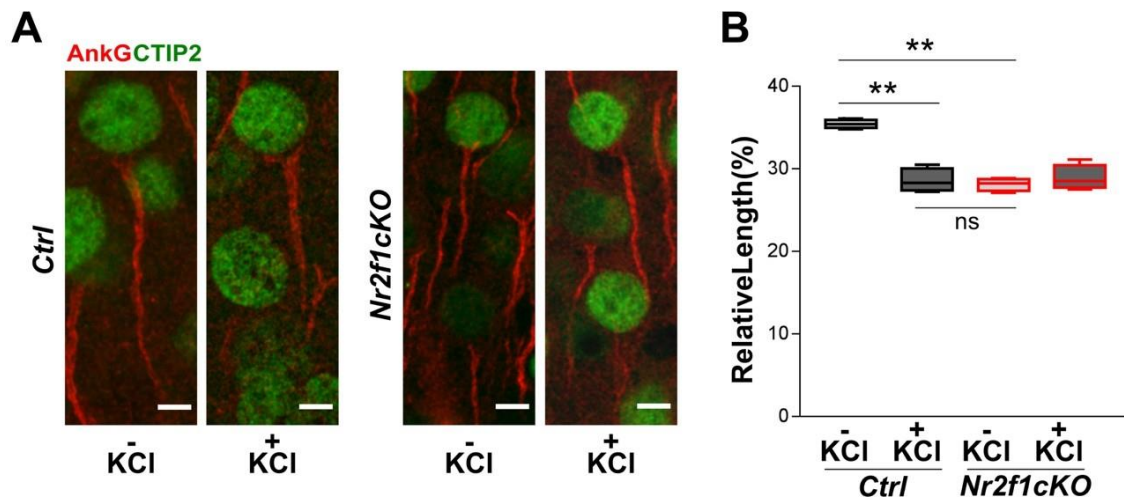


Figure S5. Mutant LVPN fail to change their AIS length upon depolarization. A) Confocal images of control and *Nr2f1cKO* LVPNs non-treated (-KCl) and treated (+KCl). In green CTIP2, in red Ankyrin. **B)** Average relative length (average length values were normalized on control values) are significantly reduced in controls after KCl treatment (*Ctrl* -KCl, 35.41 ± 0.26 ; *Ctrl* + KCl, 28.57 ± 0.71 ; $P < 0.0001$). No differences were observed in *Nr2f1cKO* cells between non-treated and treated populations. (*Nr2f1cKO* -KCl, 28.1 ± 0.3756 ; *Nr2f1cKO* + KCl; 28.9 ± 0.7714 ; $P = 0.289$). Data are represented as mean \pm SEM. Sampling and statistical tests are listed in Table S5. See also Table S5.

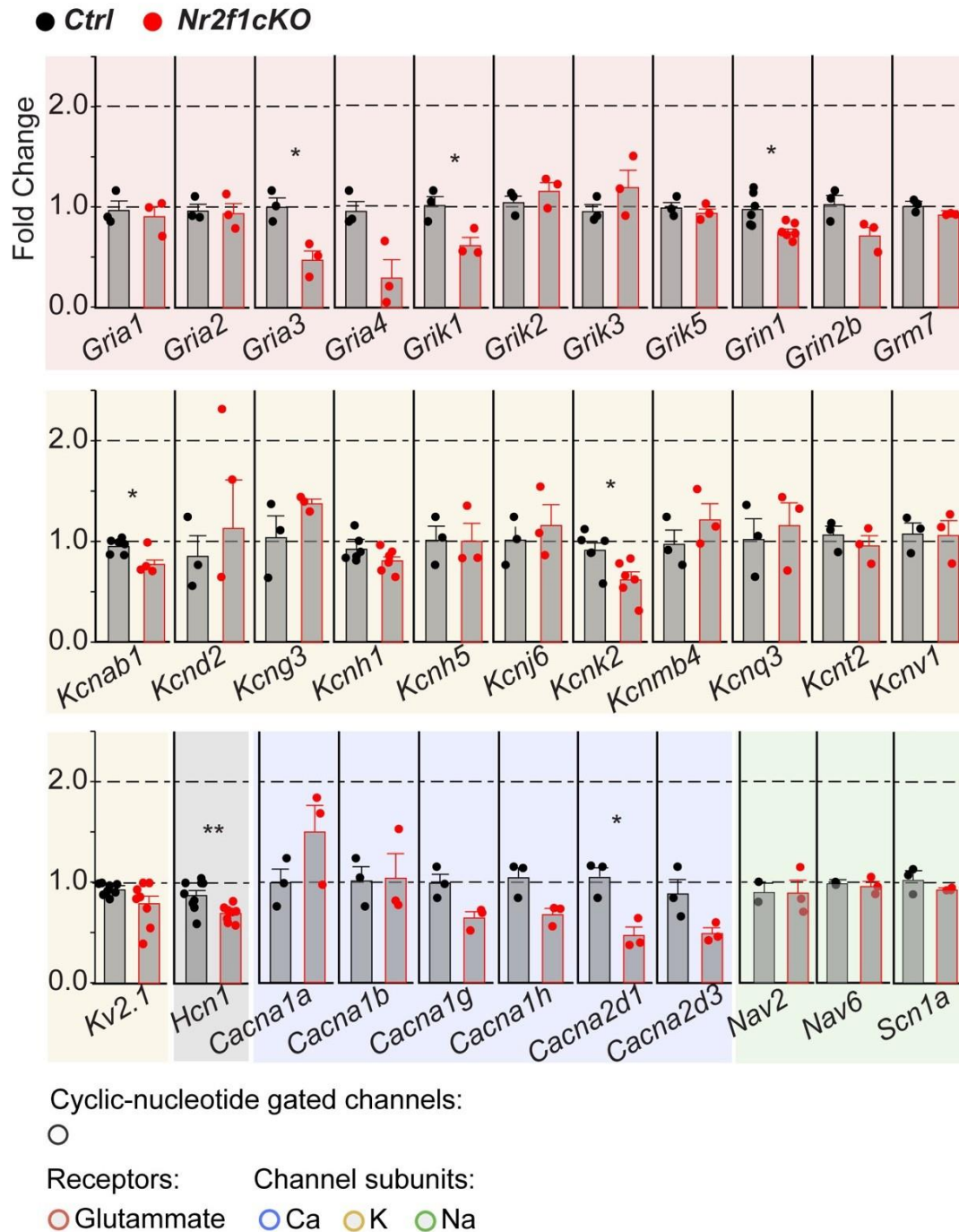


Figure S6. qPCR quantification of cortical ion channels in *Nr2f1* mutant cortices. Single qPCR quantification of P7 *Ctrl* vs *Nr2f1cKO* expression of chosen cortically (deep layers) expressed ion channel subunits and Glutamate receptors. *Ctrl* mean value is normalized to 1 to calculate fold changes in *Nr2f1cKO* conditions. *- P-Value < 0.05. P – Postnatal day. Data are represented as mean \pm SEM. Sampling and statistical tests are listed in Table S5. See also Figure 6 and Tables S4 and S5.

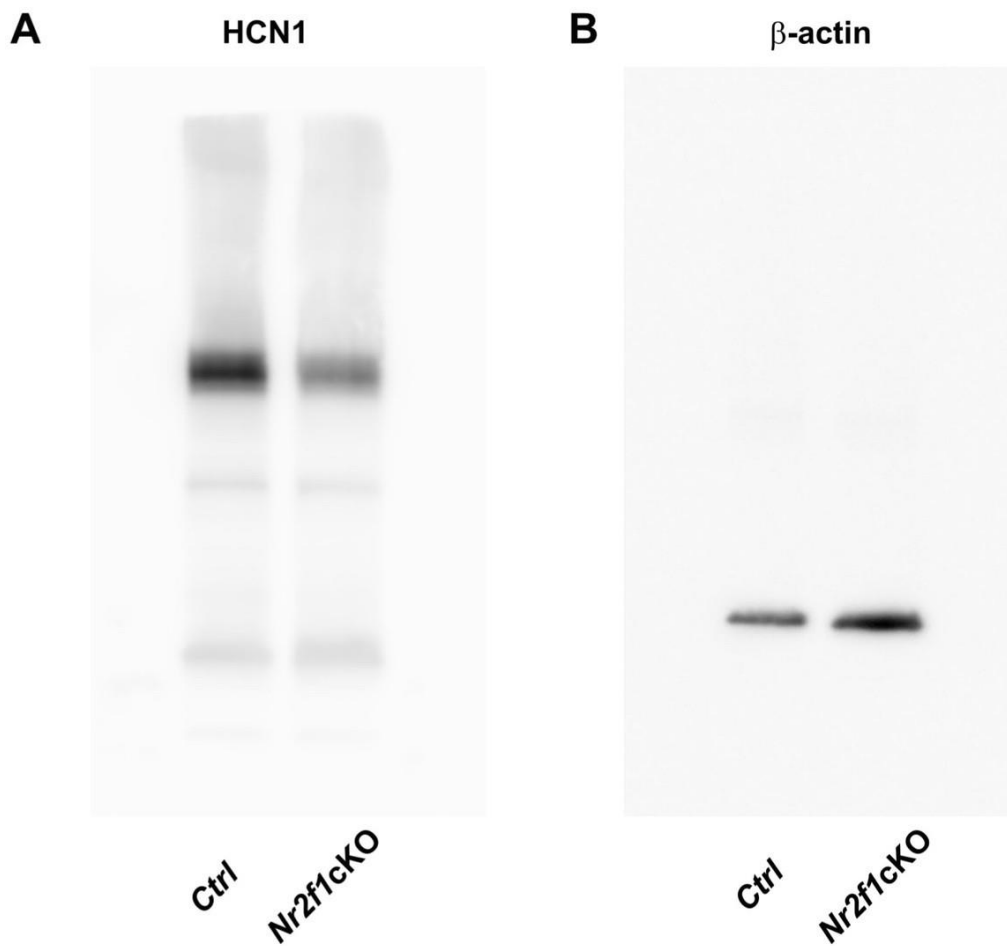


Figure S7. Full lane western blot of cortical ion channel HCN1. **A)** Western Blot of HCN1 in Ctrl and *Nr2f1* mutant cortices. Note specific downregulation of HCN1 protein in the mutant brain. **B)** Western Blot of b-actin in Ctrl and *Nr2f1* mutant cortices as an internal control. See also Figure 6B.

SUPPLEMENTARY TABLES

Ca²⁺ Transients Hz	Mean 1	s.e. 1	Mean 2	s.e. 2	Mean diff	95% conf. int.	Stat	P value
1- P1_Ctrl_M1 2- P1_Nr2f1cKO_mS1	0.031	0.0018	0.0281	0.0013	0.0029	-0.001 0.007	*	0.0464
1- P1_Ctrl_M1 2- P1_Ctrl_S1	0.031	0.0018	0.0208	0.0013	0.0102	0.006 0.015	****	< 0.0001
1- P1_Ctrl_M1 2- P4_Ctrl_M1	0.031	0.0018	0.0592	0.0018	-0.0283	-0.033 -0.023	****	< 0.0001
1- P1_Ctrl_M1 2- P4_Nr2f1cKO_mS1	0.031	0.0018	0.0579	0.0026	-0.027	-0.033 -0.021	****	< 0.0001
1- P1_Ctrl_M1 2- P4_Ctrl_S1	0.031	0.0018	0.0605	0.002	-0.0295	-0.035 -0.024	****	< 0.0001
1- P1_Nr2f1cKO_mS1 2- P1_Ctrl_S1	0.0281	0.0013	0.0208	0.0013	0.0073	0.007 0.014	****	< 0.0001
1- P1_Nr2f1cKO_mS1 2- P4_Ctrl_M1	0.0281	0.0013	0.0592	0.0018	-0.0311	-0.032 -0.023	****	< 0.0001
1- P1_Nr2f1cKO_mS1 2- P4_Nr2f1cKO_mS1	0.0281	0.0013	0.0579	0.0026	-0.0298	-0.032 -0.021	****	< 0.0001
1- P1_Nr2f1cKO_mS1 2- P4_Ctrl_S1	0.0281	0.0013	0.0605	0.002	-0.0324	-0.034 -0.024	****	< 0.0001
1- P1_Ctrl_S1 2- P4_Ctrl_M1	0.0208	0.0013	0.0592	0.0018	-0.0384	-0.043 -0.034	****	< 0.0001
1- P1_Ctrl_S1 2- P4_Nr2f1cKO_mS1	0.0208	0.0013	0.0579	0.0026	-0.0371	-0.043 -0.031	****	< 0.0001
1- P1_Ctrl_S1 2- P4_Ctrl_S1	0.0208	0.0013	0.0605	0.002	-0.0397	-0.044 -0.035	****	< 0.0001
1- P4_Ctrl_M1 2- P4_Nr2f1cKO_mS1	0.0592	0.0018	0.0579	0.0026	0.0013	-0.005 0.007	n.s.	0.6743
1- P4_Ctrl_M1 2- P4_Ctrl_S1	0.0592	0.0018	0.0605	0.002	-0.0013	-0.007 0.004	n.s.	0.6379
1- P4_Nr2f1cKO_mS1 2- P4_Ctrl_S1	0.0579	0.0026	0.0605	0.002	-0.0026	-0.009 0.004	n.s.	0.4312

Ca²⁺ Transients correlation	Mean 1	s.e. 1	Mean 2	s.e. 2	Mean diff.	95% conf. int.	Stat	P value
1- P1_Ctrl_M1 2- P1_Nr2f1cKO_mS1	0.6703	0.0939	0.6474	0.2559	0.0229	-0.612 0.657	n.s.	0.9352
1- P1_Ctrl_M1 2- P1_Ctrl_S1	0.6703	0.0939	0.707	0.3793	-0.0367	-1.009 0.935	n.s.	0.9283
1- P1_Ctrl_M1 2- P4_Ctrl_M1	0.6703	0.0939	1.415	0.2282	-0.7447	-1.273 -0.216	**	0.009
1- P1_Ctrl_M1 2- P4_Nr2f1cKO_mS1	0.6703	0.0939	1.2663	0.3163	-0.596	-1.46 0.268	n.s.	0.1343
1- P1_Ctrl_M1 2- P4_Ctrl_S1	0.6703	0.0939	2.2774	0.3223	-1.6071	-2.363 0.852	***	0.0009
1- P1_Nr2f1cKO_mS1 2- P1_Ctrl_S1	0.6474	0.2559	0.707	0.3793	-0.0597	-1.094 0.975	n.s.	0.8991
1- P1_Nr2f1cKO_mS1 2- P4_Ctrl_M1	0.6474	0.2559	1.415	0.2282	-0.7676	-1.501 -0.034	*	0.0415

1- P1_Nr2f1cKO_mS1 2- P4_Nr2f1cKO_mS1	0.6474	0.2559	1.2663	0.3163	-0.6189	-1.547 0.309	n.s.	0.1644
1- P1_Nr2f1cKO_mS1 2- P4_Ctrl_S1	0.6474	0.2559	2.2774	0.3223	-1.63	-2.513 -0.747	**	0.0014
1- P1_Ctrl_S1 2- P4_Ctrl_M1	0.707	0.3793	1.415	0.2282	-0.7079	-1.713 0.298	n.s.	0.1451
1- P1_Ctrl_S1 2- P4_Nr2f1cKO_mS1	0.707	0.3793	1.2663	0.3163	-0.5592	-1.677 0.559	n.s.	0.2869
1- P1_Ctrl_S1 2- P4_Ctrl_S1	0.707	0.3793	2.2774	0.3347	-1.5704	-2.663 - 0.477	**	0.0089
1- P4_Ctrl_M1 2- P4_Nr2f1cKO_mS1	1.415	0.2282	1.2663	0.3163	0.1487	-0.743 1.04	n.s.	0.7125
1- P4_Ctrl_M1 2- P4_Ctrl_S1	1.415	0.2282	2.2774	0.3223	-0.8624	-1.703 0.022	*	0.045
1- P4_Nr2f1cKO_mS1 2- P4_Ctrl_S1	1.2663	0.3163	2.2774	0.3223	-1.0111	-2.0073 - 0.0149	*	0.0472

Ca ²⁺ Transients Hz normalized s.d.	Mean 1	s.e. 1	Mean 2	s.e. 2	Mean diff	95% conf. int.	Stat	P value
1- P1_Ctrl_M1 2- P1_Nr2f1cKO_mS1	0.6187	0.0722	0.7741	0.2367	-0.1554	-0.739 0.428	n.s.	0.5498
1- P1_Ctrl_M1 2- P1_Ctrl_S1	0.6187	0.0722	0.7583	0.1831	-0.1396	-0.612 0.332	n.s.	0.5027
1- P1_Ctrl_M1 2- P4_Ctrl_M1	0.6187	0.0722	0.3565	0.0525	0.2622	0.068 0.456	*	0.0123
1- P1_Ctrl_M1 2- P4_Ctrl_mS1	0.6187	0.0722	0.3663	0.0627	0.2524	0.039 0.466	*	0.0249
1- P1_Ctrl_M1 2- P4_Ctrl_S1	0.6187	0.0722	0.2513	0.0338	0.3674	0.186 0.549	**	0.0014
1- P1_Nr2f1cKO_mS1 2- P1_Ctrl_S1	0.7741	0.2367	0.7583	0.1831	0.0158	-0.645 0.677	n.s.	0.9589
1- P1_Nr2f1cKO_mS1 2- P4_Ctrl_M1	0.7741	0.2367	0.3565	0.0525	0.4175	-0.163 0.998	n.s.	0.1314
1- P1_Nr2f1cKO_mS1 2- P4_Nr2f1cKO_mS1	0.7741	0.2367	0.3663	0.0627	0.4077	-0.174 0.99	n.s.	0.141
1- P1_Nr2f1cKO_mS1 2- P4_Ctrl_S1	0.7741	0.2367	0.2513	0.0338	0.5228	-0.057 1.102	n.s.	0.0697
1- P1_Ctrl_S1 2- P4_Ctrl_M1	0.7583	0.1831	0.3565	0.0525	0.4018	-0.067 0.871	n.s.	0.0807
1- P1_Ctrl_S1 2- P4_Nr2f1cKO_mS1	0.7583	0.1831	0.3663	0.0627	0.392	-0.079 0.863	n.s.	0.0882
1- P1_Ctrl_S1 2- P4_Ctrl_S1	0.7583	0.1831	0.2513	0.0338	0.507	0.037 0.976	*	0.0388
1- P4_Ctrl_M1 2- P4_Nr2f1cKO_mS1	0.3565	0.0525	0.3663	0.0627	-0.0098	-0.192 0.173	n.s.	0.9071
1- P4_Ctrl_M1 2- P4_Ctrl_S1	0.3565	0.0525	0.2513	0.0338	0.1052	-0.025 0.236	n.s.	0.1083
1- P4_Nr2f1cKO_mS1 2- P4_Ctrl_S1	0.3663	0.0627	0.2513	0.0338	0.115	-0.056 0.286	n.s.	0.1542

Active cells%	Mean 1	s.e. 1	Mean 2	s.e. 2	Mean diff	95% conf. int.	Stat	P value
1- P1_Ctrl_M1 2- P1_Nr2f1cKO_mS1	0.4286	0.079	0.7871	0.1075	-0.3585	-0.65 - 0.067	*	0.0202
1- P1_Ctrl_M1 2- P1_Ctrl_S1	0.4286	0.079	0.7283	0.1094	-0.2997	-0.591 - 0.008	*	0.0446
1- P1_Ctrl_M1 2- P4_Ctrl_M1	0.4286	0.079	0.5549	0.0801	-0.1264	-0.364 0.111	n.s.	0.2772
1- P1_Ctrl_M1 2- P4_Nr2f1cKO_mS1	0.4286	0.079	0.5358	0.0899	-0.1073	-0.375 0.161	n.s.	0.3918
1- P1_Ctrl_M1 2- P4_Ctrl_S1	0.4286	0.079	0.5689	0.1082	-0.1404	-0.424 0.144	n.s.	0.3104
1- P1_Nr2f1cKO_mS1 2- P1_Ctrl_S1	0.7871	0.1075	0.7283	0.1094	0.0588	-0.273 0.39	n.s.	0.7077
1- P1_Nr2f1cKO_mS1 2- P4_Ctrl_M1	0.7871	0.1075	0.5549	0.0801	0.2322	-0.06 0.524	n.s.	0.1089
1- P1_Nr2f1cKO_mS1 2- P4_Nr2f1cKO_mS1	0.7871	0.1075	0.5358	0.0899	0.2512	-0.061 0.564	n.s.	0.1033
1- P1_Nr2f1cKO_mS1 2- P4_Ctrl_S1	0.7871	0.1075	0.5689	0.1082	0.2182	-0.108 0.544	n.s.	0.174
1- P1_Ctrl_S1 2- P4_Ctrl_M1	0.7283	0.1094	0.5549	0.0801	0.1734	-0.118 0.465	n.s.	0.2225
1- P1_Ctrl_S1 2- P4_Nr2f1cKO_mS1	0.7283	0.1094	0.5358	0.0899	0.1925	-0.119 0.504	n.s.	0.2013
1- P1_Ctrl_S1 2- P4_Ctrl_S1	0.7283	0.1094	0.5689	0.1082	0.1594	-0.167 0.486	n.s.	0.3159
1- P4_Ctrl_M1 2- P4_Nr2f1cKO_mS1	0.5549	0.0801	0.5358	0.0899	0.0191	-0.249 0.287	n.s.	0.8772
1- P4_Ctrl_M1 2- P4_Ctrl_S1	0.5549	0.0801	0.5689	0.1082	-0.014	-0.299 0.271	n.s.	0.9184
1- P4_Nr2f1cKO_mS1 2- P4_Ctrl_S1	0.5358	0.0899	0.5689	0.1082	-0.0331	-0.338 0.272	n.s.	0.8179

Table S1. Spontaneous Ca²⁺ transient properties in acute brain slices of P1 and P4 CtrlS1, M1 of and *Nr2f1cKO* mS1 mice. Abbreviations: Hz - Ca²⁺ transient frequency, M1 - motor cortex, mS1 – motorized somatosensory cortex, P – postnatal day, S1 - somatosensory cortex, s.e. - Standard error.

	<i>Ctrl M1</i>	<i>Nr2f1cKO mS1</i>	<i>Ctrl S1</i>	p-value	test
V_{rest} (mV)	-58.48 ± 1.17	-54.62 ± 1.13	-60.26 ± 1.18	0.0028 (**)	one-way ANOVA
R_{in} (MΩ)	488.20 ± 43.97	494.80 ± 38.64	561.2 ± 36.66	0.4107	one-way ANOVA
Latency (ms)	112.3 ± 18.22	145.9 ± 23.59	133.5 ± 15.46	0.7798	Kruskal-Wallis test
Rheobase (pA)	59.00 ± 10.05	29.64 ± 3.47	61.05 ± 9.08	0.0017 (**)	Kruskal-Wallis test
$V_{threshold}$ (mV)	-32.44 ± 0.90	-32.09 ± 0.60	-30.95 ± 0.48	0.2046	Kruskal-Wallis test
AP_{amp} (mV)	72.75 ± 2.45	69.1 ± 1.11	66.65 ± 1.62	0.0708	one-way ANOVA
$AP_{half-width}$ (ms)	3.474 ± 0.1956	3.682 ± 0.1204	4.086 ± 0.1910	0.0580	one-way ANOVA
ISI (ms)	147.3 ± 18.19	175.1 ± 16.42	172.0 ± 19.92	0.6462	Kruskal-Wallis test
Sag (mV)	9.993 ± 1.48	5.38 ± 0.80	8.365 ± 0.89	0.0063 (**)	one-way ANOVA
Tau (ms)	28.57 ± 3.791	31.14 ± 3.70	28.42 ± 3.26	0.8389	Kruskal-Wallis test
MFF (Hz)	12.13 ± 0.987	17.92 ± 0.965	15.39 ± 1.202	0.0065 (**)	One-way ANOVA
C_m (pF)	64.12 ± 13.19	71.28 ± 8.70	52.78 ± 6.28	0.1977	Kruskal-Wallis test

Table S2. *Nr2f1* deficiency leads to changes in intrinsic electrophysiological properties in pyramidal neurons within the immature motor-like somatosensory cortex that are significantly different from motor and somatosensory cortex in controls. Intrinsic electrophysiological properties of layer V pyramidal neurons in acute brain slices of the immature cortex. Primary motor (M1) cortex from *control* animals (10 cells from 8 different brains), somatosensory (S1) cortex (19 cells from 8 different brains) and *Nr2f1cKO* motorized somatosensory cortex (mS1) (28 cells from 7 different brains) of P5-P8 mouse pups. V_{rest} : resting membrane potential; R_{in} : input resistance; $V_{threshold}$: action potential threshold; AP_{amp} : action potential amplitude; $AP_{half-width}$: action potential half-width; ISI: inter-spike interval; Tau: membrane time constant; MFF: maximum firing frequency; C_m : membrane capacitance. Data are represented as mean ± SEM.

Sholl analysis statistics 0-200 mm

Radius	Hypothesis	Mean 1	Mean 2	Mean Diff.	95,00% CI of diff.	Statistic	P value
0	<i>Ctrl S1 vs. cKO mS1</i>	0	0	0	-4,048 to 4,048	ns	>0,9999
	<i>cKO mS1 vs. Ctrl M1</i>	0	0	0	-4,848 to 4,848	ns	>0,9999
	<i>Ctrl S1 vs. Ctrl M1</i>	0	0	0	-5,335 to 5,335	ns	>0,9999
10	<i>Ctrl S1 vs. cKO mS1</i>	10,07	8,036	2,031	-2,017 to 6,079	ns	0,9978
	<i>cKO mS1 vs. Ctrl M1</i>	8,036	8,778	-0,7421	-5,59 to 4,106	ns	>0,9999
	<i>Ctrl S1 vs. Ctrl M1</i>	10,07	8,78	1,289	-4,046 to 6,623	ns	>0,9999
20	<i>Ctrl S1 vs. cKO mS1</i>	15,67	10,93	4,738	0,6898 to 8,786	**	0,0057
	<i>cKO mS1 vs. Ctrl M1</i>	10,93	12,78	-1,849	-6,697 to 2,999	ns	>0,9999
	<i>Ctrl S1 vs. Ctrl M1</i>	15,67	12,8	2,889	-2,446 to 8,223	ns	0,9891
30	<i>Ctrl S1 vs. cKO mS1</i>	18,87	10,36	8,51	4,461 to 12,56	****	<0,0001
	<i>cKO mS1 vs. Ctrl M1</i>	10,36	17,78	-7,421	-12,27 to -2,573	****	<0,0001
	<i>Ctrl S1 vs. Ctrl M1</i>	18,87	17,78	1,089	-4,246 to 6,423	ns	>0,9999
40	<i>Ctrl S1 vs. cKO mS1</i>	20,6	9,071	11,53	7,48 to 15,58	****	<0,0001
	<i>cKO mS1 vs. Ctrl M1</i>	9,071	17	-7,929	-12,78 to -3,081	****	<0,0001
	<i>Ctrl S1 vs. Ctrl M1</i>	20,6	17	3,6	-1,735 to 8,935	ns	0,7786
50	<i>Ctrl S1 vs. cKO mS1</i>	18,8	7,393	11,41	7,359 to 15,46	****	<0,0001
	<i>cKO mS1 vs. Ctrl M1</i>	7,393	15,11	-7,718	-12,57 to -2,87	****	<0,0001
	<i>Ctrl S1 vs. Ctrl M1</i>	18,8	15,11	3,689	-1,646 to 9,023	ns	0,7275
60	<i>Ctrl S1 vs. cKO mS1</i>	16,93	5,571	11,36	7,314 to 15,41	****	<0,0001
	<i>cKO mS1 vs. Ctrl M1</i>	5,571	12,56	-6,984	-11,83 to -2,136	****	<0,0001
	<i>Ctrl S1 vs. Ctrl M1</i>	16,93	12,56	4,378	-0,9568 to 9,712	ns	0,3138
70	<i>Ctrl S1 vs. cKO mS1</i>	14,33	4,75	9,583	5,535 to 13,63	****	<0,0001
	<i>cKO mS1 vs. Ctrl M1</i>	4,75	11,22	-6,472	-11,32 to -1,624	***	0,0005
	<i>Ctrl S1 vs. Ctrl M1</i>	14,33	11,22	3,111	-2,223 to 8,446	ns	0,9617
80	<i>Ctrl S1 vs. cKO mS1</i>	11,47	4,107	7,36	3,311 to 11,41	****	<0,0001
	<i>cKO mS1 vs. Ctrl M1</i>	4,107	8,111	-4,004	-8,852 to 0,844	ns	0,3001
	<i>Ctrl S1 vs. Ctrl M1</i>	11,47	8,111	3,356	-1,979 to 8,69	ns	0,8934
90	<i>Ctrl S1 vs. cKO mS1</i>	10	3	7	2,952 to 11,05	****	<0,0001
	<i>cKO mS1 vs. Ctrl M1</i>	3	7,111	-4,111	-8,959 to 0,7369	ns	0,2470
	<i>Ctrl S1 vs. Ctrl M1</i>	10	7,111	2,889	-2,446 to 8,223	ns	0,9891
100	<i>Ctrl S1 vs. cKO mS1</i>	7,067	2,643	4,424	0,3755 to 8,472	*	0,0160
	<i>cKO mS1 vs. Ctrl M1</i>	2,643	6,556	-3,913	-8,761 to 0,9353	ns	0,3509
	<i>Ctrl S1 vs. Ctrl M1</i>	7,067	6,556	0,5111	-4,823 to 5,846	ns	>0,9999
110	<i>Ctrl S1 vs. cKO mS1</i>	4,8	2,429	2,371	-1,677 to 6,42	ns	0,9590
	<i>cKO mS1 vs. Ctrl M1</i>	2,429	5,111	-2,683	-7,531 to 2,165	ns	0,9839
	<i>Ctrl S1 vs. Ctrl M1</i>	4,8	5,111	-0,3111	-5,646 to 5,023	ns	>0,9999
120	<i>Ctrl S1 vs. cKO mS1</i>	4,6	2,036	2,564	-1,484 to 6,613	ns	0,8843
	<i>cKO mS1 vs. Ctrl M1</i>	2,036	5,111	-3,075	-7,923 to 1,773	ns	0,8823
	<i>Ctrl S1 vs. Ctrl M1</i>	4,6	5,111	-0,5111	-5,846 to 4,823	ns	>0,9999
130	<i>Ctrl S1 vs. cKO mS1</i>	3,4	2,214	1,186	-2,863 to 5,234	ns	>0,9999
	<i>cKO mS1 vs. Ctrl M1</i>	2,214	4	-1,786	-6,634 to 3,062	ns	>0,9999
	<i>Ctrl S1 vs. Ctrl M1</i>	3,4	4	-0,6	-5,935 to 4,735	ns	0,8823

660	<i>Ctrl S1 vs. cKO mS1</i>	0	0	0	-2,803 to 2,803	ns	>0,9999
	<i>cKO mS1 vs. Ctrl M1</i>	0	0	0	-3,356 to 3,356	ns	>0,9999
	<i>Ctrl S1 vs. Ctrl M1</i>	0	0	0	-3,693 to 3,693	ns	>0,9999

Table S3. Analysis of basal dendritic complexity of layer V pyramidal neurons (LVPNs). Sholl analysis data of layer V pyramidal neurons in *Ctrl* M1 and S1 and *Nr2f1cKO* mS1 brain slices of proximal (0-200mm) and total (0-660mm) arborization. Highlighted in blue, comparisons that produced statistically significant P-values. P-values are calculated by 2way ANOVA test. **See also Figure 4 and Figure S4.**

Tables S4

Gene	Primers
<i>GAPDH</i>	Fw: GTATGACTGCACTCACGGCAAA
	Rev: TTCCCATTCTCGGCCTTG
<i>Cacna1A</i>	Fw: GGGCCCAAGAGATGTTCCAG
	Rev: TCCACAGACTGGGAGTTGGG
<i>Cacna1B</i>	Fw: CACGCAGAGGACCCACGATG
	Rev: CATCACAGCCAGTGTTCTTG
<i>Cacna1G</i>	Fw: TCAGCTGCCTGTCAACTCCC
	Rev: CCCATCACCATCCACACTGG
<i>Cacna1H</i>	Fw: ACCTACACAGGCCCGGTAC
	Rev: ATGGGACCTGGAAGGAGGTG
<i>Cacna2D1</i>	Fw: CAGGGAGGGCACTGATCTTC
	Rev: TTGATAGTGACGGGCGAAGG
<i>Cacna2D3</i>	Fw: TTAGGTGTGGCGCTCTCCAG
	Rev: GCCAAGGACACGTCAGGATG
<i>Hcn1</i>	Fw: TGCCACAGCTTTGATCCAGT
	Rev: GCGCATGTCAGCTGGTAACT
<i>Kcnab1</i>	Fw: TCCCATGGAAGAAATCGTTCCG
	Rev: CTTCCATGATCTCCATCGCG
<i>Kcng3</i>	Fw: GGAAGCCATAGAGGCAGTG
	Rev: GTGGAGTTCTCTCCACACATCTG
<i>Kcnd2</i>	Fw: CAACCGCAGTCTGGATGACC
	Rev: CGGTGAACCACCCTATGCAG
<i>Kcnh1</i>	Fw: TTAGTGCCTTTATGGGTGATCC
	Rev: GATGCCCTGACTCTCTCTCC
<i>Kcnh5</i>	Fw: CTTTCCAGACCCAGGATGCC
	Rev: TTGATTCAGTGGAGCGCCTG
<i>Kcnj6</i>	Fw: AACTGACGGAGAGGAATGGG
	Rev: TGGGTTGGGTGAATTCTGGG
<i>Kcnk2</i>	Fw: ACGTGGCAGGTGGATCAGAC
	Rev: AGTAGGCCAGCCCAACGAG
<i>Kcnmb4</i>	Fw: TTGGAAAGATGAGATCGGTTCC
	Rev: AAGCAGTGCAGGAGAGCAATC
<i>Kv2.1</i>	Fw: CGTCATCGCCATCTCTCATG
	Rev: CAGCCCACTCTCTACTAGCAA
<i>Gria1</i>	Fw: CTGGTGGTGGTGGACTGTG
	Rev: TGTCCATGAAGCCAGGTTG
<i>Gria2</i>	Fw: ATTTGGAATGGTATGGTTGGAG
	Rev: AGGCTCATGAATGGCTTCGAG
<i>Gria3</i>	Fw: TCATTCTCACGGAGGATTCCC
	Rev: CACAGCAAAGCGGAAAGCAC

Gria4	Fw: CCAGAGCCTCCCTGAAGACC
	Rev: TGCGCGCTCTCCTCTCTTTC
Grik1	Fw: AGTTGGTTCGCATGCTCTTCG
	Rev: CGAACCTTGATGCCCAATAC
Grik2	Fw: CTGGTGGAGAGTGCTTTGGG
	Rev: CCACACCCTTGCAACCCTG
Grik3	Fw: TCGCCAGATTCAGCCCTTAC
	Rev: GCCCATTCCAAACCAGAAGC
Grik5	Fw: GCCTGCGGTTGGTAGAGGAC
	Rev: TCTGCCTTCCGGTTGATGAG
Grin1	Fw: TCAGAGCACACTGTGGCTGC
	Rev: ATCGGCCAAAGGGACTGAAG
Grin2B	Fw: GGAAGTGGGAGAGGGTGGG
	Rev: CAGGACACATTTCGAGGCCAC
Scn1a	Fw: AACAAAGCTTGATTCACATACAATAAG
	Rev: AGGAGGGCGGACAAGCTG
NaV 1.2	Fw: GGGAACGCCCATCAAAGAAG
	Rev: ACGCTATCGTAGGAAGGTGG
NaV 1.6	Fw: AGTAACCCTCCAGAATGGTCCAA
	Rev: GTCTAACCAGTTCCACGGGTCT

A. List of primers used for qPCR analysis. See also Figure 6 and Figure S6.

Locus	Primers
Nr2f1 binding site at Hcn1 locus	Fw: TTTCTGCTTTCCCGTGAGAGC
	Rev: AGCCTAGCCTAGGAAGCCAG
Nr2f1 binding site at Kcnab1 locus	Fw: TGTGGTATCAGAGATGAAAGGC
	Rev: AAGGGACCTCCCAGCTCTTC
Nr2f1 binding site at Kcnk2 locus	Fw: CCCAAAGCTGGACTTGTGTAC
	Rev: TTCCCCTGATCAAATTCCATTC
Egr1 binding site at Cacna1g locus (negative control)	Fw: AGCACCAGCTCAGATCACTCC
	Rev: CAGAAGAACTGTGTCAAGAGC

B. List of primers used for qPCR analysis after ChIP. See also Figure 6.

Antigen	Provider	Catalog #	Species	Application	Working dilution
AnkG	Antibodies Inc.	75-146	Ms	IF - 1AB	1:200
CTIP2	Abcam	ab18465	Rat	IF - 1AB	1:500
NeuN	Cell Signaling	24307S	Rb	IF - 1AB	1:100
HCN1	Abcam	ab229340	Rb	IF - 1AB WB	1:100 1:1000
b-actin	Abcam	ab8277	Rb	WB	1:3000
GFP	Abcam	ab13970	Ck	ChIP	3 mg
COUP-TFI	Thermo Fisher	PA5-21611	Rb	ChIP	3 mg
Ms IgG - AF 555	Thermo Fisher	A21422	Gt	IF - 2AB	1:500
Rat IgG - AF 488	Thermo Fisher			IF - 2AB	1:500
Rb IgG - AF 647	Thermo Fisher	A32733	Gt	IF - 2AB	1:500
Rb IgG - AF 555	Thermo Fisher	A21428	Gt	IF - 2AB	1:100
Ck IgY - AF 488	Thermo Fisher	A11039	Gt	IF - 2AB	1:500
Rb IgG - HRP	BioRad	1706515	Gt	WB - 2AB	1:3000
Ms IgG - HRP	BioRad	1721011	Gt	WB - 2AB	1:3000

C. List of antibodies used in this study.

Figure		Sample number	Type and age of the samples	Test
1	D	N MEAs >=7 <i>Ctrl M1</i> N MEAs= 7 <i>Nr2f1cKO mS1</i> N MEAs= 12 <i>Ctrl S1</i> N MEAs= 10	Cultured cortical neurons DIV9	One-way ANOVA test with Bonferroni post hoc test
	E			
	F			
	G			
	H			
	D	<i>Ctrl M1</i> N channels=76 <i>Nr2f1cKO mS1</i> N channels=208 <i>Ctrl S1</i> N channels=271		
	E	<i>Ctrl M1</i> N channels=56 <i>Nr2f1cKO mS1</i> N channels=203 <i>Ctrl S1</i> N channels=170		
	F	<i>Ctrl M1</i> N channels=56 <i>Nr2f1cKO mS1</i> N channels=112 <i>Ctrl S1</i> N channels =169		
G	<i>Ctrl M1</i> N channels=56 <i>Nr2f1cKO mS1</i> N channels =114 <i>Ctrl S1</i> N channels=167			
H	<i>Ctrl M1</i> N channels=56 <i>Nr2f1cKO mS1</i> N channels =258 <i>Ctrl S1</i> N channels=256			
2	D	P1 N cells > 159 <i>Ctrl M1</i> N=165 <i>Nr2f1cKO mS1</i> N=280 <i>Ctrl S1</i> N=159 P4 N cells > 84 <i>Ctrl M1</i> N=142 <i>Nr2f1cKO mS1</i> N=369 <i>Ctrl S1</i> N=83	Acute horizontal brain sections P1 and P4	Three -way ANOVA followed by post - hoc analysis using Welch Two-samples test
	D	P1 N slices > 6 <i>Ctrl M1</i> N=7 <i>Nr2f1cKO mS1</i> N=6 <i>Ctrl S1</i> N=7		
	F	P4 N slices > 5 <i>Ctrl M1</i> N=12 <i>Nr2f1cKO mS1</i> N=12 <i>Ctrl S1</i> N=5		
3	G	N cells > 10 <i>Ctrl M1</i> N=10 (8 brains) <i>Nr2f1cKO mS1</i> N=28 (7 brains) <i>Ctrl S1</i> N=19 (8 brains)	Acute coronal brain sections P5-P8	One-way ANOVA
	H			Kruskal-Wallis test
	I			One-way ANOVA
4	B	N cells > 11 <i>Ctrl M1</i> N=11 <i>Nr2f1cKO mS1</i> N=30 <i>Ctrl S1</i> N=19	Acute coronal brain sections P5-P8	Two-way ANOVA
	C			Kruskal-Wallis
	D			One-way ANOVA
	F			One-way ANOVA
	G			One-way ANOVA
5	B	N brains=3	Coronal brain sections P7	Welch's test
	D			Unpaired t-test
	E			Unpaired t-test
	G	N brains=3	Coronal brain sections	Unpaired t-test

	A		P21	Welch's test
6	B	N cortices=4	Cortical protein extract P7	Welch's test
	C	N brains=3	Coronal brain sections P7	Welch's test
	D	N brains=3	Coronal brain sections P7	Welch's test
	E	N cortices=3		t-test followed by Benjamini-Hochberg correction
S1	A	N MEAs >=6 <i>Ctrl M1</i> N MEAs=6 <i>Nr2f1cKO mS1</i> N MEAs =6 <i>Ctrl S1</i> N MEAs =10	Cultured cortical neurons DIV9 & DIV15	One-way ANOVA test with Bonferroni post hoc test
	B	N MEAs >=4 <i>Ctrl M1</i> N MEAs =6 <i>Nr2f1cKO mS1</i> N MEAs =4 <i>Ctrl S1</i> N MEAs =8		
	C			
	D	N MEAs >=6 <i>Ctrl M1</i> N MEAs=6 <i>Nr2f1cKO mS1</i> N MEAs =6 <i>Ctrl S1</i> N MEAs=10	Cultured cortical neurons DIV15	One-way ANOVA test with Bonferroni post hoc test
	E			
	D	<i>Ctrl M1</i> N channels=330 <i>Nr2f1cKO mS1</i> N channels =377 <i>Ctrl S1</i> N channels=456		
E	<i>Ctrl M1</i> N channels=329 <i>Nr2f1cKO mS1</i> N channels =447 <i>Ctrl S1</i> N channels=458			
S2	C	P1 N slices > 6 <i>Ctrl M1</i> N=7 <i>Nr2f1cKO mS1</i> N=6 <i>Ctrl S1</i> N=7 P4 N slices > 5 <i>Ctrl M1</i> N=12 <i>Nr2f1cKO mS1</i> N=12 <i>Ctrl S1</i> N=5	Acute horizontal brain sections P1 and P4	Welch's test
S3	D	N cells > 10 <i>Ctrl M1</i> N=10 (8 brains) <i>Nr2f1cKO mS1</i> N=28 (7 brains)	Acute coronal brain sections P5-P8	One-way ANOVA (Rin), Kruskal-Wallis test (Vthreshold, ISI)
	B	<i>Ctrl S1</i> N=19 (8 brains)		One-way ANOVA (AP h-w, AP amp), Kruskal- Wallis test (Latency)
S4		N cells > 4 <i>Ctrl M1</i> N=4 <i>Nr2f1cKO mS1</i> N=23 <i>Ctrl S1</i> N=12	Acute coronal brain sections P5-P8	Two-way ANOVA
				One-way ANOVA
				One-way ANOVA
				One-way ANOVA
S5		N brains=3	Acute Coronal brain sections P21	Two-way ANOVA

S6		N cortices >3	Cortical RNA extract P7	t-test followed by Benjamini-Hochberg correction
----	--	---------------	----------------------------	--

Table S5. Experimental setup summary. Number, developmental stage and type of samples and statistical tests deployed in each experiment.

2. Paper Two

Title: *The topographic organization of cortico-pontine axonal projections is controlled by postmitotic expression of the area-patterning genes COUP-TFI/Nr2f1*

To date, it is widely known that the neuronal networks regulating voluntary movements on the one hand and locomotion or reflexes on the other are almost mutually excluded, and it is thus not surprising that those functions might be independently affected in human syndromes.

In mammals, the main circuitry of voluntary movements consists in reciprocal connections between the neocortex and the cerebellum *via* synaptic relays in the pontine nuclei, deep cerebellar nuclei, and thalamus. Furthermore, each of these regions is organized in topographically arranged maps, with different body parts represented in largely continuous somatotopic maps in the neocortex (Brodmann et al., 2006; Chapin et al., 1984; Fabri et al., 1991; Welker, 1971; Woolsey et al., 1970) and discontinuous, fractured maps in the cerebellum (Bower et al., 1981). Hence, the main role of the intercalated regions is to decode the original information so that is compatible with the topographic map of the receiving organ. Regarding the cortico-pontine connections, it has been observed that axons from layer V pyramidal neurons across the cerebral cortex project to the pontine nuclei innervating topographically organized clusters as demonstrated in monkey (Schmahmann et al., 1997), cat (Bjaalie et al., 1997), rat (T. B. Leergaard et al., 2000; Trygve B. Leergaard et al., 2000), and evidences of this organization start to emerge in mice (Henschke et al., 2020; Inoue et al., 1991; Proville et al., 2014). Within the pontine nuclei, the 3D arrangement of clustered terminal fields both preserves the overall topographical relationships of the cortical maps, and partially overlap and introduce new spatial proximities among projections from different cortical areas (Henschke et al., 2020; Trygve B. Leergaard et al., 2003, 2007; Proville et al., 2014).

According to the chrono-architectonic hypothesis of cortico-pontine circuit development (Trygve B. Leergaard et al., 1995, 2003), pontine neurons settle in the PN in a shell-like fashion in function of their birthdate (Altman et al., 1978; Kratochwil et al., 2017). The earliest cortico-pontine fibres innervate the core whereas later arriving axons progressively innervate more peripherally located pontocerebellar neurons, suggesting a causal link between birthdate and arrival time of pontine and

subcortical neurons in rodents. In terms of cortical origin, layer V neurons from the anterolateral cerebral cortex project to the central regions of the PN, while more medially located cortical neurons project to more external regions. More specifically, projections from motor areas distribute more medially and rostrally, and projections from somatosensory areas distribute in the middle and caudal part of the PN. Finally, projections from auditory and visual areas in the cortex innervate the dorsolateral parts of the PN (Trygve B. Leergaard et al., 1995, 2007).

To date, the establishment of the cortico-pontine topography is not yet completely understood and various hypotheses suggest it might be either controlled by local pontine nuclei chemo-attractive mechanisms or be intrinsically defined by factors expressed by cortico-pontine projection neurons or even that both mechanisms are acting simultaneously.

In this work, we aimed to demonstrate an intrinsic role of area patterning genes involved in early areal mapping during corticopontine topography. As an experimental model, we used the *Nr2f1* conditional mouse lines described to impinge sensory identity in cortical cells and to act on the specification, differentiation and maturation of layer V neurons (see also previous paper), which will form the corticospinal tract, one of the main tracts involved in the voluntary movement network. To do this, we first used *two conditional KO* mouse models for *Nr2f1* to specifically remove the gene from either cortical progenitor cells (*Emx1-cKO*) or cortical postmitotic neurons (*Nex-cKO*). In these models, and thanks to the cortical YFP-H reporter line, we evaluated the pattern of innervation at the level of the pontine nuclei, one of the main integration centres in the network, and other structural characteristics of the tract, such as its degree of fasciculation in the hindbrain region. These analyses showed that *Nr2f1* expression in cortical progenitor cells regulates the balance between corticopontine and corticospinal neurons whereas postmitotic expression seems to be specifically involved in topographic pontine mapping.

In the second part of the manuscript, we aimed to identify the cortical area responsible for the corticopontine topographic shift observed in *Nex-cKO* brains. Our hypothesis is that the gradient

Nr2f1 expression, high latero-posterior and low medio-anterior (Fig. 30), is contributing in establishing proper topography in the corresponding pontine regions.

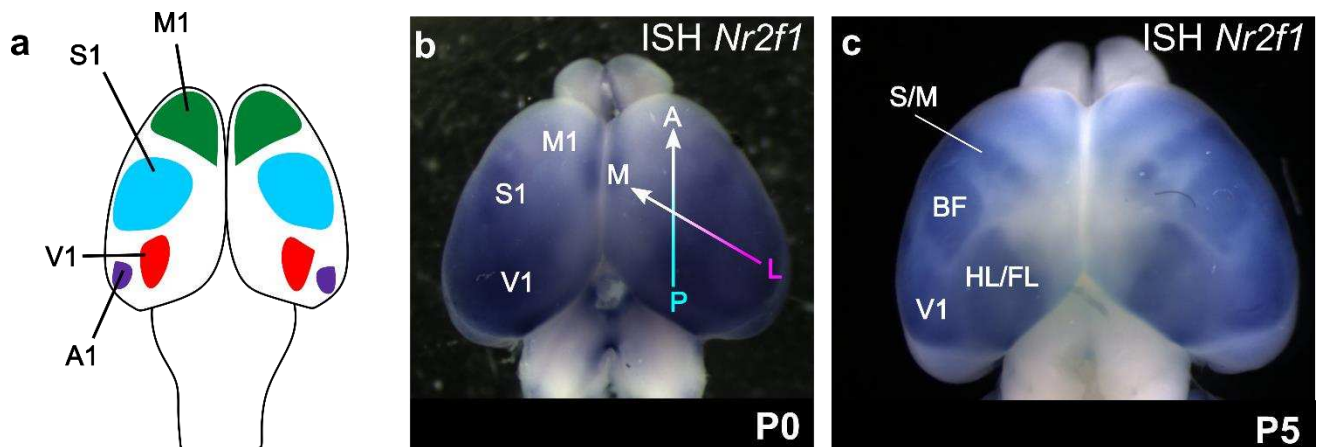


Figure 30 - *Nr2f1* cortical expression pattern. **a)** Schematic representation of functional cortical areas. *In situ* hybridization of *Nr2f1* in P0 **(b)** and P5 **(c)** mouse brains. At early postnatal stages **(b)**, *Nr2f1* is expressed in the cortex following a posterior-high/anterior-low (in cerulean) and a latero-high/medial-low (in pink) gradient, which is greatly refined at later stages **(c)**, where it is highly expressed in sensory areas and in the mixed sensory/motor area and absent from motor regions.

BF: barrel field; FL: forelimb somatosensory area; HL: hindlimb somatosensory area; LM: latero-medial; PA: postero-anterior axis; S/M: sensory/motor area.

For this task, I performed stereotaxic injections in P4-P5 pups of AAV particles carrying the reporter gene tdTomato. The experiment consisted in a series of injections in either motor or somatosensory regions of young *Ctrl* and *Nex-cKO* animals, sacrifice at age P21 through intracardiac perfusion and brain dissections. The tdTomato signal was then revealed with the help of an anti RFP antibody on 150 μ m-thick sections (see material and methods for additional information) prior imaging. The atlas registration and the spatial localization of the signal, both at the injection site and at the level of the pontine nuclei, was performed by our collaborators, expert in corticopontine topography and brain imaging (Papp et al., 2016; Puchades et al., 2019). Since a small shift of injection site in the cortex can produce a significant change in the innervation of the pontine nuclei, each mutant experiment was compared to multiple controls from both our experimental groups and public available data from the Allen brain connectivity atlas (<http://connectivity.brain-map.org/>).

Analysis of *Ctrl*s and *Nex-cKO* brains injected in motor regions gave rise to similar pattern of innervation, indicating that loss of *Nr2f1* function is not drastically affecting the topographical organization of corticopontine projections arising from frontal/motor regions where gene expression is already low at physiological levels. Conversely, *Nex-cKO* brains injected in somatosensory and more laterally located regions showed a shift in pontine innervation, compared to controls, suggesting that *Nr2f1* might contribute to the somatotopic map of corticopontine projections arising from somatosensory regions.

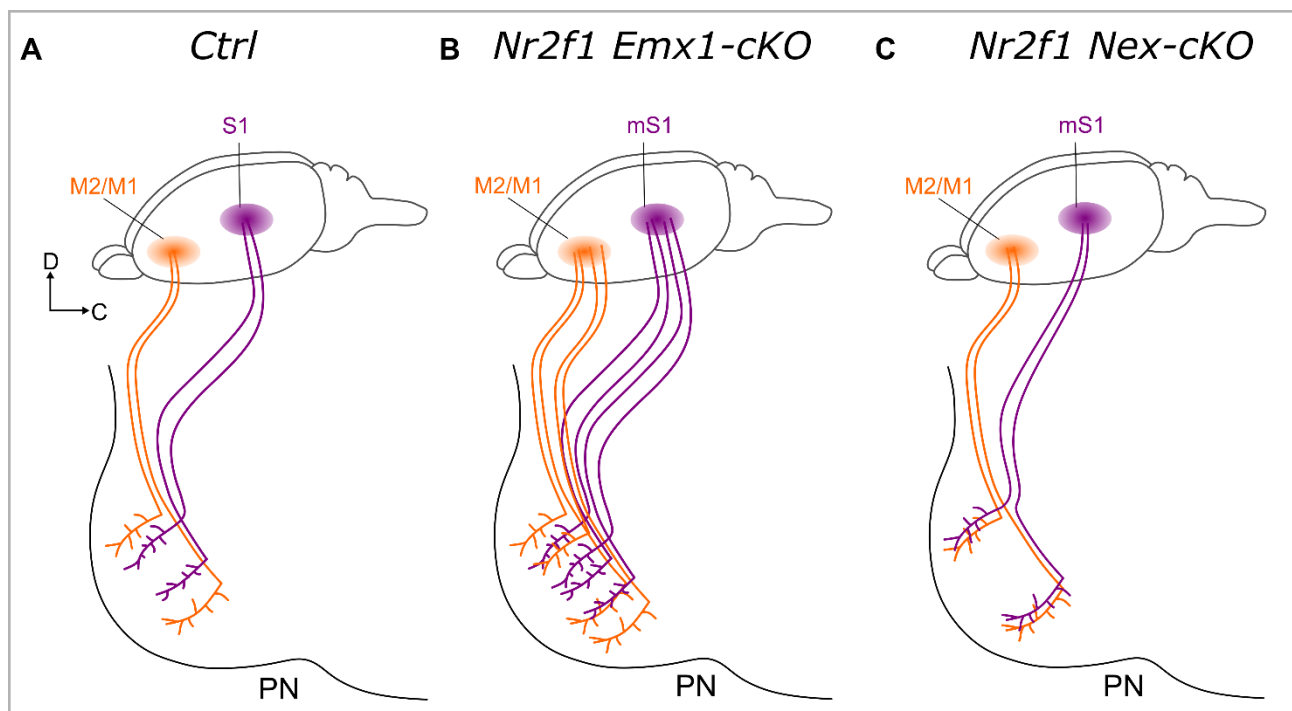


Figure 31 - Graphical summary. *a)* in mice, the topographic organization of motor and somatosensory cortical projections to the pontine nuclei (in orange and purple) relies on *Nr2f1*, an area patterning gene, for its correct establishment. Whether neurons from somatosensory areas tend to project to the inner core of the PN (purple), motor neurons instead (orange) innervate progressively more external layers within the PN. The removal of *Nr2f1* from progenitor cells (*b*) induces a generalized overproduction of corticopontine neurons, which end up projecting to the pontine nuclei in a disorganized manner. Conversely, when *Nr2f1* is depleted from postmitotic neurons (*c*), it specifically affects the ability of *mS1* neurons to reach their correct target region in the PN, and an internal-external shift of corticopontine projections is observed.

Topography of corticopontine projections is controlled by postmitotic expression of the area-mapping gene Nr2f1

Chiara Tocco^{1*}, Martin Øvsthus^{2*}, Jan G. Bjaalie², Trygve B. Leergaard^{2#}, Michèle Studer^{1#}

¹*Université Côte d'Azur, CNRS, Inserm, iBV, France*

²*Institute of Basic Medical Sciences, University of Oslo, Dept. Molecular Medicine, Oslo, Norway*

*These authors have contributed equally to the study.

#Co-last senior authors.

@Corresponding author:

Michèle Studer

iBV - Institut de Biologie Valrose

Univ. Côte d'Azur

Centre de Biochimie ; UFR Sciences

Parc Valrose, 28 avenue Valrose

06108 Nice Cedex 2

France

Tel.: +33 489150720

e-mail: Michele.studer@unice.fr

ABSTRACT

Axonal projections from layer V neurons of distinct neocortical areas are topographically organized into discrete clusters within the pontine nuclei. The mechanisms underlying the establishment of corticopontine connectivity are insufficiently understood, and it is unknown whether area patterning genes are involved in coordinating topographic projections from the neocortex to the pontine nuclei. We have investigated the arrangement of corticopontine projections in transgenic mice lacking cortical expression of the area patterning gene *Nr2f1* and exhibiting severe areal organization defects. Combining 3D digital brain atlas tools, cell-type specific *Cre*-dependent mouse lines and axonal tracing, we show that postmitotic *Nr2f1* inactivation in the developing cortex changes somatosensory-specific corticopontine projections into motor-like ones, while topographical pontine organization is largely abolished in the complete absence of *Nr2f1*. We conclude that cortical gradients of area patterning genes are directly implicated in the establishment of a topographic somatotopic map between the cortex and pontine nuclei.

INTRODUCTION

The cerebro-ponto-cerebellar system reciprocally connects the neocortex with the cerebellum via synaptic relays in the pontine nuclei, deep cerebellar nuclei, and thalamus. These pathways contribute to fine tuning and coordination of a wide range of voluntary behaviors (Brodal and Bjaalie, 1997; Svoboda and Li, 2018). To achieve proper connectivity, neuronal populations in the neocortex and cerebellum are arranged in essentially two-dimensional, topographically organized maps, with different body parts represented in largely continuous somatotopic maps in the neocortex (Chapin and Lin, 1984; Fabri and Burton, 1991; Welker, 1971; Woolsey and Van der Loos, 1970), and discontinuous, fractured maps in the cerebellum (Bower, 2011; Bower et al., 1981; Bower and Kassel, 1990; Leergaard et al., 2006; Nitschke et al., 1996; Shambes et al., 1978; Voogd, 1995; Welker, 1987). The intercalated regions of this network receive and integrate signals from the different structures, ultimately resulting in coordinating and seamlessly executing fine voluntary movements.

The pontine nuclei constitute a major synaptic relay for cerebro-cerebellar signals originating from cortical layer V (Brodal and Bjaalie, 1992; Lemon, 2008; Mihailoff et al., 1985). Axonal projections from layer V pyramidal neurons across the cerebral cortex to the pontine nuclei are organized in topographically organized clusters within the pontine nuclei, as shown in monkey (Brodal, 1978; Schmahmann and Pandya, 1997), cat (Bjaalie and Brodal, 1997), rat (Leergaard et al., 2000a; Leergaard et al., 2000b), and to some extent also in mice (Henschke and Pakan, 2020; Inoue et al., 1991; Proville et al., 2014). Within the pontine nuclei, the three-dimensional (3D) arrangement of clustered terminal fields, well described in rats, both preserves the overall topographical relationships of the cortical maps, but also partially overlap and introduce new spatial proximities among projections from different cortical areas (Leergaard, 2003; Leergaard and Bjaalie, 2007).

According to the chrono-architectonic hypothesis of cortico-pontine circuit development (Leergaard, 2003; Leergaard et al., 1995), neurons settle in the pontine nuclei in a shell-like fashion in function of their birthdate (Altman and Bayer, 1978, 1987, 1996), see also (Kratochwil et al., 2017). The earliest corticopontine fibers reach the core of the pontine nuclei where the earliest neurons have settled. Later arriving axons progressively innervate later arriving, and more peripherally

located pontocerebellar neurons, thus innervating the pontine nuclei in an inside-out fashion and suggesting a causal link between birthdate and arrival time of pontine and subcortical neurons in rodents. In terms of cortical origin, layer V neurons from the somatosensory and motor areas of the anterolateral cerebral cortex project to the central regions of the pontine nuclei, while the more medially located parts of these cortical regions project to more external regions, with projections from motor areas distributed more medially and rostrally, and projections from somatosensory areas distributed in the middle and caudal part of the pontine nuclei. Finally, projections from auditory and visual cortex innervate the dorsolateral parts of the pontine nuclei (Leergaard and Bjaalie, 1995, 2007).

The mechanisms responsible for establishing the topographic map between the neocortex and pontine nuclei are insufficiently known. The chrono-architectonic hypothesis postulates that the complex 3D topography is a product of straightforward spatio-temporal cortical gradients combined with possibly non-specific chemo-attractive mechanisms. This opens the questions of whether layer V neurons are intrinsically programmed to target specific groups of pontine neurons, or whether both intrinsic and extrinsic chemo-attractive mechanisms are directly involved in guiding proper topographical innervation to distinct subregions of the pontine nuclei. Although a plethora of molecules have been described to affect the development of the corticospinal tract (CST) (Welniarz et al., 2017), and some of them are specifically expressed in the neocortex in both progenitor cells and postmitotic neurons, little is known about cortex-specific genes being able to influence the topographic organization of corticopontine projections. Abnormal expression of cortical factors or axon guidance molecules generally results in defective growth of corticofugal axons, thus precluding any role in topographical mapping. In this study, we hypothesized that the nuclear factor *Nr2f1* (also known as COUP-TFI), a well-known area mapping gene that regulates topographic mapping of corticothalamic projections (Alfano et al., 2014; Armentano et al., 2007) and differentiation of corticospinal motor neurons and their projections (Tomassy et al., 2010), could represent one of these factors able to control topographic corticopontine mapping during corticogenesis.

To test this hypothesis and investigate the contribution of cortical genetic programs in the establishment of topographic corticopontine projections, we made use of cortico-specific *Nr2f1* conditional knockout mice (Alfano et al., 2014; Armentano et al., 2007) crossed to an *YFP-H* reporter

line (Feng et al., 2000), in which YFP is highly expressed in cortical layer V pyramidal neurons and their axonal projections (Porrero et al., 2010). The distributions of fluorescent signals were evaluated by side-by-side comparison of spatially corresponding microscopic images, and by 3D visualization of semi-quantitatively extracted point coordinate data representing labelling. Public tract-tracing data from the Allen Institute mouse brain connectivity atlas were used to demonstrate 3D topography of corticopontine projections in wild type mice, as a benchmark for further interpreting findings in the mutant mice. Next, we investigated the spatial distribution of transgenic expression of YFP signal and anterogradely labelled corticopontine projections in two independent *Nr2f1* conditional mouse lines, and control animals. Our data indicate that *Nr2f1* plays a dual role in corticopontine projection development. While its expression in cortical progenitor cells regulates the balance between corticopontine and corticospinal neurons, postmitotic expression seems to be specifically involved in topographic pontine mapping. Overall, our results demonstrate that postmitotic graded expression of area mapping genes, such as *Nr2f1*, are directly implicated in the establishment of area-specific targeting of corticopontine neurons.

RESULTS

Benchmark 3D topographic organization of corticopontine projections in wild-type mice

As a first approach to establish a 3D benchmark reference of the topographical organization of corticopontine projections in normal adult mice, we used the public *Allen Mouse Brain Connectivity Atlas* (Wang et al., 2020) to tract tracing data that has formerly aided the interpretation of the spatial distribution of YFP expressing and anterogradely labeled axons in the pontine nuclei. **Figure 1** shows a flowchart diagram of the different processing and analytic steps used for the different animal groups depicted in our workflow. Here, we first present the normal topographical organization of motor and somatosensory corticopontine projections in wild-type mice, before evaluating the YFP signal in the cortex, pontine nuclei, and medulla oblongata of *Nr2f1* mutant mice. We have semi-quantitatively characterized anterogradely labelled corticopontine projections from microscopic images shared by the *Allen Institute* as 3D data points, and co-visualized data from ten such experiments in a 3D viewer tool (**Figure 2**). Comparison of data points representing corticopontine

projections from the primary/secondary motor cortex (M1, M2; n = 5) and primary somatosensory cortex (S1; n = 5), showed that motor and somatosensory corticopontine projections target largely segregated subspaces of the pontine nuclei, with somatosensory projections located predominantly in central and caudal parts (**Figure 2E**), while projections originating from the motor cortex were located more rostrally and medially, partly surrounding the sensory projections externally (**Figure 2D**).

To further test whether motor and somatosensory corticopontine projections follow the somatotopic principles as described in rats (Leergaard and Bjaalie, 2007), we selected experiments with tracer injections located progressively more medially in the cerebral cortex, going from the representation of the face, *via* the upper limb to the lower limb representations in S1, essentially following the cortical neurogenetic gradient that ripples out from the anterolateral cortex (Smart, 1984) (see also (Leergaard and Bjaalie, 2007)). The 3D visualizations clearly show that mouse corticopontine projections are somatotopically distributed, with projections from the head or face region of S1 located centrally in the pontine nuclei, and projections from the forelimb and hindlimb located progressively more ventral and caudal (**Figure 2G**), in line with previous findings in rats (Leergaard et al., 2000a). Similarly, corticopontine projections from injections distributed from anterolateral towards medial locations across M1 and M2 were overall distributed in progressively more external subspaces, from central towards medial and rostral (**Figure 2H**). Notably, projections from injections located medially in the cerebral cortex, were distributed peripherally in the pontine nuclei, attaining a circular shape surrounding an empty central core (**Figure 2I**), in agreement with topographical distribution principles in rats (Leergaard and Bjaalie, 2007).

Taken together, our findings confirm that the somatosensory and motor neurons of the mouse cortex project to largely separate parts of the pontine nuclei (Henschke and Pakan, 2020; Inoue et al., 1991; Proville et al., 2014), with clustered terminal fields somatotopically organized in an overall 3D somatotopic map, as previously shown in rats (Leergaard et al., 2000a; Leergaard and Bjaalie, 2007). The 3D point data are used below as supplementary control data and as benchmark for interpreting YFP expression and tract-tracing results in *Nr2f1* mutant mice.

Different area-specific layer V neuron distribution between *Emx1-cKO* and *Nex-cKO* adult mutant mice

To elucidate the role of cortical areal specification on the establishment of topographical organization in mouse corticopontine projections, we first investigated the spatial organization of layer V cortical distribution and corticopontine axonal projections in *Nr2f1* deficient mice, described to display severe areal organization defects, such as an expansion of motor-like identity in presumptive somatosensory cortex (Alfano et al., 2014; Armentano et al., 2007). To this purpose, we used two well-established conditional *Nr2f1* mouse mutants. The *Nr2f1^{fl/fl}::Emx1-Cre* mouse, in which *Nr2f1* expression is abolished from cortical progenitor cells as early as mouse embryonic (E) age 9.5 (Armentano et al., 2007), and the *Nr2f1^{fl/fl}::Nex-Cre* mouse in which *Nr2f1* expression is inactivated solely in cortical postmitotic neurons (Alfano et al., 2014). Both mouse lines were crossed to the *Thy1-eYFP-H* reporter line to specifically restrict signal expression to layer V pyramidal neurons, and thus allowing proper labelling of subcortical projection neurons, including corticospinal and corticopontine fibers (Harb et al., 2016; Porrero et al., 2010). For simplicity, both lines will be named from here on *Emx1-cKO* and *Nex-cKO*, respectively.

In agreement with earlier reports (Porrero et al., 2010), we observed substantial YFP signal expression in the hippocampus, tectum, and pontine nuclei, as well as in the globus pallidus, claustrum, endopiriform nucleus, nucleus of the lateral olfactory tract, mammillary nuclei, piriform area and the substantia innominata in adult mice (**Figure 3A**). In the brain stem, signal expression was seen in the vestibular nuclei, deep cerebellar nuclei, and cerebellum. Although signal expression was present in almost the same regions in 2-months-old mutant mice as in controls, more detailed analysis of signal expression in neocortical areas revealed some distinct differences in *Emx-cKO* and *Nex-cKO* cortices relative to their respective controls, and between the two conditional lines. We used a semi-quantitative scoring system to estimate the amount of signal expression across the cerebral cortex, in areas defined by delineations in spatially registered overlay images from *Allen Mouse Brain Atlas* (**Figure 1; Figure 3B-D**). In control animals, the distribution of layer V neurons followed a rostrally high to caudally low gradient (**Figure 3A, B**), in line with the earlier documented high numbers of layer V neurons in the rostrally located motor areas, and lowest numbers in the

auditory and visual areas of the occipital cortex (Polleux et al., 1997; Porrero et al., 2010; Shepherd, 2009). In the cortex of mutant animals, this gradient was disrupted (**Figures 3C, D**). Increased YFP expression was observed caudally in the occipital and retrosplenial cortex in both groups of mutant mice, in conjunction with decreased YFP signal in frontal areas, which was particularly more pronounced in *Nex-cKO* compared to *Emx-cKO* mice (**Figures 3C-F**). Interestingly, the highest signal of YFP expression was observed in the *Emx1-cKO* somatosensory cortex, where expression was instead lower in *Nex-cKO* brains (compare **Figure 3C'' to 3D''**). Together, these data suggest a different role for *Nr2f1* in regulating layer V production across all cortical areas in progenitor cells (*Emx-cKO*) and postmitotic neurons (*Nex-cKO*).

Altered balance between corticopontine and corticospinal projections in *Emx1-cKO* and abnormal CST fasciculation

Next, we asked whether the impaired cortical distribution of YFP expressing layer V neurons in mutant mice influences the integrity of subcortical axonal projections. In all cases (mutant and controls alike), strong YFP signal expression was seen bilaterally in the main corticofugal pathways, visible as longitudinally oriented fiber bundles coursing through the caudoputamen towards the internal capsule and cerebral peduncle, passing dorsal to the pontine nuclei as the longitudinal fasciculus of the pons, and continuing through the brain stem towards the spinal cord as the pyramidal tract (**Figure 3A; Figure 4A-D**).

The majority of fibers in the cerebral peduncle are corticobulbar and terminate in the pontine nuclei (Tomasch, 1968, 1969). We therefore hypothesized that abnormal distribution of layer V neurons observed in mutant mice (**Figure 3**) might affect corticopontine innervation, which in turn could be reflected in an abnormal girth of the pontine longitudinal fascicle as it enters the pons rostrally, and to its girth as it exits the pons caudally, and continues as the pyramidal tract (**Figure 4A**). To evaluate this, we measured the dorsoventral width of the longitudinal fascicle of the pons in sequential sections along the medio-lateral axis. The measurements have been taken at rostral and caudal levels to the pontine nuclei in the three genotypes (**Figure 4E**). Surprisingly, we found the lateral

part of the fascicle to be wider at both rostral and caudal levels in *Nex-cKO* mice compared to *Emx1-cKO* and controls, while being narrower medially (see red surface in **Figure 4F,G**). This suggests that the longitudinal fascicle of the pons is flattened and expanded laterally upon *Nr2f1* inactivation in postmitotic neurons. By contrast, the diameter of the fascicle was not measurably different along the mediolateral axis in *Emx1-cKO* mice, although some statistically significant reduction was seen at more caudal levels (see blue surface in **Figure 4G**). This is also supported by quantification of the total surface of the longitudinal fascicle of the pons at rostral and caudal levels, which shows a significant surface reduction at caudal but not rostral levels in *Emx1-cKO* mice (**Figure 4H,I**), which together with reduced caudal to rostral ratio (**Figure 4J**) indicates that less fibers pass the pontine nuclei towards the brain stem. These data show an abnormal balance between corticopontine and corticospinal layer V projection neurons in *Emx1-cKO* mice and, interestingly, suggest increased fibers targeting the pontine nuclei in the absence of *Nr2f1* in cortical progenitors.

Moreover, we observed, caudal to the pontine nuclei, abnormally widespread and fasciculated fiber bundles in the pyramidal tract of mutant animals (**Figure 4C,D**). To determine whether this was a significant difference between animal groups, we estimated the degree of fiber bundle fasciculation in the pyramidal tract of *Emx1-cKO* and *Nex-cKO* mice. At locations of 250 μm and 500 μm caudal to the pontine nuclei (**Figure 4E**), we measured the total dorsoventral width of the pyramidal tract at several mediolateral levels and subtracted the width of gaps between the YFP-expressing fiber bundles at the same levels. The ratio of the total width of the pyramidal tract and width of the fibers only was used as a measure of the fasciculation index (**Figure 4K**). Interestingly, in both groups of mutant mice we found a lower degree of fasciculation in the pyramidal tract, which was more pronounced caudally (**Figure 4K**). Together, these data show that *Nr2f1* expression (both in cortical progenitor cells and postmitotic cells) influences the diameter, shape and degree of fasciculation of the pyramidal tract originating from layer V neurons.

Diffuse corticopontine projections in *Emx1-cKO* mice, and altered topography of corticopontine projections in *Nex-cKO* mice

To evaluate whether topographical organization between neocortex and pontine nuclei was affected in the absence of *Nr2f1*, we assessed the spatial distribution of YFP signal expression within the pontine nuclei by comparing intensity-normalized microscopic images of spatially corresponding sagittal sections from the brains of *Emx-cko*, *Nex-cko* and control animals (**Figure 5A,B**). In all mice, widespread signal expression was seen across most parts of the pontine nuclei (**Figure 5C-N**). A complete documentation of spatially comparable images showing YFP expression in the pontine nuclei of all mutant mice and controls is provided in **Supplementary Figures 1 and 2**.

We observed a strong YFP signal in central parts of the pontine nuclei in control brains, with the densest expression tending to surround a centrally located zone exhibiting less dense signals (**Figure 5C, F**). This region of the pontine nuclei typically receives strong projections from S1 (**Figure 2E**). Some signal expression was also visible in medial parts of the pontine nuclei (**Figure 5D, F**), which is known to receive projections from the cortical motor areas (**Figure 2D**). By contrast, signal expression was considerably lower in rostral and lateral parts of the pontine nuclei (**Figure 5E, F**), which are known to receive projections from visual and auditory areas of the cerebral cortex (Inoue et al., 1991; Leergaard and Bjaalie, 2007).

Interestingly, *Emx-cko* mice showed a relatively homogeneously distributed signal expression across all parts of the pontine nuclei, and notably also displayed more signal expression in the dorsolateral regions (**Figure 5G-J**). Signal expression was also present in the medial part of the nuclei, albeit with lower density than in the central region (**Figure 5H, I**). This observation fits well with the finding of more extensive signal expression in the occipital cortex (**Figure 3C**), which projects to the dorsolateral pontine nuclei. By comparison, the signal expression observed in *Nex-cko* animals was more constrained and predominated in rostrally and caudally located clusters extending from the cerebral peduncle towards the ventral surface of the pons, and medially surrounding a central core in which little signal was expressed (**Figure 5K-M**). These clusters were more peripherally located than the clustered signal expression observed in control animals (**Figure 5N**). Interestingly, in all *Nex-cko* cases the central region of the PN was devoid of signal expression (empty arrowheads in **Figure 5K-M**). This central region is normally innervated by projections from the face representations in S1 (**Figure 2A, E**).

Taken together, our findings show that corticopontine projections are abnormally distributed in *Nr2f1* cortical deficient mice, with more homogenously (non-specifically) distributed expression in *Emx1-cKO* mice, and more peripherally distributed signal expression in *Nex-cKO* mice, that display reduced expression in the central region of the pontine nuclei normally receiving S1 projections. In both mutant groups the signal expression was expanded to dorsolateral regions of the pontine nuclei that normally are innervated by projections from occipital cortical areas. This demonstrates that cortical *Nr2f1* graded expression in postmitotic neurons is involved in the establishment of topographically organized corticopontine projections.

Intact motor projections but altered somatosensory projections in *Nex-cKO* adult mutant mice

To more directly support our interpretation of topographical area differences observed in *Nr2f1* postmitotic mutants, we injected the AAV1-td/AAV1-CAGtdTomato anterograde viral tracer (Hwang et al., 2019) either in motor or somatosensory cortex of five days-old (P5) *Nex-cKO* mice and littermate controls. The mice were sacrificed at P21 and brains analyzed microscopically (**Figure 6A, B**). All histological sections were spatially registered to the *Allen Mouse Brain Atlas*, and the location and extent of tracer injections sites were mapped in atlas space (**Figure 6C**). For each injection site location in a *Nex-cKO* brain, control cases with the most spatially corresponding injection site were selected for comparison. Tract-tracing experiments with corresponding injection site locations in wild-type mice from the *Allen Mouse Brain Connectivity Atlas* were also used as additional controls (same cases as shown in **Figure 2**).

In all control mice, the spatial distributions of corticopontine projections were highly comparable with the labelling patterns seen in corresponding wild-type tracing data from the *Allen Mouse Brain Connectivity Atlas*. As expected, tracer injections into M1 or M2 gave rise to labelled axonal clusters located rostrally, caudally, and medially in the pontine nuclei (**Figure 6D**). Tracer injections into M1/M2 of *Nex-cKO* brains resulted in corticopontine labeling that essentially was similar to that observed in the control cases (**Figure 6D'-D'''**).

By contrast, a tracer injection into the S1 forelimb region of a *Nex-cKO* brain gave rise to abnormal distribution of corticopontine fibers (**Figure 6E**). While S1 corticopontine projections in wild-type mice typically form a large, elongated caudally located cluster and a smaller rostrally located one (**Figure 2E**), this labelling was shifted towards rostral and medial locations in the *Nex-cKO* brain (**Figures 6E'-E''**), resembling the distributions observed after tracer injections in motor areas (**Figure 2D**). This finding is again in agreement with our observation that YFP signal expression was reduced in the somatosensory receiving central part of the pontine nuclei (**Figure 5K-N**).

We conclude that corticopontine projections from the primary somatosensory cortex are abnormally patterned and shifted to resemble projections from motor areas, while the corticopontine projections from the motor cortex are less impacted by topographical differences due to postmitotic *Nr2f1* inactivation in *Nex-cKOs*.

DISCUSSION

The establishment and refinement of topographically specific mapping of connections among brain regions are a basic organizational feature of the nervous system, and their formation involves both spatial and temporal cues. To establish functionally-meaningful spatial relations between the projecting set of neurons and the receiving targets, cells in both regions need to be coordinated in terms of spatial and temporal identity, specification, migration, and axonal wiring. In several brain systems, little is known about how this coordination is achieved during development and what molecular mechanisms are involved in regulating the organization of topographic circuit assemblies.

In this study, we focused on the corticopontine topographic connectivity between different cortical areas and distinct innervated regions of the pontine nuclei. We asked whether and how spatio-temporal cortical area-patterning gradients are involved in driving topographic projections to the pontine nuclei. Using mouse genetics, tract-tracing techniques, digital brain atlas tools, and public mouse brain connectivity data, we provide novel evidence that expression of the cortical area patterning gene *Nr2f1* in layer V cortical neurons is necessary for the establishment of normal topographical organization of corticopontine projections. Our findings show that abnormal areal organization in the neocortex induced by *Nr2f1* inactivation is reflected in altered corticopontine projections as well as impaired structural integrity of the pyramidal tract. Moreover, we genetically demonstrate that while loss of *Nr2f1* from the progenitor cell pool in *Emx-cKO* mice leads to increased and abnormal cortico-pontine innervation at the expense of cortico-spinal projections, postmitotic *Nr2f1* inactivation in *Nex-cKO* mice results in altered topographic pontine mapping with reduced innervation of sensory-receiving regions. Finally, our area-specific anterograde tracing data reveal that the corticopontine projections from M1 and M2 layer V neurons are normally distributed, while projections from S1 are shifted towards more peripheral rostral and medial locations in the pontine nuclei, resembling the projections from motor areas. Overall, our data show that proper area mapping of the neocortical primordium is a pre-requisite for preserving the cortical spatial segregation within the pontine nuclei, and thus correct corticopontine topographic organization.

Methodological considerations

The primary focus of the present study was to compare 3D spatial distribution patterns in mice to reveal whether axonal distributions were similar or different in mice lacking *Nr2f1*. Spatial alignment of histological sections to a common atlas reference space was therefore crucial for making comparative observations. This was ensured by use of a two-step atlas registration method, including adjustment of section orientation and non-linear refinement (Puchades et al., 2019), and 3D comparisons of data points representing axonal labelling. The use of non-linear registration compensated for minor shape differences among brains and allowed comparison of distribution patterns among spatially relevant data. The focus on the location rather than the amount of signal expression/axonal labelling also compensated for the variation in signal expression intensity and size of tracer injections among cases. The approach to comparing axonal distributions as semi-quantitatively recorded data points in 3D was adopted from well-established methods used in earlier studies of cerebro-cerebellar organization in rats (Leergaard et al., 2000a; Leergaard and Bjaalie, 1995; Leergaard et al., 1995; Leergaard et al., 2000b; Lillehaug et al., 2002). By representing signal expression/axonal labeling as 3D point clouds, it became possible to more directly compare location and distribution patterns in 3D. For the additional benchmark data extracted from the *Allen Mouse Brain Connectivity Atlas*, we nevertheless chose to use the same sagittal image orientation as in our microscopic data, to facilitate comparison of microscopic images in addition to the 3D comparisons. The relevance and accuracy of the approach was confirmed by demonstrating that similarly located cortical tracer injections in control animals gave rise to similarly distributed labelling patterns in the pontine nuclei.

Area mapping genes and cortical topography

The cortical primordium is initially pre-specified by the combined action of secreted morphogens generated by patterning centers that will modulate expression gradients of a combination of transcription factors, largely along three orthogonal axes, the antero-posterior, medio-lateral and dorso-ventral axes (Alfano and Studer, 2012; Assimacopoulos et al., 2003). These transcription factors will determine areal fate and regulate expression of downstream molecules able to control

the topographic organization of synaptic inputs and outputs of related structures. A new emerging theme of cortical patterning relies in understanding to what extent patterns of genetic influences recapitulate the spatial topography between the cortex and subcortical brain regions (Cadwell et al., 2019). As an example, topography between the cortex and the thalamus plays a prominent functional role in processing sensory (e.g., visual, somatosensory, auditory) and motor information. Specific dorsal thalamic neurons, which relay distinct modalities of sensory or motor information, project to specific neocortical regions that need to be predisposed to become either sensory or motor. Overexpression or ectopic expression of the rostral morphogen *Fgf8* triggers either a caudal displacement of S1 together with the barrel field, or a duplication of the cortical areas receiving thalamic inputs and able to respond to peripheral stimuli, respectively (Fukuchi-Shimogori and Grove, 2001; Garel et al., 2003; Toyoda et al., 2010). Thus, thalamocortical axons are able to find their final target to form the appropriate topographical map in correct cortical domains and shows that intrinsic cortical information is directly involved in the final targeting of axons originating from the dorsal thalamus. This has also been observed with targets of *Fgf8*, such as the area mapping genes *Emx2* or *Nr2f1*, that modulate the size and positions of future cortical areas (O'Leary and Sahara, 2008). In case of *Nr2f1*, its cortical deletion results in an expansion of M1 at the expense of S1 which is caudally shifted, and thalamocortical axons reach the reduced caudal S1 where they are still able to form a tiny but discernible barrel field (Armentano et al., 2007). Thus, despite the changes in localization and size of S1, thalamocortical axons are able to adapt their targeting to form a topographic map in their appropriate cortical area in *Nr2f1* cortical mutants (Alfano et al., 2014; Armentano et al., 2007).

In light of these insights, we hypothesized that proper cortical area mapping might also be a key process underlying layer V corticopontine topographic organization, and more specifically that patterning genes, such as *Nr2f1*, are directly involved in imparting somatosensory corticopontine topography during development. This was also supported by previous evidence showing that layer V neurons are abnormally patterned in the absence of *Nr2f1*. More specifically, we showed (i) abnormal temporal and spatial specification of layer V neurons in *Nr2f1* cortical mutants (Alfano et al., 2014; Armentano et al., 2007; Tomassy et al., 2010); (ii) altered intrinsic excitability and dendrite

complexity of postnatal Nr2f1-deficient layer V projection neurons (Del Pino et al., 2020), and (iii) behavioral defects in the execution of skilled voluntary movements but not locomotion of adult Nr2f1 mutant mice (Tomassy et al., 2010). These data prompted us to propose that altered specification and functional maturation of layer V neurons in the developing cortex might also have an impact on corticopontine topography.

Our present data show that altered cortical area mapping plays an important role in corticopontine connectivity, and even more interestingly, that Nr2f1 drives corticopontine topography differently in progenitors *versus* postmitotic neurons. While Nr2f1 expressed by progenitor cells controls the balance between corticopontine and corticospinal neurons, similarly to what happens in *C. elegans* with the ortholog UNC-55 in the specification and maturation of two classes of motor neurons (Petersen et al., 2011; Zhou and Walthall, 1998), postmitotic Nr2f1 expression specifically acts in somatosensory topographic organization of corticopontine neurons. This demonstrates that specific intrinsic molecular programs of postmitotic layer V projection neurons contribute to the complex corticopontine topographical organization. Interestingly, the changes in layer V YFP expression observed in the cortex of *Nex-cKO* mice relative to control animals, with more or less normal signal expression in motor areas, reduced signal expression in somatosensory areas, and increased signal expression in visual and auditory areas in the occipital cortex, correspond well with the topographical changes in signal expression in the pontine nuclei, with normal signal expression in rostral, caudal, and medial “motor” receiving parts of the pontine nuclei, reduced expression in centrally located “sensory” receiving parts and increased signal expression in dorsolateral regions known to receive projections from the occipital cortex. This observation confirms our main conclusion that Nr2f1 is involved in determining corticopontine topographical mapping by acting on the specification and maturation of layer V neurons.

Revising the chrono-architectonic hypothesis of cortico-pontine circuit development

Previous data in developing rats have shown that pontine neurons settle in the forming pontine nuclei in a shell-like fashion according to their birthdate. Indeed, early born neurons form the central core of the pontine nuclei, while later born neurons consecutively settle around the earlier born neurons forming concentric rings (Altman and Bayer, 1987). In parallel, corticopontine axons innervate the pontine nuclei from early postnatal stages in a topographic internal-to-external corticopontine projection pattern, which is further refined through adult stages (Leergaard et al., 1995). Thus, frontal/motor neurons project rostrally and medially, parietal/somatosensory neurons project to central and caudal parts, temporal/auditory neurons to central and lateral regions, and occipital/visual neurons to lateral and rostral parts of the pontine nuclei (Leergaard and Bjaalie, 2007). This could suggest that the birthdate of pontine neurons is linked to both nucleogenesis and spatial organization of cortical inputs, and thus, that intrinsic differences in pontine neurons born at different stages might have an instructive role for corticopontine innervation. A recent study in mice showed indeed that postmitotic expression of the HOX gene *Hoxa5* guides pontine neurons to settle posteriorly within the pontine nuclei, where they are targeted by corticopontine limb somatosensory afferences (Maheshwari et al., 2020). Moreover, ectopic *Hoxa5* expression in pontine neurons is sufficient to attract cortical somatosensory inputs, regardless of their spatial position in the pontine nuclei, showing that pontine neurons can play an instructive and attractive role in topographic input connectivity of corticopontine neurons (Maheshwari et al., 2020).

Nevertheless, temporal and maturational gradients in the pontine nuclei cannot fully explain the complexity of the fine-grained somatotopic topographic connectivity pattern between cortical input and pontine neuron targets. Since the establishment of topographic maps requires multiple processes and structures, it is conceivable that the position and specific intrinsic molecular programs of both pre-synaptic afferences and post-synaptic target neurons contribute to this complex corticopontine connectivity map. Indeed, our data show that without affecting the development and maturation of pontine neurons, corticopontine layer V axons originating from somatosensory areas in the parietal cortex, with deficient *Nr2f1* expression causing abnormal spatial and temporal area identity, will target the wrong pontine region. By contrast, *Nr2f1*-deficient axons originating from motor areas in the frontal and medial cortex will innervate the pontine region normally

deputed to corticopontine motor axons. This strongly suggests that during the establishment of corticopontine topography, both structures, the neocortex and the pons need to be properly pre-patterned by factors involved in spatial and temporal control of neurogenesis, such as *Nr2f1* for the cortex, and *Hoxa5* for the pontine nuclei.

Conclusion and outlook

Our findings have contributed to unveiling a new mechanism involved in corticopontine topographic connectivity. While previous evidence pointed to the spatiotemporal maturation of pontine nuclei as the major process in guiding area-specific corticopontine projections and thus, topographic organization between cortex and pontine nuclei, here we provide novel evidence that cortical area mapping controlled by gradient expression of transcription factors, in this case *Nr2f1*, is directly involved in the establishment of corticopontine connectivity. It is plausible to propose that other factors regulating area size and positions are also involved in the same process. Overall, we propose that both structures, cortex and pontine nuclei, need to be highly coordinated during the establishment of corticopontine topography, and that distinct molecular mechanisms seem to be involved in this complex process. How precisely molecular pathways within the cortex and pontine nuclei interact with each other to coordinate proper topography is still an open question and warranted for further studies.

MATERIALS AND METHODS

Topographical map of corticopontine projections from somatosensory and motor areas

To establish a 3D benchmark map of corticopontine projections from somatosensory and motor areas in adult wild type mice, we utilized a selection of public experimental tract-tracing data available from the Allen Institute mouse brain connectivity atlas (<http://connectivity.brain-map.org/>). We selected 10 experiments in which the anterograde tracer EGFP was injected in the right primary/secondary motor cortex (n = 5) or primary somatosensory cortex (n = 5) of wild type C56BL/6J mice (**Supplementary Table 1**). Serial two photon fluorescence images were interactively inspected online using the Projection High Resolution Image viewer, and from each case, 5 sagittal oriented images of the right pontine nuclei (matching the orientation of the histological material generated from our knock-out mice), spaced at ~100 μm were captured by screen shot from the largest 3-D multiplane thumbnail viewer. The resolution of the captured images was up-sampled three times original size before they were spatially aligned to the CCFv3 using the QuickNII tool (see above). These images were used to create 3-D representations of the axonal labeling in the pontine nuclei (see below).

Animals

All mice used were bred in a C57BL6 background. Male and female animals at any stage of development were used. All experiments were conducted in accordance with the French Animal Welfare Act and European guidelines for the use of experimental animals, using protocols approved by the French Ministry of Education, Research and Innovation and the local ethics committee (CIEPAL NCE/2019–548, Nice) under authorization #15 349 and #15 350.

Nr2f1/COUP-TF1^{fl/fl} mice were crossed with *Emx1-Cre-recombinase* mice to inactivate *Nr2f1/COUP-TF1* exclusively in cortical progenitors and their progeny (Armentano et al., 2007) or with *Nex-Cre-recombinase* mice to abolish *Nr2f1/COUP-TF1* expression from postmitotic neurons (Alfano et al., 2014). Littermate *Nr2f1/COUP-TF1^{fl/fl}* mice without the presence of the *Cre-recombinase* gene (*Cre-negatives*) were considered controls (**Supplementary Table 2**). For postnatal (P)21 and adult topographic map analysis, *Emx1-cKO* and *Nex-cKO* animals were further crossed with *Thy1-eYFP-H*

mice to specifically label layer V projection neurons, as previously reported (Harb et al., 2016; Porrero et al., 2010). Mice were genotyped as previously described (Alfano et al., 2014; Armentano et al., 2007; Harb et al., 2016). Control and mutant littermates were genotyped as *Nr2f1^{fl/fl}:Thy1-eYFP-H^{T/+}* and *Nr2f1^{fl/fl}:Emx1-Cre:Thy1-eYFP-H^{T/+}* or *Nr2f1^{fl/fl}:Nex-Cre:Thy1-eYFP-H^{T/+}*, respectively. For simplicity, mutant mice are named *Emx1-cKO* and *Nex-cKO* throughout the text. Midday of the day of the observed vaginal plug was considered as embryonic day 0.5 (E0.5).

Anterograde tracing of corticospinal axons in early postnatal mice

P4-P5 animals were anesthetized on ice for 5 min and kept on ice during the whole procedure. Viral particles were produced from the AAV1-td/AAV1-CAGtdTomato (addgene #59462) plasmid by the Alexis Bemelmans (CEA, France) Company, and diluted 1:50 in TE-Buffer (Qiagen, #1018499) to a final concentration of 1.75e12 vg/ml (kindly donated by I. Dusart, Institution, Country). Approximately 0.5/1ul was injected unilaterally in different rostral-caudal and medio-lateral brain locations of control and *Nex-cKO* pups, as previously described in (Gu et al. 2017).

Microscopic imaging

Mosaic microscopic images were acquired using a Zeiss Axio Imager.M2 epifluorescence microscope equipped with a halogen lamp, a MCU 2008 motorized stage, and an EC Plan-Neofluar 10x/0.30 and an AxioCam MRm camera. ZEN blue software was used for imaging and automatic stitching. Images were exported in TIFF format and serially ordered from lateral to medial, rotated and if needed, mirrored to consistent anatomical orientation using Adobe Photoshop CS6 (RRID: SCR_014199), before being converted to PNG format and resized to 60% of original size using ImageJ (RRID:SCR_003070) with bilinear interpolation. The resized serial images were loaded into Adobe Photoshop as a stack, spatially aligned using the ventral surfaces of the pons and cerebral peduncle as landmarks, cropped and exported as individual PNG files.

For comparative analyses of topographical organization (see below), variations in YFP signal expression intensity within and between groups were normalized by adjusting the brightness and contrast of images to equal levels using a custom-made histogram matching script with ImageJ. One

selected, representative case (Experiment 5, Cre-negative, nr: 14250, **Supplementary Table 3**) was used as reference.

Spatial alignment to common 3D reference atlas

Serial sectional images were spatially registered to the *Allen Mouse Common Coordinate Framework*, version 3, 2017 edition of the delineations (CCFv3, (Wang et al., 2020) using the QuickNII software tool (RRID:SCR_016854; (Puchades et al., 2019). Multiple anatomical landmarks (hippocampus, caudoputamen, inferior and superior colliculus, and external surface of the neocortex) were used to determine the mediolateral position and orientation of the sagittal section images. For each section image, custom atlas diagrams were aligned to anatomical landmarks in the experimental images using affine transformations, with particular emphasis on matching the ventral surface of the pons and white matter tracts close to the pontine nuclei and exported as PNG images. For *Emx1-cKO* and *Nex-cKO* image series used in cortical distribution analysis and corticopontine topographical comparison analysis, the spatial registration was optimized with an additional step using the tool VisuAlign (RRID:SCR_017978), with which the custom atlas images were non-linearly adjusted to refine the fit of selected major landmarks. To co-display images and the spatially registered custom atlas images we used the software tool LocaliZoom, which is embedded in the Navigator3 image management system, developed and hosted by the Neural Systems Laboratory at the University of Oslo, Norway.

Cortical distribution analysis in *Emx1-cKO* and *Nex-cKO* mutants

Serial sectional regions of *Nex-cKO* and *Emx1-cKO* mutants superimposed with CCFv3 brain atlas underwent semi-quantitative analysis with a 5-stage scoring table based on relative density of cells in the cortical mantle (**Figure 3E**). Each brain region was scored from 0 (absent signal) to 4 (very high signal), characterized by high number of cells, dense and extensive overlap and intense signal intensity. The quantifications were summarized graphically and displayed as histograms (**Figure 3F**).

Analysis of tracer injection sites

Serial images of cortical tracer injections in *Nex-cKO* brains (**Supplementary Table 3**) and experiments taken from the *Allen Mouse Brain Connectivity Atlas*, were spatially aligned using

QuickNII and VisuAlign, as described above. The center positions of the injection sites were annotated as a point-coordinate using LocaliZoom, co-displayed with the CCFv3 atlas in the 3-D viewer tool MeshView. The mouse brain atlas of Franklin and Paxinos (Franklin and Paxinos, 2008) was used to aid the interpretation of injection site locations. This visualization was used to select spatially corresponding injection site locations for analyses of spatial distribution of corticopontine projections.

Histology and immunohistochemistry

At age P8, P21 and adulthood, animals were anesthetized by intraperitoneal injection of a mixture of Tiletamine-Zolazepam-Xylazine-Buprenorphine and intracardially perfused with PB Saline (PBS) followed by 4% paraformaldehyde (PFA) in PBS. Volumes were 15, 20 and 30 ml, respectively. Brains were removed from the skull and postfixed for 4 h at 4°C in 4% PFA, before being vibratome-sectioned in 100µm (adult samples) or 150µm (P8 and P21 samples) thick sagittal sections. All sections were incubated overnight at 4°C in a solution of 0.5% Triton X-100, 3% BSA, 10% goat serum in PBS, for permeabilization and reduction of non-specific binding of antibodies. For immunofluorescence (IF), sections were incubated for 2 days at 4°C with primary antibodies in a solution of 0.5% Triton X-100, 10% goat serum in PBS, and then overnight at 4°C with relative secondary antibodies and HOECHST diluted in PBS. For the complete list of primary and secondary antibodies, see **Supplementary Table 4**. Sections were washed several times in PBS, then transferred on Superfrost plus slides (ThermoScientific), covered and dried for 30 min to 1 h, and finally mounted with the Mowiol (Sigma-Aldrich) mounting medium.

Semi-quantitative recording and 3-D visualization of spatial distribution patterns

To investigate and compare the 3-D distributions of YFP signal expression or anterograde axonal labelling within the pontine nuclei, we used a semi-quantitative digitization approach (modified from (Leergaard and Bjaalie, 1995)). The annotation functionality in the LocaliZoom tool was used to record features of interest in the images as point coordinates, specified in the coordinate system of the reference atlas (CCFv3). LocaliZoom was thus used to represent YFP signal expression or labelled axons in the pontine nuclei as point clouds. The points were semi-quantitatively assigned to represent the overall density of signal / labelling observed in the images. To compensate for the

spacing between sections and allow inspection of point distributions perpendicularly to the section angle, the z-coordinate of each point was randomly displaced within the thickness of the gap between sections using a custom Python script. The point-coordinates were co-displayed in the 3-D interactive viewer tool MeshView (RRID:SCR_017222).

ACKNOWLEDGEMENTS

We thank Isabelle Dusart in Paris for providing us with AAV9-CAG-tdTomato viral particles produced by Alexis Bemelmans (CEA, France), Nicolaas Groeneboom and Gergely Csucs for expert technical assistance, the iBV PRISM platform for imaging support, and Sharon Yates, and Maja A. Puchades for useful discussions. This work was funded by the “Fondation Recherche Médicale; Equipe FRM 2015” #DEQ20150331750 to M.S.; by an “Investments for the Future” LabEx SIGNALIFE (grant ANR-11- LABX-0028-01) to M.S., by a PhD contract from Région PACA/Inserm and FRM 4th year PhD for C.T, with additional funding from the European Union’s Horizon 2020 Framework Program for Research and Innovation under the Specific Grant Agreement No. 785907 (Human Brain Project SGA2), Specific Grant Agreement No. 945539 (Human Brain Project SGA3), and The Research Council of Norway under Grant Agreement No. 269774 (INCF Norwegian Node) to JGB and TBL.

FIGURES and FIGURE LEGENDS

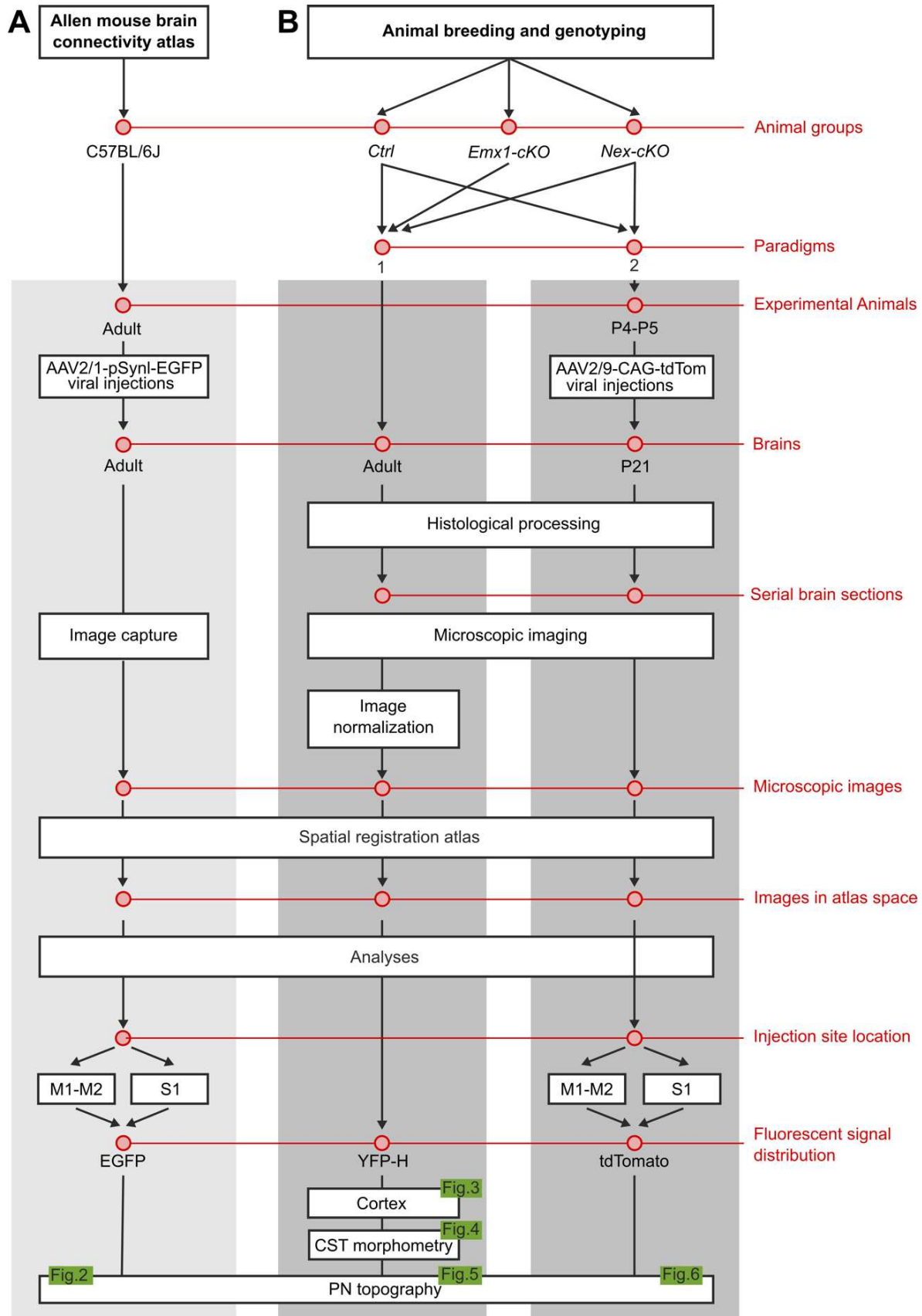


Figure 1. Experimental and analytic workflow. The left column represents the workflow followed to generate a 3-D control topographic map of corticopontine projections using public anterograde tracing data (<https://connectivity.brain-map.org/>), mapped and compared in atlas space. The central and right column represent the two paradigms investigated in conditional mouse models. The central column represents the analytic steps performed in adult control, *Emx1*-cKO and *Nex*-cKO animals (paradigm 1), whereas the right column represents the tract tracing study of the 3D topography of motor and somatosensory corticopontine projections in young control and *Nex*-cKO animals (paradigm 2). All images were spatially registered to the Allen mouse brain atlas (CCFv3; Wang et al., 2020) prior to analyses, to facilitate comparison of images and spatial distribution patterns. Results are shown in **Figures 2-7**.

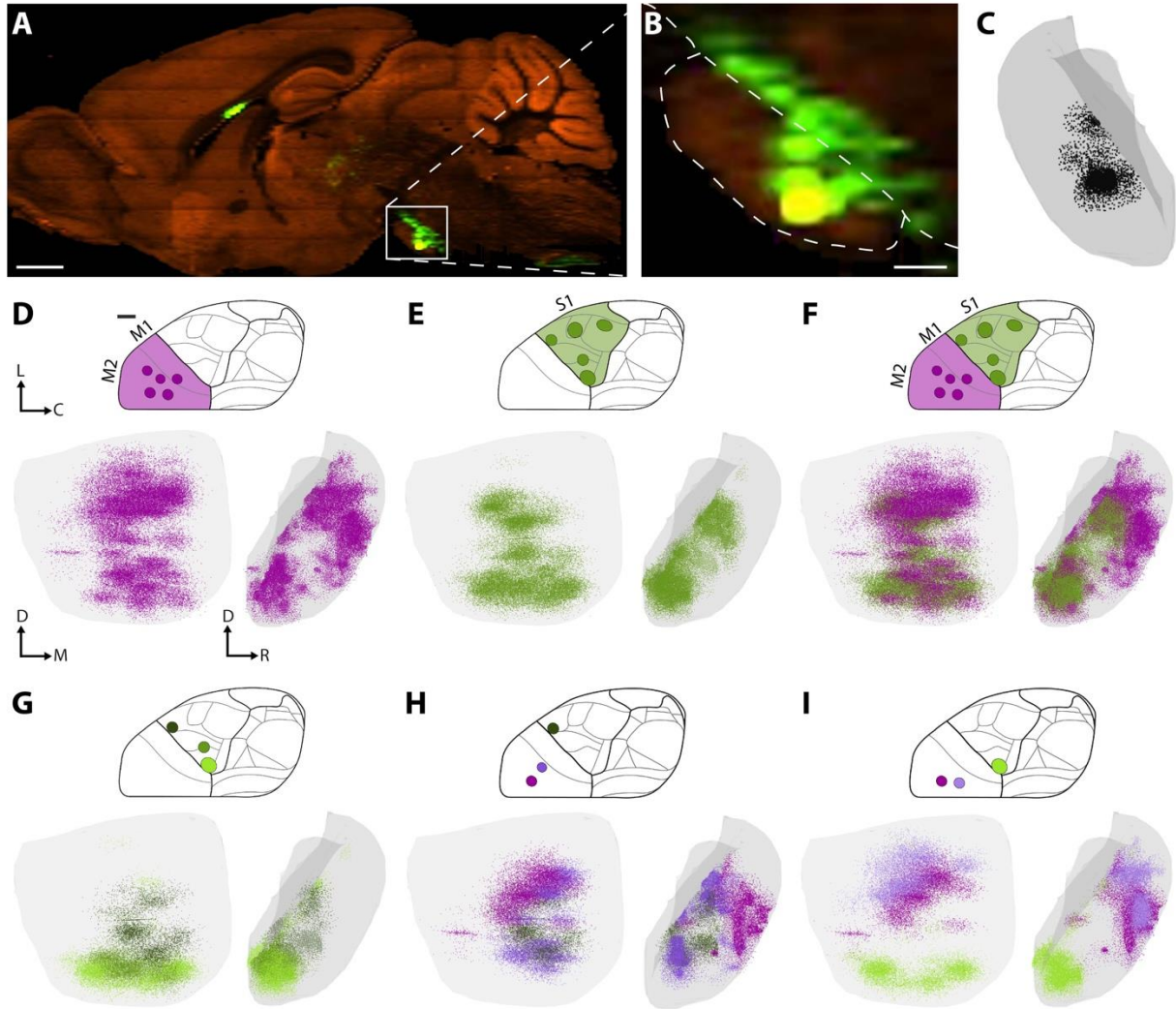


Figure 2. Topographical organization of corticopontine projections in wild-type mice. 3-D visualizations of point clouds representing spatial distribution of anterogradely labeled corticopontine axons in wild-type mice injected with anterograde tracer EGFP in the primary (M1) / secondary (M2) motor cortex. **A,B)** Sagittal tract tracing image data shown in the Allen Institute Projection High Resolution Image viewer (tracer injection in the S1 mouth representation). **C)** 3D visualization of axonal labelling semi-quantitatively represented by dots, corresponding to the observed density of labelling, inside a surface rendering of the outer boundaries of the pontine nuclei (transparent grey surface), shown in view from lateral, mirrored to match the orientation shown in **A-B**. **D-F)** 3-D visualizations dots representing the spatial distribution in the right pontine nuclei of axonal projections originating from 5 tracer injection sites in the primary (M1) and secondary (M2) motor cortex (**D**, purple points) and 5 tracer injections in the primary somatosensory (S1) cortex (**E**, green points). The data are shown in view from ventral and left. Injection site locations are indicated in the inset dorsal view map of the cerebral cortex. **F)** Co-visualization of dots representing M1 and M2 corticopontine projections from motor (**D**) and somatosensory (**E**) areas. The dot maps show that motor and somatosensory areas largely target different parts of the pontine nuclei, with projections from M1 and M2 located more peripherally towards rostral and ventral than projections from S1, but also that motor and sensory projections overlap caudally in the pontine nuclei. **G-I)** Co-visualization of color-coded dot maps representing corticopontine projections from selected combinations of cortical injections located along the orientation of cortical maturation gradients from anterolateral towards frontomedial or medial. **G)** shows the projections from three injection sites located in the S1 face, forelimb, and hindlimb representations, revealing a partly concentric arrangement of dots in the pontine nuclei, with projections from progressively more medial cortical locations are progressively shifted towards caudal. **H)** shows three other combinations of injection sites (one in S1, same case as in **G**; two in M2), also showing that a shift of injection site from interolateral towards medial corresponds to concentric shift of location from central to peripheral in the pontine nuclei, with projections from M2 surrounding the centrally located projections from S1. **I)** shows a combination of projections from three injection sites located medially in the cortex, displaced along the rostrocaudal axis, which give rise to pontine labeling that are distributed within a largely circular subspace of the pontine nuclei. D, dorsal, M, medial, R, rostral. Scale bars, 200 μm .

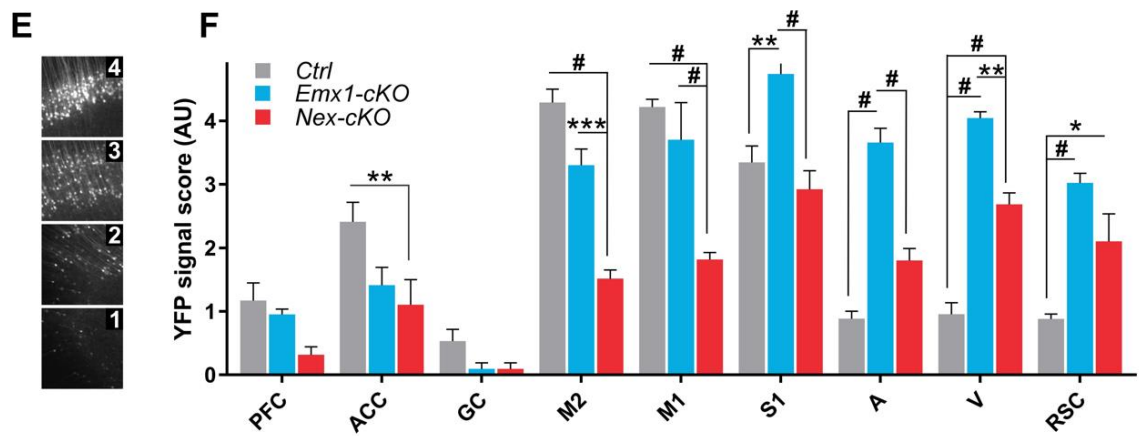
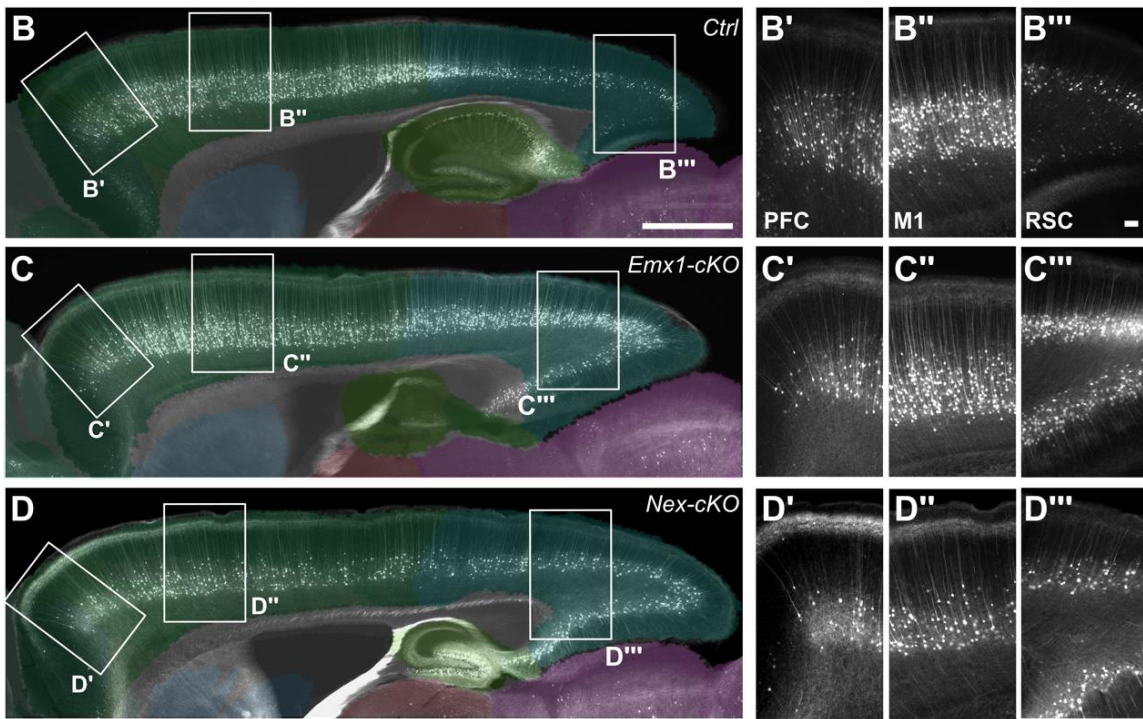
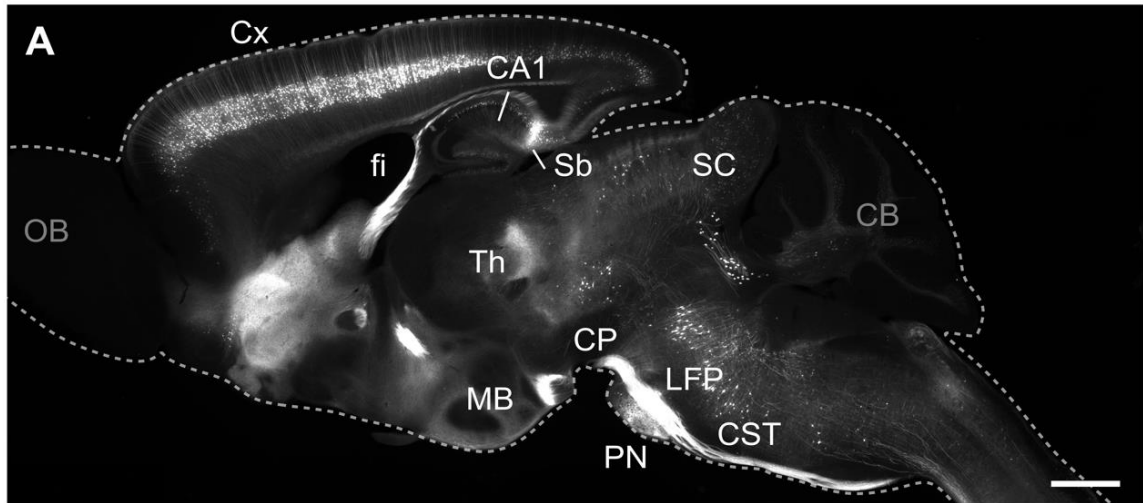


Figure 3 – Cortical distribution of YFP-positive layer V pyramidal cells in Ctrl, Emx1- and Nex-cKO adult brains. A) Representative sagittal section of a Thy1-YFP-H mouse brain. **B-D)** On the left, representative images from Ctrl, Emx1-cKO and Nex-cKO cortices. The corresponding CCFv3 atlas diagrams were superimposed on the immunofluorescence microscopic images to define the location of different cortical areas. The regions framed in **B-D** are magnified in the panels to the right (**B'-B'''**, **C'-C'''** and **D'-D'''**). **E)** The semi-quantitative scale used to score the amount of signal expression. A score of 0 was attributed when no positive cells were present in the region (not shown), 1 very few and sparse cells with low to medium signal intensity, 2 moderate number of sparse cells with moderate to high signal intensity, 3 high number of partially overlapping cells with high signal intensity and 4 very high number of extensively overlapping cells with high to very high signal intensity. **F)** Scoring of YFP-H signal expression across cortical areas in Ctrl (grey), Emx1-cKO (light blue) and Nex-cKO (red) adult animals. In Emx1-cKO samples, less cells are present in more anterior regions (M2 and M1) whereas cell density is significantly increased in central and occipital regions (S1, A, V and RSC) compared to the control condition. In Nex-cKO animals, the number of positive cells is overall smaller than Ctrl and Emx1-cKO animals. Nevertheless, Nex-cKO animals share a common trend as the Emx1-cKOs: a reduction of cell density in frontal areas (ACC, M2 and M1) and an increase in occipital areas (A, V and RSC). * < 0.05, **< 0.01, ***<0.005, ****<0.0001. Data are represented as mean ± SEM. Data were analyzed with 2way-ANOVA test and corrected for multiple comparison with the Bonferroni test. NCtrl=6, NEmx1-cKO=4 NNex-cKO=4. A: auditory cortex; ACC: anterior cingulate cortex; GC: gustatory cortex; M1: primary motor cortex; M2: secondary motor cortex; PFC: prefrontal cortex; RSC: retrosplenial cortex; S1: primary somatosensory cortex; V: visual cortex.

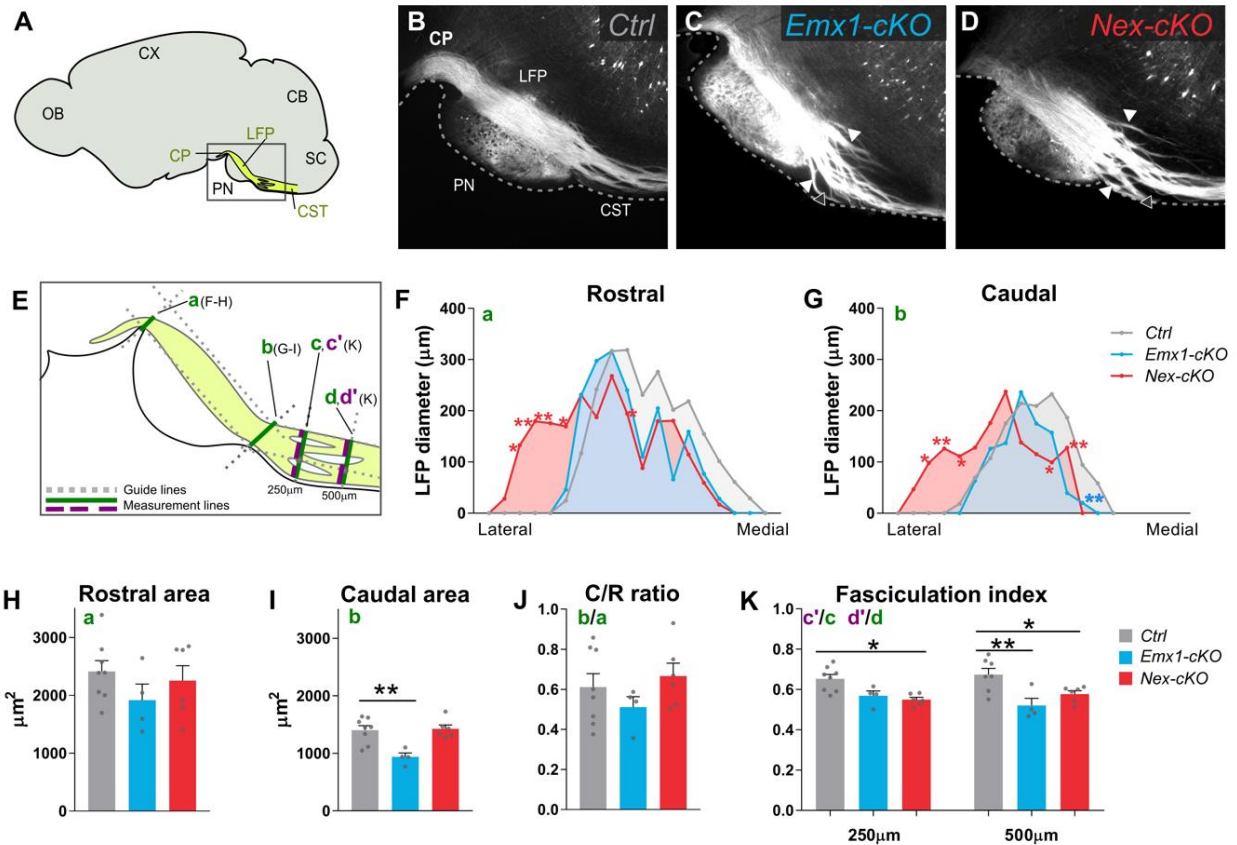


Figure 4 – Loss of *Nr2f1* function leads to misspecification of subcerebral projection neurons and CST abnormal defasciculation. **A)** Schematic diagram of a sagittal mouse brain section showing the location of the pontine nuclei (PN) and descending fiber tracts (yellow) in the cerebral peduncle (CP), longitudinal fascicle of the pons (LFP) and corticospinal tract (CST) at level of the pons. The frame indicates the region shown in **B-D** in control, *Emx1-cKO* and *Nex-cKO* animals. **E)** Diagram illustrating where the different measurements shown in **F-K** were obtained. The total dorsoventral width of the bundle expressing fluorescent signal in the descending fiber tract (red lines) was measured rostrally (**a**) and caudally (**b**) to the PN, and 250 (**c**) and 500 (**d**) μm from the caudal end of the PN. The width of separate fiber fascicles (blue lines) was measured 250 (**c'**) and 500 (**d'**) μm from the caudal end of the PN. **F-G)** Plots showing LFP diameter measurements obtained from lateral to medial before and after innervating the pontine nuclei (rostral and caudal respectively) for the three genotypes. Each measurement represents the average value of corresponding sections among distinct animals and each position on the x-axis represents a specific section of the series. **H-I)** Average values of the area under the curves in **F-G**. Generally, a comparable number of fibers reach the cerebral peduncle among the three genotypes, thus no evident differences in the rostral AUC is observed (**H**). However, after innervating the pontine nuclei, the fibers exiting the pons are less in *Emx1-cKO* brains compared to both controls and *Nex-cKO*s (**I**). The ratio between caudal and rostral AUC (**J**) shows that *Emx1-cKO* CST fibers tend to innervate the PN more than both *Ctrl*s and *Nex-cKO*. **K)** CST fasciculation index. Measurements of total thickness (red line) and fibers thickness (red and blue line respectively in schematic **E**) were performed at 250 and 500 μm from the terminal edge of the pontine nucleus. Then a ratio between the two measurements was calculated for each position. Both *Emx1-* and *Nex-cKO* show increased de-fasciculation in both locations, compared to controls. * < 0.05, ** < 0.01. Data are represented as mean \pm SEM. Data were analyzed with 2way-ANOVA test (**D-E**) or ordinary ne-way ANOVA test (**F-H and J**) and corrected for multiple comparison with the Bonferroni test. $N_{\text{Ctrl}}=8$, $N_{\text{Emx1-cKO}}=4$ $N_{\text{Nex-cKO}}=6$.

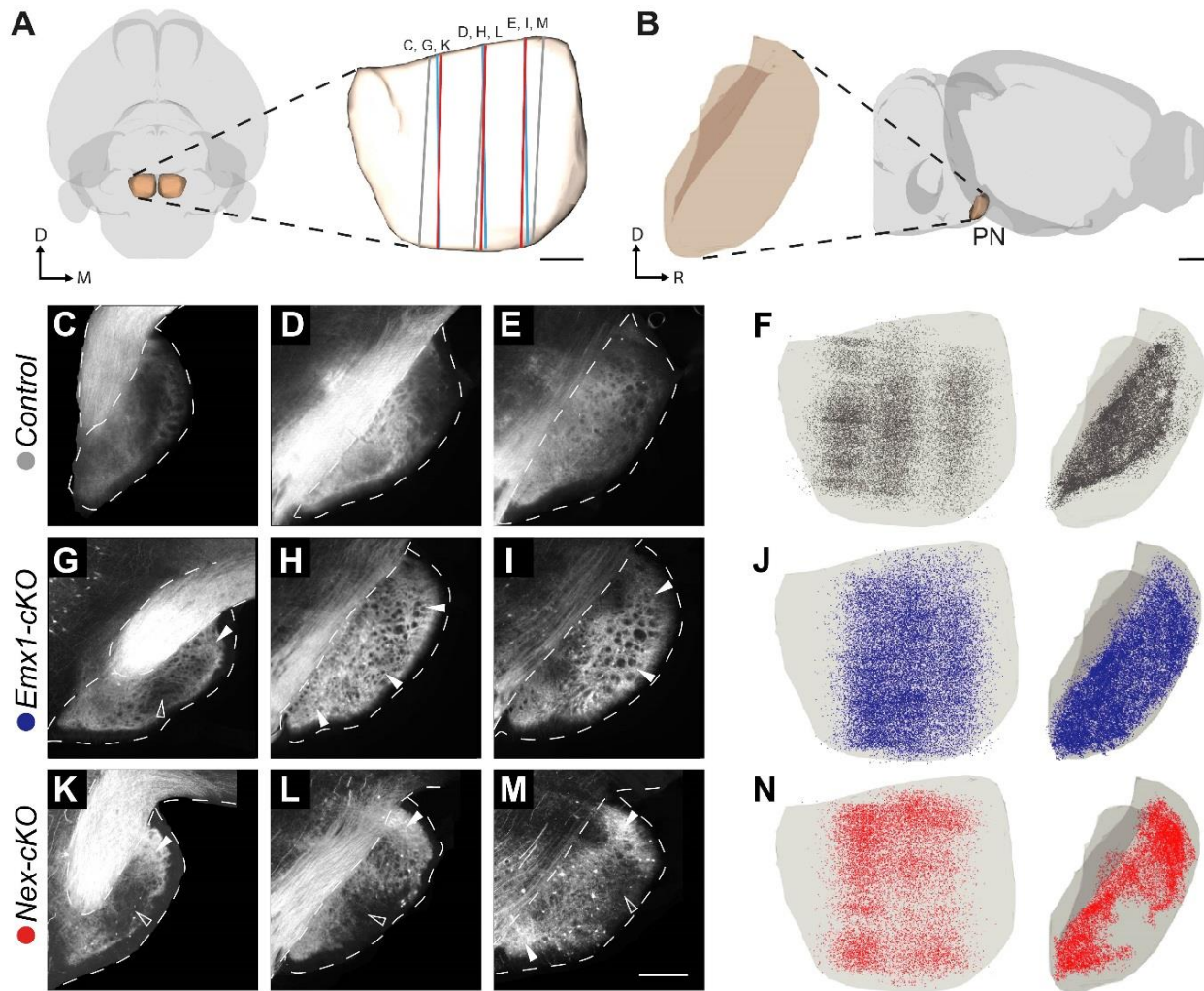


Figure 5. Distribution of YFP signal expression in the pontine nuclei in knock-out mice and controls. **A,B)** 3-D visualizations of the outer surfaces of the brain (transparent grey) and pontine nuclei (transparent brown) from the Allen mouse brain atlas in view from ventral (**A**) and left (**B**), with the pontine nuclei enlarged to demonstrate the orientation of figure panels **F, J**, and **N**. Colored lines in **A** indicate the position and orientation of the sagittal sections shown in **C-E, G-I**, and **K-M**. **C-E, G-I, K-M)** Fluorescence microscopy images of sagittal sections from different mediolateral levels of the pontine nuclei, showing the spatial distribution of YFP signal expression in control, *Emx1*-cKO, and *Nex*-cKO mice, respectively. Filled arrowheads indicate regions with increased signal expression in knock-out mice relative to controls, while non-filled arrowheads indicate regions with decreased signal expression. **F,J,N)** 3-D visualization of color coded dots representing signal expression in the pontine nuclei shown inside the outer surface of the pontine nuclei, seen from ventral and lateral (left). In control mice (**C-F**), signal expression is primarily seen in central and caudal parts of the pontine nuclei, while in *Emx1*-cKO mice (**G-J**) signal expressing is more widespread and diffuse throughout the entire pontine nuclei, notably including more peripheral parts of the pontine nuclei towards rostral, ventral and caudal (filled arrowheads in **G-I**). By contrast, in *Nex*-cKO mice (**K-N**), signal expression is reduced in the central core region of the pontine nuclei (non-filled arrowheads in **K-M**), while being increased in peripheral (rostral and caudal) regions of the pontine nuclei. R, rostral; D, dorsal; M, medial; PN, pontine nuclei. Scale bars, 1 mm in **B**, 200 μ m in **A, M**.

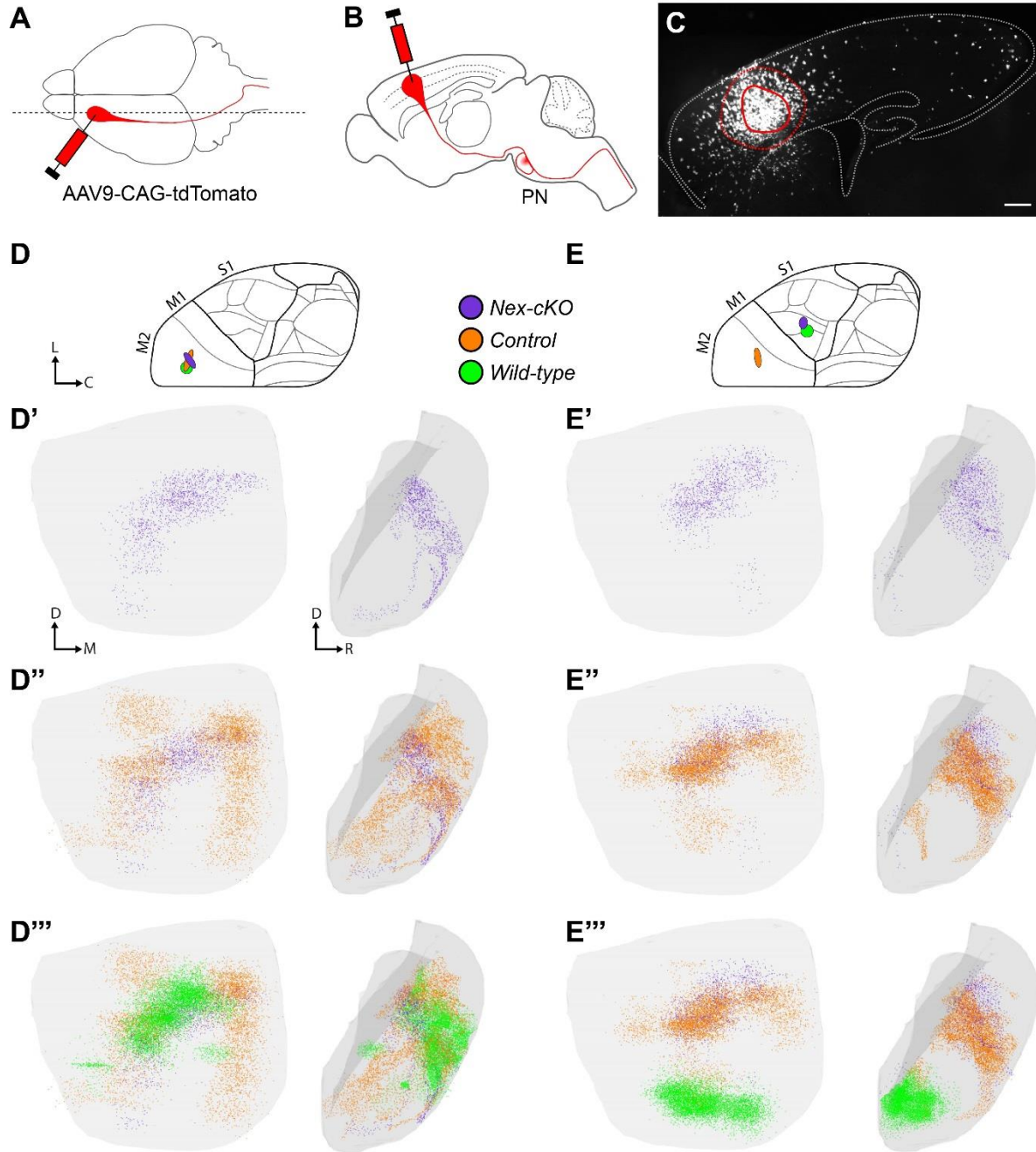


Figure 6. Anterograde tracing of corticopontine projections from motor and somatosensory areas in *Nex-cko* mice. (A,B) Diagram of the mouse brain seen in dorsal (A) and sagittal (B) view, illustrating the axonal tract tracing method used, in which the viral tracer AAV9-CAG-tdTomato is injected in the cerebral cortex of prenatal mouse pups and anterogradely transported through descending corticofugal pathways, giving rise to labelling in the pontine nuclei (PN), and other target regions (not shown). (C) Fluorescence microscopy image of sagittal section showing a tracer injection site in the secondary motor cortex. (D,E) Diagram of the right mouse brain hemisphere in view from dorsal showing cortical areas and location of injection sites in selected *Nex-cko* (purple), controls (orange), and wild type (green) mice (data from Allen mouse brain connectivity atlas). (D'-D''', E'-E''') 3D visualizations of color coded dots representing corticopontine labeling from the injection sites shown in D and E. (D') Dot maps showing that a tracer injection in the secondary motor cortex (M2) of a *Nex-cko* mouse labels corticopontine axons in a rostrally located cluster that curves towards ventral and caudal along the surface of the pontine nuclei. (D'') shows a co-visualization of the dotmap from (D', purple dots) and orange dots representing projections from similarly located tracer injection in a control mouse, which gives rise to somewhat more extensive, but largely similarly located labeling in the pontine nuclei. (D''') shows the same dots as in (D'') with addition of dots representing projections originating from a tracer injection in the same location in M2 of a wild type mice, labeling a similar cluster in the rostral pontine nuclei, thus demonstrating that corticopontine projections from M2 in *Nex-cko* are unchanged relative to those in normal control mice. (E') Dot maps showing that a tracer injection into the proximal forelimb representation in the primary somatosensory cortex (S1) of a *Nex-cko* mouse gives rise to a rostrally located cluster of labeling in the pontine nuclei. (E''), co-visualization of the same purple dots as shown (E') together with similarly located dots representing the pontine projections from a tracer injection in M2, showing that the projections from S1 in *Nex-cko* mice is highly similar to the projections seen following tracer injections in M2 (D', D'', D'''). (E''') Co-visualization of the same dots as shown in (E''), with addition of green dots representing the pontine projections from a tracer injection into the proximal forelimb representation of S1 in a wild type mouse (data from the Allen mouse brain connectivity atlas), showing that normal corticopontine projections from the S1 forelimb representation are distributed in a horizontally oriented cluster in the caudal part of the pontine nuclei. This demonstrates that corticopontine projections from S1 in *Nex-cko* mice are changed to resemble normal projections from M2. C, caudal; D, dorsal; L, lateral; M, medial; M1, primary motor cortex; M2, secondary motor cortex; PN, pontine nuclei; R, rostral; S1, primary somatosensory cortex. Scale bar, 1 mm.

REFERENCES

- Alfano, C., Magrinelli, E., Harb, K., Hevner, R.F., and Studer, M. (2014). Postmitotic control of sensory area specification during neocortical development. *Nature communications* 5, 5632.
- Alfano, C., and Studer, M. (2012). Neocortical arealization: Evolution, mechanisms and open questions. *Dev Neurobiol*.
- Altman, J., and Bayer, S.A. (1978). Prenatal development of the cerebellar system in the rat. II. Cytogenesis and histogenesis of the inferior olive, pontine gray, and the precerebellar reticular nuclei. *J Comp Neurol* 179, 49-75.
- Altman, J., and Bayer, S.A. (1987). Development of the precerebellar nuclei in the rat: IV. The anterior precerebellar extramural migratory stream and the nucleus reticularis tegmenti pontis and the basal pontine gray. *J Comp Neurol* 257, 529-552.
- Altman J, Bayer SA (1996) Development of the cerebellar system in relation to its evolution, structure and functions. CRC Press, Boca Raton.
- Armentano, M., Chou, S.J., Tomassy, G.S., Leingartner, A., O'Leary, D.D., and Studer, M. (2007). COUP-TFI regulates the balance of cortical patterning between frontal/motor and sensory areas. *Nat Neurosci* 10, 1277-1286.
- Assimacopoulos, S., Grove, E.A., and Ragsdale, C.W. (2003). Identification of a Pax6-dependent epidermal growth factor family signaling source at the lateral edge of the embryonic cerebral cortex. *J Neurosci* 23, 6399-6403.
- Bjaalie, J.G., and Brodal, P. (1997). Cat pontocerebellar network: numerical capacity and axonal collateral branching of neurones in the pontine nuclei projecting to individual parafloccular folia. *Neurosci Res* 27, 199-210.
- Bower, J.M. (2011). Functional implications of tactile projection patterns to the lateral hemispheres of the cerebellum of the albino rat: the legacy of Wally Welker. *Annals of the New York Academy of Sciences* 1225, 130-141.

Bower, J.M., Beermann, D.H., Gibson, J.M., Shambes, G.M., and Welker, W. (1981). Principles of organization of a cerebro-cerebellar circuit. Micromapping the projections from cerebral (SI) to cerebellar (granule cell layer) tactile areas of rats. *Brain, behavior and evolution* *18*, 1-18.

Bower, J.M., and Kassel, J. (1990). Variability in tactile projection patterns to cerebellar folia crus IIA of the Norway rat. *J Comp Neurol* *302*, 768-778.

Brodal, P. (1978). The corticopontine projection in the rhesus monkey. Origin and principles of organization. *Brain* *101*, 251-283.

Brodal, P., and Bjaalie, J.G. (1992). Organization of the pontine nuclei. *Neurosci Res* *13*, 83-118.

Brodal, P., and Bjaalie, J.G. (1997). Salient anatomic features of the cortico-ponto-cerebellar pathway. *Prog Brain Res* *114*, 227-249.

Cadwell, C.R., Bhaduri, A., Mostajo-Radji, M.A., Keefe, M.G., and Nowakowski, T.J. (2019). Development and Arealization of the Cerebral Cortex. *Neuron* *103*, 980-1004.

Chapin, J.K., and Lin, C.S. (1984). Mapping the body representation in the SI cortex of anesthetized and awake rats. *J Comp Neurol* *229*, 199-213.

Del Pino, I., Tocco, C., Magrinelli, E., Marcantoni, A., Ferraguto, C., Tomagra, G., Bertacchi, M., Alfano, C., Leinekugel, X., Frick, A., *et al.* (2020). COUP-TFI/Nr2f1 Orchestrates Intrinsic Neuronal Activity during Development of the Somatosensory Cortex. *Cereb Cortex* *30*, 5667-5685.

Fabri, M., and Burton, H. (1991). Ipsilateral cortical connections of primary somatic sensory cortex in rats. *J Comp Neurol* *311*, 405-424.

Feng, G., Mellor, R.H., Bernstein, M., Keller-Peck, C., Nguyen, Q.T., Wallace, M., Nerbonne, J.M., Lichtman, J.W., and Sanes, J.R. (2000). Imaging neuronal subsets in transgenic mice expressing multiple spectral variants of GFP. *Neuron* *28*, 41-51.

Fukuchi-Shimogori, T., and Grove, E.A. (2001). Neocortex patterning by the secreted signaling molecule FGF8. *Science* *294*, 1071-1074.

Franklin, K. B. J., & Paxinos, G. (2007). *The Mouse Brain in Stereotaxic Coordinates* (map). In Academic Press.

Garel, S., Huffman, K.J., and Rubenstein, J.L. (2003). Molecular regionalization of the neocortex is disrupted in *Fgf8* hypomorphic mutants. *Development* *130*, 1903-1914.

Hall RD, Lindholm EP. 1974. Organization of motor and somatosensory neocortex in the albino rat. *Brain Res* *66*:23-38

Harb, K., Magrinelli, E., Nicolas, C.S., Lukianets, N., Frangeul, L., Pietri, M., Sun, T., Sandoz, G., Grammont, F., Jabaudon, D., *et al.* (2016). Area-specific development of distinct projection neuron subclasses is regulated by postnatal epigenetic modifications. *eLife* *5*.

Henschke, J.U., and Pakan, J.M. (2020). Disynaptic cerebrocerebellar pathways originating from multiple functionally distinct cortical areas. *eLife* *9*.

Hwang, E.J., Link, T.D., Hu, Y.Y., Lu, S., Wang, E.H., Lilascharoen, V., Aronson, S., O'Neil, K., Lim, B.K., and Komiyama, T. (2019). Corticostriatal Flow of Action Selection Bias. *Neuron* *104*, 1126-1140 e1126.

Inoue, K., Terashima, T., and Inoue, Y. (1991). Postnatal development of the pontine projections from the visual cortex of the mouse. *Okajimas Folia Anat Jpn* *67*, 479-492.

Kratochwil, C.F., Maheshwari, U., and Rijli, F.M. (2017). The Long Journey of Pontine Nuclei Neurons: From Rhombic Lip to Cortico-Ponto-Cerebellar Circuitry. *Front Neural Circuits* *11*, 33.

Leergaard, T.B. (2003). Clustered and laminar topographic patterns in rat cerebro-pontine pathways. *Anat Embryol (Berl)* *206*, 149-162.

Leergaard, T.B., Alloway, K.D., Mutic, J.J., and Bjaalie, J.G. (2000a). Three-dimensional topography of corticopontine projections from rat barrel cortex: correlations with corticostriatal organization. *J Neurosci* *20*, 8474-8484.

Leergaard, T.B., and Bjaalie, J.G. (1995). Semi-automatic data acquisition for quantitative neuroanatomy. MicroTrace--computer programme for recording of the spatial distribution of neuronal populations. *Neurosci Res* 22, 231-243.

Leergaard, T.B., and Bjaalie, J.G. (2007). Topography of the complete corticopontine projection: from experiments to principal Maps. *Front Neurosci* 1, 211-223.

Leergaard, T.B., Lakke, E.A., and Bjaalie, J.G. (1995). Topographical organization in the early postnatal corticopontine projection: a carbocyanine dye and 3-D computer reconstruction study in the rat. *J Comp Neurol* 361, 77-94.

Leergaard, T.B., Lillehaug, S., De Schutter, E., Bower, J.M., and Bjaalie, J.G. (2006). Topographical organization of pathways from somatosensory cortex through the pontine nuclei to tactile regions of the rat cerebellar hemispheres. *Eur J Neurosci* 24, 2801-2812.

Leergaard, T.B., Lyngstad, K.A., Thompson, J.H., Taeymans, S., Vos, B.P., De Schutter, E., Bower, J.M., and Bjaalie, J.G. (2000b). Rat somatosensory cerebropontocerebellar pathways: spatial relationships of the somatotopic map of the primary somatosensory cortex are preserved in a three-dimensional clustered pontine map. *J Comp Neurol* 422, 246-266.

Lemon, R.N. (2008). Descending pathways in motor control. *Annu Rev Neurosci* 31, 195-218.

Lillehaug, S., Oyan, D., Leergaard, T.B., and Bjaalie, J.G. (2002). Comparison of semi-automatic and automatic data acquisition methods for studying three-dimensional distributions of large neuronal populations and axonal plexuses. *Network* 13, 343-356.

Maheshwari, U., Kraus, D., Vilain, N., Holwerda, S.J.B., Cankovic, V., Maiorano, N.A., Kohler, H., Satoh, D., Sigrist, M., Arber, S., *et al.* (2020). Postmitotic Hoxa5 Expression Specifies Pontine Neuron Positional Identity and Input Connectivity of Cortical Afferent Subsets. *Cell reports* 31, 107767.

Mihailoff, G.A., Lee, H., Watt, C.B., and Yates, R. (1985). Projections to the basilar pontine nuclei from face sensory and motor regions of the cerebral cortex in the rat. *J Comp Neurol* 237, 251-263.

Nitschke, M.F., Kleinschmidt, A., Wessel, K., and Frahm, J. (1996). Somatotopic motor representation in the human anterior cerebellum. A high-resolution functional MRI study. *Brain* 119 (Pt 3), 1023-1029.

O'Leary, D.D., and Sahara, S. (2008). Genetic regulation of arealization of the neocortex. *Curr Opin Neurobiol* 18, 90-100.

Petersen, S.C., Watson, J.D., Richmond, J.E., Sarov, M., Walthall, W.W., and Miller, D.M., 3rd (2011). A transcriptional program promotes remodeling of GABAergic synapses in *Caenorhabditis elegans*. *J Neurosci* 31, 15362-15375.

Polleux, F., Dehay, C., and Kennedy, H. (1997). The timetable of laminar neurogenesis contributes to the specification of cortical areas in mouse isocortex. *J Comp Neurol* 385, 95-116.

Porrero, C., Rubio-Garrido, P., Avendano, C., and Clasca, F. (2010). Mapping of fluorescent protein-expressing neurons and axon pathways in adult and developing Thy1-eYFP-H transgenic mice. *Brain Res* 1345, 59-72.

Proville, R.D., Spolidoro, M., Guyon, N., Dugue, G.P., Selimi, F., Isope, P., Popa, D., and Lena, C. (2014). Cerebellum involvement in cortical sensorimotor circuits for the control of voluntary movements. *Nat Neurosci* 17, 1233-1239.

Puchades, M.A., Csucs, G., Ledergerber, D., Leergaard, T.B., and Bjaalie, J.G. (2019). Spatial registration of serial microscopic brain images to three-dimensional reference atlases with the QuickNII tool. *PLoS One* 14, e0216796.

Schmahmann, J.D., and Pandya, D.N. (1997). Anatomic organization of the basilar pontine projections from prefrontal cortices in rhesus monkey. *J Neurosci* 17, 438-458.

Shambes, G.M., Gibson, J.M., and Welker, W. (1978). Fractured somatotopy in granule cell tactile areas of rat cerebellar hemispheres revealed by micromapping. *Brain, behavior and evolution* 15, 94-140.

Shepherd, G.M. (2009). Intracortical cartography in an agranular area. *Front Neurosci* 3, 337-343.

Smart, I.H. (1984). Histogenesis of the mesocortical area of the mouse telencephalon. *J Anat* 138 (Pt 3), 537-552.

Svoboda, K., and Li, N. (2018). Neural mechanisms of movement planning: motor cortex and beyond. *Curr Opin Neurobiol* 49, 33-41.

Tomasch, J. (1968). The overall information carrying capacity of the major afferent and efferent cerebellar cell and fiber systems. *Confin Neurol* 30, 359-367.

Tomasch, J. (1969). The numerical capacity of the human cortico-pontocerebellar system. *Brain Res* 13, 476-484.

Tomassy, G.S., De Leonibus, E., Jabaudon, D., Lodato, S., Alfano, C., Mele, A., Macklis, J.D., and Studer, M. (2010). Area-specific temporal control of corticospinal motor neuron differentiation by COUP-TFI. *Proc Natl Acad Sci U S A* 107, 3576-3581.

Toyoda, R., Assimacopoulos, S., Wilcoxon, J., Taylor, A., Feldman, P., Suzuki-Hirano, A., Shimogori, T., and Grove, E.A. (2010). FGF8 acts as a classic diffusible morphogen to pattern the neocortex. *Development* 137, 3439-3448.

Wang, Q., Ding, S.L., Li, Y., Royall, J., Feng, D., Lesnar, P., Graddis, N., Naeemi, M., Facer, B., Ho, A., *et al.* (2020). The Allen Mouse Brain Common Coordinate Framework: A 3D Reference Atlas. *Cell* 181, 936-953 e920.

Voogd, J. (1995) Cerebellum. In Bannister, L.H., Berry, M.M., Collins, P., Dyson, M., Dussek, J.E. & Ferguson, M.W.J., (Eds), *Gray's Anatomy*. Churchill Livingstone, New York, pp. 1027-1065.

Welker, C. (1971). Microelectrode delineation of fine grain somatotopic organization of (Sml) cerebral neocortex in albino rat. *Brain Res* 26, 259-275.

Welker W (1987) Spatial organization of somatosensory projections to granule cell cerebellar cortex: functional and connectional implications of fractured somatotopy (summary of Wisconsin studies). In: King JS (ed) *New concepts in cerebellar neurobiology*. Liss, New York, pp 239-280

Welniarz, Q., Dusart, I., and Roze, E. (2017). The corticospinal tract: Evolution, development, and human disorders. *Dev Neurobiol* 77, 810-829.

Woolsey, T.A., and Van der Loos, H. (1970). The structural organization of layer IV in the somatosensory region (SI) of mouse cerebral cortex. The description of a cortical field composed of discrete cytoarchitectonic units. *Brain Res* 17, 205-242.

Zhou, H.M., and Walthall, W.W. (1998). UNC-55, an orphan nuclear hormone receptor, orchestrates synaptic specificity among two classes of motor neurons in *Caenorhabditis elegans*. *J Neurosci* 18, 10438-10444.

Zingg, B., Hintiryan, H., Gou, L., Song, M.Y., Bay, M., Bienkowski, M.S., Foster, N.N., Yamashita, S., Bowman, I., Toga, A.W., *et al.* (2014). Neural networks of the mouse neocortex. *Cell* 156, 1096-1111.

TABLES

Supplementary Table 1

Allen mouse brain connectivity database					
Experiment number #	Sex	Age (± 2)	Genotype	Injection site	Figure of appearance
114290938	male	P56	C57BL/6J	Primary somatosensory cortex, mouth region	Fig. 2
112229814	male	P56	C57BL/6J	Primary somatosensory cortex, upper limb region	Fig. 2 and 6
112952510	male	P56	C57BL/6J	Secondary motor cortex	Fig. 2 and 6
114292355	male	P56	C57BL/6J	Primary somatosensory cortex, lower limb region	Fig. 2
126908007	male	P56	C57BL/6J	Primary somatosensory cortex, nose region	Fig. 2
127084296	male	P56	C57BL/6J	Secondary motor cortex	Fig. 2
127866392	male	P56	C57BL/6J	Primary somatosensory cortex, barrel field region	Fig. 2
141602484	male	P56	C57BL/6J	Secondary motor cortex	Fig. 2
141603190	male	P56	C57BL/6J	Secondary motor cortex	Fig. 2
585025284	male	P56	C57BL/6J	Secondary motor cortex	Fig. 2

Supplementary Table 2

Adult					
Exp. #	Animal #	Sex	Age	Genotype	Figure of appearance
1	13588	female	P33	<i>Thy1-eYFP^{T/+}; Nr2f1^{fl/fl}</i>	Fig. 3, 4, 5 and Suppl. Fig.1, 2
1	13587	female	P33	<i>Thy1-eYFP^{T/+}; Nr2f1^{fl/fl}; NEX-Cre</i>	Fig. 3, 4, 5 and Suppl. Fig.1, 2
2	13585	male	P62	<i>Thy1-eYFP^{T/+}; Nr2f1^{fl/fl}; NEX-Cre</i>	Fig. 3, 4, 5 and Suppl. Fig.1, 2
3	13809	male	P57	<i>Thy1-eYFP^{T/+}; Nr2f1^{fl/fl}; NEX-Cre</i>	Fig. 3, 4, 5 and Suppl. Fig.1, 2
4	14258	male	P57	<i>Thy1-eYFP^{T/+}; Nr2f1^{fl/fl}</i>	Fig. 3, 4, 5 and Suppl. Fig.1, 2
4	14260	male	P57	<i>Thy1-eYFP^{T/+}; Nr2f1^{fl/fl}; NEX-Cre</i>	Fig. 3, 4, 5 and Suppl. Fig.1, 2
5	13805	male	P55	<i>Thy1-eYFP^{T/+}; Nr2f1^{fl/fl}; NEX-Cre</i>	Fig. 3, 4, 5 and Suppl. Fig.1, 2
5	14250	male	P72	<i>Thy1-eYFP^{T/+}; Nr2f1^{fl/fl}</i>	Fig. 3, 4, 5 and Suppl. Fig.1, 2
5	15170	male	P75	<i>Thy1-eYFP^{T/+}; Nr2f1^{fl/fl}</i>	Fig. 3, 4, 5 and Suppl. Fig.1, 2
6	16922	male	P76	<i>Thy1-eYFP^{T/+}; Nr2f1^{fl/fl}; EMX1-Cre</i>	Fig. 3, 4, 5 and Suppl. Fig.1, 2
6	16923	male	P76	<i>Thy1-eYFP^{T/+}; Nr2f1^{fl/fl}</i>	Fig. 3, 4, 5 and Suppl. Fig.1, 2
6	16924	male	P76	<i>Thy1-eYFP^{T/+}; Nr2f1^{fl/fl}</i>	Fig. 3, 4, 5 and Suppl. Fig.1, 2
6	16926	male	P76	<i>Thy1-eYFP^{T/+}; Nr2f1^{fl/fl}; EMX1-Cre</i>	Fig. 3, 4, 5 and Suppl. Fig.1, 2
7	17882	male	P72	<i>Thy1-eYFP^{T/+}; Nr2f1^{fl/fl}; EMX1-Cre</i>	Fig. 3, 4, 5 and Suppl. Fig.1, 2
8	18046	female	P109	<i>Thy1-eYFP^{T/+}; Nr2f1^{fl/fl}; EMX1-Cre</i>	Fig. 3, 4, 5 and Suppl. Fig.1, 2
8	18166	female	P98	<i>Thy1-eYFP^{T/+}; Nr2f1^{fl/fl}</i>	Fig. 3, 4, 5 and Suppl. Fig.1, 2
8	18271	female	P87	<i>Thy1-eYFP^{T/+}; Nr2f1^{fl/fl}</i>	Fig. 3, 4, 5 and Suppl. Fig.1, 2

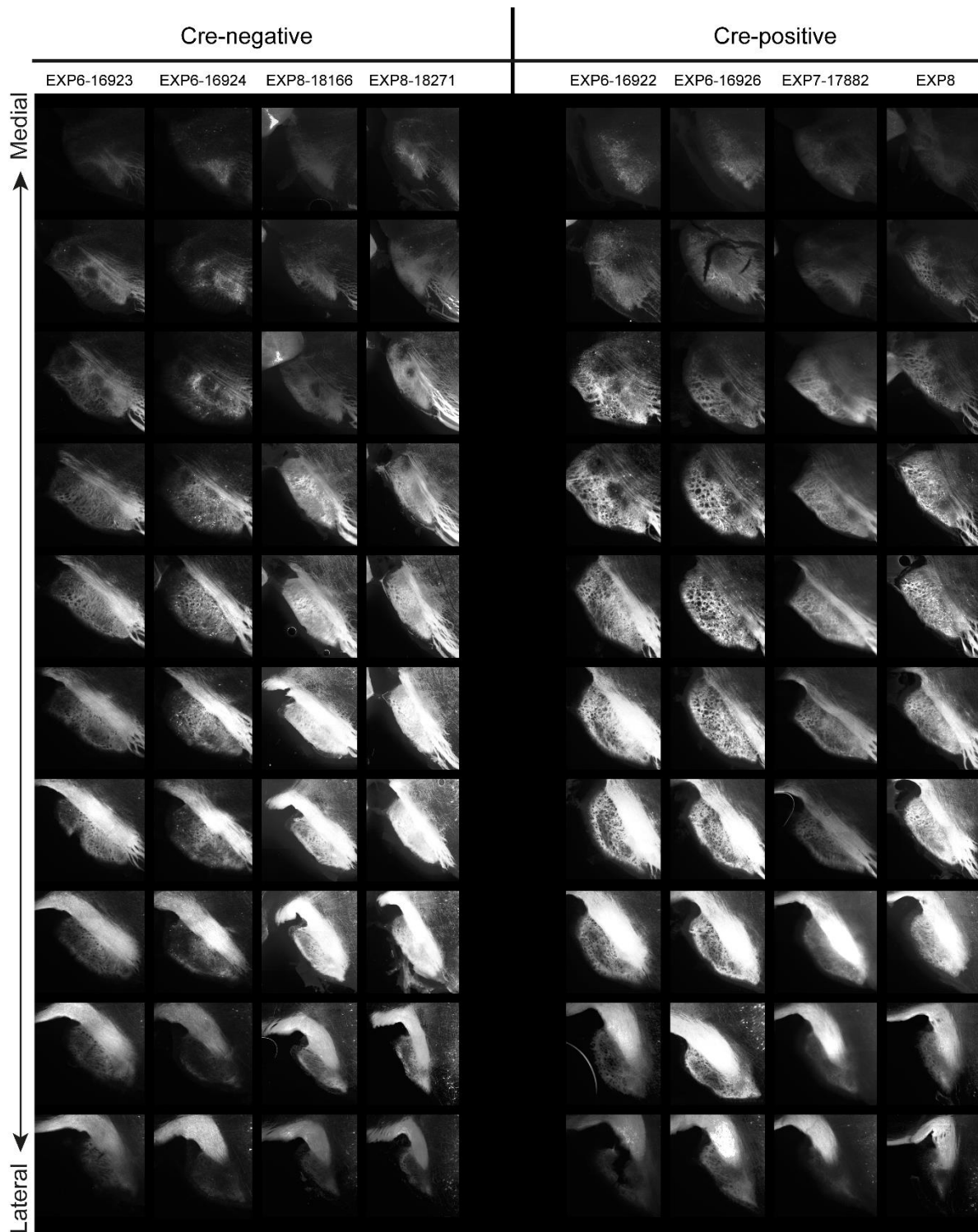
Supplementary Table 3

P21 – unilateral CST tracing			
<i>Motor cortex</i>			
Experiment #	Animal #	Genotype	Used for analyses in
2	11643_13	<i>Ctrl</i>	Fig. 6D
2	11643_16	<i>Nex-cKO</i>	Fig. 6D
2	11643_17	<i>Nex-cKO</i>	Fig. 6D
2	11796_2	<i>Ctrl</i>	Fig. 6D
2	11796_8	<i>Ctrl</i>	Fig. 6D
2	11796_9	<i>Ctrl</i>	Fig. 6D
3	18035_1	<i>Ctrl</i>	Fig. 6D
3	18035_2	<i>Ctrl</i>	Fig. 6D
3	18035_7	<i>Ctrl</i>	Fig. 6D
3	18035_3	<i>Nex-cKO</i>	Fig. 6D
3	18035_4	<i>Nex-cKO</i>	Fig. 6D
3	18035_8	<i>Nex-cKO</i>	Fig. 6D
4	19423_2	<i>Ctrl</i>	Fig. 6D
4	19423_3	<i>Ctrl</i>	Fig. 6D
4	19423_4	<i>Nex-cKO</i>	Fig. 6D
4	19423_5	<i>Nex-cKO</i>	Fig. 6D
<i>Somatosensory cortex</i>			
4	19423_7	<i>Nex-cKO</i>	Fig. 6E

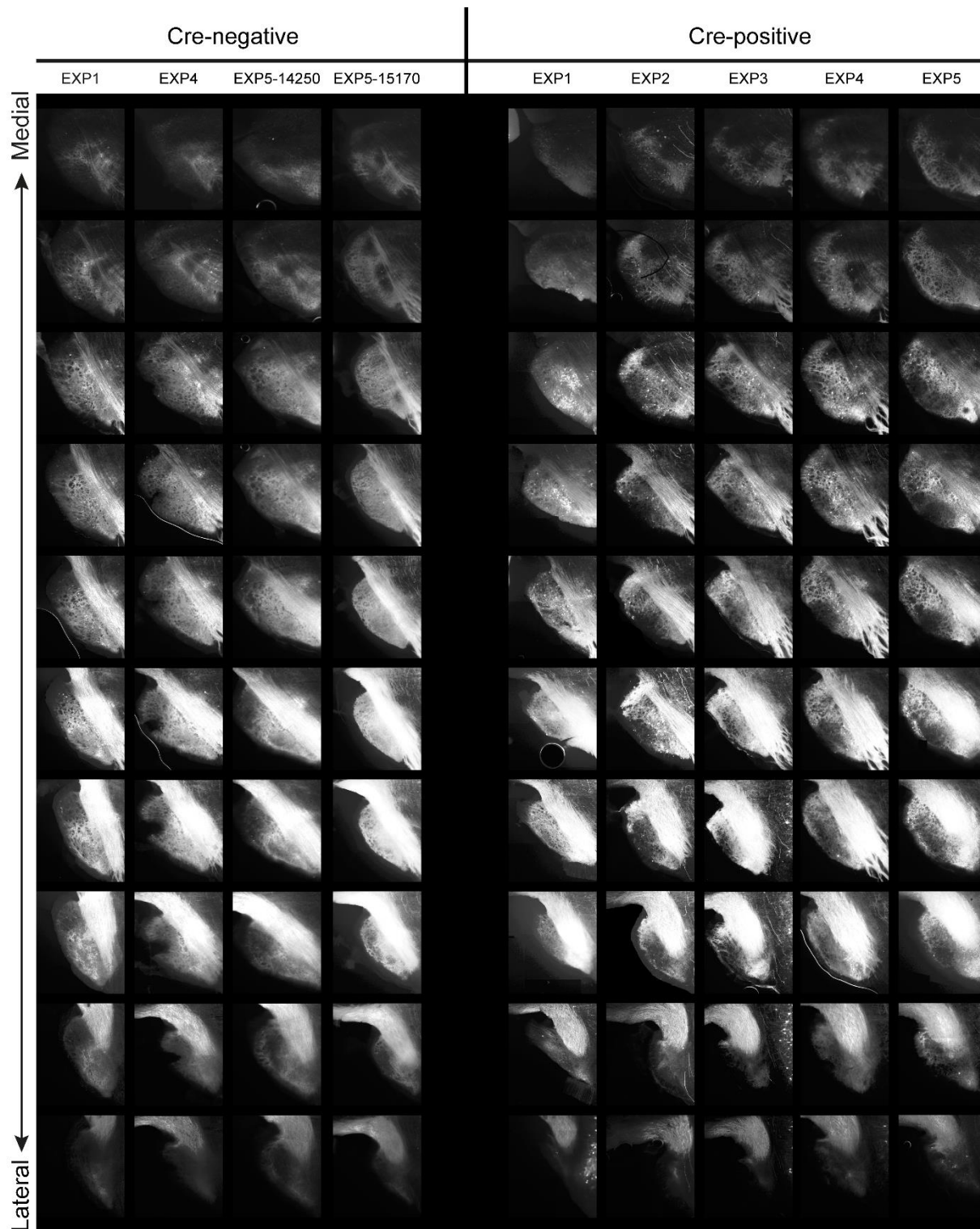
Supplementary Table 4

List of primary and secondary antibodies used in this study.

Antigen	Provider	Catalog #	Species	Working dilution
GFP	Abcam	Ab13970	Ck	1:500
RFP	Abcam	Ab 124754	Rb	1:500
FLAG (DYKDDDDK Epitope)	NOVUS	NBP-1-06712	Rat	1:500
Ck IgY - AF 488	Thermo Fisher	A11039	Gt	1:500
Rb IgG - AF 555	Thermo Fisher	A21428	Gt	1:500
Rat IgG - AF 594	Thermo Fisher	A11007	Gt	1:500



Supplementary figure 1: Sagittal sectional images from medial to lateral of the pontine nuclei in Emx1-cKO control and mutant mice. Sagittal sectional images are organized in columns, from medial to lateral, for Emx1-cKO cre-negative control cases on the left and Emx1-cKO cre-positive mutant cases on the right. Experimental case numbers are shown above each column. The rows show images in corresponding mediolateral position.



Supplementary figure 2: Sagittal sectional images from medial to lateral of the pontine nuclei in Nex-cKO control and mutant mice. Sagittal sectional images are organized in columns from medial to lateral for Nex-cKO cre-negative control cases on the left and Nex-cKO cre-positive mutant cases on the right. Experimental case numbers are shown above each column. The rows show images in corresponding mediolateral position.

3. Additional results

a. Assessing dendrites spine density of cortical layer V pyramidal neurons in *Nr2f1* cKO models

In the first part of the results, we investigated several morphological and structural aspects of pyramidal neurons that are known to influence and be influenced by fluctuation in the electrophysiological state of the cell. We introduced the concept of intrinsic excitability and described it as the likelihood of a cell to become active and fire action potentials. Despite that, it has been reported that several mechanisms are often put in place to restore a normal range of firing activity, when the excitability is perturbed, in order to maintain the network in a physiological state. In the previous chapters, we have already reported the adaptation of the AIS structure to affect its efficiency to fire action potentials and the modification of the dendritic arborization, as a way to control the effective number of neuron-neuron connections and the propagation of the signal among the circuit.

Here, I will focus on another structure that can affect and be affected by changes in the intrinsic excitability of a cell: the density and nature of dendritic spines.

Spines are a heterogeneous group of small membranous structures protruding from the main dendrites for an average length of 0.5 to 2 μm and density of 1-10 spines per 10 μm . Curiously, dendritic spines are very rarely found in lower organisms, suggesting that their origins might be related to the insurgence of a more complex and advanced nervous system, such that of mammals. Spines represent the postsynaptic compartment for the majority of excitatory (glutamatergic) synapses, and their activity is essential for synaptic transmission and plasticity and ultimately for learning and memory.

Before moving on with the results, I will briefly introduce how and when spines are generated during brain development, their structure and classification and finally, their physiological and pathological functions.

i. Spine density dynamics variation relative to the developmental stage, cell type and cortical region of belonging

Although the establishment of spines begins prenatally, their refinement is a much long-lasting event, which protracts all along early postnatal life, and a certain degree of plasticity is even persisting into adulthood (Moyer et al., 2018).

Typically, in mammals synaptogenesis is predominantly happening during early postnatal development, and then spine density decreases during adolescence and until adulthood, when it stabilizes. In rodents, and specifically on LVPNs dendrites, there is a huge increase in the number of filopodia during the first two postnatal weeks. *In vivo* imaging analyses show that these structures are highly dynamic, with just the 3% of them persisting for more than a couple of days and eventually transforming into mature spines (Lendvai et al., 2000; Zuo et al., 2005). Throughout adolescence and adulthood, the number of filopodia steadily decreases until they are just a small fraction of the overall pool. Concomitantly, spines continue to be generated and to mature, as well as they will dismantle and progressively eliminated. In a first time, during adolescence, the elimination rate is higher than generation rate, thus leading to a general decrease of the spine density. Then, during adulthood, the elimination slows down to reach an equilibrium point, and the number of spines remains stable (Holtmaat et al., 2005; Trachtenberg et al., 2002; Zuo et al., 2005).

Interestingly, this process is observed in other cortical neuron populations, although the specific dynamics vary considerably among cell types and cortical regions. For instance, as a result of reduced turnover during adolescence, adult LII/III projection neurons show a higher spine density than adult LVPNs (Tjia et al., 2017). Moreover, when compared among different cortical regions, LVPNs show slightly different dynamics (Majewska et al., 2006). To date, it is still under debate whether these differences are intrinsically defined or are imparted by the local neuronal circuits in which they are involved.

ii. The structure of mature dendritic spines

Classical anatomical studies of fixed brains led to the definition of four main morphological classes: thin, stubby mushroom and cup-shaped or bifurcated spines. In addition, a fifth category is

represented by filopodia, a highly dynamic structure which is thought to be both a precursor of mature spines, and an inactive transitory state towards which mature spines revert to when local factors such as synaptic activity is required.

Other than based on their morphology, spines can be defined based upon the organelles and molecules they contain. Generally speaking, larger spines contain more and more diverse organelles than smaller spines. One of the most characteristic structures is the post synaptic density (PSD), which is localized on the head of the spine and faces the presynaptic active zone of an adjacent neuron. The PSD is where both AMPA and NMDA glutamate receptors localize and the bigger the structure is, the more receptors it can host. Not only this, but a correlation between head size and AMPA content has also been reported, with bigger spines often showing an accumulation of AMPA receptors at the expense of a reduced pool of NMDA receptors, whereas smaller spines show a complementary asset (Kasai et al., 2003).

iii. Functions and pathological dysfunctions of dendritic spines

The peculiar shape of the spines is functional to the compartmentalization of chemical and electrical signalling within individual synapses. Moreover, specific morphological characteristics, such as head width and neck diameter, might influence how single unities work. For example, small stubby spines with thinner necks accumulate Ca^{2+} much faster than bigger spines with thicker necks. This, together with a higher content in NMDA receptors, would result in increased susceptibility to LTP – an activity-driven increase of synaptic transmission- making this class of spines the putative responsible for synaptic plasticity (Matsuzaki et al., 2004). On the contrary, large mushroom spines are much more resilient, and seem to be the one responsible to ensure memory (Kasai et al., 2003; Matsuzaki et al., 2004).

At any given time, neural circuits have to be rather stable, so that the activity range always falls into physiological conditions but at the same time permissive towards changes in connectivity and synaptic strength which occur during developmental stages and learning and memory processes. At the cellular level, this equilibrium is pursued through different adaptive mechanisms and one among them is the regulation of the synaptic strength. For instance, when the E/I ratio is perturbed, and an excessive inhibition is registered, a cell which is part of the network might register an increase of

the number of spines and/or their glutamate receptors pool, producing an increase of the firing rate. The other way around happens if the cell is involved in an over-excited circuit (Tien et al., 2018).

Given their implication in several essential processes, it might not be surprising that defects in the dendritic spine functions lead to cognitive dysfunctions in humans. The first evidence of this association is traced back to the 1974, when post-mortem Golgi staining on brains from patients affected by intellectual disability (ID) showed a general reduction of mature spines and a relative augmentation of filopodia. More recently, spine defects have also been reported in post-mortem samples of Autism Spectrum Disorder (ASD) patients. In this case, a significant increase in spine density has been observed in layer II-III pyramidal cells in several cortical regions. Dendritic spines aberrations have also been discovered in several genetic diseases, such as Fragile-X Syndrome (augmentation of immature spines on cortical pyramidal cells) and Rett and Down Syndromes (reduction of mature spines and abnormal accumulation of immature filopodia).

Genetic animal models have successfully been used to recapitulate those findings and to investigate the molecular mechanisms underlying the defective spinogenesis and its involvement in the pathogenesis of neurodevelopmental diseases.

In the previous chapters we elucidated the role of *Nr2f1* in regulating intrinsic excitability and network activity of young neurons. Furthermore, BBSOAS patients show intellectual disability and ASD features, suggesting a possible impairment in dendritic spines maturation and stability. Being the maturation of dendritic spines a process that happens in differentiating neurons rather than progenitor cells, we decided to focus our analyses on the *Nex-CKO* mouse line, where *Nr2f1* is ablated solely from the postmitotic neurons.

iv. Results

To test the hypothesis of *Nr2f1* being involved in spine production, elimination and/or maturation, I took advantage of the *Thy1-eYFP-H* transgenic reporter mouse line previously introduced (Porrero et al., 2010). Both controls and *Nex-cKO* were crossed with the reporter mouse line, and the endogenous YFP signal was exploited for the high-resolution imaging of dendrites and spines (Fig. 32).

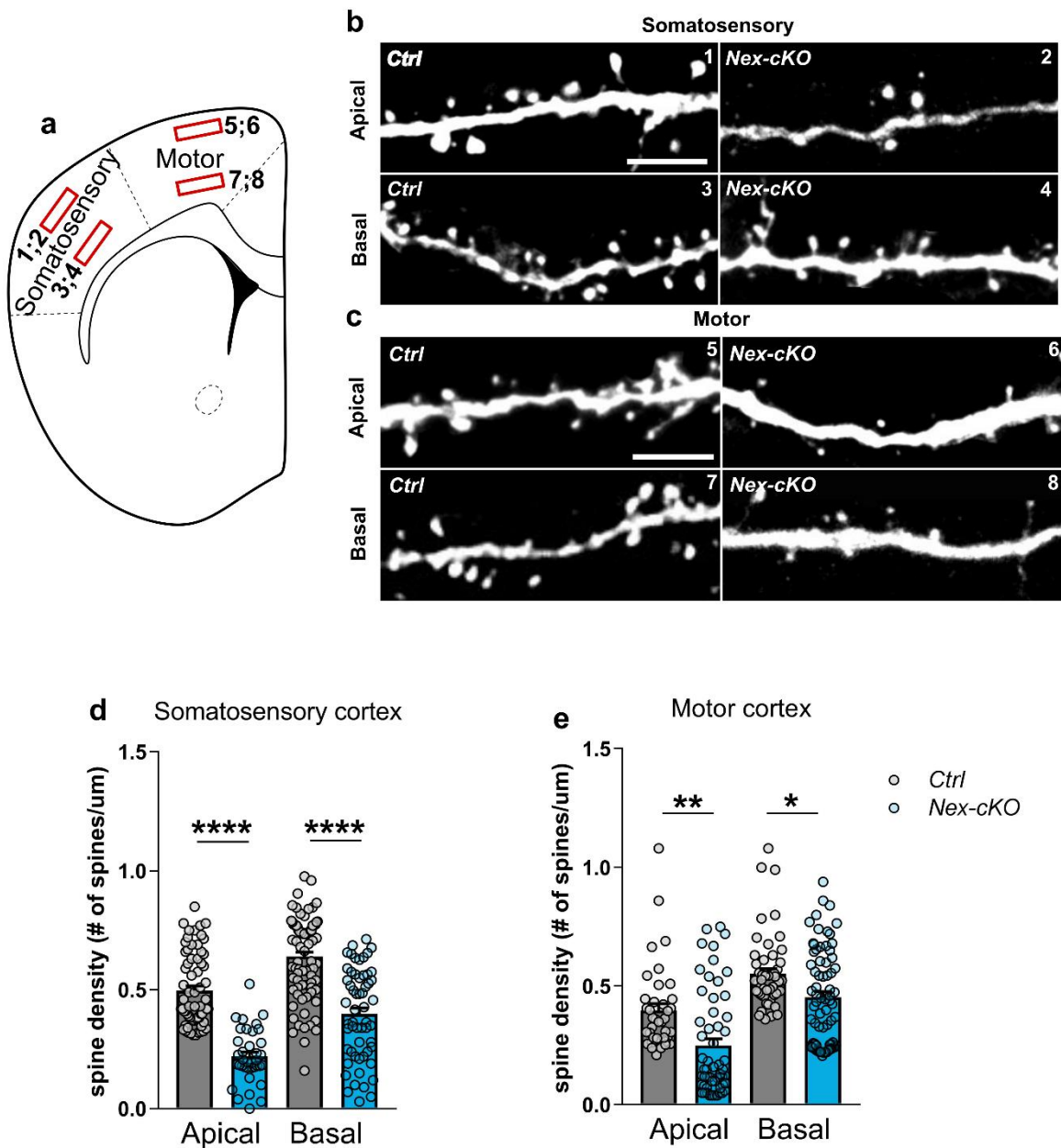


Figure 32- Loss of Nr2f1 leads to reduction of spines in Nex-cKO adult brains. **a)** Schematic representation of a coronal brain section and the location of motor and somatosensory cortex. The red boxes represent the position of the figures in **b** and **c**. **b)** Representative dendrites from the somatosensory cortex of control and mutant brains, in apical (**1-2**) and basal (**3-4**) positions. **c)** Representative dendrites from the motor cortex of control and mutant brains, in apical (**5-6**) and basal (**7-8**) position. In **d** and **e**, spine density has been calculated as the ratio between the number of spines for segment and the length of the segment. The bars represent the average value for each region and position, whereas the dots represent the values of individual segments and the variability of the samples. The data have been analysed by 1wayANOVA test and corrected for multiple correction with the Bonferroni's test. Analyses have been performed on the average values of N=3 animals. (****< 0.001; **= 0.0018; *= 0.0236).

The density of spines was quantified as the ratio between the number of spines and the length of the analysed dendritic segment. Sampling of the segments has been performed in both the apical and the basal dendritic arborization individually (**Fig. 32a-c**). For the basal portion, differentiation among primary, secondary or higher degree dendrites was not possible due to the high number of positive cells. Hence, a single mixed population has been analysed. For the apical portion instead, the primary dendrite has been excluded from the analysis, whereas secondary and higher degree dendrites could not be distinguished. The analysis has been performed in both motor and somatosensory areas. In general, spine density has been found reduced in all the analysed regions (**Fig. 32d-e**).

Next, the morphological characteristics of the spines, as readout of their maturation, was analysed. To do that, neck length, head width and number of heads have been measured for each spine and then used to classify the spines in four classes (**Fig. 33a**). In both somatosensory (**Fig. 33b-c**) and motor (**Fig. 33d-e**) regions and in apical and basal positions, the distribution among classes does not seem to be affected by the absence of Nr2f1.

These data together suggest that Nr2f1 might affect the balance between production and elimination rate in adult brains, but it seems to have no effect on spine maturation.

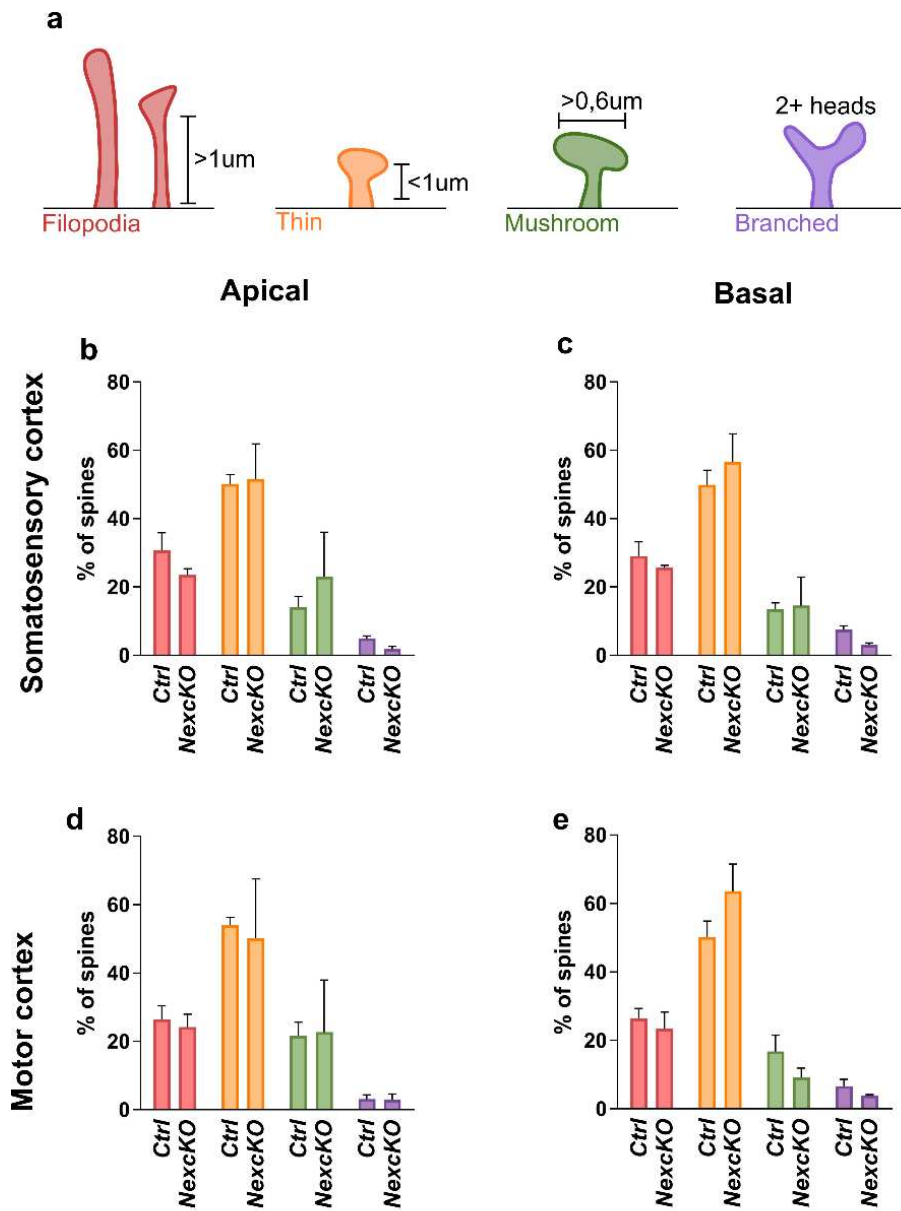


Figure 33 - Loss of Nr2f1 does not affect spine maturation in Nex-cKO mutants. *a)* Schematic representation of spine classes considered in this analysis. *In b, c, d and e,* the values are calculated as percentage of a specific class of spines on the total number of spines. The bars represent the average value for each region and position. The data have been analysed by 2wayANOVA test and corrected for multiple correction. Analyses have been performed on the average values of N=3 animals.

More experiments need to be provided to elucidate where exactly Nr2f1 acts in the process of synaptogenesis and whether reduced number of synapses in adult brains is the result of defective synaptogenesis at early stages of brain development or of abnormal imbalance of spine production and elimination. Specifically, the analysis the spine density at different developmental stages can help understanding at what time exactly the defect originates, whereas *in vivo* time-lapse analysis can tell us more about spine dynamics in the adult brains of mutant animals.

a. Assessing topographic map of thalamo-cortical and cortico-pontine projections in a genetic rescue model for *Nr2f1* loss of function.

Although a plethora of molecules have been described to affect CST development (Welniarz et al., 2007), and some of them are specifically expressed in the neocortex in both progenitor cells and postmitotic neurons, very little is known about cortex-specific genes being able to influence the topographic projection map within the PN. Abnormal expression of these factors generally results in projection defects, suggesting that establishment of proper identity and cell fate in the cortex can influence subcerebral layer Vb projection neuron ability to correctly reach their targets. The postmitotic transcription factor *Bhlhb5* (also known as BHLHE22) for example, has been reported to influence the ability of the CST to trespass the mid-hindbrain boundary (MHB) and enter the spinal cord (Joshi et al. 2008). Interestingly, in *Nr2f1* cortical mutants, *Bhlhb5* cortical expression is drastically reduced (Alfano et al., 2014), suggesting that the two genes could regulate CST development by acting in the same molecular pathway.

In the Paper 2 attached above, we utilized cortico-specific *Nr2f1* conditional knockout mice to investigate the contribution of cortical genetic programs in the establishment of topographic corticopontine projections. In these animals, we analyzed the 3D spatial distribution of the reporter gene *Thy1-YFP-H* (Porrero et al., 2010) in serial microscopic images and find that loss of *Nr2f1* from the progenitor cell pool results in an imbalance ratio of corticopontine and corticospinal projections, whereas the loss of function of the gene in postmitotic neurons leads to aberrant pattern of PN innervation (**see Result – Paper two for additional information**).

In this chapter, we aimed to assess whether *Nr2f1* and *Bhlhb5* are functionally related in the topographic organization of corticothalamic and corticopontine projections.

Previously in the lab, the presence of *Nr2f1* binding sites on the regulatory sequence of *Bhlhb5* was assessed via MatInspector (<http://www.genomatix.de/en/produkte/genomatix-software-suite.html>), ECR browser (<http://ecrbase.dcode.org>) and ChromAnalyzer (Montemayor et al., 2010) and six binding sites were identified upstream of the ORF of the *Bhlhb5* locus with variable evolutionary conservation in mammals. Then, to assess whether *Nr2f1* binds to these sites *in vivo*,

a CHIP assay was performed on E14.5 telencephalic tissue with a well-used antibody against Nr2f1 (Parisot et al., 2017). QPCR analysis of immunoprecipitated material showed a high enrichment of a site located – 2,7kb of the initiation transcription site of *Bhlhb5*, suggesting direct regulation of *Bhlhb5* by Nr2f1.

During my thesis, I started investigating whether the two genes were functionally interconnected in the differentiation process of corticopontine and corticospinal fibers. For this purpose, I overexpressed *Bhlhb5* in *Nex-cKO* E13.5 embryos, taking advantage of the *in utero* electroporation technique (see Materials and Methods for the detailed protocol). The aim was to re-express *Bhlhb5* in Nr2f1-deficient layer V neurons of S1 to demonstrate that *Bhlhb5* is involved in corticopontine connectivity downstream of Nr2f1. Briefly, the technique consists in injecting one or more genetic constructs into the lateral ventricle of mice embryos and induces the cellular internalization of the plasmid(s) with the use of pulsed electric current, without removing the embryos from the uterus. In this way, the embryogenesis can carry on after the surgery, and the effects of the genetic modification can be evaluated at later stages of embryonic or postnatal development. Furthermore, since the internalization of the plasmids is affecting cells facing the ventricle surface, and that only progenitors are present at this site, by controlling the embryonic time of the experiments, it is possible to target only progenitors that give rise to specific subtype of neurons (i.e. E12.5 injections targets predominantly layer VI-producing progenitors, E13.5 layer V etc.). Hence, to functionally assess the role of *Bhlhb5* expression in CST formation and connectivity, we re-expressed *Bhlhb5* in layer V neurons of Nr2f1 *Nex-cKO* and control brains by *in utero* electroporating an expression construct containing a *Bhlhb5* cDNA flanked by flox sites and a GFP-expressing sequence at E13.5, a time of high production of layer V neurons. Since the plasmid is flanked by lox sites, *Bhlhb5* will be expressed only upon *Nex* activity, thus in early postmitotic neurons. In this way high *Bhlhb5* expression cannot have an undesirable effect in progenitor cells. The reporter construct “spaghetti monster” (pCAG_smFP FLAG, addgene #59756) and the mCherry plasmid (addgene #108685) were also co-electroporated for allowing a better visualization of layer V axons and a quick reveal of the injection site after brain dissection, respectively. Electroporated brains were then assessed at P7.

Although the results here shown are very preliminary, it is worth noticing that thanks to the use of the enhanced spaghetti monster reporter plasmid, I was able to consistently track subcerebral projections through the entirety of the tract, from the injection site (**Fig. 34A,D,G**) to its terminals in the thalamus (**Fig. 34B',E',H'**) and the pontine nuclei (**Fig. 34C',F',H''**). We will at first confirm whether by solely injecting the tracer plasmid in control and *Nex-cKO* animals, we are able to recapitulate the topographic corticothalamic shift previously described (Alfano, 2014). Preliminary results show that while S1 layer V projections target the PoM thalamic nucleus in controls as expected (Bureau et al., 2006) (**Fig.34B, B'**), layer V projections in S1 *Nex-cKO* cortices seem to target PoM but also VL thalamic neurons (**Fig.34E, E'**), in line with a partial S1 to M1 change. The data upon re-expression of *Bhlhb5* in *Nex-cKO* brains seem to be more uncertain, even if layer V axons seemingly reaching the PoM and VPM nucleus (**Fig.34H, H'**).

Moreover, while corticopontine terminals nicely target the center of the PN in controls (**Fig.34C, C'**), in line with the arrival of S1 axons, as expected (Trygve B. Leergaard et al., 1995), the pattern of terminals in *Nex-cKO* PN seems to be extended by covering other regions that only the somatosensory arriving afferences(**Fig.34F, F'**). Re-expression of *Bhlhb5* seems to change the pattern of corticopontine, but at this stage this is not clear yet and needs more analysis (**Fig.34H, H''**). Since the injection sites differ among experiments (even if always targeting the putative somatosensory area), I will need to do more experiments and the data here presented need to be carefully compared to the brain atlas sections for correct locations. This part will be finalized with the help of our collaborators in Norway.

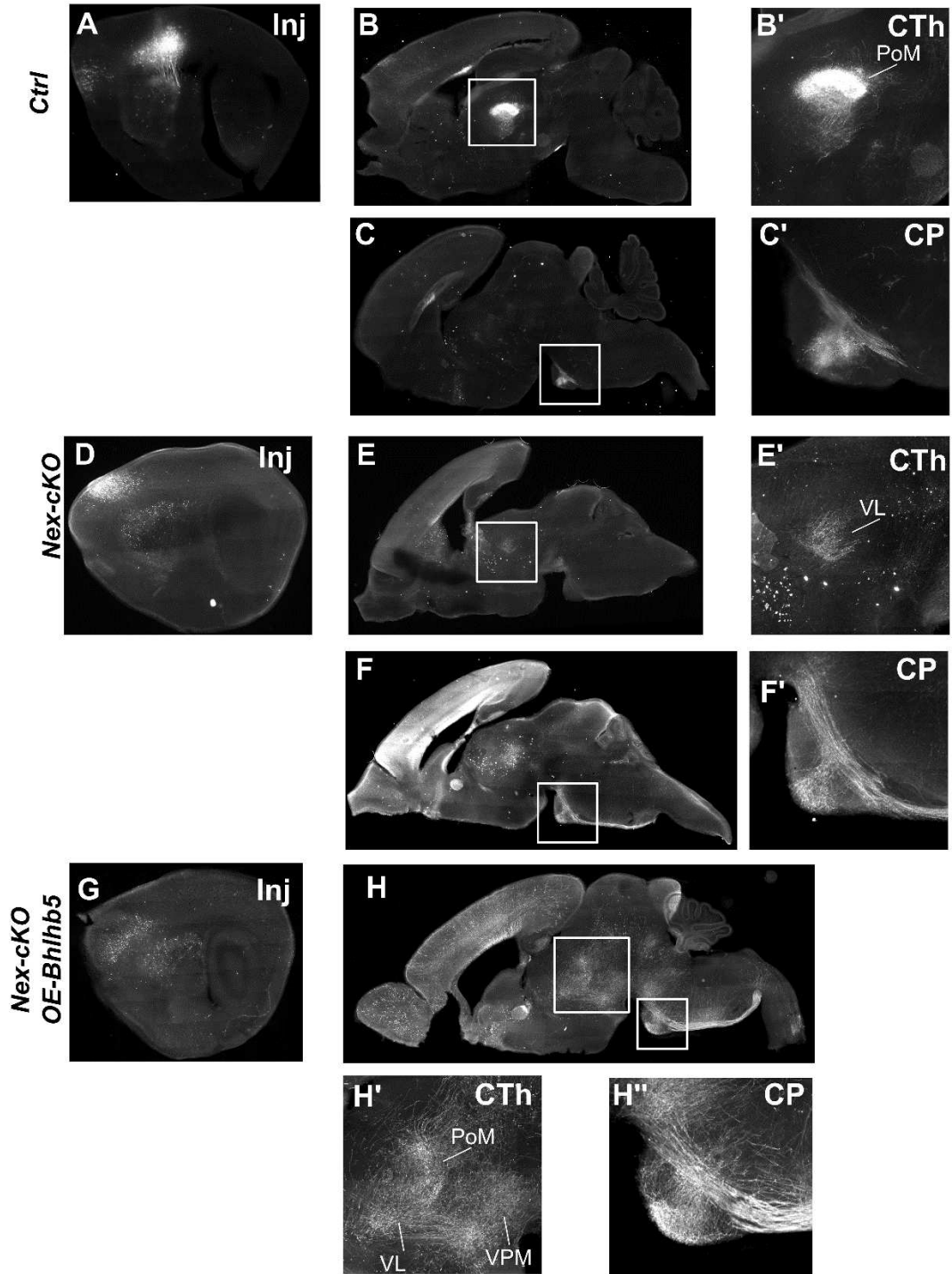


Figure 34 - Assessing *Nr2f1/Bhlhb5* functional relationship via *in utero* electroporation. Representative sections of injections sites and tracing in control (A-C), Nex-cKO (D-F) and Nex-cKO;Bhlhb5-OE (G-h) P7 brains. A,D,G) site of injection; B,E,H) whole brain sections and magnifications (B'-B''',E'-E''',H'-H''') of corticothalamic projections. C,F,I) whole brain sections and magnifications (C',F',I') of corticothalamic projections.

CTh: corticothalamic; CP: corticopontine; Inj: injection site; PoM: posteromedial nucleus; VPM: ventral posteromedial nucleus; VL: ventrolateral nucleus.

Annex A

Publication of LVPNs P7 reconstructed cells on the neuromorpho.org database

Since 2006, [Neuromorpho.org](https://neuromorpho.org) with the help of over 500 laboratories worldwide is collecting and publishing digitally reconstructed neurons that are associated with peer-reviewed publications. Here, more than one thousand different classes of neurons from over 300 brain regions and dozens of animal models are represented (**Fig. 35**), and one hundred thousand and counting cell reconstructions are stored and indexed to facilitate data sharing and provide the neuroscientific community with the biggest depository of 3D neurons structures and associated metadata.

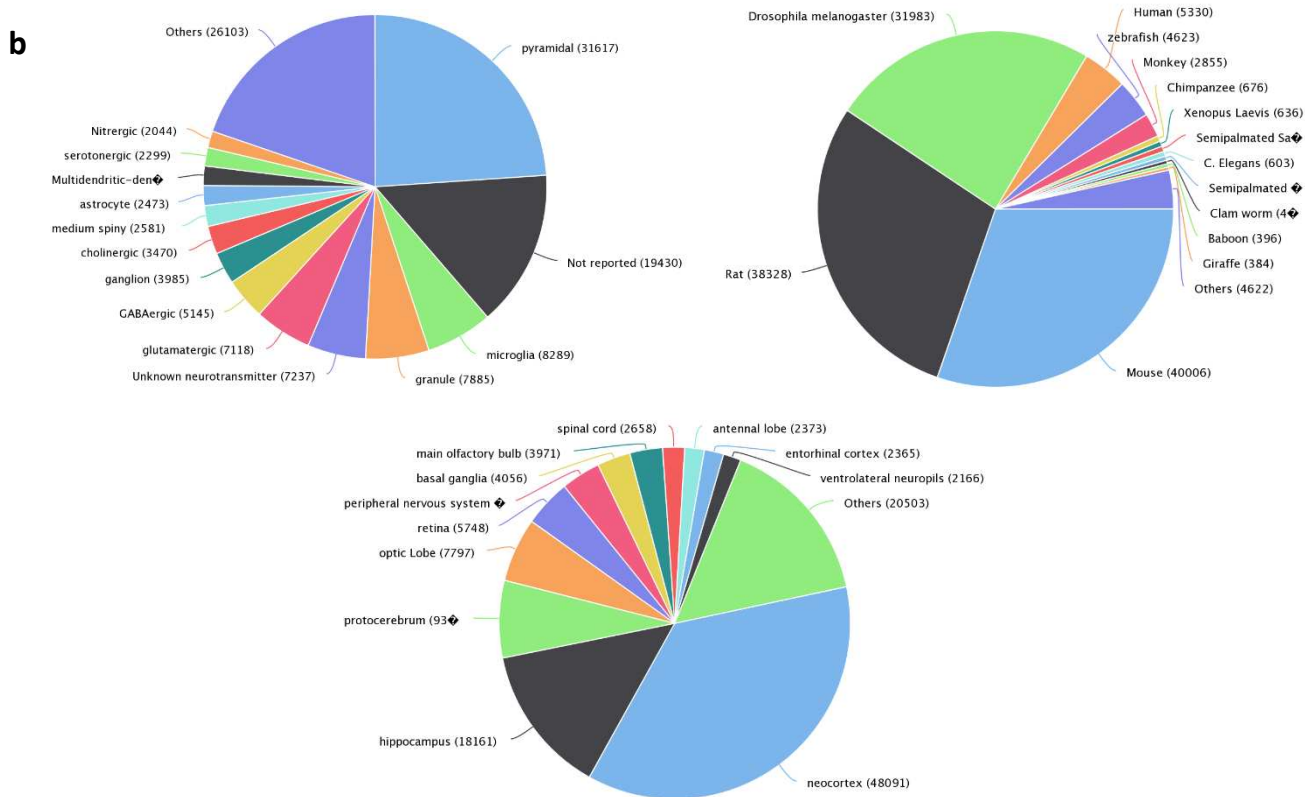


Figure 35 - Neuromorpho.org cells' classification. In the database, cells can be browsed based on their type (a), animal species (b) or brain region (c).

In November 2020, the LVPNs used for the electrophysiological and morphological analyses in del Pino et al. 2020 have been approved for publication in the database and are now available at the following link [ADD LINK AS SOON AS IT'S AVAILABLE](#). Specifically, as reported in the paper, we

analysed three different groups of pyramidal neurons: the populations of LVPNs of the motor and somatosensory cortex of control animals and those from the motorized somatosensory cortex of mutant animals.

To better highlight our contribution, in the next section I will present the main aspect of the database and how the information is stored and displayed on the website. Finally, I will present a selection of cells from each experimental group and their relative morphometric information, as published in the main article.

Once selected a specific archive the website allows users to scroll through it and have a quick look at the different reconstructions and key information on the cell, such as its location and type. From this overview, we can visualize a 2D snapshot of each cell structure, with basal dendrites represented in green, the apical dendrite in magenta and the axon (when available) in grey (Fig. 36).

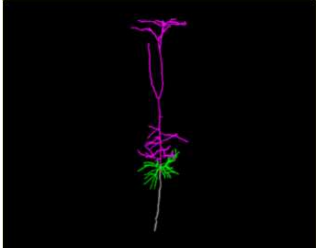
From here, by clicking on the cell name, the viewer is redirected to the detailed sheet for that specific entry.

The screenshot shows the NeuroMorpho.Org website interface. At the top, there is a logo for NeuroMorpho.Org and a version number: Version 8.0.69 - Released: 2020-11-05 - Content: 139593 neurons. Below the logo is a navigation bar with links: HOME, BROWSE, SEARCH, LITERATURE COVERAGE, TERMS OF USE, HELP. The main content area displays a search result for 61 neurons found. Three neurons are listed as examples:

- MS_p19c5**: Archive Name: Studer, Species Name: mouse, Structural Domains: Dendrites, No Soma, Axon, Physical Integrity: Dendrites & Axon Complete, Morphological Attributes: Diameter, 3D, Angles, Region1: neocortex, Region2: somatosensory, Region3: primary somatosensory, layer 5, Main Cell Type: principal cell, Class2: pyramidal, Class3: Not reported.
- MS_p3c8**: Archive Name: Studer, Species Name: mouse, Structural Domains: Dendrites, No Soma, No Axon, Physical Integrity: Dendrites Complete, Morphological Attributes: Diameter, 3D, Angles, Region1: neocortex, Region2: somatosensory, Region3: primary somatosensory, layer 5, Main Cell Type: principal cell, Class2: pyramidal, Class3: Not reported.
- MS_p18c5**: Archive Name: Studer, Species Name: mouse, Structural Domains: Dendrites, No Soma, No Axon, Physical Integrity: Dendrites Complete, Morphological Attributes: Diameter, 3D, Angles, Region1: neocortex, Region2: somatosensory, Region3: primary somatosensory, layer 5, Main Cell Type: principal cell, Class2: pyramidal, Class3: Not reported.

Figure 36 – Example of Neuromorpho archive

Here is where users can find access to the 3D tracing images and thanks to the inbuilt tools, the cell reconstruction can also be visualized in the 3D space, rotated and zoomed in. Moreover, all the available metadata are listed in this page.



[Morphology File \(Standardized\)](#)
[Morphology File \(Original\)](#)
[Log File \(Standardized\)](#)
[Log File \(Original\)](#)

[3D Neuron Viewer - Java, legacy](#)
[3D Neuron Viewer - WebGL, novel](#)
[Animation](#)

Reference Article

Related Article Reference : COUP-TFI/Nr2f1 Orchestrates Intrinsic Neuronal Activity during Development of the Somatosensory Cortex.

Measurements

Soma Surface	: N/A
Number of Stems	: 2
Number of Bifurcations	: 60
Number of Branches	: 122
Overall Width	: 169.89 μm
Overall Height	: 759.17 μm
Overall Depth	: 98.05 μm
Average Diameter	: 1.94 μm
Total Length	: 4742.93 μm
Total Surface	: 28650.3 μm^2
Total Volume	: 16127.5 μm^3
Max Euclidean Distance	: 543.9 μm
Max Path Distance	: 669.71 μm
Max Branch Order	: 23
Average Contraction	: 0.94
Total Fragmentation	: 5651
Partition Asymmetry	: 0.57
Average Rall's Ratio	: 1.84
Average Bifurcation Angle Local	: 52.49°
Average Bifurcation Angle Remote	: 71.03°
Fractal Dimension	: 1.02

Details about selected neuron

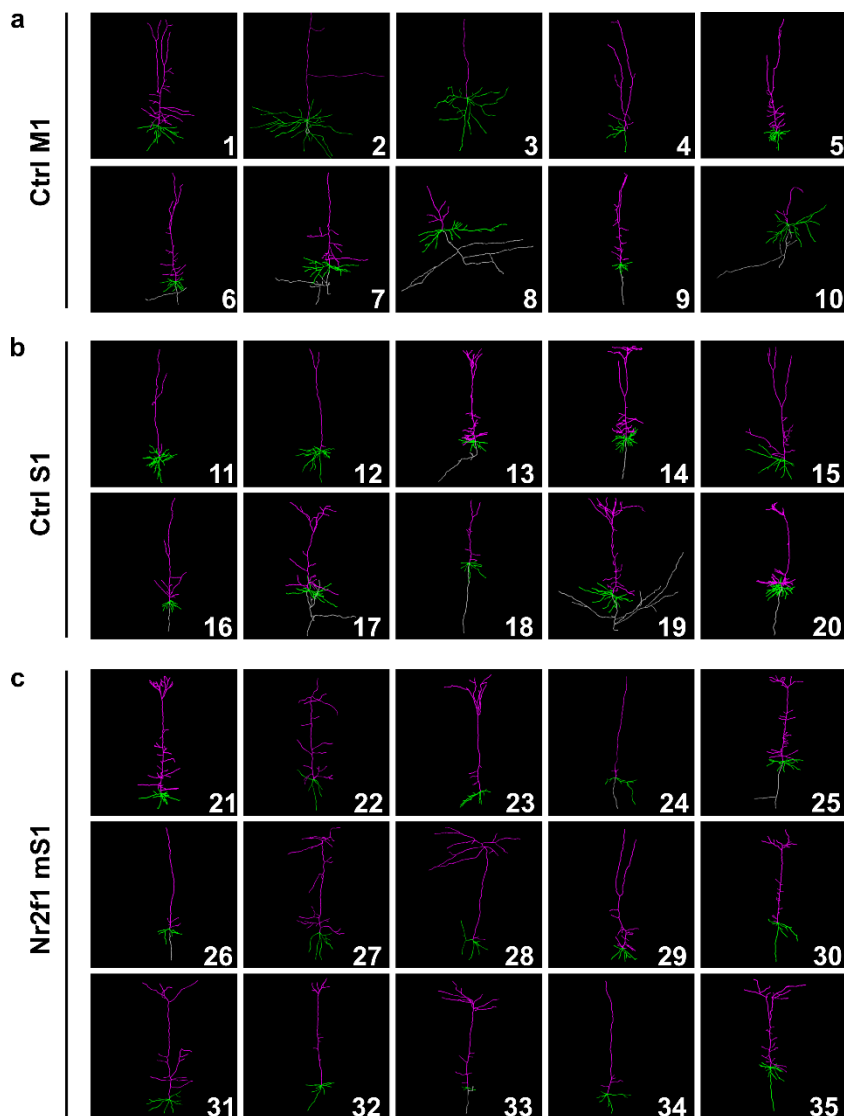
NeuroMorpho.Org ID	: NMO_152189
Neuron Name	: MS_p8c2
Archive Name	: Studer
Species Name	: mouse
Strain	: C57B6
Structural Domains	: Dendrites, No Soma, Axon
Physical Integrity	: Dendrites Complete, Axon Incomplete
Morphological Attributes	: Diameter, 3D, Angles
Min Age	: 5.0 days
Max Age	: 8.0 days
Gender	: Male/Female
Min Weight	: Not reported
Max Weight	: Not reported
Development	: young
Primary Brain Region	: neocortex
Secondary Brain Region	: somatosensory
Tertiary Brain Region	: primary somatosensory, layer 5
Primary Cell Class	: principal cell
Secondary Cell Class	: pyramidal
Tertiary Cell Class	: Not reported
Original Format	: Imaris.hoc
Experiment Protocol	: In vitro
Experimental Condition	: Control
Staining Method	: biocytin
Slicing Direction	: coronal
Slice Thickness	: 300 μm
Tissue Shrinkage	: Not reported
Objective Type	: oil
Magnification	: 25x
Reconstruction Method	: Imaris
Date of Deposition	: 2020-09-07
Date of Upload	: 2020-10-28
Persistence Vector	: MS_p8c2.pvec
Note	: Cells were traced by Chiara Tocco

Figure 37 - Example of a cell sheet

For each cell, the original publication is reported, together with a list of basic measurements and general information on the animal used (strain, age and genotype for instance), brain region and cell type of belonging and finally the experimental setup. All the information, and the 3D reconstructions are downloadable from the website (**Fig. 37**).

LVPNs present morphological differences among classes and genotypes

As described in del Pino et al., early during postnatal development, the LVPNs from the putative motor and somatosensory regions of control animals show subtle morphological differences at the level of the basal dendrites, and mutant cells show even more clear changes compared to controls. Moreover, a noteworthy level of heterogeneity has been observed in all classes. In the Neuromorpho.org database it is possible to have a general overview of the cell populations and to highlight both their differences and common features.



It is easy to appreciate for example, how cells from the control M1 region present different levels of complexity (Fig. 38a), with the extremes being cell number 2 (C2, more complex) and number 4 (C4, less complex). By going back to the data, we see how the basal dendrite complexity index (bDCI) of C2 is approximately 7 times bigger than C4 (28704 vs 4035) and that C2 branches 56% more than C4 (28 bifurcations versus only 18). Furthermore, if we compare the two Sholl curves, this

Figure 38 - Panel of selected representative cells. LVPNs of the control M1 (a), control S1 (b) and mutant mS1 (c).

difference in complexity is even more evident (**Fig. 39**) with C2 intersecting more concentric spheres and more times than C4, suggesting the more complex cell has a higher number of longer basal dendrites than its simplest counterpart.

The same range of diversity is observed in the control S1 and the mutant motorized S1 cell populations. Despite this high intra-group variability, mutant cells appear to be on average more simplified than both M1 and S1 control cells, as described in the main paper. This tendency is once again pretty obvious when looking at the cell pool in his entirety (**Fig. 38**). By taking as examples cell number 35 (C35) as a very complex mutant cell and cell number 33 (C33) as a very simple one (**Fig. 38c**), we see how both of them show a lower bDCI than both example cells from M1 (C35= 2463 and C33= 549 compared to C2= 28704 and C4=4035). By comparing their Sholl curves, C33 is evidently more simplified than both M1 cells, whereas C35 shows a profile that is almost as complex as the simplest M1 cell (**Fig. 39**).

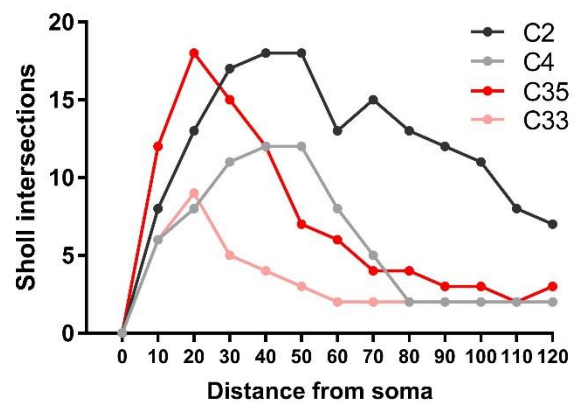


Figure 39 - Sholl curves of four example cells

Hence, although the neuromorpho.org depository is a great tool to have a quick overview of a huge variety of cells and allows sharing and comparing databases from different labs around the globe, to avoid misinterpretations and wrong assumptions, it is crucial that the information in it is backed up by peer reviewed publications and solid analyses and documentation of those parameters that are not directly deducible from the 3D reconstructions. The fact that, by considering only a couple of examples for each genotype, we are not able to exactly reproduce the results published in del Pino et al., is a clear indication of the complexity of the analyses there performed. In fact, the high heterogeneity of our cell pools required a big enough number of replicates to allow us to observe differences among the groups.

Annexe B

Whole brain tissue clearing and imaging as a tool to study tract malformations in *Nr2f1* mutant animals.

In previous parts of my thesis (**results – paper two**, and **additional results – b**) the main topic of the study was represented by assessing structural and connectivity features of long and complex tract through the mouse brain of control and mutant animals. In general, we mainly implied 2D analysis methods, and recurred to digital reconstruction approaches to build up 3D models of our network of interest. In the past decades, several protocols (Tian et al., 2020) have been developed to allow whole tissue clearing and staining, making the study of structure in the 3D space possible.

During my thesis, I dedicated some time to the setup of one of these protocols (modified from Belle et al., 2017) in order to recapitulate the several defects of innervation (Alfano, Magrinelli, Harb, Hevner, et al., 2014; Armentano et al., 2007; Tomassy et al., 2010b, Tocco et al., in preparation; Jurkute et al., in preparation) observed in *Nr2f1* animals. Although much work is still required for the optimization of the protocol for young adult and adult brains, experiments performed at early stages of embryonic development were successfully performed (see Methods for further details) and integrated into a manuscript which is now under revision.

The general aim of this work is to study pathophysiological mechanisms of visual impairments observed in BBSOAS patients and *Nr2f1* heterozygous (*HET*) and null (*KO*) mice. It has been previously reported that loss of *Nr2f1* function in mice affects the early patterning of the developing optic vesicle and leads to abnormal retinogenesis, disruption of radial glial cell axonal guidance from the neural retina into the optic stalk and defective formation of the optic nerve (Bertacchi, Gruart, et al., 2019), recapitulating various OD abnormalities described in BBSOAS patients (D. G. M. M. Bosch et al., 2014; C. A. Chen et al., 2016).

To further characterize the formation and the structure of the optic nerve in *Nr2f1 HET* and *KO* eyes, and to visualize the axonal pathway of the radial glial cells in its entirety, we took advantage of Tuj1 immunostaining on clarified whole embryonic heads, followed by light-sheet imaging and three-dimensional (3D) reconstructions. After dissection, E13.5 embryo heads from *WT*, *HET* and *KO*

animals were processed as in (Belle et al., 2017), but some modifications to the original protocol were made. For example, in the original methods, the samples were initially dehydrated into incremental MetOH solutions and the endogenous signal was quenched by placing the samples in H₂O₂ for one over-night in the cold and then rehydrated, prior immunostaining. Since our samples were very delicate and easily damageable, we removed the initial dehydration and rehydration steps, and performed a rather quick quenching step at higher temperatures (see Methods for more details). The immunostaining steps, that originally were covering up to three weeks depending on the size of the sample, were instead performed in a shorter period of time. Several tests have been accomplished to find the right duration to ensure a homogeneous staining and at the same time to preserve the tissue integrity.

The first results obtained are depicted in **Fig. 40**. With the use of a Tuj1+ antibody, we were able to reveal the entirety of neuronal projections (**Fig. 40A,B** in grayscale) and signal segmentation was required to highlight the signal coming from the retina (**Fig. 40A,B** in dark green) and the optic nerve (**Fig. 40A,B** in light green). By isolating the signal from retina and optic nerve, the retinal defect (**Fig. 40C,C',D,D'**) and the misguidance of Tuj1+ fibre was readily apparent in the 3D optic nerve reconstruction (**Fig. 40E-G**). Virtual transverse sectioning at different levels showed spanning of the morphological defect along the whole length of the developing mutant optic nerves, with the axons failing to shift dorsally and fill the dorsal-most half of the optic nerve as it happens in WT samples (**Fig. 40** insets 1-4).

Taken together, these early developmental defects impinge on the final morphology and fibre organization within the developing optic nerve, with the impact being more severe in *KO* mice than in *HET* mice.

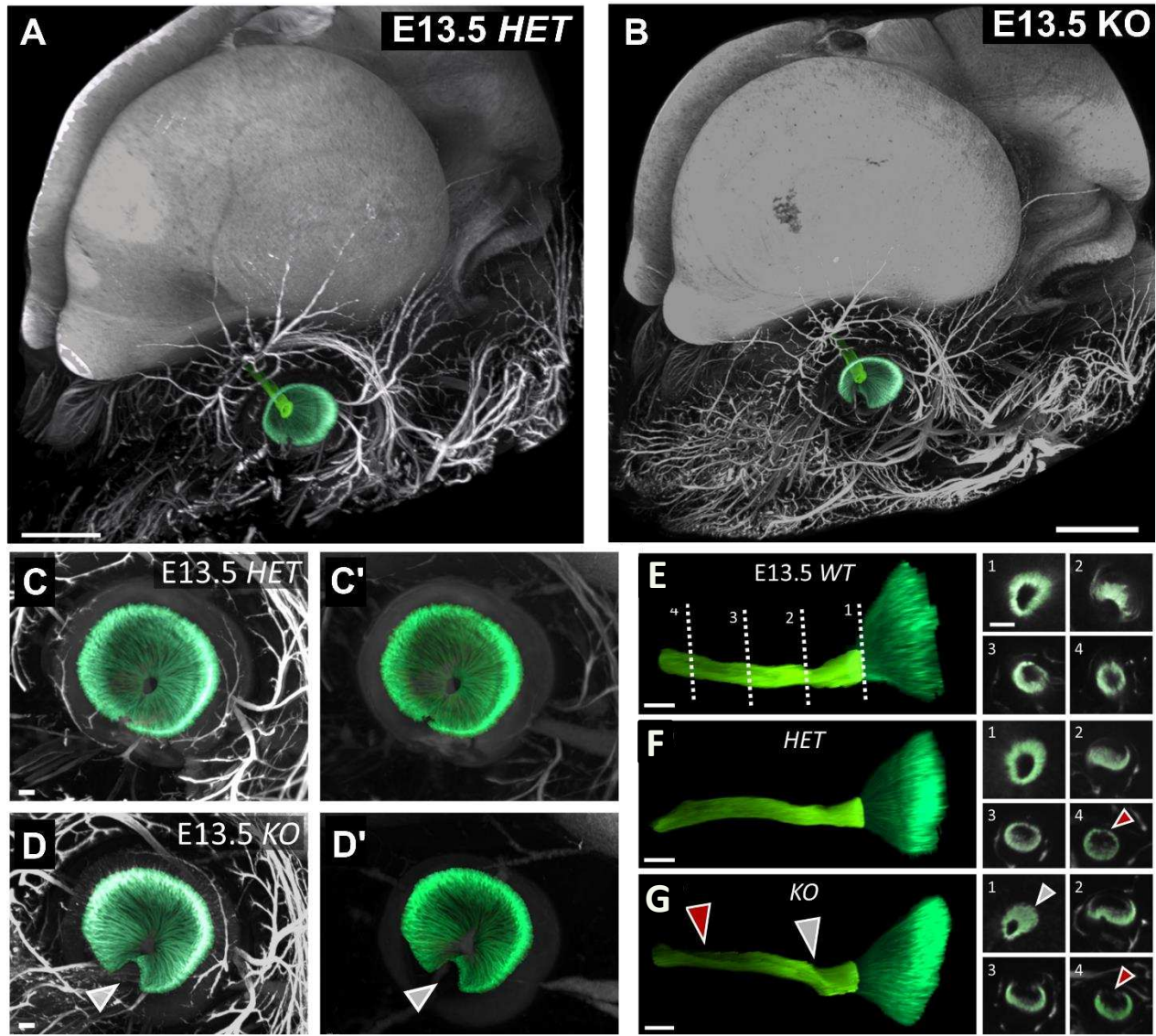


Figure 40 - Assessing optic nerve malformations via tissue clearing and 3D imaging techniques. A,B) whole head view of E13.5 HET and KO pups. In green, segmentation and 3D segmentation of retina and optic nerve. C-D) Frontal-view 3D reconstruction of E13.5 HET and KO pups. Arrowhead is pointing to the malformation of the retina in KO animals. E-F) lateral view of retina and optic nerve of WT, HET and KO E13.5 animals. Arrowheads are point to proximal (grey panel G and inset 1) and distal (red, panel G and insets 4) optic nerve defective formation.

DISCUSSION AND PERSPECTIVES

During brain development, the establishment of proper local and long-range connectivity is regulated by a plethora of transcription factors directing cell proliferation, migration and differentiation (Dennis D M O'Leary & Sahara, 2008) but also spontaneous activity (Andreae & Burrone, 2018; Antón-Bolaños et al., 2019; Kirischuk et al., 2017) and axonal wiring in a time-, space- and dose-dependent way. However, the specific genetic programs coordinated by these factors remain largely unexplored. Although it has been initially proposed that cortical identity was primordially driven by mitotically expressed patterning genes (Greig et al., 2013; Dennis D.M. O'Leary et al., 2007), in the last decade a growing literature started to emerge, elucidating the role of postmitotic regulation of arealization, cell fate determination and axon guidance (Alfano et al., 2014; Fazel Darbandi et al., 2018; Harb et al., 2016; Zhenyong Huang et al., 2009; Joshi et al., 2008; C. F. Wang et al., 2017; Zembrzycki et al., 2015). Moreover, it also turned out that patterning genes maintained their expression during late events of corticogenesis, i.e., at postnatal stages and even in adulthood, suggesting that they might play different roles during brain development and maturation. Below, I will discuss some of these aspects in the context of the data obtained during my thesis work.

Mitotic and post-mitotic dual role of neocortical area patterning genes

Several factors are either expressed in progenitor cells (i.e. Pax6, Emx2 and Sp8) or in postmitotic neurons (i.e. Lmo4, Bhlhb5 and Tbr1) whereas few others are expressed both mitotically and postmitotically in the developing pre- and post-natal neocortex. At present, deciphering their multiple role constitutes an open challenge also because several of these genes turned out to be causative of neurodevelopmental diseases (Barkovich et al., 2012; Parrini et al., 2016). The use of *constitutive* and *conditional knockouts* in the mouse system has helped in starting to untangle their multiple roles and distinct mechanisms of action are starting to emerge.

Lhx2 for example, is expressed in both progenitor cells and postmitotic neurons and plays distinct roles in the two temporal windows. For instance, its expression in cortical progenitors is fundamental for the barrel cortex patterning and its correct thalamocortical initial innervation (Shetty et al., 2013), whereas at later stages it specifically acts on thalamocortical arborization within

the layer IV (Zembrzycki et al., 2015). Hence, deletion of *Lhx2* in progenitors leads to complete agenesis of the barrel cortex, which in turn affects arrival and innervation of thalamocortical afferences (Shetty et al., 2013). Conversely, postmitotic loss-of-function does not affect the initial specification of layer IV neurons nor thalamocortical fibres entering the cortical plate (Zembrzycki et al., 2015), but instead it impairs the final maturation of the barrels (C. F. Wang et al., 2017).

Nr2f1, also known as COUP-TFI, is one of the most studied arealization genes and is also expressed in both progenitor cells and postmitotic neurons. This nuclear receptor is now recognised to impart sensory features to cortical differentiating neurons and simultaneously inhibiting cell intrinsic “motorizing” processes (Alfano et al., 2014). Whether its cortical loss-of-function is elicited mitotically or postmitotically, it leads to frontal motor area expansion and sensory areas substantial altered in size and position (Alfano et al., 2014; Armentano et al., 2007). This structural impairment in turn influences the establishment of topographic cortico-thalamic and thalamo-cortical connectivity (Alfano et al., 2014; Armentano et al., 2007). Similar to *Lhx2*, we also started to decipher distinctive roles between mitotic and postmitotic *Nr2f1* functions. While mitotic *Nr2f1* expression seems to be mainly involved in modulating the progenitor rate of distinct progenitor subtypes, apical versus basal RGC production, in a regionalized fashion and in line with its high caudal to low rostral expression gradient (Bertacchi et al., 2020), postmitotic modulation (loss- or gain-of-function) acts mainly in area- and laminar-dependent specification of neocortical neurons (Alfano et al., 2014). For example, proper layer IV specification into stellate cells, the major recipient cortical cells of thalamic inputs, also depend on *Nr2f1* (PMID: 31395862), and most probably on postmitotic *Nr2f1* expression (*unpublished data from the host lab*). Moreover, hippocampal development, migration and function also depend on *Nr2f1* progenitor expression in the hippocampal primordium (Flore et al., 2016), whereas absence of *Nr2f1* in postmitotic cells, only slightly affect hippocampal morphogenesis (Parisot et al., 2017). This indicates that *Nr2f1* can play multiple and pleiotropic roles during brain organization and that it might acts differently in function of the developmental time and cell-type, most probably because of its ability to bind to several targets and partners (reviewed in Bertacchi et al., 2019). It is thus not surprising that haploinsufficiency of the gene is sufficient to induce a pathological syndrome in humans (Bosch paper), and that full *KO* (in which both alleles are affected) will lead to birth lethality in mice (Armentano et al., 2006).

To further unravel novel mechanisms underlying areal organization that depend on *Nr2f1*, my thesis work challenged *Nr2f1* functions in local network maturation as well as long-range connectivity in two distinct cortical-specific conditional mouse lines, in which the deletion of the gene is carried out either in progenitor or postmitotic cells. We show that loss of *Nr2f1* in progenitor cells give rise to the most severe impairments, such as altered intrinsic electrophysiological properties, dendrite complexity and network synchronicity, even if we have not tested these properties in a postmitotic mouse model. However, we also observed that postmitotic *Nr2f1* inactivation leads to dendritic spine reduction, suggesting that postmitotic expression might directly be involved in intrinsic neuronal bioelectric properties. Regarding subcerebral connectivity, we observed that while full cortical *Nr2f1* inactivation leads to an imbalance between production of corticopontine and corticospinal projection neurons, the inactivation of the gene solely in the postmitotic pool leads to more subtle defects, such an altered topographic map between the cortex and the pontine nuclei.

In my thesis, I decided to focus on the morphological and functional properties of layer V pyramidal neurons (LVPNs), as a paradigm of network establishment and maturation in the mammalian neocortex. Since these cells constitute the main cortical population involved in the regulation of fine voluntary movements, we reasoned that a defective specification or maturation of these cells might be at the basis of the behavioural impairment observed upon loss of *Nr2f1* (Contesse et al., 2019; Tomassy et al., 2010). Furthermore, over the past decades, developmental, anatomical and functional features of LVPNs have been thoroughly investigated, making these cells the most studied neocortical neuron types and the ideal benchmark for understanding the genetic basis of physiological and pathological cortical network development (Ramaswamy & Markram, 2015).

***Nr2f1* controls spontaneous network activity in neocortical progenitor cells.**

After intrinsic genetic programs prime the emerging neocortex to develop into an organized pattern of functional areas, prenatal thalamic input (Antón-Bolaños et al., 2019) and sensory-driven activity (Simi & Studer, 2018) coordinate the refinement of the cortical map. Local spontaneous

electric activity, which autonomously synchronizes large groups of neurons independently of sensory stimulation and contributes to the development of neuronal circuits (Andreae & Burrone, 2018; Antón-Bolaños et al., 2019; Kirischuk et al., 2017; Luhmann & Khazipov, 2018), is also known to set the initial blueprint of cortical network organization by triggering the formation of a primordial pattern of activity (Corlew et al., 2004; Uhlén et al., 2015), and ultimately influencing long-range connectivity. Indeed, its alteration during cortical development leads to defective progenitor behavior, cell migration and formation of dysfunctional cortical circuits (Kirkby et al., 2013; Li et al., 2013). The close interactions between identity patterning genes, thus intrinsic genetic regulation, and early activity function, i.e., intrinsic spontaneous activity, has never been well defined and became the topic of my first paper. To date, how spontaneous activity is genetically regulated remains also largely unknown.

In Del Pino et al., 2020, we proposed that *Nr2f1* might regulate spontaneous activity and intrinsic excitability within the immature somatosensory cortex during early postnatal development. The analyses of several cell-intrinsic electrophysiological and morphological characteristics of LVPNs indicated that *Nr2f1* loss-of-function in neocortical progenitors leads to alterations in network spontaneous activity as early as P0, and to several altered intrinsic excitability parameters (i.e., more depolarized resting membrane potential or a decreased expression of voltage sag (I_h)) as well as morphological dendrite abnormalities in postnatal LVPNs. Furthermore, we showed that the regulation of electric properties was elicited through the regulation of expression of voltage-gated ion channels in pyramidal glutamatergic neurons. In fact, we discovered that upon loss of *Nr2f1*, several glutamate (*Gria3*, *Grin1* and *Grik1*), calcium (*Cacna2d1*), potassium (*Kcnab1* and *Kcnk2*) and non-selective cyclic-nucleotide gated (*Hcn1*) channels were abnormally expressed in the cortex of postnatal mutants. In particular, we demonstrated that *Hcn1* - known to contribute to intrinsic neural excitability and spontaneous rhythmic activity in the brain (Z. Huang et al., 2009) – protein levels were downregulated in layer V soma and dendrites in *Nr2f1* mutant cortices. Moreover, *Hcn1* transcript expression levels seemed to be directly regulated by *Nr2f1*, as demonstrated by ChIP experiments, thus representing one key player, most probably among many others not identified yet, during the establishment of neuronal synchronicity in the developing neocortex.

The implication of *Nr2f1* in determining cortical network development reinforces the newly emerging link between area patterning and lamination genes, the establishment of primitive activity network, and their potential long-term effects (Boillot et al., 2016; Murase et al., 2016). Furthermore, *Tbr1*, a factor involved in layer VI cell specification in the developing neocortex (Cánovas et al., 2015; Han et al., 2011; McKenna et al., 2011), was also reported to directly and positively regulate *Hcn1* transcription by acting on Ih current and sag response in postmitotic neurons (Fazel Darbandi et al., 2018). We thus propose that the fine regulation of *Hcn1* expression levels might be a common mechanism of early transcriptional regulators to modulate spontaneous network activity within the developing cortex.

Nevertheless, many open questions remain to be addressed on how *Nr2f1* triggers early network maturation, and whether affected activity is a direct or indirect phenomenon due to *Nr2f1* loss-of-function. While we show that *Hcn1* transcript levels are directly modulated by *Nr2f1*, we still do not know whether the altered expression of other channels shown in our work (and most probably others that we have not identified yet) is just a consequence of altered *Hcn1* pacemaker activity or whether other channels are also directly regulated by *Nr2f1*. We speculate that their expression levels might be a secondary effect of the *Hcn1*-dependent early alterations in the overall network activity. Similar mechanisms where network activity alterations influence the expression of ion channels are also observed in other structures, such as the hippocampus, where the induction of increased bursting activity and seizures persistently alters *Hcn* channels expression (Chen et al., 2001).

To test this premise, two strategies might be implied:

On the one side, to directly test whether altered excitability might be directly involved in layer V differentiation and maturation, we could inhibit cell excitability through the overexpression of the inward rectifier potassium channel *Kir2.1* either by electroporating a plasmid expressing *Kir2.1* (already available in the lab) by IUE or by injecting a virus expressing *Kir2.1* (kind gift from G. Fishell, Harvard, USA) (Baronas & Kurata, 2014). In general, inward rectifiers are active at the resting membrane potential and conduct inward potassium (K⁺) currents by contributing to the maintenance of the resting potential and limiting the probability of the cell to reach the

depolarization state and fire action potentials (Hibino et al., 2010; Lu, 2004; Nichols & Lopatin, 1997). Despite their name, several Kir channels do not show a very strong inward current; Kir2.1 on the other side, is considered the strongest rectifier, making it a very suitable tool to control cell excitability (Burrone et al., 2002; Johns et al., 1999). We hypothesise that by overexpressing Kir2.1 channel in early postmitotic brains of controls and *Nr2f1* animals *via* IUE or viral injection, we could rescue the dendritic structural defects and the impaired expression of ion channels, which we interpreted as a consequence of augmented intrinsic excitability of mutant cells.

On the other side, we could pharmacologically impair Hcn1 functionality in wild type animals and test whether it recapitulate the phenotype observed in *Nr2f1* mutant mice. Interestingly, the pharmacological inhibition of Hcn1 function *in vivo via* the drug ZD7288, and confirmed by reduction of I_h current in cortical neurons, leads to abnormal execution of skilled motor tasks, tested by single pellet skilled reaching test, thus highlighting a novel role of Hcn1 in cortical maturation leading to distinct behaviours (Boychuk et al., 2017). A similar test in *Nr2f1 cKO* conditions produced similar results (Tomassy et al., 2010), prompting us to suggest a functional role of *Nr2f1* through Hcn1 in the regulation of fine voluntary movements.

Corticopontine *versus* corticospinal fate determination in progenitor cells is under the control of *Nr2f1*

As suggested by their name, cortical area patterning genes are the principal factors regulating topographic organization in the developing neocortex. A fast expanding field of investigation is trying to decipher the role of these genes in influencing the topographical organization existing between the cortex and its subcortical targets (Cadwell et al., 2019).

One of the most extensively studied circuits in topographical organization of two distinct structures, besides the retinotectal topographic map (Kaprielian & Patterson, 1994; Simmons et al., 1982), is represented by the connectivity between the cortex and the thalamus (Antón-Bolaños et al., 2018). During cortical development, specific thalamic neurons project towards distinct cortical

regions refining the parcellation of neocortical sensory or motor areas in a topographic way (visual thalamic nuclei will project to visual cortex, somatosensory thalamic nuclei to S1 cortex, etc). Genetic impairment of cortical arealization leads to shift in thalamocortical targeting, suggesting proper cell intrinsic cortical information is important for attracting thalamic afferences in the right place and at the correct time (Fukuchi-Shimogori & Grove, 2001; Dennis D M O’Leary & Sahara, 2008).

Loss of *Nr2f1* function in the developing neocortex produces an abnormal expansion of the fronto-motor cortex at the expense of sensory areas, regardless whether it is elicited in progenitors or postmitotic neurons (Alfano, 2014; Armentano et al., 2007). Nevertheless, the caudally shifted and significantly smaller S1 region is still capable of accurately attracting thalamocortical afferences in a topographic organized way.

Encouraged by previous data in the thalamocortical system and by the behavioural impairments in fine voluntary movement execution (Tomassy et al., 2010), we aimed to investigate whether *Nr2f1* could also contribute to the correct establishment of layer V pyramidal neuron axonal projections towards the pons and spinal cord and, more specifically, to the organization of the corticopontine topographic map.

For this purpose, we implied tract-tracing techniques and digital brain atlas tools to precisely map axon terminal within the pontine nuclei of control and *Nr2f1* mutant mice. With the help of our collaborators, experts in corticopontine topography, and the *Allen Brain Atlas Connectivity Map* (Q. Wang et al., 2020), we first demonstrated the existence of a corticopontine topographical map in mice, similar to the one previously described in rats (Leergaard et al., 1995). Then, we used our two independent *Nr2f1* conditional mice (*Nr2f1 Emx cKO* and *Nex cKO*) to assess corticospinal projections. Our findings show that the loss of cortical *Nr2f1* function leads to an increased de-fasciculation of the corticospinal tract, implying a role of *Nr2f1* in maintaining CST integrity. Moreover, and interestingly, loss of *Nr2f1* in progenitors results in increased innervation of corticopontine axons in the pontine nuclei at the expense of corticospinal axons which we quantified to be reduced in the *Emx-cKO* model (see Fig. 4 in the attached manuscript). This imbalance between corticopontine and corticospinal projection neurons reminds the role played by *UNC-55*, the

ortholog gene of *Nr2f1*, in *C. elegans* in the conversion of a class of motor neurons into another one, and the subsequent change of connectivity (Mimi Zhou & Walthall, 1998; Petersen et al., 2011). This implies that *Nr2f1*, similarly to UNC-55, might control a set of genes that distinguish these two subclasses of neurons. The Iroquois-like homeodomain protein seems to be an interesting UNC-55 target in driving the correct fate of dorsal versus ventral motor neuron synapses in *C.elegans* (Petersen et al., 2011), but nothing is known on possible downstream targets of *Nr2f1* in mammals. Nevertheless, we know that the LIM homeodomain *Lmo4* and the bHLH transcription factor *Bhlhb5* are involved in driving corticopontine versus corticospinal connectivity, respectively (Cederquist et al., 2013). In *Nr2f1* mutant mice, *Lmo4* is highly upregulated in somatosensory cortex after birth and concomitantly *Bhlhb5*, normally expressed only in sensory cortex, is downregulated (Alfano, 2014; Harb et al., 2016). Thus, the imbalance between production of corticopontine versus corticospinal within layer V, might be due to the deregulation between *Lmo4* and *Bhlhb5*. Abnormal upregulation of *Lmo4* by LVPNs might push layer V neurons to become corticopontine and innervate in higher numbers the pontine nuclei, while downregulation of *Bhlhb5* might be involved in generating less layer V neurons reaching the spinal cord, and/or, as proposed below, in corticopontine topographic organization. This is a hypothesis, that we might test in the future.

Postmitotic role of *Nr2f1* in the establishment of the cortico-pontine topographic map

The outcome of *Nr2f1* loss-of-function in postmitotic neurons resulted in a different kind of defect, i.e., altered topographic pontine innervation, with less projections reaching sensory-receiving regions and an atypical accumulation of fibres in motor-receiving regions. Furthermore, the analysis of anterograde tracing from motor and somatosensory cortical areas indicated that the topographic abnormalities previously observed, originate mainly from somatosensory than from motor layer V projection neurons, in line with the cortical pattern of expression of *Nr2f1* (Armentano et al., 2006; Zhou et al., 1999). This was a surprising but very exciting outcome and confirmed that *Nr2f1* is directly involved in topographic mapping.

We hypothesise that the different outcomes we observe are due to the different degree of cell commitment when they undergo *Nr2f1* inactivation. In particular, when progenitor cells, known to

be very plastic in terms of fate, stop producing *Nr2f1*, they might still have a broad range of possible differentiation paths to pursue, whereas postmitotic neurons might be more committed to a particular fate but still plastic to more advanced differentiation processes, such as excitability, maturation and axon targeting. In this case, *Nr2f1* postmitotic inactivation had no effect on the production of corticopontine *versus* corticospinal neurons, but more on the fine topographic mapping between cortex and pontine neurons. Loss of postmitotic *Nr2f1* guided somatosensory corticopontine axons to innervate motor targets instead of somatosensory types of targets within the pontine nuclei. Similarly to what observed in *Lhx2* mutant animals, mitotic loss of function bears a more penetrant phenotype (i.e. abolishment of layer IV neuron specification and barrel field formation) than its postmitotic counterpart (i.e. impaired final steps of thalamocortical innervation and barrels maturation) (Shetty et al., 2013; C. F. Wang et al., 2017; Zembrzycki et al., 2015). Another example is the dual role of *Pax6* in the visual system (Pratt et al., 2000; Sebastián-Serrano et al., 2012). Once again, an early loss of function in progenitor cells affect their survival, ultimately leading to eye agenesis, whereas a late inactivation of the gene in postmitotic retinal ganglion cells does not affect their viability, but rather impair their response to the growth factor SFRP1.

Despite a temporal correlation between cortical maturation and pontine pattern of innervation has been proposed long time ago (Leergaard et al., 1995), to date very little is known about the genetic programs regulating the precise topographic organization of corticopontine afferences and various hypotheses suggests the process might depend on intrinsic factors expressed by cortical neurons or by local pontine permissive and instructive cues (D. D.M. O'Leary et al., 1991).

It has been recently reported that the postmitotic expression of the homeobox gene *Hoxa5* in migrating pontine neurons is sufficient to instruct them in settling posteriorly in the developing pontine nuclei and to attract descending corticopontine afferences specifically from the limb representation in the somatosensory cortex (Maheshwari et al., 2020), corroborating the hypothesis of an instructive role for pontine cells in the topographical organization of corticopontine projections. Conversely, our work represents a first evidence for the direct involvement of cortical gradients, in this case under the control of *Nr2f1* (but possibly also of other cortical transcription factors), in the establishment of a topographic corticopontine map. Hence, we propose that

molecular cascades distinctively acting in both structures, the neocortex and the pontine nuclei, are crucial for the completion of this process.

How exactly the process is regulated, remains still largely unknown and further investigations are needed in order to identify potential *Nr2f1* effectors and/or cofactors.

As mentioned above, the postmitotic transcription factor *Bhlhb5* could be an interesting candidate. The gene, which have been previously reported to be strongly downregulated in the absence of *Nr2f1* (Alfano et al., 2014), also presents several *Nr2f1* binding sites in its regulatory sequence (*unpublished*). Specifically, ChIP assays followed by qPCR have revealed that one site in particular was highly enriched, suggesting a direct regulatory function of *Nr2f1* on *Bhlhb5* transcription (*unpublished*). Since *Bhlhb5* *KO* mice display similar connectivity defects, with subcerebral projections stopping at the level of the cerebral peduncle at the expense of corticospinal projections (Joshi et al., 2008), we decided to test whether *Bhlhb5* was downstream of *Nr2f1* in regulating cortico-pontine and cortico-spinal specification, including topography. To do so, I electroporated a Cre-inducible *Bhlhb5* vector (flanked by *lox* sites) that re-express *Bhlhb5* in *Nr2f1*-deficient neurons thanks to the use of the *Nes Cre-recombinase*. By re-establishing *Bhlhb5* expression *via in utero* electroporation into the forming neocortex of E13.5 mice and by taking advantage of the high-performance tracer spaghetti monster, my first preliminary data point to a possible change of corticothalamic and corticopontine connectivity, but more data need to be produced to assess whether the topographic defects observed in *Nr2f1* mutant projections are recovered upon *Bhlhb5* re-expression. To definitely prove that *Bhlhb5* can be a valuable candidate in topographic organization, overexpression of *Bhlhb5* in wild-type brains, particularly in the motor cortex where expression is low, would represent a complementary approach to the *Bhlhb5* re-expression in *Nr2f1* postmitotic mutant mice.

Overall, my thesis work helped identifying novel roles for the arealization gene *Nr2f1* in layer V late specification and maturation. Its implication in the establishment of proper electrophysiological properties on the one hand, and subcortical connectivity on the other hand represented a first important step towards deciphering *Nr2f1* mechanisms of action during the development of the mammalian neocortex. Moreover, because of the recent discovery of a novel developmental

syndrome caused by mutation on the NR2F1 coding sequence (Bosch et al., 2014; Rech et al., 2020), deciphering the genetic basis of its function becomes of crucial importance for better understanding the pathogenesis of the symptoms reported in humans.

References

- Akintunde, A., & Buxton, D. F. (1992). Origins and collateralization of corticospinal, corticopontine, corticorubral and corticostriatal tracts: a multiple retrograde fluorescent tracing study. *Brain Research*. [https://doi.org/10.1016/0006-8993\(92\)91629-5](https://doi.org/10.1016/0006-8993(92)91629-5)
- Alcamo, E. A., Chirivella, L., Dautzenberg, M., Dobreva, G., Fariñas, I., Grosschedl, R., & McConnell, S. K. (2008). *Satb2* Regulates Callosal Projection Neuron Identity in the Developing Cerebral Cortex. *Neuron*. <https://doi.org/10.1016/j.neuron.2007.12.012>
- Alfano, C. (2014). The nuclear receptors COUP-TF: A long-lasting experience in forebrain assembly. *Cellular and Molecular Life Sciences*, *71*(1), 43–62. <https://doi.org/10.1007/s00018-013-1320-6>
- Alfano, C., Magrinelli, E., Harb, K., Hevner, R. F., & Studer, M. (2014). Postmitotic control of sensory area specification during neocortical development. *Nature Communications*, *5*(1), 5632. <https://doi.org/10.1038/ncomms6632>
- Alfano, C., & Studer, M. (2013). Neocortical arealization: Evolution, mechanisms, and open questions. *Developmental Neurobiology*, *73*(6), 411–447. <https://doi.org/10.1002/dneu.22067>
- Alfano, C., Viola, L., Heng, J. I. T., Pirozzi, M., Clarkson, M., Flore, G., de Maio, A., Schedl, A., Guillemot, F., & Studer, M. (2011). COUP-TFI promotes radial migration and proper morphology of callosal projection neurons by repressing *Rnd2* expression. *Development*, *138*(21), 4685–4697. <https://doi.org/10.1242/dev.068031>
- Allène, C., Cattani, A., Ackman, J. B., Bonifazi, P., Aniksztejn, L., Ben-Ari, Y., & Cossart, R. (2008). Sequential generation of two distinct synapse-driven network patterns in developing neocortex. *Journal of Neuroscience*. <https://doi.org/10.1523/JNEUROSCI.3733-08.2008>
- Allene, C., & Cossart, R. (2010). Early NMDA receptor-driven waves of activity in the developing neocortex: Physiological or pathological network oscillations? In *Journal of Physiology*. <https://doi.org/10.1113/jphysiol.2009.178798>
- Allio, A., Calorio, C., Franchino, C., Gavello, D., Carbone, E., & Marcantoni, A. (2015). Bud extracts from *Tilia tomentosa* Moench inhibit hippocampal neuronal firing through GABAA and benzodiazepine receptors activation. *Journal of Ethnopharmacology*. <https://doi.org/10.1016/j.jep.2015.06.016>
- Altman, J., & Bayer, S. A. (1978). Development of the diencephalon in the rat. I. Autoradiographic study of the time of origin and settling patterns of neurons of the hypothalamus. *Journal of Comparative Neurology*. <https://doi.org/10.1002/cne.901820511>
- Altman, J., and Bayer, S.A. (1987). Development of the precerebellar nuclei in the rat: IV. The anterior precerebellar extramural migratory stream and the nucleus reticularis tegmenti pontis and the basal pontine gray. *J Comp Neurol* *257*, 529-552.

- Altman J, Bayer SA (1996) Development of the cerebellar system in relation to its evolution, structure and functions. CRC Press, Boca Raton.
- Anderson, O. D. (1975). Moving Average Processes. *The Statistician*. <https://doi.org/10.2307/2987925>
- Andreae, L. C., & Burrone, J. (2018). The role of spontaneous neurotransmission in synapse and circuit development. In *Journal of Neuroscience Research*. <https://doi.org/10.1002/jnr.24154>
- Antón-Bolaños, N., Espinosa, A., & López-Bendito, G. (2018). Developmental interactions between thalamus and cortex: a true love reciprocal story. *Current Opinion in Neurobiology*, 52, 33–41. <https://doi.org/10.1016/j.conb.2018.04.018>
- Antón-Bolaños, N., Sempere-Ferràndez, A., Guillamón-Vivancos, T., Martini, F. J., Pérez-Saiz, L., Gezelius, H., Filipchuk, A., Valdeolmillos, M., & López-Bendito, G. (2019). Prenatal activity from thalamic neurons governs the emergence of functional cortical maps in mice. *Science*. <https://doi.org/10.1126/science.aav7617>
- Arber, S. (2017). Organization and function of neuronal circuits controlling movement. *EMBO Molecular Medicine*. <https://doi.org/10.15252/emmm.201607226>
- Arber, S., & Costa, R. M. (2018). Connecting neuronal circuits for movement. In *Science*. <https://doi.org/10.1126/science.aat5994>
- Arlotta, P., Molyneaux, B. J., Chen, J., Inoue, J., Kominami, R., & MacKlis, J. D. (2005). Neuronal subtype-specific genes that control corticospinal motor neuron development in vivo. *Neuron*. <https://doi.org/10.1016/j.neuron.2004.12.036>
- Armentano, M., Chou, S.-J. J., Srubek Tomassy, G., Leingärtner, A., O’Leary, D. D. M., Studer, M., Tomassy, G. S., Leingärtner, A., O’Leary, D. D. M., & Studer, M. (2007). COUP-TFI regulates the balance of cortical patterning between frontal/motor and sensory areas. *Nat Neurosci*, 10(10), 1277–1286. <https://doi.org/10.1038/nn1958>
- Armentano, M., Filosa, A., Andolfi, G., & Studer, M. (2006). COUP-TFI is required for the formation of commissural projections in the forebrain by regulating axonal growth. *Development (Cambridge, England)*, 133, 4151–4162. <https://doi.org/10.1242/dev.02600>
- Asante, C. O., Chu, A., Fisher, M., Benson, L., Beg, A., Scheiffele, P., & Martin, J. (2010). Cortical control of adaptive locomotion in wild-type mice and mutant mice lacking the ephrin-Eph effector protein $\alpha 2$ -chimaerin. *Journal of Neurophysiology*. <https://doi.org/10.1152/jn.00671.2010>
- Assimacopoulos, S., Grove, E.A., and Ragsdale, C.W. (2003). Identification of a Pax6-dependent epidermal growth factor family signaling source at the lateral edge of the embryonic cerebral cortex. *J Neurosci* 23, 6399-6403.
- Ayoub, A. E., & Kostovic, I. (2009). New horizons for the subplate zone and its pioneering neurons.

In *Cerebral Cortex*. <https://doi.org/10.1093/cercor/bhp025>

- Bagnard, D., Chounlamountri, N., Püschel, A. W., & Bolz, J. (2001). Axonal surface molecules act in combination with semaphorin 3A during the establishment of corticothalamic projections. *Cerebral Cortex*. <https://doi.org/10.1093/cercor/11.3.278>
- Bagri, A., Marín, O., Plump, A. S., Mak, J., Pleasure, S. J., Rubenstein, J. L. R., & Tessier-Lavigne, M. (2002). Slit proteins prevent midline crossing and determine the dorsoventral position of major axonal pathways in the mammalian forebrain. *Neuron*. [https://doi.org/10.1016/S0896-6273\(02\)00561-5](https://doi.org/10.1016/S0896-6273(02)00561-5)
- Barbelanne, M., & Tsang, W. Y. (2014). Molecular and cellular basis of autosomal recessive primary microcephaly. In *BioMed Research International* (Vol. 2014). <https://doi.org/10.1155/2014/547986>
- Barkovich, A. J., Guerrini, R., Kuzniecky, R. I., Jackson, G. D., & Dobyns, W. B. (2012). A developmental and genetic classification for malformations of cortical development: Update 2012. In *Brain*. <https://doi.org/10.1093/brain/aws019>
- Baronas, V. A., & Kurata, H. T. (2014). Inward rectifiers and their regulation by endogenous polyamines. In *Frontiers in Physiology*. <https://doi.org/10.3389/fphys.2014.00325>
- Basaldella, E., Takeoka, A., Sigrist, M., & Arber, S. (2015). Multisensory Signaling Shapes Vestibulo-Motor Circuit Specificity. *Cell*. <https://doi.org/10.1016/j.cell.2015.09.023>
- Bayraktar, O. A., Fuentealba, L. C., Alvarez-Buylla, A., & Rowitch, D. H. (2015). Astrocyte development and heterogeneity. *Cold Spring Harbor Perspectives in Biology*. <https://doi.org/10.1101/cshperspect.a020362>
- Bedogni, F., Hodge, R. D., Elsen, G. E., Nelson, B. R., Daza, R. A. M., Beyer, R. P., Bammler, T. K., Rubenstein, J. L. R., & Hevner, R. F. (2010). Tbr1 regulates regional and laminar identity of postmitotic neurons in developing neocortex. *Proceedings of the National Academy of Sciences of the United States of America*. <https://doi.org/10.1073/pnas.1002285107>
- Belle, M., Godefroy, D., Couly, G., Malone, S. A., Collier, F., Giacobini, P., & Chédotal, A. (2017). Tridimensional Visualization and Analysis of Early Human Development. *Cell*, 169(1), 161-173.e12. <https://doi.org/10.1016/j.cell.2017.03.008>
- Bender, R. A., & Baram, T. Z. (2008). Hyperpolarization activated cyclic-nucleotide gated (HCN) channels in developing neuronal networks. *Progress in Neurobiology*. <https://doi.org/10.1016/j.pneurobio.2008.09.007>
- Berger, T., Larkum, M. E., & Lüscher, H. R. (2001). High Ih channel density in the distal apical dendrite of layer V pyramidal cells increases bidirectional attenuation of EPSPs. *Journal of Neurophysiology*. <https://doi.org/10.1152/jn.2001.85.2.855>
- Bertacchi, M., Gruart, A., Kaimakis, P., Allet, C., Serra, L., Giacobini, P., Delgado-García, J. M., Bovolenta, P., & Studer, M. (2019). Mouse Nr2f1 haploinsufficiency unveils new pathological

- mechanisms of a human optic atrophy syndrome. *EMBO Molecular Medicine*, 11(8). <https://doi.org/10.15252/emmm.201910291>
- Bertacchi, M., Parisot, J., & Studer, M. (2019). The pleiotropic transcriptional regulator COUP-TFI plays multiple roles in neural development and disease. *Brain Research*, 1705, 75–94. <https://doi.org/10.1016/j.brainres.2018.04.024>
- Bertacchi, M., Romano, A. L., Loubat, A., Mau-them, F. T., Willems, M., Faivre, L., Kien, P. K. Van, Perrin, L., Sorlin, A., Kuentz, P., Philippe, C., & Garde, A. (2020). Altered regional progenitor dynamics in the neocortex of a BBSOA disease mouse model. *EMBO Journal*.
- Bjaalie, J.G., and Brodal, P. (1997). Cat pontocerebellar network: numerical capacity and axonal collateral branching of neurones in the pontine nuclei projecting to individual parafloccular folia. *Neurosci Res* 27, 199-210.
- Bjaalie, J. G., Sudbø, J., & Brodal, P. (1997). Corticopontine terminal fibres form small scale clusters and large scale lamellae in the cat. *NeuroReport*. <https://doi.org/10.1097/00001756-199705060-00019>
- Blankenship, A. G., Hamby, A. M., Firl, A., Vyas, S., Maxeiner, S., Willecke, K., & Feller, M. B. (2011). The role of neuronal connexins 36 and 45 in shaping spontaneous firing patterns in the developing retina. *Journal of Neuroscience*. <https://doi.org/10.1523/JNEUROSCI.5640-10.2011>
- Boillot, M., Lee, C. Y., Allene, C., Leguern, E., Baulac, S., & Rouach, N. (2016). LGI1 acts presynaptically to regulate excitatory synaptic transmission during early postnatal development. *Scientific Reports*. <https://doi.org/10.1038/srep21769>
- Bojanek, E. K., Mosconi, M. W., Guter, S., Betancur, C., Macmillan, C., & Cook, E. H. (2020). Clinical and neurocognitive issues associated with Bosch-Boonstra-Schaaf optic atrophy syndrome: A case study. *American Journal of Medical Genetics, Part A*, 182(1), 213–218. <https://doi.org/10.1002/ajmg.a.61409>
- Bonzanni, M., DiFrancesco, J. C., Milanese, R., Campostrini, G., Castellotti, B., Bucchi, A., Baruscotti, M., Ferrarese, C., Franceschetti, S., Canafoglia, L., Ragona, F., Freri, E., Labate, A., Gambardella, A., Costa, C., Rivolta, I., Gellera, C., Granata, T., Barbuti, A., & DiFrancesco, D. (2018). A novel de novo HCN1 loss-of-function mutation in genetic generalized epilepsy causing increased neuronal excitability. *Neurobiology of Disease*. <https://doi.org/10.1016/j.nbd.2018.06.012>
- Borello, U., Madhavan, M., Vilinsky, I., Faedo, A., Pierani, A., Rubenstein, J., & Campbell, K. (2014). Sp8 and COUP-TF1 reciprocally regulate patterning and fgf signaling in cortical progenitors. *Cerebral Cortex*. <https://doi.org/10.1093/cercor/bhs412>
- Bosch, D. G. D. G. M., Boonstra, F. N., de Leeuw, N., Pfundt, R., Nillesen, W. M., de Ligt, J., Gilissen, C., Jhangiani, S., Lupski, J. R., Cremers, F. P. P. M., & de Vries, B. B. A. B. (2015). Novel genetic causes for cerebral visual impairment. *European Journal of Human Genetics*, May, 1–6. <https://doi.org/10.1038/ejhg.2015.186>

- Bosch, D. G. M. M., Boonstra, F. N., Gonzaga-Jauregui, C., Xu, M., De Ligt, J., Jhangiani, S., Wiszniewski, W., Muzny, D. M., Yntema, H. G., Pfundt, R., Vissers, L. E. L. M. L. M., Spruijt, L., Blokland, E. A. W. W., Chen, C. A., Lewis, R. A., Tsai, S. Y., Gibbs, R. A., Tsai, M. J., Lupski, J. R., ... Schaaf, C. P. (2014). NR2F1 mutations cause optic atrophy with intellectual disability. *American Journal of Human Genetics*, *94*(2), 303–309. <https://doi.org/10.1016/j.ajhg.2014.01.002>
- Bosley, T. M. T. M., Salih, M. A. A. M., Jen, J. C. C., Lin, D. D. D. M., Oystreck, D., Abu-Amero, K. K. K., MacDonald, D. B. B., Al Zayed, Z., al Dhalaan, H., Kansu, T., Stigsby, B., & Baloh, R. W. W. (2005). Neurologic features of horizontal gaze palsy and progressive scoliosis with mutations in ROBO3. *American Journal of Ophthalmology*. <https://doi.org/10.1016/j.ajo.2005.06.013>
- Bouet, V., Boulouard, M., Toutain, J., Divoux, D., Bernaudin, M., Schumann-Bard, P., & Freret, T. (2009). The adhesive removal test: A sensitive method to assess sensorimotor deficits in mice. *Nature Protocols*. <https://doi.org/10.1038/nprot.2009.125>
- Bower, J. M., Beermann, D. H., Gibson, J. M., Shambes, G. M., & Welker, W. (1981). Principles of organization of a cerebro-cerebellar circuit: Micromapping the projections from cerebral (SI) to cerebellar (Granule Cell Layer) tactile areas of rats. *Brain, Behavior and Evolution*. <https://doi.org/10.1159/000121772>
- Bower, J.M. (2011). Functional implications of tactile projection patterns to the lateral hemispheres of the cerebellum of the albino rat: the legacy of Wally Welker. *Annals of the New York Academy of Sciences* 1225, 130-141.
- Bower, J.M., and Kassel, J. (1990). Variability in tactile projection patterns to cerebellar folia crus IIA of the Norway rat. *J Comp Neurol* 302, 768-778.
- Boychuk, J. A., Farrell, J. S., Palmer, L. A., Singleton, A. C., Pittman, Q. J., & Teskey, G. C. (2017). HCN channels segregate stimulation-evoked movement responses in neocortex and allow for coordinated forelimb movements in rodents. *Journal of Physiology*. <https://doi.org/10.1113/JP273068>
- Brager, D. H., Akhavan, A. R., & Johnston, D. (2012). Impaired Dendritic Expression and Plasticity of h-Channels in the *fmr1*-/y Mouse Model of Fragile X Syndrome. *Cell Reports*. <https://doi.org/10.1016/j.celrep.2012.02.002>
- Brager, D. H., & Johnston, D. (2007). Plasticity of intrinsic excitability during long-term depression is mediated through mGluR-dependent changes in I_h in hippocampal CA1 pyramidal neurons. *Journal of Neuroscience*. <https://doi.org/10.1523/JNEUROSCI.3520-07.2007>
- Britanova, O., de Juan Romero, C., Cheung, A., Kwan, K. Y., Schwark, M., Gyorgy, A., Vogel, T., Akopov, S., Mitkovski, M., Agoston, D., Šestan, N., Molnár, Z., & Tarabykin, V. (2008). *Satb2* Is a Postmitotic Determinant for Upper-Layer Neuron Specification in the Neocortex. *Neuron*. <https://doi.org/10.1016/j.neuron.2007.12.028>
- Brodal, P. (2010). The central nervous system: Structure and function (4th ed.). In *The central nervous system: Structure and function (4th ed.)*.

- Brodal, P. (1978). The corticopontine projection in the rhesus monkey. Origin and principles of organization. *Brain* 101, 251-283.
- Brodal, P., and Bjaalie, J.G. (1992). Organization of the pontine nuclei. *Neurosci Res* 13, 83-118.
- Brodal, P., and Bjaalie, J.G. (1997). Salient anatomic features of the cortico-ponto-cerebellar pathway. *Prog Brain Res* 114, 227-249.
- Brodmann, K., & Garey, L. J. (2006). Brodmann's localisation in the cerebral cortex: The principles of comparative localisation in the cerebral cortex based on cytoarchitectonics. In *Brodmann's Localisation in the Cerebral Cortex: The Principles of Comparative Localisation in the Cerebral Cortex Based on Cytoarchitectonics*. <https://doi.org/10.1007/b138298>
- Bureau, I., Von Paul, F. Saint, & Svoboda, K. (2006). Interdigitated paralemniscal and lemniscal pathways in the mouse barrel cortex. *PLoS Biology*. <https://doi.org/10.1371/journal.pbio.0040382>
- Burrone, J., O'Byrne, M., & Murthy, V. N. (2002). Multiple forms of synaptic plasticity triggered by selective suppression of activity in individual neurons. *Nature*. <https://doi.org/10.1038/nature01242>
- Buxbaum, J. D., Silverman, J. M., Smith, C. J., Greenberg, D. A., Kilifarski, M., Reichert, J., Cook, E. H., Fang, Y., Song, C. Y., & Vitale, R. (2002). Association between a GABRB3 polymorphism and autism. *Molecular Psychiatry*. <https://doi.org/10.1038/sj.mp.4001011>
- Cadwell, C. R., Bhaduri, A., Mostajo-Radji, M. A., Keefe, M. G., & Nowakowski, T. J. (2019). Development and Arealization of the Cerebral Cortex. In *Neuron*. <https://doi.org/10.1016/j.neuron.2019.07.009>
- Cánovas, J., Berndt, F. A., Sepúlveda, H., Aguilar, R., Veloso, F. A., Montecino, M., Oliva, C., Maass, J. C., Sierralta, J., & Kukuljan, M. (2015). The specification of cortical subcerebral projection neurons depends on the direct repression of TBR1 by CTIP1/BCL11a. *Journal of Neuroscience*. <https://doi.org/10.1523/JNEUROSCI.0169-15.2015>
- Caviness, V. S., & Frost, D. O. (1980). Tangential organization of thalamic projections to the neocortex in the mouse. *Journal of Comparative Neurology*. <https://doi.org/10.1002/cne.901940205>
- Cederquist, G. Y., Azim, E., Shnider, S. J., Padmanabhan, H., & Macklis, J. D. (2013). Lmo4 establishes rostral motor cortex projection neuron subtype diversity. *Journal of Neuroscience*. <https://doi.org/10.1523/JNEUROSCI.5140-12.2013>
- Chapin, J. K., & Lin, C. -S. (1984). Mapping the body representation in the SI cortex of anesthetized and awake rats. *Journal of Comparative Neurology*. <https://doi.org/10.1002/cne.902290206>
- Chen, B., Schaevitz, L. R., & McConnell, S. K. (2005). Fezl regulates the differentiation and axon targeting of layer 5 subcortical projection neurons in cerebral cortex. *Proceedings of the*

National Academy of Sciences of the United States of America.
<https://doi.org/10.1073/pnas.0508732102>

- Chen, B., Wang, S. S., Hattox, A. M., Rayburn, H., Nelson, S. B., & McConnell, S. K. (2008). The Fezf2-Ctip2 genetic pathway regulates the fate choice of subcortical projection neurons in the developing cerebral cortex. *Proceedings of the National Academy of Sciences of the United States of America*, *105*(32), 11382–11387. <https://doi.org/10.1073/pnas.0804918105>
- Chen, C. A., Bosch, D. G. M. M., Cho, M. T., Rosenfeld, J. A., Shinawi, M., Lewis, R. A., Mann, J., Jayakar, P., Payne, K., Walsh, L., Moss, T., Schreiber, A., Schoonveld, C., Monaghan, K. G., Elmslie, F., Douglas, G., Boonstra, F. N., Millan, F., Cremers, F. P. M. M., ... Schaaf, C. (2016). The expanding clinical phenotype of Bosch-Boonstra-Schaaf optic atrophy syndrome: 20 new cases and possible genotype-phenotype correlations. *Genetics in Medicine*, *18*(11), 1143–1150. <https://doi.org/10.1038/gim.2016.18>
- Chen, K., Aradi, I., Thon, N., Eghbal-Ahmadi, M., Baram, T. Z., & Soltesz, I. (2001). Persistently modified h-channels after complex febrile seizures convert the seizure-induced enhancement of inhibition to hyperexcitability. *Nature Medicine*. <https://doi.org/10.1038/85480>
- Cho, M. W., & Choi, M. Y. (2012). Spontaneous organization of the cortical structure through endogenous neural firing and gap junction transmission. *Neural Networks*. <https://doi.org/10.1016/j.neunet.2012.03.002>
- Cho, R. H., Segawa, S., Mizuno, A., & Kaneko, T. (2004). Intracellularly labeled pyramidal neurons in the cortical areas projecting to the spinal cord: I. Electrophysiological properties of pyramidal neurons. *Neuroscience Research*. <https://doi.org/10.1016/j.neures.2004.08.006>
- Chow, C. W., Halliday, J. L., Anderson, R. M. D., Danks, D. M., & Fortune, D. W. (1985). Congenital absence of pyramids and its significance in genetic diseases. *Acta Neuropathologica*. <https://doi.org/10.1007/BF00687014>
- Christophe, E., Doerflinger, N., Lavery, D. J., Molnár, Z., Charpak, S., & Audinat, E. (2005). Two populations of layer V pyramidal cells of the mouse neocortex: Development and sensitivity to anesthetics. *Journal of Neurophysiology*. <https://doi.org/10.1152/jn.00076.2005>
- Cohen, L. G., Meer, J., Tarkka, I., Bierner, S., Leiderman, D. B., Dubinsky, R. M., Sanes, J. N., Jabbari, B., Branscum, B., & Hallett, M. (1991). Congenital mirror movements. Abnormal organization of motor pathways in two patients. *Brain*. <https://doi.org/10.1093/brain/114.1.381>
- Contesse, T., Ayrault, M., Mantegazza, M., Studer, M., & Deschaux, O. (2019a). Hyperactive and anxiolytic-like behaviors result from loss of COUP-TFI/Nr2f1 in the mouse cortex. *Genes, Brain and Behavior*, *18*(7). <https://doi.org/10.1111/gbb.12556>
- Contesse, T., Ayrault, M., Mantegazza, M., Studer, M., & Deschaux, O. (2019b). Hyperactive and anxiolytic-like behaviors result from loss of COUP-TFI/Nr2f1 in the mouse cortex. *Genes, Brain and Behavior*, *18*(7). <https://doi.org/10.1111/gbb.12556>

- Coonan, J. R., Greferath, U., Messenger, J., Hartley, L., Murphy, M., Boyd, A. W., Dottori, M., Galea, M. P., & Bartlett, P. F. (2001). Development and reorganization of corticospinal projections in EphA4 deficient mice. *Journal of Comparative Neurology*. <https://doi.org/10.1002/cne.1064>
- Cooney, A. J., Tsai, S. Y., O'Malley, B. W., & Tsai, M. J. (1992). Chicken ovalbumin upstream promoter transcription factor (COUP-TF) dimers bind to different GGTC A response elements, allowing COUP-TF to repress hormonal induction of the vitamin D₃, thyroid hormone, and retinoic acid receptors. *Molecular and Cellular Biology*. <https://doi.org/10.1128/mcb.12.9.4153>
- Corlew, R., Bosma, M. M., & Moody, W. J. (2004). Spontaneous, synchronous electrical activity in neonatal mouse cortical neurones. *Journal of Physiology*. <https://doi.org/10.1113/jphysiol.2004.071621>
- Cossette, P., Liu, L., Brisebois, K., Dong, H., Lortie, A., Vanasse, M., Saint-Hilaire, J. M., Carmant, L., Verner, A., Lu, W. Y., Wang, Y. T., & Rouleau, G. A. (2002). Mutation of GABRA1 in an autosomal dominant form of juvenile myoclonic epilepsy. *Nature Genetics*. <https://doi.org/10.1038/ng885>
- Cotterill, E., Charlesworth, P., Thomas, C. W., Paulsen, O., & Eglon, S. J. (2016). A comparison of computational methods for detecting bursts in neuronal spike trains and their application to human stem cell-derived neuronal networks. *Journal of Neurophysiology*. <https://doi.org/10.1152/jn.00093.2016>
- Creutzfeldt, O. D. (1977). Generality of the functional structure of the neocortex. *Naturwissenschaften*, 64(10), 507–517. <https://doi.org/10.1007/BF00483547>
- Dahme, M., Bartsch, U., Martini, R., Anliker, B., Schachner, M., & Mantei, N. (1997). Disruption of the mouse L1 gene leads to malformations of the nervous system. *Nature Genetics*. <https://doi.org/10.1038/ng1197-346>
- Del Pino, I., Brotons-Mas, J. R., Marques-Smith, A., Marighetto, A., Frick, A., Marín, O., & Rico, B. (2017). Abnormal wiring of CCK+ basket cells disrupts spatial information coding. *Nature Neuroscience*. <https://doi.org/10.1038/nn.4544>
- DeLong, M. R. (1972). Activity of basal ganglia neurons during movement. *Brain Research*. [https://doi.org/10.1016/0006-8993\(72\)90118-7](https://doi.org/10.1016/0006-8993(72)90118-7)
- delPino, I., García-Frigola, C., Dehorter, N., Brotons-Mas, J. R., Alvarez-Salvado, E., MartínezdeLagrán, M., Ciceri, G., Gabaldón, M. V., Moratal, D., Dierssen, M., Canals, S., Marín, O., & Rico, B. (2013). Erbb4 Deletion from Fast-Spiking Interneurons Causes Schizophrenia-like Phenotypes. *Neuron*. <https://doi.org/10.1016/j.neuron.2013.07.010>
- Demyanenko, G. P., Riday, T. T., Tran, T. S., Dalal, J., Darnell, E. P., Brennaman, L. H., Sakurai, T., Grumet, M., Philpot, B. D., & Maness, P. F. (2011). NrCAM deletion causes topographic mistargeting of thalamocortical axons to the visual cortex and disrupts visual acuity. *Journal of Neuroscience*. <https://doi.org/10.1523/JNEUROSCI.4467-10.2011>

- Demyanenko, G. P., Siesser, P. F., Wright, A. G., Brennaman, L. H., Bartsch, U., Schachner, M., & Maness, P. F. (2011). L1 and CHL1 cooperate in thalamocortical axon targeting. *Cerebral Cortex*. <https://doi.org/10.1093/cercor/bhq115>
- Di Meglio, T., Nguyen-Ba-Charvet, K. T., Tessier-Lavigne, M., Sotelo, C., & Chédotal, A. (2008). Molecular mechanisms controlling midline crossing by precerebellar neurons. *Journal of Neuroscience*. <https://doi.org/10.1523/JNEUROSCI.0078-08.2008>
- Donoghue, J. P., & Wise, S. P. (1982). The motor cortex of the rat: Cytoarchitecture and microstimulation mapping. *Journal of Comparative Neurology*. <https://doi.org/10.1002/cne.902120106>
- Dottori, M., Hartley, L., Galea, M., Paxinos, G., Polizzotto, M., Kilpatrick, T., Bartlett, P. F., Murphy, M., Köntgen, F., & Boyd, A. W. (1998). EphA4 (Sek1) receptor tyrosine kinase is required for the development of the corticospinal tract. *Proceedings of the National Academy of Sciences of the United States of America*. <https://doi.org/10.1073/pnas.95.22.13248>
- Dow, R. S. (1942). CEREBELLAR ACTION POTENTIALS IN RESPONSE TO STIMULATION OF THE CEREBRAL CORTEX IN MONKEYS AND CATS. *Journal of Neurophysiology*. <https://doi.org/10.1152/jn.1942.5.2.121>
- Dufour, A., Seibt, J., Passante, L., Depaepe, V., Ciossek, T., Frisé, J., Kullander, K., Flanagan, J. G., Polleux, F., & Vanderhaeghen, P. (2003). Area Specificity and Topography of Thalamocortical Projections Are Controlled by ephrin/Eph Genes. *Neuron*, 39(3), 453–465. [https://doi.org/10.1016/S0896-6273\(03\)00440-9](https://doi.org/10.1016/S0896-6273(03)00440-9)
- Dumitrescu, A. S., Evans, M. D., & Grubb, M. S. (2016). Evaluating Tools for Live Imaging of Structural Plasticity at the Axon Initial Segment. *Frontiers in Cellular Neuroscience*, 10(November), 1–17. <https://doi.org/10.3389/fncel.2016.00268>
- Esposito, M. S., Capelli, P., & Arber, S. (2014). Brainstem nucleus MdV mediates skilled forelimb motor tasks. *Nature*, 508(7496), 351–356. <https://doi.org/10.1038/nature13023>
- Evans, M. D., Dumitrescu, A. S., Kruijssen, D. L. H., Taylor, S. E., Grubb, M. S., Evans, M. D., Dumitrescu, A. S., Kruijssen, D. L. H., Taylor, S. E., & Grubb, M. S. (2015). Rapid Modulation of Axon Initial Segment Length Influences Repetitive Spike Firing Article Rapid Modulation of Axon Initial Segment Length Influences Repetitive Spike Firing. *CellReports*, 13(6), 1233–1245. <https://doi.org/10.1016/j.celrep.2015.09.066>
- Evans, R. M., & Mangelsdorf, D. J. (2014). Nuclear receptors, RXR, and the big bang. In *Cell*. <https://doi.org/10.1016/j.cell.2014.03.012>
- F.Nitschke, M., Kleinschmidt, A., Wessel, K., & Frahm, J. (1996). Somatotopic motor representation in the human anterior cerebellum. *Brain*. <https://doi.org/10.1093/brain/119.3.1023>
- Fabri, M., & Burton, H. (1991). Ipsilateral cortical connections of primary somatic sensory cortex in rats. *Journal of Comparative Neurology*. <https://doi.org/10.1002/cne.903110310>

- Fame, R. M., MacDonald, J. L., & Macklis, J. D. (2011). Development, specification, and diversity of callosal projection neurons. In *Trends in Neurosciences*. <https://doi.org/10.1016/j.tins.2010.10.002>
- Fan, J., Stemkowski, P. L., Gandini, M. A., Black, S. A., Zhang, Z., Souza, I. A., Chen, L., & Zamponi, G. W. (2016). Reduced hyperpolarization-activated current contributes to enhanced intrinsic excitability in cultured hippocampal neurons from PrP^{-/-} mice. *Frontiers in Cellular Neuroscience*. <https://doi.org/10.3389/fncel.2016.00074>
- Fan, Y., Fricker, D., Brager, D. H., Chen, X., Lu, H. C., Chitwood, R. A., & Johnston, D. (2005). Activity-dependent decrease of excitability in rat hippocampal neurons through increases in Ih. *Nature Neuroscience*. <https://doi.org/10.1038/nn1568>
- Farmer, S. F., Ingram, D. A., & Stephens, J. A. (1990). Mirror movements studied in a patient with Klippel-Feil syndrome. *The Journal of Physiology*. <https://doi.org/10.1113/jphysiol.1990.sp018222>
- Farr, T. D., & Whishaw, I. Q. (2002). Quantitative and qualitative impairments in skilled reaching in the mouse (*Mus musculus*) after a focal motor cortex stroke. *Stroke*. <https://doi.org/10.1161/01.STR.0000020714.48349.4E>
- Fatemi, S. H., Folsom, T. D., Reutiman, T. J., & Thuras, P. D. (2009). Expression of GABAB Receptors Is Altered in Brains of Subjects with Autism. *Cerebellum*. <https://doi.org/10.1007/s12311-008-0075-3>
- Faulkner, R. L., Coble, J., Jones, E. G., Low, L. K., Liu, X.-B. B., Cheng, H.-J. J., Coble, J., Jones, E. G., & Cheng, H.-J. J. (2008). Dorsal turning of motor corticospinal axons at the pyramidal decussation requires plexin signaling. *Neural Development*, 3, 21. <https://doi.org/10.1186/1749-8104-3-21>
- Favuzzi, E., Deogracias, R., Marques-Smith, A., Maeso, P., Jezequel, J., Exposito-Alonso, D., Balia, M., Kroon, T., Hinojosa, A. J., Maraver, E. F., & Rico, B. (2019). Neurodevelopment: Distinct molecular programs regulate synapse specificity in cortical inhibitory circuits. *Science*. <https://doi.org/10.1126/science.aau8977>
- Fazel Darbandi, S., Robinson Schwartz, S. E., Qi, Q., Catta-Preta, R., Pai, E. L.-L., Mandell, J. D., Everitt, A., Rubin, A., Krasnoff, R. A., Katzman, S., Tastad, D., Nord, A. S., Willsey, A. J., Chen, B., State, M. W., Sohal, V. S., & Rubenstein, J. L. R. (2018). Neonatal Tbr1 Dosage Controls Cortical Layer 6 Connectivity. *Neuron*, 100(4), 831-845.e7. <https://doi.org/10.1016/j.neuron.2018.09.027>
- Feng, G., Mellor, R.H., Bernstein, M., Keller-Peck, C., Nguyen, Q.T., Wallace, M., Nerbonne, J.M., Lichtman, J.W., and Sanes, J.R. (2000). Imaging neuronal subsets in transgenic mice expressing multiple spectral variants of GFP. *Neuron* 28, 41-51.
- Finger, J. H., Bronson, R. T., Harris, B., Johnson, K., Przyborski, S. A., & Ackerman, S. L. (2002). The netrin 1 receptors Unc5h3 and Dcc are necessary at multiple choice points for the guidance of corticospinal tract axons. *Journal of Neuroscience*. <https://doi.org/10.1523/jneurosci.22-23-10346.2002>

- Flore, G., Di Ruberto, G., Parisot, J., Sannino, S., Russo, F., Illingworth, E. A., Studer, M., & De Leonibus, E. (2016). Gradient COUP-TFI Expression Is Required for Functional Organization of the Hippocampal Septo-Temporal Longitudinal Axis. *Cerebral Cortex*, bhv336. <https://doi.org/10.1093/cercor/bhv336>
- Franklin, K. B. J., & Paxinos, G. (2007). The Mouse Brain in Stereotaxic Coordinates (map). In Academic Press.
- Frotscher, M., Chai, X., Bock, H. H., Haas, C. A., Förster, E., & Zhao, S. (2009). Role of Reelin in the development and maintenance of cortical lamination. In *Journal of Neural Transmission*. <https://doi.org/10.1007/s00702-009-0228-7>
- Fukuchi-Shimogori, T., & Grove, E. A. (2001). Neocortex patterning by the secreted signaling molecule FGF8. *Science*. <https://doi.org/10.1126/science.1064252>
- Gao, W. J., & Zheng, Z. H. (2004). Target-specific differences in somatodendritic morphology of layer V pyramidal neurons in rat motor cortex. *Journal of Comparative Neurology*. <https://doi.org/10.1002/cne.20224>
- Garaschuk, O., Hanse, E., & Konnerth, A. (1998). Developmental profile and synaptic origin of early network oscillations in the CA1 region of rat neonatal hippocampus. *Journal of Physiology*. <https://doi.org/10.1111/j.1469-7793.1998.219bu.x>
- Garel, S., Huffman, K.J., and Rubenstein, J.L. (2003). Molecular regionalization of the neocortex is disrupted in Fgf8 hypomorphic mutants. *Development* 130, 1903-1914.
- Gavello, D., Calorio, C., Franchino, C., Cesano, F., Carabelli, V., Carbone, E., & Marcantoni, A. (2018). Early Alterations of Hippocampal Neuronal Firing Induced by Abeta42. *Cerebral Cortex*. <https://doi.org/10.1093/cercor/bhw377>
- Gavello, D., Rojo-Ruiz, J., Marcantoni, A., Franchino, C., Carbone, E., & Carabelli, V. (2012). Leptin counteracts the hypoxia-induced inhibition of spontaneously firing hippocampal neurons: A microelectrode array study. *PLoS ONE*. <https://doi.org/10.1371/journal.pone.0041530>
- Geisen, M. J., Di Meglio, T., Pasqualetti, M., Ducret, S., Brunet, J. F., Chedotal, A., & Rijli, F. M. (2008). Hox paralog group 2 genes control the migration of mouse pontine neurons through slit-Robo signaling. *PLoS Biology*. <https://doi.org/10.1371/journal.pbio.0060142>
- Goebbels, S., Bormuth, I., Bode, U., Hermanson, O., Schwab, M. H., & Nave, K.-A. (2006). Genetic targeting of principal neurons in neocortex and hippocampus of NEX-Cre mice. *Genesis*, 44(12), 611–621. <https://doi.org/10.1002/dvg.20256>
- Gorski, J. A., Talley, T., Qiu, M., Puelles, L., Rubenstein, J. L. R., & Jones, K. R. (2002). Cortical excitatory neurons and glia, but not GABAergic neurons, are produced in the Emx1-expressing lineage. *The Journal of Neuroscience: The Official Journal of the Society for Neuroscience*. <https://doi.org/20026564>
- Greig, L. C., Woodworth, M. B., Galazo, M. J., Padmanabhan, H., & Macklis, J. D. (2013). Molecular

- logic of neocortical projection neuron specification, development and diversity. *Nature Reviews Neuroscience*, 14(11), 755–769. <https://doi.org/10.1038/nrn3586>
- Grove, E. A., & Fukuchi-Shimogori, T. (2003). Generating the cerebral cortical area map. In *Annual Review of Neuroscience*. <https://doi.org/10.1146/annurev.neuro.26.041002.131137>
- Grubb, M. S., & Burrone, J. (2010). Activity-dependent relocation of the axon initial segment fine-tunes neuronal excitability. *Nature*. <https://doi.org/10.1038/nature09160>
- Gu, C., Rodriguez, E. R., Reimert, D. V., Shu, T., Fritzsche, B., Richards, L. J., Kolodkin, A. L., & Ginty, D. D. (2003). Neuropilin-1 conveys semaphorin and VEGF signaling during neural and cardiovascular development. *Developmental Cell*. [https://doi.org/10.1016/S1534-5807\(03\)00169-2](https://doi.org/10.1016/S1534-5807(03)00169-2)
- Gulledge, A. T., & Bravo, J. J. (2016). Neuron morphology influences axon initial segment plasticity. *ENeuro*, 3(February), 1–24. <https://doi.org/10.1523/ENEURO.0085-15.2016>
- Gundersen, H., & Solitare, G. B. (1968). Mirror Movements in Patients with the Klippel-Feil Syndrome: Neuropathologic Observations. *Archives of Neurology*. <https://doi.org/10.1001/archneur.1968.00470360097009>
- Haller, S., Wetzel, S. G., & Lütsch, J. (2008). Functional MRI, DTI and neurophysiology in horizontal gaze palsy with progressive scoliosis. *Neuroradiology*. <https://doi.org/10.1007/s00234-007-0359-1>
- Hamada, M. S., Goethals, S., De Vries, S. I., Brette, R., & Kole, M. H. P. (2016). Covariation of axon initial segment location and dendritic tree normalizes the somatic action potential. *Proceedings of the National Academy of Sciences of the United States of America*. <https://doi.org/10.1073/pnas.1607548113>
- Hamasaki, T., Leingärtner, A., Ringstedt, T., & O’Leary, D. D. M. (2004). EMX2 regulates sizes and positioning of the primary sensory and motor areas in neocortex by direct specification of cortical progenitors. *Neuron*. <https://doi.org/10.1016/j.neuron.2004.07.016>
- Han, W., Kwan, K. Y., Shim, S., Lam, M. M. S., Shin, Y., Xu, M., Zhu, Y., Li, M., & Šestan, N. (2011). TBR1 directly represses Fezf2 to control the laminar origin and development of the corticospinal tract. *Proceedings of the National Academy of Sciences of the United States of America*. <https://doi.org/10.1073/pnas.1016723108>
- Harb, K., Magrinelli, E., Nicolas, C. S., Lukianets, N., Frangeul, L., Pietri, M., Sun, T., Sandoz, G., Grammont, F., Jabaudon, D., Studer, M., & Alfano, C. (2016). Area-specific development of distinct projection neuron subclasses is regulated by postnatal epigenetic modifications. *ELife*, 5(JANUARY2016), 1–25. <https://doi.org/10.7554/eLife.09531>
- Hatanaka, Y., Zhu, Y., Torigoe, M., Kita, Y., & Murakami, F. (2016). From migration to settlement: The pathways, migration modes and dynamics of neurons in the developing brain. In *Proceedings of the Japan Academy Series B: Physical and Biological Sciences*.

<https://doi.org/10.2183/pjab.92.1>

- Hattox, A. M., & Nelson, S. B. (2007). Layer V neurons in mouse cortex projecting to different targets have distinct physiological properties. *Journal of Neurophysiology*, 98(6), 3330–3340. <https://doi.org/10.1152/jn.00397.2007>
- Hwang, E.J., Link, T.D., Hu, Y.Y., Lu, S., Wang, E.H., Lilascharoen, V., Aronson, S., O'Neil, K., Lim, B.K., and Komiyama, T. (2019). Corticostriatal Flow of Action Selection Bias. *Neuron* 104, 1126-1140 e1126.
- Henning, Y., Osadnik, C., & Malkemper, E. P. (2019). EyeCi: Optical clearing and imaging of immunolabeled mouse eyes using light-sheet fluorescence microscopy. In *Experimental Eye Research*. <https://doi.org/10.1016/j.exer.2018.12.001>
- Henschke, J. U., & Pakan, J. M. P. (2020). Disynaptic cerebrocerebellar pathways originating from multiple functionally distinct cortical areas. *ELife*. <https://doi.org/10.7554/ELIFE.59148>
- Hibino, H., Inanobe, A., Furutani, K., Murakami, S., Findlay, I., & Kurachi, Y. (2010). Inwardly rectifying potassium channels: Their structure, function, and physiological roles. In *Physiological Reviews*. <https://doi.org/10.1152/physrev.00021.2009>
- Hofstetter, K. M., & Ehret, G. (1992). The auditory cortex of the mouse: Connections of the ultrasonic field. *Journal of Comparative Neurology*. <https://doi.org/10.1002/cne.903230306>
- Holtmaat, A. J. G. D., Trachtenberg, J. T., Wilbrecht, L., Shepherd, G. M., Zhang, X., Knott, G. W., & Svoboda, K. (2005). Transient and persistent dendritic spines in the neocortex in vivo. *Neuron*. <https://doi.org/10.1016/j.neuron.2005.01.003>
- Hu, B. (2003). Functional organization of lemniscal and nonlemniscal auditory thalamus. *Experimental Brain Research*. <https://doi.org/10.1007/s00221-003-1611-5>
- Huang, Z., Walker, M. C., & Shah, M. M. (2009). Loss of Dendritic HCN1 Subunits Enhances Cortical Excitability and Epileptogenesis. *Journal of Neuroscience*, 29(35), 10979–10988. <https://doi.org/10.1523/jneurosci.1531-09.2009>
- Huang, Zhenyong, Kawase-Koga, Y., Zhang, S., Visvader, J., Toth, M., Walsh, C. A., & Sun, T. (2009). Transcription factor Lmo4 defines the shape of functional areas in developing cortices and regulates sensorimotor control. *Developmental Biology*, 327(1), 132–142. <https://doi.org/10.1016/j.ydbio.2008.12.003>
- Hwung, Y. P., Wang, L. H., Tsai, S. Y., & Tsai, M. J. (1988). Differential binding of the chicken ovalbumin upstream promoter (COUP) transcription factor to two different promoters. *Journal of Biological Chemistry*.
- Inoue, K., Terashima, T., & Inoue, Y. (1991). Postnatal Development of the Pontine Projections from the Visual Cortex of the Mouse. *Okajimas Folia Anatomica Japonica*. https://doi.org/10.2535/ofaj1936.67.6_479

- Jabaudon, D. (2017). Fate and freedom in developing neocortical circuits. *Nature Communications*, 8(May), 1–9. <https://doi.org/10.1038/ncomms16042>
- Jansen, A., & Andermann, E. (2005). Genetics of the polymicrogyria syndromes. In *Journal of Medical Genetics*. <https://doi.org/10.1136/jmg.2004.023952>
- Jen, J. C., Chan, W. M., Bosley, T. M., Wan, J., Carr, J. R., Rüb, U., Shattuck, D., Salamon, G., Kudo, L. C., Ou, J., Lin, D. D. M., Salih, M. A. M., Kansu, T., Al Dhalaan, H., Al Zayed, Z., MacDonald, D. B., Stigsby, B., Plaitakis, A., Dretakis, E. K., ... Engle, E. C. (2004). Mutations in a human ROBO gene disrupt hindbrain axon pathway crossing and morphogenesis. *Science*. <https://doi.org/10.1126/science.1096437>
- Johns, D. C., Marx, R., Mains, R. E., O'Rourke, B., & Marbán, E. (1999). Inducible genetic suppression of neuronal excitability. *Journal of Neuroscience*. <https://doi.org/10.1523/jneurosci.19-05-01691.1999>
- Jones, L., López-Bendito, G., Gruss, P., Stoykova, A., & Molnár, Z. (2002). Pax6 is required for the normal development of the forebrain axonal connections. *Development*.
- Joshi, P. S., Molyneaux, B. J., Feng, L., Xie, X., Macklis, J. D., & Gan, L. (2008). Bhlhb5 Regulates the Postmitotic Acquisition of Area Identities in Layers II-V of the Developing Neocortex. *Neuron*, 60(2), 258–272. <https://doi.org/10.1016/j.neuron.2008.08.006>
- Juric-Sekhar, G., & Hevner, R. F. (2019). Malformations of Cerebral Cortex Development: Molecules and Mechanisms. In *Annual Review of Pathology: Mechanisms of Disease*. <https://doi.org/10.1146/annurev-pathmechdis-012418-012927>
- Kandel, E. R., & Kandel, E.; Schwartz, J.; Jessel, T. M. (1991). Principles of Neural Science, Fifth Edition | AccessNeurology | McGraw-Hill Medical. In *Elsevier*.
- Kaneko, T., Caria, M. A., & Asanuma, H. (1994). Information processing within the motor cortex. II. Intracortical connections between neurons receiving somatosensory cortical input and motor output neurons of the cortex. *Journal of Comparative Neurology*. <https://doi.org/10.1002/cne.903450203>
- Kaprielian, Z., & Patterson, P. H. (1994). The molecular basis of retinotectal topography. In *BioEssays*. <https://doi.org/10.1002/bies.950160102>
- Kasai, H., Matsuzaki, M., Noguchi, J., Yasumatsu, N., & Nakahara, H. (2003). Structure-stability-function relationships of dendritic spines. In *Trends in Neurosciences*. [https://doi.org/10.1016/S0166-2236\(03\)00162-0](https://doi.org/10.1016/S0166-2236(03)00162-0)
- Kasper, E. M., Larkman, A. U., Lübke, J., & Blakemore, C. (1994). Pyramidal neurons in layer 5 of the rat visual cortex. I. Correlation among cell morphology, intrinsic electrophysiological properties, and axon targets. *Journal of Comparative Neurology*. <https://doi.org/10.1002/cne.903390402>

- Kilb, W., & Frotscher, M. (2016). Cajal-Retzius cells: organizers of cortical development. *E-Neuroforum*, 7(4), 82–88. <https://doi.org/10.1007/s13295-016-0031-5>
- Kim, D., & Ackerman, S. L. (2011). The UNC5C netrin receptor regulates dorsal guidance of mouse hindbrain axons. *Journal of Neuroscience*. <https://doi.org/10.1523/JNEUROSCI.5254-10.2011>
- Kirschuk, S., Sinning, A., Blanquie, O., Yang, J. W., Luhmann, H. J., & Kilb, W. (2017). Modulation of neocortical development by early neuronal activity: Physiology and pathophysiology. In *Frontiers in Cellular Neuroscience*. <https://doi.org/10.3389/fncel.2017.00379>
- Kirkby, L. A., Sack, G. S., Firl, A., & Feller, M. B. (2013). A role for correlated spontaneous activity in the assembly of neural circuits. In *Neuron*. <https://doi.org/10.1016/j.neuron.2013.10.030>
- Koenigkam-Santos, M., de Castro, M., Versiani, B. R., Diniz, P. R. B., & Santos, A. C. (2010). Kallmann syndrome and mirror movements: White matter quantitative evaluation with magnetic resonance imaging. *Journal of the Neurological Sciences*. <https://doi.org/10.1016/j.jns.2010.02.010>
- Kole, M. H. P., Bräuer, A. U., & Stuart, G. J. (2007). Inherited cortical HCN1 channel loss amplifies dendritic calcium electrogenesis and burst firing in a rat absence epilepsy model. *Journal of Physiology*. <https://doi.org/10.1113/jphysiol.2006.122028>
- Kole, M. H. P., & Stuart, G. J. (2012). Signal Processing in the Axon Initial Segment. In *Neuron*. <https://doi.org/10.1016/j.neuron.2012.01.007>
- Kordeli, E., Lambert, S., & Bennett, V. (1995). Ankyrin(G). A new ankyrin gene with neural-specific isoforms localized at the axonal initial segment and node of Ranvier. *Journal of Biological Chemistry*. <https://doi.org/10.1074/jbc.270.5.2352>
- Kostovic, I., & Rakic, P. (1990). Developmental history of the transient subplate zone in the visual and somatosensory cortex of the macaque monkey and human brain. *Journal of Comparative Neurology*. <https://doi.org/10.1002/cne.902970309>
- Krams, M., Quinton, R., Ashburner, J., Friston, K. J., Frackowiak, R. S. J., Bouloux, P. M. G., & Passingham, R. E. (1999). Kallmann's syndrome: Mirror movements associated with bilateral corticospinal tract hypertrophy. *Neurology*. <https://doi.org/10.1212/wnl.52.4.816>
- Kratochwil, C. F., Maheshwari, U., & Rijli, F. M. (2017). The Long Journey of Pontine Nuclei Neurons: From Rhombic Lip to Cortico-Ponto-Cerebellar Circuitry. *Frontiers in Neural Circuits*, 11(May), 1–19. <https://doi.org/10.3389/fncir.2017.00033>
- Kuba, H. (2010). Plasticity at the axon initial segment. *Communicative & Integrative Biology*. <https://doi.org/10.4161/cib.3.6.13242>
- Kuba, H., Oichi, Y., & Ohmori, H. (2010). Presynaptic activity regulates Na⁺ channel distribution at the axon initial segment. *Nature*. <https://doi.org/10.1038/nature09087>
- Kwan, K. Y., Šestan, N., & Anton, E. S. (2012). Transcriptional co-regulation of neuronal migration

- and laminar identity in the neocortex. In *Development*. <https://doi.org/10.1242/dev.069963>
- Lai, T., Jabaudon, D., Molyneaux, B. J., Azim, E., Arlotta, P., Menezes, J. R. L., & Macklis, J. D. (2008). SOX5 Controls the Sequential Generation of Distinct Corticofugal Neuron Subtypes. *Neuron*. <https://doi.org/10.1016/j.neuron.2007.12.023>
- Leergaard, T. B., Alloway, K. D., Mutic, J. J., & Bjaalie, J. G. (2000). Three-dimensional topography of corticopontine projections from rat barrel cortex: Correlations with corticostriatal organization. *Journal of Neuroscience*. <https://doi.org/10.1523/jneurosci.20-22-08474.2000>
- Leergaard, Trygve B., & Bjaalie, J. G. (2007). Topography of the complete corticopontine projection: From experiments to principal maps. *Frontiers in Neuroscience*, *1*(1), 211–223. <https://doi.org/10.3389/neuro.01.1.1.016.2007>
- Leergaard, Trygve B., Bjaalie, J. G., Devor, A., Wald, L. L., & Dale, A. M. (2003). In vivo tracing of major rat brain pathways using manganese-enhanced magnetic resonance imaging and three-dimensional digital atlas. *NeuroImage*. <https://doi.org/10.1016/j.neuroimage.2003.07.009>
- Leergaard, Trygve B., Lakke, E. A. J. F., & Bjaalie, J. G. (1995). Topographical organization in the early postnatal projection: A carbocyanine dye and 3-D computer reconstruction study in the rat. *Journal of Comparative Neurology*, *361*(1), 77–94. <https://doi.org/10.1002/cne.903610107>
- Leergaard, Trygve B., Lillehaug, S., De Schutter, E., Bower, J. M., & Bjaalie, J. G. (2006). Topographical organization of pathways from somatosensory cortex through the pontine nuclei to tactile regions of the rat cerebellar hemispheres. *European Journal of Neuroscience*, *24*(10), 2801–2812. <https://doi.org/10.1111/j.1460-9568.2006.05150.x>
- Leergaard, Trygve B., Lyngstad, K. A., Thompson, J. H., Taeymans, S., Vos, B. P., De Schutter, E., Bower, J. M., & Bjaalie, J. G. (2000). Rat somatosensory cerebropontocerebellar pathways: Spatial relationships of the somatotopic map of the primary somatosensory cortex are preserved in a three-dimensional clustered pontine map. *Journal of Comparative Neurology*. [https://doi.org/10.1002/\(SICI\)1096-9861\(20000626\)422:2<246::AID-CNE7>3.0.CO;2-R](https://doi.org/10.1002/(SICI)1096-9861(20000626)422:2<246::AID-CNE7>3.0.CO;2-R)
- Leergaard, T.B., Alloway, K.D., Mutic, J.J., and Bjaalie, J.G. (2000a). Three-dimensional topography of corticopontine projections from rat barrel cortex: correlations with corticostriatal organization. *J Neurosci* *20*, 8474-8484.
- Leergaard, T.B., and Bjaalie, J.G. (1995). Semi-automatic data acquisition for quantitative neuroanatomy. MicroTrace--computer programme for recording of the spatial distribution of neuronal populations. *Neurosci Res* *22*, 231-243.
- Leighton, P. A., Mitchell, K. J., Goodrich, L. V., Lu, X., Pinson, K., Scherz, P., Skarnes, W. C., & Tessier-Lavigne, M. (2001). Defining brain wiring patterns and mechanisms through gene trapping in mice. *Nature*. <https://doi.org/10.1038/35065539>
- Lein, E. S., Hawrylycz, M. J., Ao, N., Ayres, M., Bensinger, A., Bernard, A., Boe, A. F., Boguski, M. S.,

- Brockway, K. S., Byrnes, E. J., Chen, L., Chen, L., Chen, T. M., Chin, M. C., Chong, J., Crook, B. E., Czaplinska, A., Dang, C. N., Datta, S., ... Jones, A. R. (2007). Genome-wide atlas of gene expression in the adult mouse brain. *Nature*. <https://doi.org/10.1038/nature05453>
- Lemon, R.N. (2008). Descending pathways in motor control. *Annu Rev Neurosci* 31, 195-218.
- Lemon, R. N., Landau, W., Tutssel, D., & Lawrence, D. G. (2012). Lawrence and Kuypers (1968a, b) revisited: Copies of the original filmed material from their classic papers in Brain. *Brain*. <https://doi.org/10.1093/brain/aws037>
- Lendvai, B., Stern, E. A., Chen, B., & Svoboda, K. (2000). Experience-dependent plasticity of dendritic spines in the developing rat barrel cortex in vivo. *Nature*. <https://doi.org/10.1038/35009107>
- Leng, X., Cooney, A. J., Tsai, S. Y., & Tsai, M. J. (1996). Molecular mechanisms of COUP-TF-mediated transcriptional repression: evidence for transrepression and active repression. *Molecular and Cellular Biology*. <https://doi.org/10.1128/mcb.16.5.2332>
- Leone, D. P., Panagiotakos, G., Heavner, W. E., Joshi, P., Zhao, Y., Westphal, H., & McConnell, S. K. (2017). Compensatory Actions of Ldb Adaptor Proteins During Corticospinal Motor Neuron Differentiation. *Cerebral Cortex (New York, N.Y. : 1991)*. <https://doi.org/10.1093/cercor/bhw003>
- Leterrier, C. (2018). The Axon Initial Segment: An Updated Viewpoint. *The Journal of Neuroscience*, 38(9), 2135–2145. <https://doi.org/10.1523/jneurosci.1922-17.2018>
- Li, H., Fertuzinhos, S., Mohns, E., Hnasko, T. S., Verhage, M., Edwards, R., Sestan, N., & Crair, M. C. (2013). Laminar and Columnar Development of Barrel Cortex Relies on Thalamocortical Neurotransmission. *Neuron*. <https://doi.org/10.1016/j.neuron.2013.06.043>
- Li, S., Qiu, F., Xu, A., Price, S. M., & Xiang, M. (2004). Barhl1 Regulates Migration and Survival of Cerebellar Granule Cells by Controlling Expression of the Neurotrophin-3 Gene. *Journal of Neuroscience*. <https://doi.org/10.1523/JNEUROSCI.4444-03.2004>
- Li, Y., Muffat, J., Omer, A., Bosch, I., Lancaster, M. A., Sur, M., Gehrke, L., Knoblich, J. A., & Jaenisch, R. (2017). Induction of Expansion and Folding in Human Cerebral Organoids. *Cell Stem Cell*. <https://doi.org/10.1016/j.stem.2016.11.017>
- Lillehaug, S., Oyan, D., Leergaard, T.B., and Bjaalie, J.G. (2002). Comparison of semi-automatic and automatic data acquisition methods for studying three-dimensional distributions of large neuronal populations and axonal plexuses. *Network* 13, 343-356.
- Liu, Q., Dwyer, N. D., & O'Leary, D. D. M. (2000). Differential expression of COUP-TFI, CHL1, and two novel genes in developing neocortex identified by differential display PCR. *Journal of Neuroscience*. <https://doi.org/10.1523/jneurosci.20-20-07682.2000>
- Liu, Y., Shi, J., Lu, C. C., Wang, Z. B., Lyuksyutova, A. I., Song, X., & Zou, Y. (2005). Ryk-mediated Wnt repulsion regulates posterior-directed growth of corticospinal tract. *Nature Neuroscience*. <https://doi.org/10.1038/nn1520>

- Lodato, S., Tomassy, G. S., De Leonibus, E., Uzcategui, Y. G., Andolfi, G., Armentano, M., Touzot, A., Gaztelu, J. M., Arlotta, P., De La Prida, L. M., & Studer, M. (2011). Loss of COUP-TFI alters the balance between caudal ganglionic eminence- and medial ganglionic eminence-derived cortical interneurons and results in resistance to epilepsy. *Journal of Neuroscience*. <https://doi.org/10.1523/JNEUROSCI.6580-10.2011>
- Loots, G., & Ovcharenko, I. (2007). ECRbase: Database of evolutionary conserved regions, promoters, and transcription factor binding sites in vertebrate genomes. *Bioinformatics*. <https://doi.org/10.1093/bioinformatics/btl546>
- López-Bendito, G., Flames, N., Ma, L., Fouquet, C., Di Meglio, T., Chedotal, A., Tessier-Lavigne, M., & Marín, O. (2007). Robo1 and Robo2 cooperate to control the guidance of major axonal tracts in the mammalian forebrain. *Journal of Neuroscience*. <https://doi.org/10.1523/JNEUROSCI.4605-06.2007>
- López-Mascaraque, L., & De Castro, F. (2004). Protocortex versus protomap: A perspective from the olfactory bulb. *Revista de Neurologia*. <https://doi.org/10.33588/rn.3902.2004347>
- Lu, Z. (2004). Mechanism of rectification in inward-rectifier K⁺ channels. In *Annual Review of Physiology*. <https://doi.org/10.1146/annurev.physiol.66.032102.150822>
- Luhmann, H. J., & Khazipov, R. (2018). Neuronal activity patterns in the developing barrel cortex. In *Neuroscience*. <https://doi.org/10.1016/j.neuroscience.2017.05.025>
- Luhmann, H. J., Sinning, A., Yang, J. W., Reyes-Puerta, V., Stüttgen, M. C., Kirischuk, S., & Kilb, W. (2016). Spontaneous neuronal activity in developing neocortical networks: From single cells to large-scale interactions. In *Frontiers in Neural Circuits*. <https://doi.org/10.3389/fncir.2016.00040>
- Lupica, C. R., Bell, J. A., Hoffman, A. F., & Watson, P. L. (2001). Contribution of the hyperpolarization-activated current (I_h) to membrane potential and GABA release in hippocampal interneurons. *Journal of Neurophysiology*. <https://doi.org/10.1152/jn.2001.86.1.261>
- Magee, J. C. (1998). Dendritic hyperpolarization-activated currents modify the integrative properties of hippocampal CA1 pyramidal neurons. *Journal of Neuroscience*. <https://doi.org/10.1523/jneurosci.18-19-07613.1998>
- Maheshwari, U., Kraus, D., Vilain, N., Holwerda, S. J. B., Cankovic, V., Maiorano, N. A., Kohler, H., Satoh, D., Sigrist, M., Arber, S., Kratochwil, C. F., Di Meglio, T., Ducret, S., & Rijli, F. M. (2020). Postmitotic Hoxa5 Expression Specifies Pontine Neuron Positional Identity and Input Connectivity of Cortical Afferent Subsets. *Cell Reports*, *31*(11), 107767. <https://doi.org/10.1016/j.celrep.2020.107767>
- Majewska, A. K., Newton, J. R., & Sur, M. (2006). Remodeling of synaptic structure in sensory cortical areas In Vivo. *Journal of Neuroscience*. <https://doi.org/10.1523/JNEUROSCI.4454-05.2006>
- Maness, P. F., & Schachner, M. (2007). Neural recognition molecules of the immunoglobulin

- superfamily: Signaling transducers of axon guidance and neuronal migration. In *Nature Neuroscience*. <https://doi.org/10.1038/nn1827>
- Manuel, M., Georgala, P. A., Carr, C. B., Chanas, S., Kleinjan, D. A., Martynoga, B., Mason, J. O., Molinek, M., Pinson, J., Pratt, T., Quinn, J. C., Simpson, T. I., Tyas, D. A., van Heyningen, V., West, J. D., & Price, D. J. (2007). Controlled overexpression of Pax6 in vivo negatively auto-regulates the Pax6 locus, causing cell-autonomous defects of late cortical progenitor proliferation with little effect on cortical arealization. *Development*. <https://doi.org/10.1242/dev.02764>
- Marcorelles, P., & Laquerriere, A. (2010). Neuropathology of holoprosencephaly. In *American Journal of Medical Genetics, Part C: Seminars in Medical Genetics*. <https://doi.org/10.1002/ajmg.c.30249>
- Marillat, V., Sabatier, C., Failli, V., Matsunaga, E., Sotelo, C., Tessier-Lavigne, M., & Chédotal, A. (2004). The slit receptor Rig-1/Robo3 controls midline crossing by hindbrain precerebellar neurons and axons. *Neuron*. <https://doi.org/10.1016/j.neuron.2004.06.018>
- Marín, O., Baker, J., Puelles, L., & Rubenstein, J. L. R. (2002). Patterning of the basal telencephalon and hypothalamus is essential for guidance of cortical projections. *Development*.
- Marini, C., Porro, A., Rastetter, A., Dalle, C., Rivolta, I., Bauer, D., Oegema, R., Nava, C., Parrini, E., Mei, D., Mercer, C., Dhamija, R., Chambers, C., Coubes, C., Thévenon, J., Kuentz, P., Julia, S., Pasquier, L., Dubourg, C., ... Depienne, C. (2018). HCN1 mutation spectrum: From neonatal epileptic encephalopathy to benign generalized epilepsy and beyond. *Brain*. <https://doi.org/10.1093/brain/awy263>
- Martínez-Cerdeño, V., & Noctor, S. C. (2014). Cajal, Retzius, and Cajal-Retzius cells. In *Frontiers in Neuroanatomy*. <https://doi.org/10.3389/fnana.2014.00048>
- Massengill, J. L., Smith, M. A., Son, D. I., & O'Dowd, D. K. (1997). Differential expression of K(4-AP) currents and Kv3.1 potassium channel transcripts in cortical neurons that develop distinct firing phenotypes. *Journal of Neuroscience*. <https://doi.org/10.1523/jneurosci.17-09-03136.1997>
- Matsuzaki, M., Honkura, N., Ellis-Davies, G. C. R., & Kasai, H. (2004). Structural basis of long-term potentiation in single dendritic spines. *Nature*. <https://doi.org/10.1038/nature02617>
- Matyas, F., Sreenivasan, V., Marbach, F., Wacogne, C., Barsy, B., Mateo, C., Aronoff, R., & Petersen, C. C. H. (2010). Motor control by sensory cortex. *Science*. <https://doi.org/10.1126/science.1195797>
- Mayston, M. J., Harrison, L. M., Quinton, R., Stephens, J. A., Krams, M., & Bouloux, P. M. G. (1997). Mirror movements in X-linked Kallmann's syndrome. I. A neurophysiological study. *Brain*. <https://doi.org/10.1093/brain/120.7.1199>
- McKenna, W. L., Betancourt, J., Larkin, K. A., Abrams, B., Guo, C., Rubenstein, J. L. R., & Chen, B. (2011). Tbr1 and Fezf2 regulate alternate corticofugal neuronal identities during neocortical development. *Journal of Neuroscience*. <https://doi.org/10.1523/JNEUROSCI.4131-10.2011>

- Mihailoff, G.A., Lee, H., Watt, C.B., and Yates, R. (1985). Projections to the basilar pontine nuclei from face sensory and motor regions of the cerebral cortex in the rat. *J Comp Neurol* 237, 251-263.
- Mihailoff, G. A., Adams, C. E., & Woodward, D. J. (1984). An autoradiographic study of the postnatal development of sensorimotor and visual components of the corticopontine system. *Journal of Comparative Neurology*. <https://doi.org/10.1002/cne.902220110>
- Mimi Zhou, H., & Walthall, W. W. (1998). UNC-55, an orphan nuclear hormone receptor, orchestrates synaptic specificity among two classes of motor neurons in *Caenorhabditis elegans*. *Journal of Neuroscience*. <https://doi.org/10.1523/jneurosci.18-24-10438.1998>
- Mitchell, B. D., & Macklis, J. D. (2005). Large-scale maintenance of dual projections by callosal and frontal cortical projection neurons in adult mice. *Journal of Comparative Neurology*. <https://doi.org/10.1002/cne.20428>
- Molyneaux, B. J., Arlotta, P., Hirata, T., Hibi, M., & Macklis, J. D. (2005). Fezl is required for the birth and specification of corticospinal motor neurons. *Neuron*. <https://doi.org/10.1016/j.neuron.2005.08.030>
- Molyneaux, B. J., Arlotta, P., Menezes, J. R. L., & Macklis, J. D. (2007). Neuronal subtype specification in the cerebral cortex. *Nature Reviews Neuroscience*, 8(6), 427–437. <https://doi.org/10.1038/nrn2151>
- Montemayor, C., Montemayor, O. A., Ridgeway, A., Lin, F., Wheeler, D. A., Pletcher, S. D., & Pereira, F. A. (2010). Genome-wide analysis of binding sites and direct target genes of the orphan nuclear receptor NR2F1/COUP-TFI. *PLoS ONE*, 5(1). <https://doi.org/10.1371/journal.pone.0008910>
- Moody, W. J., & Bosma, M. M. (2005). Ion channel development, spontaneous activity, and activity-dependent development in nerve and muscle cells. In *Physiological Reviews*. <https://doi.org/10.1152/physrev.00017.2004>
- Moreno-Juan, V., Filipchuk, A., Antón-Bolaños, N., Mezzera, C., Gezelius, H., Andrés, B., Rodríguez-Malmierca, L., Susín, R., Schaad, O., Iwasato, T., Schüle, R., Rutlin, M., Nelson, S., Ducret, S., Valdeolmillos, M., Rijli, F. M., & López-Bendito, G. (2017). Prenatal thalamic waves regulate cortical area size prior to sensory processing. *Nature Communications*. <https://doi.org/10.1038/ncomms14172>
- Mosconi, M. W., Kay, M., D’Cruz, A. M., Seidenfeld, A., Guter, S., Stanford, L. D., & Sweeney, J. A. (2009). Impaired inhibitory control is associated with higher-order repetitive behaviors in autism spectrum disorders. *Psychological Medicine*, 39(9), 1559–1566. <https://doi.org/10.1017/S0033291708004984>
- Moyer, C. E., & Zuo, Y. (2018). Cortical dendritic spine development and plasticity: insights from in vivo imaging. In *Current Opinion in Neurobiology*. <https://doi.org/10.1016/j.conb.2018.06.002>
- Murase, S., Lantz, C. L., Kim, E., Gupta, N., Higgins, R., Stopfer, M., Hoffman, D. A., & Quinlan, E. M.

- (2016). Matrix Metalloproteinase-9 Regulates Neuronal Circuit Development and Excitability. *Molecular Neurobiology*. <https://doi.org/10.1007/s12035-015-9295-y>
- Nat, R., Apostolova, G., & Dechant, G. (2013). Telencephalic Neurogenesis Versus Telencephalic Differentiation of Pluripotent Stem Cells. In *Trends in Cell Signaling Pathways in Neuronal Fate Decision*. <https://doi.org/10.5772/54251>
- Nolan, M. F., Malleret, G., Dudman, J. T., Buhl, D. L., Santoro, B., Gibbs, E., Vronskaya, S., Buzsáki, G., Siegelbaum, S. A., Kandel, E. R., & Morozov, A. (2004). A behavioral role for dendritic integration: HCN1 channels constrain spatial memory and plasticity at inputs to distal dendrites of CA1 pyramidal neurons. *Cell*. <https://doi.org/10.1016/j.cell.2004.11.020>
- O'Leary, D. D.M., Heffner, C. D., Kutka, L., Lopez-Mascaraque, L., Missias, A., & Reinoso, B. S. (1991). A target-derived chemoattractant controls the development of the corticopontine projection by a novel mechanism of axon targeting. *Development*.
- O'Leary, D. D. M. (1989). Do cortical areas emerge from a protocortex? *Trends in Neurosciences*, 12(10), 400–406. [https://doi.org/10.1016/0166-2236\(89\)90080-5](https://doi.org/10.1016/0166-2236(89)90080-5)
- O'Leary, D. D. M., Chou, S. J., & Sahara, S. (2007). Area patterning of the mammalian cortex. *Neuron*, 56(2), 252–269. <https://doi.org/10.1016/j.neuron.2007.10.010>
- O'Leary, D. D. M., & Sahara, S. (2008). Genetic regulation of arealization of the neocortex. *Current Opinion in Neurobiology*, 18(1), 90–100. <https://doi.org/10.1016/j.conb.2008.05.011>
- O'Leary, D. D. M., Schlaggar, B. L., & Stanfield, B. B. (1992). The specification of sensory cortex: Lessons from cortical transplantation. *Experimental Neurology*. [https://doi.org/10.1016/0014-4886\(92\)90234-H](https://doi.org/10.1016/0014-4886(92)90234-H)
- O'Leary, D. D. M., & Terashima, T. (1988). Cortical axons branch to multiple subcortical targets by interstitial axon budding: Implications for target recognition and “waiting periods.” *Neuron*, 1(10), 901–910. [https://doi.org/10.1016/0896-6273\(88\)90147-X](https://doi.org/10.1016/0896-6273(88)90147-X)
- Oh, S. W., Harris, J. A., Ng, L., Winslow, B., Cain, N., Mihalas, S., Wang, Q., Lau, C., Kuan, L., Henry, A. M., Mortrud, M. T., Ouellette, B., Nguyen, T. N., Sorensen, S. A., Slaughterbeck, C. R., Wakeman, W., Li, Y., Feng, D., Ho, A., ... Zeng, H. (2014). A mesoscale connectome of the mouse brain. *Nature*. <https://doi.org/10.1038/nature13186>
- Okada, T., Keino-Masu, K., & Masu, M. (2007). Migration and nucleogenesis of mouse precerebellar neurons visualized by in utero electroporation of a green fluorescent protein gene. *Neuroscience Research*, 57(1), 40–49. <https://doi.org/10.1016/j.neures.2006.09.010>
- Olson, E. C. (2014). Analysis of preplate splitting and early cortical development illuminates the biology of neurological disease. In *Frontiers in Pediatrics*. <https://doi.org/10.3389/fped.2014.00121>
- Oswald, M. J., Tantirigama, M. L. S., Sonntag, I., Hughes, S. M., & Empson, R. M. (2013). Diversity of

- layer 5 projection neurons in the mouse motor cortex. *Frontiers in Cellular Neuroscience*, 7(October), 1–18. <https://doi.org/10.3389/fncel.2013.00174>
- Özdinler, P. H., & Macklis, J. D. (2006). IGF-I specifically enhances axon outgrowth of corticospinal motor neurons. *Nature Neuroscience*. <https://doi.org/10.1038/nn1789>
- Paixão, S., Balijepalli, A., Serradj, N., Niu, J., Luo, W., Martin, J. H., & Klein, R. (2013). EphrinB3/EphA4-mediated guidance of ascending and descending spinal tracts. *Neuron*. <https://doi.org/10.1016/j.neuron.2013.10.006>
- Papp, E. A., Leergaard, T. B., Csucs, G., & Bjaalie, J. G. (2016). Brain-Wide Mapping of Axonal Connections: Workflow for Automated Detection and Spatial Analysis of Labeling in Microscopic Sections. *Frontiers in Neuroinformatics*, 10(April), 1–11. <https://doi.org/10.3389/fninf.2016.00011>
- Parisot, J., Flore, G., Bertacchi, M., & Studer, M. (2017). COUP-TFI mitotically regulates production and migration of dentate granule cells and modulates hippocampal Cxcr4 expression. *Development (Cambridge)*. <https://doi.org/10.1242/dev.139949>
- Parrini, E., Conti, V., Dobyns, W. B., & Guerrini, R. (2016). Genetic basis of brain malformations. In *Molecular Syndromology*. <https://doi.org/10.1159/000448639>
- Pearson, R. A., Catsicas, M., Becker, D. L., Bayley, P., Lüneborg, N. L., & Mobbs, P. (2004). Ca²⁺ signalling and gap junction coupling within and between pigment epithelium and neural retina in the developing chick. *European Journal of Neuroscience*. <https://doi.org/10.1111/j.0953-816X.2004.03338.x>
- Petersen, A. V., Cotel, F., & Perrier, J. F. (2017). Plasticity of the Axon Initial Segment: Fast and Slow Processes with Multiple Functional Roles. *Neuroscientist*. <https://doi.org/10.1177/1073858416648311>
- Petersen, S. C., Watson, J. D., Richmond, J. E., Sarov, M., Walthall, W. W., & Miller, D. M. (2011). A transcriptional program promotes remodeling of GABAergic synapses in *Caenorhabditis elegans*. *Journal of Neuroscience*. <https://doi.org/10.1523/JNEUROSCI.3181-11.2011>
- Polleux, F., Dehay, C., and Kennedy, H. (1997). The timetable of laminar neurogenesis contributes to the specification of cortical areas in mouse isocortex. *J Comp Neurol* 385, 95-116.
- Poolos, N. P., Bullis, J. B., & Roth, M. K. (2006). Modulation of h-channels in hippocampal pyramidal neurons by p38 mitogen-activated protein kinase. *Journal of Neuroscience*. <https://doi.org/10.1523/JNEUROSCI.2069-06.2006>
- Poolos, N. P., Migliore, M., & Johnston, D. (2002). Pharmacological upregulation of h-channels reduces the excitability of pyramidal neuron dendrites. *Nature Neuroscience*. <https://doi.org/10.1038/nn891>

- Porrero, C., Rubio-Garrido, P., Avendaño, C., & Clascá, F. (2010). Mapping of fluorescent protein-expressing neurons and axon pathways in adult and developing Thy1-eYFP-H transgenic mice. *Brain Research*, *1345*, 59–72. <https://doi.org/10.1016/j.brainres.2010.05.061>
- Powell, A. W., Sassa, T., Wu, Y., Tessier-Lavigne, M., & Polleux, F. (2008). Topography of thalamic projections requires attractive and repulsive functions of netrin-1 in the ventral telencephalon. *PLoS Biology*. <https://doi.org/10.1371/journal.pbio.0060116>
- Pratt, T., Vitalis, T., Warren, N., Edgar, J. M., Mason, J. O., & Price, D. J. (2000). A role for Pax6 in the normal development of dorsal thalamus and its cortical connections. *Development*.
- Proville, R. D., Spolidoro, M., Guyon, N., Dugué, G. P., Selimi, F., Isope, P., Popa, D., & Léna, C. (2014). Cerebellum involvement in cortical sensorimotor circuits for the control of voluntary movements. *Nature Neuroscience*. <https://doi.org/10.1038/nn.3773>
- Puchades, M. A., Csucs, G., Ledergerber, D., Leergaard, T. B., & Bjaalie, J. G. (2019). Spatial registration of serial microscopic brain images to three-dimensional reference atlases with the QuickNII tool. *PLoS ONE*. <https://doi.org/10.1371/journal.pone.0216796>
- Qiu, Y., Cooney, A. J., Kuratani, S., DeMayo, F. J., Tsai, S. Y., & Tsai, M. J. (1994). Spatiotemporal expression patterns of chicken ovalbumin upstream promoter- transcription factors in the developing mouse central nervous system: Evidence for a role in segmental patterning of the diencephalon. *Proceedings of the National Academy of Sciences of the United States of America*. <https://doi.org/10.1073/pnas.91.10.4451>
- Qiu, Yuhong, Pereira, F. A., DeMayo, F. J., Lydon, J. P., Tsai, S. Y., & Tsai, M. J. (1997). Null mutation of mCOUP-TFI results in defects in morphogenesis of the glossopharyngeal ganglion, axonal projection, and arborization. *Genes and Development*. <https://doi.org/10.1101/gad.11.15.1925>
- Quandt, K., Frech, K., Karas, H., Wingender, E., & Werner, T. (1995). MatInd and matInspector: New fast and versatile tools for detection of consensus matches in nucleotide sequence data. *Nucleic Acids Research*. <https://doi.org/10.1093/nar/23.23.4878>
- R Development Core Team, R. (2011). R: A Language and Environment for Statistical Computing. In *R Foundation for Statistical Computing*. <https://doi.org/10.1007/978-3-540-74686-7>
- Rakic, P. (1988). Specification of Cerebral Cortical Areas Cortical Neurons Originate Outside the. *Science (New York, N.Y.)*, *241*, 170–176.
- Rakic, P., Ayoub, A. E., Breunig, J. J., & Dominguez, M. H. (2009). Decision by division: making cortical maps. In *Trends in Neurosciences*. <https://doi.org/10.1016/j.tins.2009.01.007>
- Ramaswamy, S., & Markram, H. (2015). Anatomy and physiology of the thick-tufted layer 5 pyramidal neuron. *Frontiers in Cellular Neuroscience*, *9*(JUNE), 1–29. <https://doi.org/10.3389/fncel.2015.00233>

- Rech, M. E., McCarthy, J. M., Chen, C. A., Edmond, J. C., Shah, V. S., Bosch, D. G. M., Berry, G. T., Williams, L., Madan-Khetarpal, S., Niyazov, D., Shaw-Smith, C., Kovar, E. M., Lupo, P. J., & Schaaf, C. P. (2020). Phenotypic expansion of Bosch–Boonstra–Schaaf optic atrophy syndrome and further evidence for genotype–phenotype correlations. *American Journal of Medical Genetics, Part A, October 2019*, 1–12. <https://doi.org/10.1002/ajmg.a.61580>
- Robertson, J., Hatton, C., Emerson, E., & Baines, S. (2015). Prevalence of epilepsy among people with intellectual disabilities: A systematic review. In *Seizure*. <https://doi.org/10.1016/j.seizure.2015.03.016>
- Roerig, B., & Feller, M. B. (2000). Neurotransmitters and gap junctions in developing neural circuits. In *Brain Research Reviews*. [https://doi.org/10.1016/S0165-0173\(99\)00069-7](https://doi.org/10.1016/S0165-0173(99)00069-7)
- Roessmann, U., & Hori, A. (1985). Agyria (lissencephaly) with anomalous pyramidal crossing. Case report and review of literature. *Journal of the Neurological Sciences*. [https://doi.org/10.1016/0022-510X\(85\)90146-7](https://doi.org/10.1016/0022-510X(85)90146-7)
- Rubenstein, J. L. R., & Rakic, P. (1999). Genetic control of cortical development. In *Cerebral Cortex*. <https://doi.org/10.1093/cercor/9.6.521>
- Rünker, A. E., O’Tuathaigh, C., Dunleavy, M., Morris, D. W., Little, G. E., Corvin, A. P., Gill, M., Henshall, D. C., Waddington, J. L., Mitchell, K. J., Tuathaigh, C. O., Dunleavy, M., Morris, D. W., Little, G. E., Aiden, P., Ru, A. E., Gill, M., Henshall, D. C., Waddington, J. L., ... Mitchell, K. J. (2011). Mutation of Semaphorin-6A disrupts limbic and cortical connectivity and models neurodevelopmental psychopathology. *PLoS ONE*, 6(11). <https://doi.org/10.1371/journal.pone.0026488>
- Rünker, A. E., Rünker, A. E., Little, G. E., Suto, F., Fujisawa, H., & Mitchell, K. J. (2008). *Semaphorin-6A controls guidance of corticospinal tract axons at multiple choice points multiple choice points*. December. <https://doi.org/10.1186/1749-8104-3-34>
- Saito, T., & Nakatsuji, N. (2001). Efficient gene transfer into the embryonic mouse brain using in vivo electroporation. *Developmental Biology*. <https://doi.org/10.1006/dbio.2001.0439>
- Schallert, T., Fleming, S. M., Leasure, J. L., Tillerson, J. L., & Bland, S. T. (2000). CNS plasticity and assessment of forelimb sensorimotor outcome in unilateral rat models of stroke, cortical ablation, parkinsonism and spinal cord injury. *Neuropharmacology*. [https://doi.org/10.1016/S0028-3908\(00\)00005-8](https://doi.org/10.1016/S0028-3908(00)00005-8)
- Schellekens, W., Petridou, N., & Ramsey, N. F. (2018). Detailed somatotopy in primary motor and somatosensory cortex revealed by Gaussian population receptive fields. *NeuroImage*. <https://doi.org/10.1016/j.neuroimage.2018.06.062>
- Schindelin, J., Arganda-Carreras, I., Frise, E., Kaynig, V., Longair, M., Pietzsch, T., Preibisch, S., Rueden, C., Saalfeld, S., Schmid, B., Tinevez, J. Y., White, D. J., Hartenstein, V., Eliceiri, K., Tomancak, P., & Cardona, A. (2012). Fiji: An open-source platform for biological-image analysis. In *Nature Methods*. <https://doi.org/10.1038/nmeth.2019>

- Schindelin, J., Rueden, C. T., Hiner, M. C., & Eliceiri, K. W. (2015). The ImageJ ecosystem: An open platform for biomedical image analysis. In *Molecular Reproduction and Development*. <https://doi.org/10.1002/mrd.22489>
- Schmahmann, J. D., & Pandya, D. N. (1997). The cerebrocerebellar system. *International Review of Neurobiology*. [https://doi.org/10.1016/s0074-7742\(08\)60346-3](https://doi.org/10.1016/s0074-7742(08)60346-3)
- Schneggenburger, R., & Rosenmund, C. (2015). Molecular mechanisms governing Ca²⁺ regulation of evoked and spontaneous release. In *Nature Neuroscience*. <https://doi.org/10.1038/nn.4044>
- Schwarz, C., & Thier, P. (1999). Binding of signals relevant for action: Towards a hypothesis of the functional role of the pontine nuclei. In *Trends in Neurosciences*. [https://doi.org/10.1016/S0166-2236\(99\)01446-0](https://doi.org/10.1016/S0166-2236(99)01446-0)
- Sebastián-Serrano, A., Sandonis, A., Cardozo, M., Rodríguez-Tornos, F. M., Bovolenta, P., & Nieto, M. (2012). Pax6 expression in postmitotic neurons mediates the growth of axons in response to SFRP1. *PLoS ONE*. <https://doi.org/10.1371/journal.pone.0031590>
- Shah, M. M. (2014). Cortical HCN channels: Function, trafficking and plasticity. *Journal of Physiology*. <https://doi.org/10.1113/jphysiol.2013.270058>
- Shambes, G.M., Gibson, J.M., and Welker, W. (1978). Fractured somatotopy in granule cell tactile areas of rat cerebellar hemispheres revealed by micromapping. *Brain, behavior and evolution* 15, 94-140.
- Shepherd, G.M. (2009). Intracortical cartography in an agranular area. *Front Neurosci* 3, 337-343.
- Shetty, A. S., Godbole, G., Maheshwari, U., Padmanabhan, H., Chaudhary, R., Muralidharan, B., Hou, P. S., Monuki, E. S., Kuo, H. C., Rema, V., & Tole, S. (2013). Lhx2 regulates a cortex-specific mechanism for barrel formation. *Proceedings of the National Academy of Sciences of the United States of America*. <https://doi.org/10.1073/pnas.1311158110>
- Shinmyo, Y., Riyadh, M. A., Ahmed, G., Naser, I. Bin, Hossain, M., Takebayashi, H., Kawasaki, H., Ohta, K., & Tanaka, H. (2015). Draxin from neocortical neurons controls the guidance of thalamocortical projections into the neocortex. *Nature Communications*. <https://doi.org/10.1038/ncomms10232>
- Shinohara, M., Zhu, Y., & Murakami, F. (2013). Four-dimensional analysis of nucleogenesis of the pontine nucleus in the hindbrain. *Journal of Comparative Neurology*. <https://doi.org/10.1002/cne.23353>
- Simi, A., & Studer, M. (2018). Developmental genetic programs and activity-dependent mechanisms instruct neocortical area mapping. *Current Opinion in Neurobiology*, 53, 96–102. <https://doi.org/10.1016/j.conb.2018.06.007>
- Simmons, P. A., Lemmon, V., & Pearlman, A. L. (1982). Afferent and efferent connections of the striate and extrastriate visual cortex of the normal and reeler mouse. *Journal of Comparative*

Neurology. <https://doi.org/10.1002/cne.902110308>

- Simonyan, K. (2019). Recent advances in understanding the role of the basal ganglia. *F1000Research*. <https://doi.org/10.12688/f1000research.16524.1>
- Smart, I.H. (1984). Histogenesis of the mesocortical area of the mouse telencephalon. *J Anat* 138 (Pt 3), 537-552.
- Squire, L. E., Berg, D., Bloom, F. E., du Lac, S., Ghosh, A., & Spitzer, N. C. (2013). *Fundamental Neuroscience*. In *Fundamental Neuroscience*. Elsevier. <https://doi.org/10.1016/C2010-0-65035-8>
- Srivatsa, S., Parthasarathy, S., Molnár, Z., & Tarabykin, V. (2015). Sip1 downstream effector ninein controls neocortical axonal growth, ipsilateral branching, and microtubule growth and stability. *Neuron*. <https://doi.org/10.1016/j.neuron.2015.01.018>
- Starkey, M. L., Barritt, A. W., Yip, P. K., Davies, M., Hamers, F. P. T., McMahon, S. B., & Bradbury, E. J. (2005). Assessing behavioural function following a pyramidotomy lesion of the corticospinal tract in adult mice. *Experimental Neurology*. <https://doi.org/10.1016/j.expneurol.2005.06.017>
- Sun, T., & Hevner, R. F. (2014). Growth and folding of the mammalian cerebral cortex: from molecules to malformations. In *Nature Reviews Neuroscience*. <https://doi.org/10.1038/nrn3707>
- Supèr, H., Soriano, E., & Uylings, H. B. M. (1998). The functions of the preplate in development and evolution of the neocortex and hippocampus. *Brain Research Reviews*. [https://doi.org/10.1016/S0165-0173\(98\)00005-8](https://doi.org/10.1016/S0165-0173(98)00005-8)
- Suter, B. A., Migliore, M., & Shepherd, G. M. G. (2013). Intrinsic electrophysiology of mouse corticospinal neurons: A class-specific triad of spike-related properties. *Cerebral Cortex*. <https://doi.org/10.1093/cercor/bhs184>
- Svoboda, K., and Li, N. (2018). Neural mechanisms of movement planning: motor cortex and beyond. *Curr Opin Neurobiol* 49, 33-41.
- Swinnen, N., Smolders, S., Avila, A., Notelaers, K., Paesen, R., Ameloot, M., Brône, B., Legendre, P., & Rigo, J.-M. (2013). Complex invasion pattern of the cerebral cortex by microglial cells during development of the mouse embryo. *Glia*, 61(2), 150–163. <https://doi.org/10.1002/glia.22421>
- Tamburin, S., Manganotti, P., Zanette, G., & Fiaschi, A. (2002). Cutaneomotor integration in human hand motor areas: somatotopic effect and interaction of afferents. *Experimental Brain Research*.
- Tan, X., & Shi, S. H. (2013). Neocortical neurogenesis and neuronal migration. In *Wiley Interdisciplinary Reviews: Developmental Biology*. <https://doi.org/10.1002/wdev.88>
- Ten Donkelaar, H. J., Lammens, M., Wesseling, P., Hori, A., Keyser, A., & Rotteveel, J. (2004). Development and malformations of the human pyramidal tract. In *Journal of Neurology*.

<https://doi.org/10.1007/s00415-004-0653-3>

- Tennant, K. A., Asay, A. L., Allred, R. P., Ozburn, A. R., Kleim, J. A., & Jones, T. A. (2010). The vermicelli and capellini handling tests: Simple quantitative measures of dexterous forepaw function in rats and mice. *Journal of Visualized Experiments*. <https://doi.org/10.3791/2076>
- Terashima, T., Inoue, K., Inoue, Y., & Mikoshiba, K. (1987). Thalamic connectivity of the primary motor cortex of normal and reeler mutant mice. *Journal of Comparative Neurology*. <https://doi.org/10.1002/cne.902570309>
- Thuault, S. J., Malleret, G., Constantinople, C. M., Nicholls, R., Chen, I., Zhu, J., Panteleyev, A., Vronskaya, S., Nolan, M. F., Bruno, R., Siegelbaum, S. A., & Kandel, E. R. (2013). Prefrontal cortex HCN1 channels enable intrinsic persistent neural firing and executive memory function. *Journal of Neuroscience*. <https://doi.org/10.1523/JNEUROSCI.2427-12.2013>
- Tian, T., Yang, Z., & Li, X. (2020). Tissue clearing technique: Recent progress and biomedical applications. In *Journal of Anatomy*. <https://doi.org/10.1111/joa.13309>
- Tien, N., & Kerschensteiner, D. (2018). *Homeostatic plasticity in neural development*. 1–7.
- Tissir, F., Bar, I., Jossin, Y., & Goffinet, A. M. (2005). Protocadherin Celsr3 is crucial in axonal tract development. *Nature Neuroscience*. <https://doi.org/10.1038/nn1428>
- Tjia, M., Yu, X., Jammu, L. S., Lu, J., & Zuo, Y. (2017). Pyramidal neurons in different cortical layers exhibit distinct dynamics and plasticity of apical dendritic spines. *Frontiers in Neural Circuits*. <https://doi.org/10.3389/fncir.2017.00043>
- Tlamsa, A. P., & Brumberg, J. C. (2010). Organization and morphology of thalamocortical neurons of mouse ventral lateral thalamus. *Somatosensory and Motor Research*. <https://doi.org/10.3109/08990221003646736>
- Tolkien J. R. R. (1991). *The lord of the rings*. HarperCollins.
- Tomasch, J. (1968). The overall information carrying capacity of the major afferent and efferent cerebellar cell and fiber systems. *Confin Neurol* 30, 359-367.
- Tomasch, J. (1969). The numerical capacity of the human cortico-pontocerebellar system. *Brain Res* 13, 476-484.
- Tomassy, G. S., De Leonibus, E., Jabaudon, D., Lodato, S., Alfano, C., Mele, A., Macklis, J. D., & Studer, M. (2010). Area-specific temporal control of corticospinal motor neuron differentiation by COUP-TFI. *Proceedings of the National Academy of Sciences of the United States of America*, 107(8), 3576–3581. <https://doi.org/10.1073/pnas.0911792107>
- Touzot, A., Ruiz-Reig, N., Vitalis, T., & Studer, M. (2016). Molecular control of two novel migratory paths for CGE-derived interneurons in the developing mouse brain. *Development (Cambridge)*. <https://doi.org/10.1242/dev.131102>

- Toyoda, R., Assimacopoulos, S., Wilcoxon, J., Taylor, A., Feldman, P., Suzuki-Hirano, A., Shimogori, T., and Grove, E.A. (2010). FGF8 acts as a classic diffusible morphogen to pattern the neocortex. *Development* 137, 3439-3448.
- Trachtenberg, J. T., Chen, B. E., Knott, G. W., Feng, G., Sanes, J. R., Welker, E., & Svoboda, K. (2002). Long-term in vivo imaging of experience-dependent synaptic plasticity in adult cortex. *Nature*. <https://doi.org/10.1038/nature01273>
- Tritsch, N. X., Yi, E., Gale, J. E., Glowatzki, E., & Bergles, D. E. (2007). The origin of spontaneous activity in the developing auditory system. *Nature*. <https://doi.org/10.1038/nature06233>
- Tseng, G. -F, & Prince, D. A. (1993). Heterogeneity of rat corticospinal neurons. *Journal of Comparative Neurology*. <https://doi.org/10.1002/cne.903350107>
- Uhlén, P., Fritz, N., Smedler, E., Malmersjö, S., & Kanatani, S. (2015). Calcium signaling in neocortical development. *Developmental Neurobiology*. <https://doi.org/10.1002/dneu.22273>
- Vale, T. C., Pedroso, J. L., Rivero, R. L. M., Mandeli, A. S., Dias-da-Silva, M. R., & Barsottini, O. G. (2017). Lack of decussation of pyramids in Kallmann syndrome presenting with mirror movements. In *Journal of the Neurological Sciences*. <https://doi.org/10.1016/j.jns.2016.11.051>
- van Tilborg, E., de Theije, C. G. M., van Hal, M., Wagenaar, N., de Vries, L. S., Benders, M. J., Rowitch, D. H., & Nijboer, C. H. (2018). Origin and dynamics of oligodendrocytes in the developing brain: Implications for perinatal white matter injury. In *GLIA*. <https://doi.org/10.1002/glia.23256>
- van Welie, I., Remme, M. W. H., van Hooft, J. A., & Wadman, W. J. (2006). Different levels of Ih determine distinct temporal integration in bursting and regular-spiking neurons in rat subiculum. *Journal of Physiology*. <https://doi.org/10.1113/jphysiol.2006.113944>
- Viswanathan, S., Williams, M. E., Bloss, E. B., Stasevich, T. J., Speer, C. M., Nern, A., Pfeiffer, B. D., Hooks, B. M., Li, W. P., English, B. P., Tian, T., Henry, G. L., Macklin, J. J., Patel, R., Gerfen, C. R., Zhuang, X., Wang, Y., Rubin, G. M., & Looger, L. L. (2015). High-performance probes for light and electron microscopy. *Nature Methods*, 12(6), 568–576. <https://doi.org/10.1038/nmeth.3365>
- Voogd, J. (1995) Cerebellum. In Bannister, L.H., Berry, M.M., Collins, P., Dyson, M., Dussek, J.E. & Ferguson, M.W.J., (Eds), *Gray's Anatomy*. Churchill Livingstone, New York, pp. 1027-1065.
- Wang, C. F., Hsing, H. W., Zhuang, Z. H., Wen, M. H., Chang, W. J., Briz, C. G., Nieto, M., Shyu, B. C., & Chou, S. J. (2017). Lhx2 Expression in Postmitotic Cortical Neurons Initiates Assembly of the Thalamocortical Somatosensory Circuit. *Cell Reports*. <https://doi.org/10.1016/j.celrep.2017.01.001>
- Wang, Q., Ding, S.L., Li, Y., Royall, J., Feng, D., Lesnar, P., Graddis, N., Naemi, M., Facer, B., Ho, A., et al. (2020). The Allen Mouse Brain Common Coordinate Framework: A 3D Reference Atlas. *Cell* 181, 936-953 e920.

- Wang, Y., Thekdi, N., Smallwood, P. M., Macke, J. P., & Nathans, J. (2002). Frizzled-3 is required for the development of major fiber tracts in the rostral CNS. *Journal of Neuroscience*. <https://doi.org/10.1523/jneurosci.22-19-08563.2002>
- Wang, Z., Xu, N. L., Wu, C. P., Duan, S., & Poo, M. M. (2003). Bidirectional changes in spatial dendritic integration accompanying long-term synaptic modifications. *Neuron*. [https://doi.org/10.1016/S0896-6273\(02\)01189-3](https://doi.org/10.1016/S0896-6273(02)01189-3)
- Watson, C., Paxinos, G., & Puelles, L. (2012). The Mouse Nervous System. In *The Mouse Nervous System*. <https://doi.org/10.1016/C2009-0-00185-8>
- Wefelmeyer, W., Puhl, C. J., & Burrone, J. (2016). Homeostatic Plasticity of Subcellular Neuronal Structures: From Inputs to Outputs. In *Trends in Neurosciences*. <https://doi.org/10.1016/j.tins.2016.08.004>
- Welker W (1987) Spatial organization of somatosensory projections to granule cell cerebellar cortex: functional and connectational implications of fractured somatotopy (summary of Wisconsin studies). In: King JS (ed) New concepts in cerebellar neurobiology. Liss, New York, pp 239-280
- Weimann, J. M., Zhang, Y. A., Levin, M. E., Devine, W. P., Brûlet, P., & McConnell, S. K. (1999). Cortical neurons require Otx1 for the refinement of exuberant axonal projections to subcortical targets. *Neuron*. [https://doi.org/10.1016/S0896-6273\(00\)81030-2](https://doi.org/10.1016/S0896-6273(00)81030-2)
- Welker, C. (1971). Microelectrode delineation of fine grain somatotopic organization of Sml cerebral neocortex in albino rat. *Brain Research*. [https://doi.org/10.1016/S0006-8993\(71\)80004-5](https://doi.org/10.1016/S0006-8993(71)80004-5)
- Welniarz, Q., Dusart, I., & Roze, E. (2017). The corticospinal tract: Evolution, development, and human disorders. *Developmental Neurobiology*, 810–829. <https://doi.org/10.1002/dneu.22455>
- Welniarz, Q., Morel, M. P., Pourchet, O., Gallea, C., Lamy, J. C., Cincotta, M., Doulazmi, M., Belle, M., Méneret, A., Trouillard, O., Ruiz, M., Brochard, V., Meunier, S., Trembleau, A., Vidailhet, M., Chédotal, A., Dusart, I., & Roze, E. (2017). Non cell-autonomous role of DCC in the guidance of the corticospinal tract at the midline. *Scientific Reports*. <https://doi.org/10.1038/s41598-017-00514-z>
- Williams, R. S., Swisher, C. N., Jennings, M., Ambler, M., & Caviness, V. S. (1984). Cerebro-ocular dysgenesis (Walker-Warburg syndrome): Neuropathologic and etiologic analysis. *Neurology*. <https://doi.org/10.1212/wnl.34.12.1531>
- Williams, S. R., & Stuart, G. J. (2000). Site independence of EPSP time course is mediated by dendritic I(h) in neocortical pyramidal neurons. *Journal of Neurophysiology*. <https://doi.org/10.1152/jn.2000.83.5.3177>
- Williams, S. R., & Stuart, G. J. (2003). Voltage- and site-dependent control of the somatic impact of dendritic IPSPs. *Journal of Neuroscience*. <https://doi.org/10.1523/jneurosci.23-19-07358.2003>
- Wonders, C. P., & Anderson, S. A. (2006). The origin and specification of cortical interneurons.

Nature Reviews. Neuroscience, 7(9), 687–696. <https://doi.org/10.1038/nrn1954>

- Woolsey, T. A., & Van der Loos, H. (1970). The structural organization of layer IV in the somatosensory region (S I) of mouse cerebral cortex. *Brain Research*. [https://doi.org/10.1016/0006-8993\(70\)90079-x](https://doi.org/10.1016/0006-8993(70)90079-x)
- Wright, A. G., Demyanenko, G. P., Powell, A., Schachner, M., Enriquez-Barreto, L., Tran, T. S., Polleux, F., & Maness, P. F. (2007). Close homolog of L1 and neuropilin 1 mediate guidance of thalamocortical axons at the ventral telencephalon. *Journal of Neuroscience*. <https://doi.org/10.1523/JNEUROSCI.2888-07.2007>
- Wu, S. P., Lee, D. K., DeMayo, F. J., Tsai, S. Y., & Tsai, M. J. (2010). Generation of ES cells for conditional expression of nuclear receptors and coregulators in vivo. *Molecular Endocrinology*. <https://doi.org/10.1210/me.2010-0068>
- Yamada, R., & Kuba, H. (2016). Structural and functional plasticity at the axon initial segment. *Frontiers in Cellular Neuroscience*. <https://doi.org/10.3389/fncel.2016.00250>
- Yamamoto, N., & López-Bendito, G. (2012). Shaping brain connections through spontaneous neural activity. *European Journal of Neuroscience*. <https://doi.org/10.1111/j.1460-9568.2012.08101.x>
- Zelina, P., Blockus, H., Zagar, Y., Péres, A., Friocourt, F., Wu, Z., Rama, N., Fouquet, C., Hohenester, E., Tessier-Lavigne, M., Schweitzer, J., Roest Crolius, H., & Chédotal, A. (2014). Signaling switch of the axon guidance receptor Robo3 during vertebrate evolution. *Neuron*. <https://doi.org/10.1016/j.neuron.2014.11.004>
- Zembrzycki, A., Chou, S. J., Ashery-Padan, R., Stoykova, A., & O'Leary, D. D. M. (2013). Sensory cortex limits cortical maps and drives top-down plasticity in thalamocortical circuits. *Nature Neuroscience*. <https://doi.org/10.1038/nn.3454>
- Zhang, K., Yu, F., Zhu, J., Han, S., Chen, J., Wu, X., Chen, Y., Shen, T., Liao, J., Guo, W., Yang, X., Wang, R., Qian, Y., Yang, J., Cheng, L., Zhao, Y., Hui, C. C., Li, J., Peng, G., ... Tang, K. (2020). Imbalance of Excitatory/Inhibitory Neuron Differentiation in Neurodevelopmental Disorders with an NR2F1 Point Mutation. *Cell Reports*, 31(3), 1.e1-1.e25. <https://doi.org/10.1016/j.celrep.2020.03.085>
- Zhang, Y., Bonnan, A., Bony, G., Ferezou, I., Pietropaolo, S., Ginger, M., Sans, N., Rossier, J., Oostra, B., LeMasson, G., & Frick, A. (2014). Dendritic channelopathies contribute to neocortical and sensory hyperexcitability in Fmr1-/- mice. *Nature Neuroscience*. <https://doi.org/10.1038/nn.3864>
- Zhou, C., Tsai, S. Y., & Tsai, M. J. (2001). COUP-TFI: An intrinsic factor for early regionalization of the neocortex. *Genes and Development*. <https://doi.org/10.1101/gad.913601>
- Zhou, Cheng, Qiu, Y., Pereira, F. A., Crair, M. C., Tsai, S. Y., & Tsai, M. J. (1999). The nuclear orphan receptor COUP-TFI is required for differentiation of subplate neurons and guidance of thalamocortical axons. *Neuron*. [https://doi.org/10.1016/S0896-6273\(00\)81032-6](https://doi.org/10.1016/S0896-6273(00)81032-6)

- Zhou, D., Lambert, S., Malen, P. L., Carpenter, S., Boland, L. M., & Bennett, V. (1998). Ankyrin(G) is required for clustering of voltage-gated Na channels at axon initial segments and for normal action potential firing. *Journal of Cell Biology*. <https://doi.org/10.1083/jcb.143.5.1295>
- Zingg, B., Hintiryan, H., Gou, L., Song, M.Y., Bay, M., Bienkowski, M.S., Foster, N.N., Yamashita, S., Bowman, I., Toga, A.W., et al. (2014). Neural networks of the mouse neocortex. *Cell* 156, 1096-1111.
- Zuo, Y., Lin, A., Chang, P., & Gan, W. B. (2005). Development of long-term dendritic spine stability in diverse regions of cerebral cortex. *Neuron*. <https://doi.org/10.1016/j.neuron.2005.04.001>